Infrared spectroscopic analysis of prostate tissue: Evaluation of different glass substrate and their influence on cancer detection, with a view for clinical translation

A thesis submitted to The University of Manchester for
the degree of Doctor of Philosophy in the Faculty of Science and Engineering

2022

Yu Zheng

School of Engineering /Department of Chemical Engineering

Abstract

Spectral histopathology (SHP) using glass slides is a promising method for cancer detection. In order to achieve clinical application, it is very important to find the effect of glass type on detection results. The project has studied the influence of glass type on infrared spectra, tissue histopathological classification and cancer detection by two experimental methods. The backgrounds of experiment 1 and 2 were selected tissue-free areas (blank glass, glue & coverslip) and blank glass, respectively. In addition, glue removal by Matlab is an essential data process due to the existence of glue and coverslip in the H&E stained tissue sample. Therefore, finding the most suitable experimental method and glue removal method are also the project's important aims.

Due to the partly opaque, the infrared transmission window for glass slides is 2000-3800 cm^{-1}. Only hydroxyl and its related groups are shown in the infrared spectra of the blank glass slide. The comparison of spectra on 12 blank glass slides indicates that most glass slides cannot be discriminated by infrared spectra except for glass D.

A series of prostate tissue sections from the same BPH patient are mound on the 12 different glass slides. Stroma and epithelium are used for studying tissue classification because they are important compositions and have a high proportion of prostate tissue. The results show that the tissue classification on the same glass slide has very high accuracy (above 98.40%) for both experiments. In addition, tissue classification accuracies for most classifiers tested on different glass slides are above 90.57%. Good performance means that the type of glass slide has a minor influence on tissue classification before removing the glue.

Only 6 glass slides are commonly used for tissue work in 12 glass slides. A series of adjacent tissue slices are mounted on the 6 glass slides, which are from 4 patients (2 BPH & 2 CaP). The accuracies of cancer detection on the same glass slide for

experiments 1 and 2 are 97.00% and 92.00%, respectively. However, the worse result on different glass slides indicates that the type of glass slide has an impact on cancer detection.

The purpose of glue removal is correct the bands in 3400-3450 cm^{-1} and 3400-3600 cm^{-1}, which are related to glue and coverslip, respectively. However, after removing the glue, tissue classification and cancer detection accuracy on the same glass slides are reduced. It means that glue has a contribution to tissue classification and cancer detection.

Experiment 1 always had higher accuracy than experiment 2. The type of glass slide has a slight influence on tissue classification but has a huge effect on cancer detection. Therefore, the type of glass slide must be consistent during cancer detection by SHP, and experiment 1 is the most suitable method.

Keywords: Infrared spectral histopathology (SHP), glass slides, cancer detection, tissue classification, glue removal

Contents

List of Figures

List of Tables

Abbreviation

ANN	Artificial Neural Nets
ATR	Attenuated Total Reflection
BaF_2	Barium fluoride
BPH	Benign Prostatic Hyperplasia
CaF_2	Calcium fluoride
CT	Computed Tomography
CaP	Prostate Cancer
DRE	Digital Rectal Examination
EFSW	Electric Field Standing Wave effect
EMSC	Extended Multiplicative Scattering Correction
FPA	Focal Plane Array
FTIR	Fourier Transform Infrared
GIMP	GNU Image Manipulation Program
H&E	Haematoxylin and Eosin
HCA	Hierarchical Cluster Analysis
IRE	Internal Reflection Element
LDA	Linear Discriminant Analysis
LSCOV	Least-squares with known Covariance
MCT	Mercury Cadmium Telluride
MRI	Magnetic Resonance Imaging
PC	Principle Component
PCA	Principle Component Analysis
PC-DFA	Principal Component Discriminant Function Analysis
PSA	Prostate Specific Antigen
QCL	Quantum Cascade Laser
ROC	Receiver Operating Characteristic
RmieSc	Resonant Mie Scattering Correction
SHP	Spectral Histopathology
SNR	Signal to Noise Ratio
SVM	Support Vector Machines
TRUS-b	Transrectal Ultrasonography

Declaration

No portion of the work referred to in the thesis has beenc submitted in support of an application for another degree or qualification of this or any other university or other institute of learning

Yu Zheng

Copyright

Acknowledgement

First of all, I would like to many thank my supervisor Professor Peter Gardner, who has been patiently guided my study since I was an MSc student. In the past four years, he gave me a lot of encouragement and advice in my study, which made me more confident.

Secondly, I would like to thank Doctor Alex Henderson, who helped me a lot with my data processing. He provided me with training in Matlab and equipment.

I obtained much help and love during my study. Thanks to all of members in Gardner group.

Finally, big thanks to my parents for their support and encouragement during the studying.

Chapter 1

Introduction

1.1 Prostate Cancer

Nowadays, cancer is a significant disease threatening human life worldwide. According to the GLOBOCAN data, there were 19.3 million new cancer cases and 10.0 million deaths worldwide in 2020, with breast, lung, colorectal, and prostate cancer being the most common cancer types diagnosed. By 2040, it is estimated that there will be 28.4 million new cancer cancers each year[1]. A critical point for successful cancer treatment and prognosis is early diagnosis[2]. Therefore, in certain case, cancer screening has been an effective way to control cancer[2][3].

Prostate cancer (CaP) is the second most frequent malignant tumour in men, especially in Europe and America[1][4]. At present, prostate cancer screening modalities include prostate-specific antigen (PSA) detection, digital rectal exam (DRE), magnetic resonance imaging (MRI) and transrectal ultrasound-guided puncture biopsy[3][5]. The biopsy result is a "gold standard" for prostate cancer detection.

The diagnosis results are from pathologists' judgment, which is subjective and time-consuming. According to the information on the NHS website, it usually takes a few days to get diagnosis results after the biopsy[6]. The speed of diagnosis is slow, in part caused by the massive workload of pathologists. Automated pre-screening sample is a potential method of reducing the pathologists' workload.

1.2 Infrared Spectral Histopathology

Infrared spectral histopathology (SHP) is a promising diagnostic tool for various cancer detection. SHP interprets tissue characterisation and classification based on infrared chemical images and computer data processing. In recent years, many studies have shown that SHP could distinguish many types of cancer with high sensitivity and specificity, such as lung cancer[7][8][9], colon cancer[10][11][12], breast

cancer[13][14][15], and prostate cancer[16] [17].

SHP is based on spectral measurement, which depends on the biochemical information of tissue. In comparison, the pathological examination is based on tissue morphology and architecture [18]. In addition, SHP is also a label-free and non-destructive processing. Therefore, SHP can give a diagnostic interpretation for a histopathological sample and could be applied in pre-screening processing in clinical applications.

1.3 Clinical application of SHP

Suppose SHP is applied as a pre-screening process in clinical applications. In that case, SHP could be used to detect the normal samples, which do not contain cancer, and the diagnostic result will be given quickly to the patient. In contrast, the rest of the suspicious and cancerous samples diagnosed by SHP would be given to the pathologists for expert examination and reporting of the final diagnosis. This idea reduces the pathologist's workload, increases the detection speed, and ensures the accuracy of cancer detection.

Not disturbing the current pathological process is very important to achieve the clinical application of SHP. Therefore, it is better for SHP to use the same preserved tissue samples which are used for pathological examination. The tissue block is preserved in formalin and processed by additional solutions to prepare the permanent tissue samples. Then the tissue is placed in paraffin wax and cut into thin slices (4-8μm) after the wax has hardened. The thin tissue sections are stained with dyes and then mounted on glass slides with glue and coverslip. Haematoxylin and Eosin (H&E) are the most common dyes in clinical applications [19].

1.4 Glass substrate for SHP

It is essential for SHP clinical application to keep the existing pathological process. Therefore, the sample preparation process is not disturbed, and the same permanent tissue sample would be used for pre-screening by SHP. Thus, the glass slides would be used as a substrate.

Infrared chemical images used for SHP are measured by Fourier transform infrared spectroscopy (FTIR). Due to the high transparency across a wide infrared range, the conventional substrates for FTIR are calcium fluoride (CaF_2) and barium fluoride (BaF_2), which are used in most of the studies of SHP. However, there are many reasons why CaF_2 and BaF_2 are not particularly suitable for clinical application. First, a new sample preparation step needs to be added if using these substrates, and the traditional sample preparation process would be disturbed. Second, automated equipment normally required for tissue preparation cannot be used because CaF_2 and BaF_2 are fragile [17]. Manual operation is time-consuming. In addition, the price of CaF_2 and BaF_2 are very high, which is around £60 per slide. It would be uneconomic for clinical practice.

Given these significant limitations, is it feasible to use glass as the substrate? Compared with CaF_2 and BaF_2, glass is more robust and significantly cheaper (about £0.7 per slide). However, the glass substrate also has some disadvantages. The glass's thickness and composition affect the fingerprint range's spectral data[20]. For example, the thickness of the coverslip is only around 0.13-0.17mm. Some studies have compared the spectra on the different types of coverslips. The results indicated that according to the spectral data from the fingerprint and lipid range, the cancerous and non-cancerous cell lines could be separated[21][22].

But the glass slides used in this project is histopathology glass slide, and the thickness is around 1mm. The spectral data from fingerprint region cannot be obtained for

histopathology glass slides due to the partly opaque in the infrared region. Thus, the infrared window for the glass slide is in the high wavenumber range (2500-3800 cm^{-1}) [23].

Therefore, most of the critical biological peaks used for further data processing are obscured, and the only useful peak observed is the amide A band (3298 cm^{-1}). Despite this, previous studies have shown that SHP could distinguish prostate cancerous tissue from benign tissue on glass substrates with high sensitivity and accuracy [17][24]. Thus, SHP could discriminate between cancerous and normal tissue on the glass slides.

Because cancer detection in clinical pathological examination depends on the tissue morphological detail, the type of glass slides does not affect detection results. However, the glass substrate would be measured during SHP, and at present, there is a wide range of types of glass slides used in clinical practice. Therefore, it is vital for the clinical application of SHP to study whether the different types of glass could affect the detection result.

1.5 Objective of the project

This project is a fundamental study for the clinical application of SHP, and the aim is to find the impact of glass types on cancer detection. In the project, non-cancerous and cancerous tissue are from benign prostatic hyperplasia (BPH) and CaP patients, respectively. There are 12 different brands of glass slides in total, and only six of them are more suitable for tissue work. In addition, there are two experimental methods for measuring the tissue by FTIR. So it is meaningful to find the best experimental method for SHP.

The project is divided into three main studies presented in chapter 4, chapter 6, chapter 7 . In addition, chapter 5 compared the different methods of glue removal and found the

most suitable way for tissue classification and cancer detection in chapters 6 and 7.

Chapter 4 studies the spectral difference for 12 blank glass slides by comparing the infrared spectra of 12 blank glass slides. Therefore, this part's purpose is to study the effect of the type of glass slide on infrared spectra.

In general, prostate tissue is made of epithelium, stroma, blood and secretion[18]. The prostate secretion is a watery liquid. Cancer detection by SHP can be based on the spectra of different kinds of tissue, and the accuracy is slightly different[17]. The stroma and epithelium are used for further cancer detection because they are important compositions for prostate tissue and are always used in many SHP studies. Thus, before studying cancer detection, it is necessary for chapter 6 to study the effect of glass types on tissue classification. Samples in this part are a series of adjacent tissue sections from the same benign prostatic hyperplasia (BPH) patient mounted on the 12 glass slides.

Chapter 7 studies the effect of glass slide type on cancer detection. Samples in this chapter are a series of adjacent tissue sections from 4 patients (2 BPH & 2 CaP) individually mounted on the 6 glass slides. In addition, four tissue sections in paraffin and without H&E stained are mounted on CaF_2 and regarded as a control set.

In addition, all tissue sections are mounted on the glass slides with glue and coverslip. Therefore, the glue has a specific influence on the spectra, and it is necessary to remove the effect of glue from the spectra. Chapter 5 compares the different methods and fit ranges of glue removal and finds the most suitable glue removal method applied in the spectra in chapters 6 and 7.

1.6 Reference

[1] H. Sung *et al.*, 'Global Cancer Statistics 2020: GLOBOCAN Estimates of Incidence and Mortality Worldwide for 36 Cancers in 185 Countries', *CA. Cancer J. Clin.*, vol. 71, no. 3, pp. 209–249, 2021.

[2] R. C. Wender, O. W. Brawley, S. A. Fedewa, T. Gansler, and R. A. Smith, 'A blueprint for cancer screening and early detection: Advancing screening's contribution to cancer control', *CA. Cancer J. Clin.*, vol. 69, no. 1, pp. 50–79, Jan. 2019.

[3] R. A. Smith *et al.*, 'Cancer screening in the United States, 2018: A review of current American Cancer Society guidelines and current issues in cancer screening', *CA. Cancer J. Clin.*, vol. 68, no. 4, pp. 297–316, Jul. 2018.

[4] G. Gandaglia *et al.*, 'Epidemiology and Prevention of Prostate Cancer', *Eur. Urol. Oncol.*, vol. 4, no. 6, pp. 877–892, Dec. 2021.

[5] R. W. Stewart, S. Lizama, K. Peairs, H. F. Sateia, and Y. Choi, 'Screening for prostate cancer', *Seminars in Oncology*. 2017.

[6] 'Biopsy - NHS'. [Online]. Available: https://www.nhs.uk/conditions/biopsy/. [Accessed: 02-Jan-2022].

[7] X. Mu *et al.*, 'Statistical analysis of a lung cancer spectral histopathology (SHP) data set', *Analyst*, vol. 140, no. 7, pp. 2449–2464, 2015.

[8] A. Akalin *et al.*, 'Classification of malignant and benign tumors of the lung by infrared spectral histopathology (SHP).', *Lab. Invest.*, vol. 95, no. 4, pp. 406–21, 2015.

[9] F. Großerueschkamp *et al.*, 'Marker-free automated histopathological annotation of lung tumour subtypes by FTIR imaging', *Analyst*, vol. 140, no. 7, pp. 2114–2120, 2015.

[10] C. Kuepper, F. Großerueschkamp, A. Kallenbach-Thieltges, A. Mosig, A. Tannapfel, and K. Gerwert, 'Label-free classification of colon cancer grading using infrared spectral histopathology', *Faraday Discuss.*, vol. 187, pp. 105–118, 2016.

[11] J. Nallala *et al.*, ‘Infrared spectral histopathology for cancer diagnosis: a novel approach for automated pattern recognition of colon adenocarcinoma.’, *Analyst*, vol. 139, no. 16, pp. 4005–4015, 2014.

[12] A. Kallenbach-Thieltges, F. Gro??er??schkamp, A. Mosig, M. Diem, A. Tannapfel, and K. Gerwert, ‘Immunohistochemistry, histopathology and infrared spectral histopathology of colon cancer tissue sections’, *J. Biophotonics*, vol. 6, no. 1, pp. 88–100, 2013.

[13] M. W. Kissin, G. Q. Della Rovere, D. Easton, and G. Westbury, ‘Risk of lymphoedema following the treatment of breast cancer’, *Br. J. Surg.*, vol. 73, no. 7, pp. 580–584, 1986.

[14] B. Bird, K. Bedrossian, N. Laver, M. Miljković, M. J. Romeo, and M. Diem, ‘Detection of breast micro-metastases in axillary lymph nodes by infrared micro-spectral imaging.’, *Analyst*, vol. 134, no. 6, pp. 1067–76, 2009.

[15] M. J. Pilling, A. Henderson, and P. Gardner, ‘Quantum Cascade Laser Spectral Histopathology: Breast Cancer Diagnostics Using High Throughput Chemical Imaging’, *Anal. Chem.*, vol. 89, no. 14, pp. 7348–7355, 2017.

[16] E. Gazi *et al.*, ‘Applications of Fourier transform infrared microspectroscopy in studies of benign prostate and prostate cancer. A pilot study’, *J. Pathol.*, vol. 201, no. 1, pp. 99–108, 2003.

[17] M. J. Pilling, A. Henderson, J. H. Shanks, M. D. Brown, N. W. Clarke, and P. Gardner, ‘Infrared spectral histopathology using haematoxylin and eosin (H&E) stained glass slides: a major step forward towards clinical translation’, *Analyst*, vol. 142, no. 8, pp. 1258–1268, 2017.

[18] M. Pilling and P. Gardner, ‘Fundamental developments in infrared spectroscopic imaging for biomedical applications’, *Chem. Soc. Rev.*, vol. 45, no. 7, pp. 1935–1957, 2016.

[19] M. Slaoui and L. Fiette, ‘Histopathology Procedures: From Tissue Sampling to Histopathological Evaluation’, 2010.

[20] M. Kansiz, L. M. Dowling, I. Yousef, O. Guaitella, F. Borondics, and J. Sulé-Suso, ‘Optical Photothermal Infrared Microspectroscopy Discriminates for the

First Time Different Types of Lung Cells on Histopathology Glass Slides', *Anal. Chem.*, vol. 93, no. 32, pp. 11081–11088, 2021.

[21] A. V. Rutter, J. Crees, H. Wright, D. G. Van Pittius, I. Yousef, and J. Sulé-Suso, 'Fourier transform infrared spectra of cells on glass coverslips. A further step in spectral pathology', *Analyst*, vol. 143, no. 23, pp. 5711–5717, 2018.

[22] A. V. Rutter *et al.*, 'Identification of a Glass Substrate to Study Cells Using Fourier Transform Infrared Spectroscopy: Are We Closer to Spectral Pathology?', *Appl. Spectrosc.*, vol. 74, no. 2, pp. 178–186, 2020.

[23] R. a Shaw, H. H. Eysel, K. Z. Liu, and H. H. Mantsch, 'Infrared spectroscopic analysis of biomedical specimens using glass substrates.', *Anal. Biochem.*, vol. 259, no. 2, pp. 181–6, 1998.

[24] P. Bassan, J. Mellor, J. Shapiro, K. J. Williams, M. P. Lisanti, and P. Gardner, 'Transmission FT-IR chemical imaging on glass substrates: Applications in infrared spectral histopathology', *Anal. Chem.*, vol. 86, no. 3, pp. 1648–1653, 2014.

Chapter 2

Literature Review

2.1 Cancer

Cancer is one of the prevalent life-threatening diseases. According to the World Health Organization (WHO) data in 2020, about 10 million people died from cancer. Furthermore, there were approximately 19.3 million new cancer cases [1].

The most frequently diagnosed cancers in the world include breast cancer, lung cancer, prostate cancer, nonmelanoma of skin and colon cancer[1][2]. At present, the incidence and mortality of several common cancers worldwide are still increasing[3]. However, treatments for many late-stage cancers are still poor or relatively ineffective. Therefore, it is crucial for patients' treatment to develop and improve the early diagnosis methods of various kinds of cancer so that treatments can be started earlier. Currently, the main techniques of clinical cancer diagnosis include endoscopy, medical imaging methods[4], such as magnetic resonance imaging (MRI), computed tomography (CT), B-ultrasound, X-ray imaging, mammography, various biochemical tests and histopathology based on microscope observation of tissue morphology[5][6].

The combination of histopathology and imaging methods is still the most critical standard cancer diagnostic method. However, the pathological diagnosis operation process is non-quantitative, time-consuming and subjective[7]. Although the diagnostic accuracy of CT and MRI is improved, the price is higher. Fourier transforms infrared spectrometer (FTIR) is a simple analytical method with high accuracy compared with other methods.

2.2 Application of Infrared Spectroscopic Imaging

Infrared spectroscopy and microscopic imaging are powerful tools for studying the chemical composition and spatial distribution of complex substances. The development of infrared spectroscopic imaging includes three broad areas: data recording,

interpretation of recorded data, and information extraction[8]. Hence, due to the development of theory consisting of many approaches, higher performing instrumentation, and better algorithms and computation [8], many applications have been widely used in analytical chemistry, materials science[9][10], forensic science[11][12], food industry[13] and biomedicine[7][14]. In particular, biomedical diagnostics and analysis have been extensively studied in the biomedical field[7][15][16].

Fourier transform infrared (FTIR) microscopy is a higher-performing commercial instrumentation. Its application has been extended from the chemical field to the biomedical field and from studying the structure of nucleic acid, proteins, and other biological macromolecules to investigating the composition of more complex tissues and cells[8][17]. In principle, FTIR spectroscopy can give information regarding the structure and chemical properties of the samples at the molecular level. However, in complex cells and tissues, the overall spectrum is the superposition of the spectra of the constituent molecules. Spectral differences, however, can reveal the biochemical changes of pathological tissues and cells in the process of carcinogenesis[6]. At present, FTIR has been widely used in the study of cancerous tissues and cells[18][19][20].

The cell is the basic unit of structure and function of the organism, and its elemental chemical compositions are carbohydrates, lipids, protein, nucleic acid and other biological macromolecules. The cancerisation of cells or tissues is always accompanied by changes in the conformation, relative content and surrounding environment of the above biological macromolecules[18]. The infrared spectrum of the cells or tissue is composed of the vibrational spectra of these biological macromolecules[21]. The infrared spectral characteristics of the biological macromolecules are shown in Table 2.1.

Table2. 1 The main bands of the biological macromolecules in the infrared range

Wavenumber (cm^{-1})	Mode of vibration
3300	The amide A and OH
~3075	The amide B
~2959	Asymmetric stretching of C-H in CH_3
~2925	Asymmetric stretching of C-H in CH_2
~2872	Symmetric stretching of C-H in CH_3
~2852	Symmetric stretching of C-H in CH_2
~1741	Symmetric stretching of CO in lipids
~1650	Amide Ⅰ
~1550	Amide Ⅱ
~1467	Scissoring C-H bending (CH_2)
~1396	Scissoring C-H bending (CH_3)
1310-1240	Amide Ⅲ
1250-1220	Asymmetric P=O stretching in PO_2
~1085	Symmetric P=O stretching in PO_2

Therefore, according to the infrared spectrum of tissue or cells, information about the structure of biological macromolecules that make up tissue or cells can be obtained, and then the normal and cancerous tissue or cell can be identified by using the difference of the spectral information, which provides the potential for the diagnosis of cancer at the molecular level. Many researchers have used FTIR to study cells or tissues of prostate cancer[16], [22]–[25], breast cancer[26]–[28], lung cancer[29][30], colon cancer[19][31][32], renal cancer[33], brain cancer[34], and so on. The results of these studies have a good performance on cancer detection and indicated that the application of FTIR is a potential method for cancer detection.

2.2.1 Application in Prostate Cancer Detection

Prostate cancer is one of the most common cancers that endanger men's health. Prostate cancer ranks second in the world in cancer morbidity and fifth in mortality[1]. Early detection and treatment can significantly improve patients' survival rate and life quality. Therefore, it is very important to find a method for the early diagnosis of prostate cancer. Currently, the main diagnostic procedures for prostate cancer are digital rectal examination (DRE) and the use of prostate specific antigen (PSA) as an indicator for biopsy. Although the prostate biopsy guided by transrectal ultrasonography (TRUS-b)

is a gold standard for prostate cancer diagnosis, there is the possibility of misdiagnosis according to the indicator of PSA. Furthermore, the biopsy is an invasive examination that may lead to overdiagnosis of prostate cancer[35]. Therefore, finding an early detection method for prostate cancer is still a critical problem in prostate cancer treatment.

Gleason grading is used to assess the mortality risk and predict prostate cancer's outcome [36]. From 1966 to 1974, Donald Gleason modified and developed the Gleason grading system[37]. There are five histologic patterns, which are from pattern 1 to pattern 5. The grading score is calculated by adding the most and second most common patterns. Therefore, the range of grading scores is from 2 to 10[38]. Commonly, the higher scores, the higher malignancy [5][36].

In 2005, the Gleason score was codified by the international society of urological pathology (ISUP) and became the recommended prostate cancer grading system[39]. In 2014, the ISUP Gleason grading conference defined a new grading system. Gleason grading scores are divided into five grade groups, and the lowest score is 6. The five grade groups in the new grading system are shown in table 2.2 [38][40]. The latest modification for pathologic grading guidelines was in 2019. It recommended the approaches to report Gleason patterns quantities and minor Gleason patterns and summarised the challenge with the development of multiparametric magnetic resonance imaging (mpMRI)-targeted biopsies[41][42].

In recent years, there have been many studies to detect prostate cancer by infrared spectroscopy. According to the results of Gazi's et al. study[23], FTIR microspectroscopy could be a promising method to diagnose prostate cancer. The study used FTIR microspectroscopy to compare the spectra of prostate cancer cell lines derived from different metastatic sites and tissue from benign and malignant prostate. The spectra can be used to discriminate the benign and malignant prostate cells depending on the ratio of peak intensities at 1030 $cm^{-1}$and 1080 cm^{-1}, corresponding

to the glycogen and phosphate vibrations, respectively. Furthermore, on the basis of the ratio, the malignant content can also be estimated. Based on cell metabolic activities, the paper gave reasonable explanations for the different levels of glycogen and zinc between the normal and cancerous prostate cells. The explanations also proved that it is reliable to distinguish benign and malignant cells according to the peak area ratio of 1030 $cm^{-1}$and 1080 cm^{-1}.

Table2. 2 International society of urological pathology 2014 grade

Grade group	Gleason score
1	6 (3+3)
2	7 (3+4)
3	7 (4+3)
4	8 (4+4 or 3+5 or 5+3)
5	9 – 10

The results of data processing in this paper showed that the principal component analysis (PCA) could successfully separate the spectra of prostate cancer cell lines from different metastatic sites. In addition, there was a good separation for benign and malignant glands of different Gleason grades tissue by directly entering the spectral intensities into the linear discriminate algorithm (LDA). Moreover, it proved that the LDA-FTIR could be a potential method for cancer detection [23].

However, this study also had some limitations. Firstly, the study just proved that it was possible to discriminate the benign and malignant prostate cells by imaging FTIR microspectroscopy. There was no specific quantification evidence to show the separation results. Secondly, the number of benign and cancerous samples were only 2 and 3, respectively. The small-scale study meant that it might not be statistically significant. Therefore, further studies were conducted using FTIR imaging.

In 2006, an additional study was performed by E Gazi[43]. In this study, serial sections of prostate cancer tissue were diagnosed by the clinical pathologist and FTIR-LDA, respectively. Furthermore, according to the Gleason score and FTIR-LDA scored

system, the detection results were compared. However, the correlation of the two methods was low (20%) by using the stringent-rule criteria because the Gleason grading and FTIR-LDA grading were based on tissue architecture and biochemical composition, respectively. The results showed that the FTIR-LDA scores were always higher than the Gleason scores, which indicated that the malignant cell had developed more aggressive phenotypes before the architecture of the tissue changed. While the correlation of the two methods was greater by using the three-band Gleason criteria (Gleason scores <7, =7, >7), in which the sensitivity and specificity for FTIR-LDA score were $\geq$70% and >81%. Similarly, when using the cut-off point of $\geq$8, the sensitivity and specificity are71% and 67%, respectively. Although compared with the results of Gleason scores, the sensitivity was lower by 14% for the FTIR-LDA score. The specificity was higher than 4%. The result indicated that the incorrect prediction for prostate cancer metastatic behaviour was lower by using the FTIR-LDA score system. This would be more important for the FTIR-LDA score system as a complementary method to be applied in the clinic in the future. According to the similar performance in tumour metastatic behaviour prediction by two grading methods, FTIR-LDA was a viable method to classify malignant prostatic tumours.

The sample number in Gazi's further study was 40, which was higher than the study in 2003. However, it still needs to build an extensive data set for further testing. The low sensitivity and specificity may also be caused by the small number of samples section of the same tumour. However, the clinical detection results are from the overall performances of several sections of the same tumour[43].

In 2009, Baker also achieved prostate cancer grading by another data analysis method. Principal Component Discriminant Function Analysis (PC-DFA) was used to differentiate the spectra. The results of this study showed that prostate cancer could be graded with high sensitivity and specificity by FTIR microspectroscopy combined with PC-DFA. Similarly to the Gazi study in 2006 [43], this study also used the three-band Gleason criteria (Gleason scores <7, =7, >7), but the sensitivity and specificity

increased to 83.6% and 86%, respectively. It indicated that the FTIR PC-DFA diagnostic model was better than FTIR-LDA. The spectra in Amide, C–H, CH_2 and CH_3 regions are different for tissues with different Gleason scores. In this study, amide and lipid regions were also used to discriminate low-grade cancer from high-grade cancer [44]. The biochemical components had changed before the tissue structure changed. It leads to the cancer grading by the conventional pathological method being usually lower than that by the spectroscopic grading method [43]. Therefore, this study achieved the separation between locally confined and locally invasive prostate cancer by an observer independent criterion. It is very important for the diagnosis, prognostication and treatment planning in different stages of prostate cancer.

However, this study also contained some limitations. The major limitation was that the novel spectral grading system was still based on the observer dependent Gleason grading system. This means that problems in the Gleason grading system may still exist in the new grading system. Secondly, the scale of the study was still small, so it was important for further work to increase the number and type of the sample. Thirdly, the detector of FTIR microspectroscopy used in this study was a single point detector. Compared with the linear array and focal plane array detectors, single point detectors have the disadvantages of being time-consuming to use, and mapping produces low imaging quality.

To instead the manual judgment of biopsy, Kwak et al. studied automated recognition of prostate cancer tissue [45][46]. To pre-define prostate tissue, they developed computer information and management and decision-support system. The database in this system contained tissue images, clinical information and more measurement data (e.g. IR chemical imaging). According to computing tissue morphologic similarity (TMS) score and morphological features, the retrieval system could be trained. This system could define prostate cancer tissue automatedly with high accuracy (around 80%)[46]. In 2014, Bassan also studied rapid automated cell-type recognition by random forest classifier based on infrared imaging[47].

Both Gazi [23], [43]and Baker [44] studies used paraffin-embedded formalin-fixed prostate cancer tissues. In order to achieve high throughput, a tissue microarray system has also s been used. Prostate tissue microarrays were used in Fernandez's study in 2005[48]. The prostate tissue consists of normal epithelium, fibrous stroma, mixed stroma, muscle, nerve, lymphocytes, stone, ganglion, endothelium and blood. The different histology classes have different chemical compositions, which leads to the spectra of different histology classes being also different[48]. In this study, each pixel of prostate tissue imaging was assigned histopathologic recognition. In addition, the tissue segmentation was automated by Metric classification. Furthermore, according to the epithelial pixel spectra, the benign and malignant cells can be differentiated because prostate cancer is derived from the epithelial cell. In addition, compared with the conventional immunohistochemical approach, the samples used in the vibrational spectroscopic approach did not need to be stained, which could eliminate the influence of dye or molecular probe. Although the study has achieved the accurate segmentation of prostate tissue and separation between the malignant and the benign epithelial cell, cancer grading for prostate microarray tissue by FTIR was not validated in this study, which would be researched in further study.

The samples (tissue specimen and tissue microarray) used in the abovementioned studies are paraffin-embedded formalin-fixed prostate cancer tissue. Because of the infrared absorption of paraffin, the paraffin could affect the spectra. The deparaffinisation of the tissue for spectroscopic evaluation is very important. Therefore, it is necessary to build a standard protocol to remove the paraffin and assess whether paraffin removal can affect spectral pathology. And depending on the results of Hughes's study in 2014 [49], although the paraffin removal could lead to leached out unbound tissue lipid, the locked lipid that was mainly in the membranes could still be detected, and these lipid signals were useful for spectral pathology. Paraffin-related peaks at 1426, 2846, 2954 cm^{-1} and the evidence of paraffin removal is that the methylene vibrations are at a stable baseline[49]. The study compared the spectral

information of methylene vibration when the tissue is washed by different solvents (hexane and xylene) with different immersion times. The results showed that there was a steady state after the tissue was immersed for 10 min and no major difference between the use of hexane and the xylene. However, hexane is more flammable than xylene[49]. Therefore, the suggestion of deparaffinisation for paraffin-embedded formalin-fixed prostate cancer tissue is dewaxed by xylene for 5 – 10 min.

Characterisation of normal and malignant prostate tissue by FTIR microspectroscopy imaging was also studied on snap frozen tissue[50]. According to the FTIR spectroscopy, Pezzei et al. investigated the process of cancer in detail by identifying the change in the molecular components and histopathological morphology. Compared with the paraffin-embedded formalin-fixed tissue, snap frozen prostate tissue could maintain the topographic integrity of the tissue and avoid time-consuming extraction, purification and separation steps.

2.2.2 Application in Breast Cancer Detection

Breast cancer is one of the primary malignant tumours in women, and its morbidity and mortality are increasing [1]. Breast exam, mammogram images, breast ultrasound, histopathological examination of biopsy samples, and breast magnetic resonance imaging have been widely used in the diagnosis of benign and malignant breast tissue[5][51]. However, such techniques have different inaccuracies in detection. Therefore, new methods for breast cancer diagnosis are helpful for increasing detection accuracy.

In 1995, Marc et al. compared the FTIR spectra of breast cancer and normal tissue biopsies. Their study has found an increase in phosphodiester groups, Amide I and Amide II bands for cancerous tissues[52]. In 1999, Ci et al. investigated the spectral difference among normal, benign (hyperplasia, fibroadenoma) and cancerous frozen breast tissue samples[53]. The spectral differences among the four types of breast are

mainly expressed in the peak at 970 cm^{-1}, and the ratio of absorbance of the peak at 1459 cm^{-1} and 1239 cm^{-1}. It indicated the content of nucleic acids and collagen has significate implications for different types of breast tissue.

The main path of metastasis of breast cancer is via the lymph nodes [54]. Surgery has always been the primary treatment for breast cancer [55]. Surgery for breast cancer includes the management of the primary site of cancer and axillary dissection. Axillary lymph node dissection is always the main treatment of breast cancer surgery [56]. It provides accurate axillary lymph node staging, removes potential metastatic lymph nodes and achieves better regional control. However, there are serious side effects after an operation, such as arm lymphedema and shoulder dysfunction.[56]. With the development of imaging technology, more and more breast cancers at the early stages are being detected. For these early-diagnosed cancers, only a small number of patients have axillary lymph node metastases. Therefore, axillary lymph node dissection does not bring any benefit to those patients without axillary lymph node metastases.

Sentinel lymph nodes are the first lymph nodes to contact the primary site of cancer and are the first lymph node to receive cancer metastasis[57]. In theory, if the sentinel lymph nodes do not have free metastatic breast cancer cells, the probability of breast metastasis of other lymph nodes is tiny. Sentinel lymph node biopsy can avoid the routine axillary lymph node dissection for early breast cancer stage patients without axillary lymph node metastases, and reduce the complications of operation and improve the life quality of the patients.

However, the sentinel lymph node biopsy depends on the pathologists' experience. Many misdiagnoses remain in routine histopathology. Therefore, it is very important to find an alternative method to find micro-metastases accurately and effectively. Bird et al. [58] reproduced the structure of axillary lymph nodes and diagnosed free metastatic breast cancer cells by infrared micro-spectral imaging combined with multivariate statistical analysis in 2009. Using hierarchical cluster analysis (HCA), the tissue image

was classified into different cluster images. Pathologists could compare the cluster images with H&E images obtained from the same tissue to give the best morphological interpretations. This study also demonstrated that SHP was a promising method for deparaffinised tissue to classify tissue and identify abnormal cells.

The study by Bird [58] also compared the classification results of paraffined and deparaffinised tissues. The paraffin had a very strong contribution at the C-H stretching (3000 - 2800 cm^{-1}) and (1490 - 1350 cm^{-1}). Therefore, spectral ranges of paraffined tissue in data analysis were 1800 - 1496 $cm^{-1}$and 1350 - 900 cm^{-1}. While the spectral range of deparaffinised tissue was 1800 - 900 cm^{-1}. The results showed that for T-lymphocyte and breast cancer, there were large differences between deparaffinised and paraffined spectra, which was caused by the change of secondary structure of the protein and hydration of the tissue during the deparaffinisation process. There was a better classification result by analysing the paraffined spectral data because spectra of deparaffinised tissue were contaminated by dispersive artefacts. There were different results between this study and that by Hughes et al.[49], which was caused by different infrared operation modes. Transflection was used in this study, while Hughes et al. used transmission.

The study by Bird [58] also met the challenge of detecting micro-metastatic cancer cells. Because the size of a cancer cell is only ~25 μm and only a few cancer cells are present in micro-metastases, to differentiate the cancer cell correctly, it requires the pixel resolution of the FTIR microscope to be of the order of only 5-10 μm. In addition, chemical structural details of cancers and biological molecules could be understood precisely and accurately by combining spectroscopy and Artificial Intelligence (AI)[59]. This study was improved by the application of Artificial Neural Nets (ANN), and the results demonstrated that ANN could classify spectral data and consume less time than HCA[58].

Maria et al. compared the spectral difference of Non-malignant (MCF10A), malignant

non-metastatic MCF7 and metastatic MDA breast cell lines[51]. For MCF7 cell line, there were a blue shift of amide I and II bands and higher intensity of nucleic acid bands. In addition, these three types of cell lines could be separated by the ratiometric analysis of peaks' areas. The study indicated FTIR micro-spectroscopy could be a potential method to diagnose breast cancer at the cytological level.

Many studies have proven that the SHP could achieve structural classification and cancerous detection for breast tissue. In order to be a complementary method for clinical application in the future, SHP not only needs to have high accuracy in cancer detection but also needs to have high speed and high throughput for detection. Compared with the FTIR system, the development of quantum cascade laser (QCL) infrared imaging systems means that tissue imaging can be achieved with high speed and high throughput [60]. In 2017, using QCL coupled with a machine learning approach, Pilling et al. accurately separated the breast tissue microarrays into four histological classes and diagnosed malignant from the non-malignant tissue by stroma spectra with high sensitivity and specificity[28].

The breast tissue core was composed of epithelium, stroma, blood and necrosis[28]. In addition, the mean spectra of each histological class were significantly different. All of the tissue cores were separated into training and test set randomly. The same number of spectra of each class were used to train the random forest classifier, and the acceptance threshold was 0.6. Then the classifier was used to classify all pixels in chemical images of the test set. Compared with brightfield images of H&E stained tissue cores, the chemical images have a good agreement for each class.

All pixels of the other class in each tissue core was removed by the random forest classifier, and the stromal spectra were isolated. The study using fivefold cross-validation, trained a new classifier to detect malignant and non-malignant stroma. According to the result of the ROC curve, there was a good separation between malignant and non-malignant stromal spectra. In addition, there was high accuracy

regarding the differentiation of non-malignant and malignant stroma using the acceptance threshold of 0.6. Moreover, the cancerous sample could be detected according to the proportion of the malignant stroma, which is commonly close to 1. This study indicated that stroma is a good indicator of breast cancer [28].

In the study by Pilling[28], the spectra were obtained by a QCL coupled with an FPA detector. However, due to the coherence effect between the sample and coherent light, the signal to noise ratio of the spectra was poor. Although the single point acquisition could reduce the interference effect and improve the spectral quality, it could reduce the throughput and detection speed. Compared with the clinical classification results, the coherence effects only had minimal impact on classification accuracy. In addition, this study indicated that FPA-based QCL imaging using the continuous frequency spectra had high accuracy in differentiating malignant and non-malignant stroma, and it also proved that it could be viable to use discrete frequency spectra for cancer diagnosis, which would improve the throughput and detection speed [28].

2.2.3 Application in other cancer Detection

The SHP is also applied to other types of cancer diagnosis in recent years, such as lung cancer[29], [30], [61], colon cancer[19], [20], [31], [32], renal tumours [33] and brain cancer[62].

There are also some developments in lung cancer detection. CT, chest radiography (X-ray), sputum cytology, and MRI scan are the main clinical techniques for the diagnosis of lung cancer[6]. Lung cancer is divided into small cell lung cancer (SCLC) and non-small cell lung cancer (NSCLC). The major types of NSCLC are adenocarcinoma (ADC) and squamous cell carcinoma (SqCC) [61]. There are also some different subtypes for ADC, such as lepidic, acinar, papillary, micropapillary and solid predominant ADC[63]. Because of the different prognoses of the subtypes, discrimination of subtypes is very important in lung cancer detection. However, it is the

main challenge for pathologists due to the histological heterogeneity in the subtypes[29]. Therefore, finding a complementary method to improve the detection accuracy is necessary.

SHP has been applied to lung cancer diagnosis in many studies. Mu et al. [30] used different multivariate statistical methods to process the infrared spectral dataset, which composes of 3880 samples from 374 patients. The results showed that there was 95% accuracy in distinct normal, necrotic and cancerous tissue, while 90% accuracy in classifying SCLC, SqCC and ADC. The study reported by Groberueschkamp et al. [29] using FTIR image analysed using a random forest classifier not only achieved the lung cancer classification but also, for the first time, identified subtypes of ADC in the marker-free fresh-frozen tissue slides.

The sputum spectra could also be biomarkers for detecting lung cancer with high accuracy. Paul et al. collected the spectra of sputum from 1800 – 950 cm^{-1}. The spectral difference between cancer and normal sputum may be from changes in protein, nucleic acid and glycogen levels in tumours, and the peaks at 964 cm^{-1}, 1024 cm^{-1}, 1411 cm^{-1}, 1577 $cm^{-1}$and 1656 cm^{-1}[64].

Many types of research about different kinds of cancer use the infrared technique. Bergner et al. collected FTIR imaging from 22 brain metastasis tissue sections with H&E stained. The correct classification rates by support vector machines (SVMs) for brain tissue, necrosis and carcinoma are 98.8%, 98.4% and 94.4%, respectively [47]. In 2013, Uckermann et al. discriminated the FTIR spectral difference between glioblastoma cells with high and low content of CD133 (cluster of differentiation 133)-positive cells by unsupervised cluster analysis [65]. A method for automatically identifying colon tissue types and areas of colon adenocarcinoma was explored by Kallenbach et al. in 2013 [32]. Ukkonen et al. used FTIR imaging to study the relationship between cancer progression and the tumour microenvironment (TME) of invading melanoma and oral carcinoma cells[66]. Wald et al. identified the main cell

types in melanoma cancer with high accuracy (above 90%) by FTIR imaging combined with a supervised partial least squares discriminant analysis (PLS-DA) model [67].

2.2.4 Application in Cancer Detection on Glass Substrate

Many studies have proven that the SHP is a promising method to detect cancer. Further work is exploring the most suitable protocol and achieving clinical application. The substrate of most SHP studies using transmission mode operation is an infrared transparent substrate, such as calcium fluoride (CaF_2) or barium fluoride (BaF_2) [7]. However, these transmission substrates are expensive and fragile, which could contribute to high costs and make them unsuitable for use in automated tissue preparation equipment [68]. Manual tissue preparation would lead to reduced throughput and detection speed and eliminate many advantages of the SHP. Thus, to achieve the clinical application of infrared SHP and become a complementary diagnostic tool, a major step is making infrared chemical imaging fit into a current cancer diagnosis workflow. Currently, tissue biopsy and analysis by a pathologist is the gold standard of cancer detection. Glass substrates are used for tissue biopsy because they are cheap and robust. However, the vital drawback of glass is its opacity in most of the useful mid-infrared spectral regions.

In 1998, a study researched by Anthony Shaw [69] demonstrated that it was possible to carry out clinical analyses and diagnostic spectral classification using the glass substrate in spite of limited transparency in the mid-IR region. However, the samples in this study were dried serum, amniotic fluid and synovial fluid films rather than tissue specimens and tissue microarrays. In addition, the study was for the determination of fetal lung maturity and differential diagnosis of arthritis rather than cancer detection. The results showed that there were enough features to diagnose different kinds of arthritis only using the absorption above 2000 cm^{-1}. The analytical and diagnostic accuracy of the IR spectral classification method was similar for films dried on a glass slide and CaF_2 slides. Although this research was not used for cancer detection, it gave a general idea

for the IR spectral classification method using a glass slide to achieve the clinical application of disease diagnosis.

In recent years, the results of several studies also indicate that it is possible to achieve infrared SHP for cancer diagnosis using glass slides. In 2014, Bassan et al. [70] classified each breast tissue core into four basic cell type classes only by the high wavenumber transmission window (2500-3800 cm^{-1}) of glass substrates. Moreover, differentiating malignant and non-malignant tissue cores only based on the epithelium cell had a reasonable accuracy. In order to reduce the spectral distortion and prevent chemical alteration caused by the reagent, tissue cores used in this study still remained embedded in the paraffin. Because of the appearance of paraffin, the wavenumber region 2700-3000 cm^{-1} was truncated, and the infrared region used in this study was 3000-3700cm^{-1}. According to the mean spectra of the four different classes (epithelium, stroma, blood and necrosis), there was a difference in peak position, peak width and intensity of the shoulder. By using the training set database extracted from two breast tissue cores, four features were used to discriminate between different classes, which included the ratio of absorbances: 3380:3400 cm^{-1}, 3520:3530 cm^{-1}, 3350:3390 cm^{-1} and area under spectral region from 3109 to 3580 cm^{-1}. Then, a random forest classifier could be constructed using the above four features. The test set was consisted of the remaining 69 cores and using a probability acceptance threshold of 0.95, the spectra in the test set were classified with high accuracy [70].

To investigate the viable ability of breast cancer detection only using high wavenumber region, all of the epithelial spectra conducted a new database and the discriminatory features used to differentiate malignant and non-malignant epithelium were the ratio of absorbance: 3160:3170 cm^{-1}, 3190:3220 cm^{-1}, , 3200:3220 cm^{-1}, 3110:3220 $cm^{-1}$and 3120:3460 cm^{-1}. Then according to the visualised result processed by PCA, it was able to separate the malignant from non-malignant epithelial breast tissue cores by using the ratio of absorbance: 3160:3170 cm^{-1} and 3190:3220 cm^{-1}[70]. However,

this limitation lacked specific accuracy for differentiating malignant and non-malignant tissue.

Bussan's study [70] proved that the SHP on glass substrates was a viable method for breast cancer discrimination. However, the sample in his research was unstained tissue, which was still different from the samples used in clinical biopsy analysis. It will not fit into the standard pathologist workflow. Therefore, Pilling et al. [68] carried out a study in 2017 using haematoxylin and eosin (H&E) stained prostate tissue microarrays on a glass slide. The results demonstrated that by using H&E stained samples, rapid automated spectral histology could be achieved with high classification accuracy. Furthermore, the different degrees of staining does not affect the classification accuracy.

The samples in Pilling's study were formalin-fixed paraffin-embedded prostate tissue. Before being stained, the samples need to be dewaxed by xylene and rehydrated by graded ethanol [68]. This deparaffinised processing would alter tissue chemical composition and change the spectra. The results from a study by Pijanka et al. [71] showed that the H&E stain process could lead to the appearance of a new peak at 1387 cm^{-1} and disappearance of some lipid peaks at 2850 cm^{-1} and 2920 cm^{-1}. However, comparing the chemical image of prostate tissue at 3298 cm^{-1} (Amide A) and brightfield visible image, there was great agreement in morphology [68]. The tissue core was still separated into epithelium, stroma, blood and secretion. According to the mean spectra of each histological class, there was a distinct difference in the Amide A band. Therefore, it was possible to discriminate different histological classes by the amide A band [68]. The study using the random forest classifier quickly achieved the automated histological classification with high accuracy. Every class was denoted by a different colour, producing a false colour image, which had an excellent agreement with the visible brightfield image.

The high agreement of the false colour image indicated that the infrared chemical image could classify the histological classes correctly using the H&E stained prostate tissue on glass. However, the staining process was still a variable factor. The different tissue

cores could possibly have different degrees of stain. Nine serial sections of benign prostatic hyperplasia (BPH) with different immersion times were used in this study to explore the influence of different degrees of stain on histological classification [68]. The different degrees of H&E stain tissues were used as training and test sets, and the correct classification results indicated that the different degrees of stain had no effect on the classification accuracy.

The main purpose of the research is to achieve cancer detection by SHP. Because epithelium and stroma are the main constituents of prostate cancer tissue in Pilling's study [68], each H&E stained sample was identified into four classes: normal epithelium, malignant epithelium, normal stroma and malignant stroma. A new random forest classifier was constructed by training and validation sets and then used to classify the test set with high accuracy for each class (above 95%). The cancerous tissue cores were detected according to the high malignant epithelium and stroma percentage.

Besides the accuracy of the histological classification, the high throughput is also essential. The study consumed 51.5 hours of measurement time for 182 cores [68]. In order to further improve the translation speed, further study needs to optimise spectral collection parameters and find the trade-off between spectral quality and throughput. Further work is required to validate the SHP as a reliable method for cancer diagnosis by detecting a large number of samples from more independent patients and also carrying out studies on different cancer types. The final target is to achieve the SHP clinical application for cancer detection.

Similarly, Tang et al. used FTIR images of H&E stained tissue on glass slides to do breast cancer prediction[72]. There were 120 breast tissue biopsy cores from different patients. The cancerous core could be classified with high accuracy (95.8%) by AdaBoost algorithm classification, which has been proven to be more robust than random forest [73]. In addition, the classification threshold is optimised to reduce the false-negative rate of cancer diagnosis, and the best threshold is 0.1.

Both Pilling and Tang's studies achieved cancer detection on the histopathology glass slide (thickness is 1mm), which would lead to the absorption of the mid-IR spectrum in the fingerprint region. Rutter et al. found that spectral data from the fingerprint region could be obtained if the tissue was mounted on a thinner glass slide, such as a coverslip (thickness is around 0.12–0.17 mm) [74]. Three types of cell lines (peripheral blood mononuclear cells, a leukaemia cell line and a lung cancer cell line) mounted on glass coverslips could be separated by PCA. In 2020, Rutter et al. studied the previous three types of cell lines and lymph node tissue mounted on four different types of glass coverslips [75]. They found all types of coverslip could provide spectra from 1800 cm^{-1} to 1550 cm^{-1}. But one type of coverslip has the better spectral quality and the spectral range could be down to 1350 cm^{-1}. PCA could achieve the separation between different cell lines based on the spectra in the lipid region and fingerprint region.

For the histopathology glass slide (thickness is 1mm), to obtain the spectra in the fingerprint region, Optical Photothermal Infrared Microspectroscopy (O-PTIR) could be used instead of the FTIR imaging system. O-PTIR could get high-quality spectra from the lipid region (3000-2700 cm^{-1}) and fingerprint region (1770-950 cm^{-1}). Kansiz et al. used O-PTIR and achieved the separation between lung cancer cells and non-malignant lung cells mounted on glass slides, and the classification accuracy ranged from 96% to 99% [76].

Infrared spectroscopy could be a diagnostic and prognostic tool and be applied in the clinical system. However, many challenges still need to be overcome[77]. For spectroscopic histopathology, although the measurement is carried by an FTIR microscope with FPA detector, it still needs several hours to get the spectra from a large tissue or TMA. Some studies have suggested only measuring some spectral biomarkers rather than the whole spectral range[47][78]. Data processing and analysis is a critical stage after collecting spectral data. Many appropriate data analysis strategies and typical algorithms are used to solve clinical and biological research questions. The data

analysis approach includes exploratory data analysis, classification of samples, quantitative analysis and explanatory analysis[77]. Hence, finding a suitable method is critical for the data analysis phase. Although many challenges in the clinical translation of vibrational spectroscopy, it is still a significant technique for developing disease diagnosis and prognosis.

2.3 Reference

[1] H. Sung *et al.*, 'Global Cancer Statistics 2020: GLOBOCAN Estimates of Incidence and Mortality Worldwide for 36 Cancers in 185 Countries', *CA. Cancer J. Clin.*, vol. 71, no. 3, pp. 209–249, 2021.

[2] L. A. Torre, F. Bray, R. L. Siegel, J. Ferlay, J. Lortet-tieulent, and A. Jemal, 'Global Cancer Statistics, 2012', *CA. cancer J. Clin.*, vol. 65, no. 2, pp. 87–108, 2015.

[3] R. L. Siegel, K. D. Miller, and A. Jemal, 'Cancer statistics, 2017', *CA. Cancer J. Clin.*, vol. 67, no. 1, pp. 7–30, 2017.

[4] F. Duffaud and P. Therasse, '[New guidelines to evaluate the response to treatment in solid tumors]', *Bull Cancer*, vol. 87, no. 12, pp. 881–886, 2000.

[5] R. A. Smith *et al.*, 'Cancer screening in the United States, 2018: A review of current American Cancer Society guidelines and current issues in cancer screening', *CA. Cancer J. Clin.*, vol. 68, no. 4, pp. 297–316, Jul. 2018.

[6] A. R. M. Al-shamasneh and U. H. B. Obaidellah, 'Artificial Intelligence Techniques for Cancer Detection and Classification: Review Study', *Eur. Sci. J.*, vol. 13, no. 3, pp. 342–370, 2017.

[7] M. Pilling and P. Gardner, 'Fundamental developments in infrared spectroscopic imaging for biomedical applications', *Chem. Soc. Rev.*, vol. 45, no. 7, pp. 1935–1957, 2016.

[8] J I .Epstein, Jr Allsbrook ' The 2005 International Society of Urological Pathology (ISUP) consensus conference on Gleason grading of prostatic carcinoma ', *The American journal of surgical pathology* , vol. 29, no. 9, pp. 1228–1242, 2005.

[9] L. Cséfalvayová, M. Strlič, and H. Karjalainen, 'Quantitative NIR chemical imaging in heritage science', *Anal. Chem.*, vol. 83, no. 13, pp. 5101–5106, 2011.

[10] S. Serranti, A. Gargiulo, and G. Bonifazi, 'Classification of polyolefins from building and construction waste using NIR hyperspectral imaging system',

Resour. Conserv. Recycl., vol. 61, pp. 52–58, 2012.

[11] Q. Wang *et al.*, 'Estimation of the late postmortem interval using FTIR spectroscopy and chemometrics in human skeletal remains', *Forensic Sci. Int.*, vol. 281, pp. 113–120, Dec. 2017.

[12] J. D. Fredericks, P. Bennett, A. Williams, and K. D. Rogers, 'FTIR spectroscopy: A new diagnostic tool to aid DNA analysis from heated bone', *Forensic Sci. Int. Genet.*, vol. 6, no. 3, pp. 375–380, May 2012.

[13] V. Fernández-Ibáñez, T. Fearn, A. Soldado, and B. de la Roza-Delgado, 'Development and validation of near infrared microscopy spectral libraries of ingredients in animal feed as a first step to adopting traceability and authenticity as guarantors of food safety', *Food Chem.*, vol. 121, no. 3, pp. 871–877, 2010.

[14] T. Puchert, D. Lochmann, J. C. Menezes, and G. Reich, 'A multivariate approach for the statistical evaluation of near-infrared chemical images using Symmetry Parameter Image Analysis (SPIA)', *Eur. J. Pharm. Biopharm.*, vol. 78, no. 1, pp. 117–124, 2011.

[15] S. Magalhães, B. J. Goodfellow, and A. Nunes, 'FTIR spectroscopy in biomedical research: how to get the most out of its potential', 2021.

[16] M. A. Mackanos and C. H. Contag, 'FTIR microspectroscopy for improved prostate cancer diagnosis' Trends in biotechnology, 2009, 27(12): 661-663..

[17] S. Kumar, A. Srinivasan, and F. Nikolajeff, 'Role of Infrared Spectroscopy and Imaging in Cancer Diagnosis', *Curr. Med. Chem.*, vol. 25, no. 9, pp. 1055–1072, 2017.

[18] J. Doherty, G. Cinque, and P. Gardner, 'Single-cell analysis using Fourier transform infrared microspectroscopy', *Appl. Spectrosc. Rev.*, vol. 52, no. 6, pp. 560–587, 2017.

[19] C. Kuepper, F. Großerueschkamp, A. Kallenbach-Thieltges, A. Mosig, A. Tannapfel, and K. Gerwert, 'Label-free classification of colon cancer grading using infrared spectral histopathology', *Faraday Discuss.*, vol. 187, pp. 105–118, 2016.

[20] A. A. Ahmadzai *et al.*, 'Determination using synchrotron radiation-based Fourier transform infrared microspectroscopy of putative stem cells in human adenocarcinoma of the intestine: corresponding benign tissue as a template', *Appl. Spectrosc.*, vol. 68, no. 8, pp. 812–822, 2014.

[21] Z. Movasaghi, S. Rehman, and I. U. Rehman, 'Fourier transform infrared (FTIR) spectroscopy of biological tissues', *Applied Spectroscopy Reviews*, vol. 43, no. 2. pp. 134–179, 2008.

[22] C. Hughes *et al.*, 'Assessment of paraffin removal from prostate FFPE sections using transmission mode FTIR-FPA imaging', *Anal. Methods*, vol. 6, no. 4, p. 1028, 2014.

[23] E. Gazi *et al.*, 'Applications of Fourier transform infrared microspectroscopy in studies of benign prostate and prostate cancer. A pilot study', *J. Pathol.*, vol. 201, no. 1, pp. 99–108, 2003.

[24] R. Bhargava, 'Towards a practical Fourier transform infrared chemical imaging protocol for cancer histopathology', *Anal. Bioanal. Chem.*, 2007.

[25] E. Gazi *et al.*, 'A Correlation of FTIR Spectra Derived from Prostate Cancer Biopsies with Gleason Grade and Tumour Stage', *Eur. Urol.*, vol. 50, no. 4, pp. 750–761, 2006.

[26] R. Baker, K. D. Rogers, N. Shepherd, and N. Stone, 'New relationships between breast microcalcifications and cancer', British journal of cancer, 2010, 103(7): 1034-1039. British journal of cancer, 2010, 103(7): 1034-1039..

[27] S. Kumar, C. Desmedt, D. Larsimont, C. Sotiriou, and E. Goormaghtigh, 'Change in the microenvironment of breast cancer studied by FTIR imaging', *Analyst*, vol. 138, no. 14, p. 4058, 2013.

[28] M. J. Pilling, A. Henderson, and P. Gardner, 'Quantum Cascade Laser Spectral Histopathology: Breast Cancer Diagnostics Using High Throughput Chemical Imaging', *Anal. Chem.*, vol. 89, no. 14, pp. 7348–7355, 2017.

[29] F. Großerueschkamp *et al.*, 'Marker-free automated histopathological annotation of lung tumour subtypes by FTIR imaging', *Analyst*, vol. 140, no. 7, pp. 2114–2120, 2015.

[30] X. Mu *et al.*, 'Statistical analysis of a lung cancer spectral histopathology (SHP) data set', *Analyst*, vol. 140, no. 7, pp. 2449–2464, 2015.

[31] J. Nallala *et al.*, 'Infrared spectral histopathology for cancer diagnosis: a novel approach for automated pattern recognition of colon adenocarcinoma.', *Analyst*, vol. 139, no. 16, pp. 4005–4015, 2014.

[32] A. Kallenbach-Thieltges, F. Groschkamp, A. Mosig, M. Diem, A. Tannapfel, and K. Gerwert, 'Immunohistochemistry, histopathology and infrared spectral histopathology of colon cancer tissue sections', *J. Biophotonics*, vol. 6, no. 1, pp. 88–100, 2013.

[33] V. Šablinskas *et al.*, 'Infrared spectroscopic imaging of renal tumor tissue', *J. Biomed. Opt.*, vol. 16, no. 9, p. 096006, 2011.

[34] F.Scholkmann, S.Kleiser, A J .Metz, et al., ' A review on continuous wave functional near-infrared spectroscopy and imaging instrumentation and methodology ', *J. Neuroimage. Opt*., vol. 85, pp.6-27, 2014.

[35] M. N. Simmons, R. K. Berglund, and J. S. Jones, 'A practical guide to prostate cancer diagnosis and management', *Cleve. Clin. J. Med.*, vol. 78, no. 5, pp. 321–331, 2011.

[36] P. M. Pierorazio, P. C. Walsh, A. W. Partin, and J. I. Epstein, 'Prognostic Gleason grade grouping: data based on the modified Gleason scoring system', *BJU Int.* |, vol. 111, pp. 753–760, 2013.

[37] D. F. Gleason, G. T. Mellinger, and L. J. Ardving, 'Prediction of prognosis for prostatic adenocarcinoma by combined histological grading and clinical staging', *J. Urol.*, vol. 111, no. 1, pp. 58–64, 1974.

[38] J. I. Epstein *et al.*, 'A Contemporary Prostate Cancer Grading System: A Validated Alternative to the Gleason Score', *Eur. Urol.*, vol. 69, no. 3, pp. 428–435, 2016.

[39] G. J. L. H. Van Leenders *et al.*, 'The 2019 International Society of Urological Pathology (ISUP) Consensus Conference on Grading of Prostatic Carcinoma', *Am. J. Surg. Pathol.*, vol. 44, no. 8, pp. E87–E99, 2020.

[40] J. I. Epstein, L. Egevad, M. B. Amin, B. Delahunt, J. R. Srigley, and P. A.

Humphrey, 'The 2014 international society of urological pathology (ISUP) consensus conference on gleason grading of prostatic carcinoma definition of grading patterns and proposal for a new grading system', *Am. J. Surg. Pathol.*, vol. 40, no. 2, pp. 244–252, 2016.

[41] K. A. Iczkowski, G. J. L. H. Van Leenders, and T. H. Van Der Kwast, 'The 2019 International Society of Urological Pathology (ISUP) Consensus Conference on Grading of Prostatic Carcinoma', *Am. J. Surg. Pathol.*, vol. 45, no. 7, pp. 1005–1007, 2021.

[42] N. Mottet *et al.*, 'EAU-EANM-ESTRO-ESUR-SIOG Guidelines on Prostate Cancer—2020 Update. Part 1: Screening, Diagnosis, and Local Treatment with Curative Intent', *Eur. Urol.*, vol. 79, no. 2, pp. 243–262, 2021.

[43] E. Gazi *et al.*, 'A Correlation of FTIR Spectra Derived from Prostate Cancer Biopsies with Gleason Grade and Tumour Stage', *Eur. Urol.*, vol. 50, no. 4, pp. 750–761, Oct. 2006.

[44] M. J. Baker, E. Gazi, M. D. Brown, J. H. Shanks, N. W. Clarke, and P. Gardner, 'Investigating FTIR based histopathology for the diagnosis of prostate cancer', *J. Biophotonics*, vol. 2, no. 1–2, pp. 104–113, 2009.

[45] J. T. Kwak, S. M. Hewitt, S. Sinha, and R. Bhargava, 'Multimodal microscopy for automated histologic analysis of prostate cancer', BMC cancer, 11(1): 1-16，2011.

[46] J. T. Kwak, S. M. Hewitt, A. A. Kajdacsy-balla, S. Sinha, and R. Bhargava, 'Automated prostate tissue referencing for cancer detection and diagnosis', *BMC Bioinformatics*, pp. 1–12, 2016.

[47] P. Bassan, A. Sachdeva, J. H. Shanks, M. D. Brown, N. W. Clarke, and P. Gardner, 'Automated high-throughput assessment of prostate biopsy tissue using infrared spectroscopic chemical imaging Automated high-throughput assessment of prostate biopsy tissue using infrared spectroscopic chemical imaging', Medical Imaging 2014: Digital Pathology. Vol. 9041. SPIE, 2014.

[48] D. C. Fernandez, R. Bhargava, S. M. Hewitt, and I. W. Levin, 'Infrared

spectroscopic imaging for histopathologic recognition', *Nat. Biotechnol.*, vol. 23, no. 4, pp. 469–474, 2005.

[49] C. Hughes, L. Gaunt, M. Brown, N. W. Clarke, and P. Gardner, 'Assessment of paraffin removal from prostate FFPE sections using transmission mode FTIR-FPA imaging ', Analytical Methods, 6(4): 1028-1035.2014.

[50] C. Pezzei *et al.*, 'Characterisation of normal and malignant prostate tissue by Fourier transform infrared microspectroscopy', *Mol. Biosyst.*, vol. 6, no. 11, pp. 2287–2295, 2010.

[51] M. Lasalvia, V. Capozzi, and G. Perna, 'Comparison of FTIR spectra of different breast cell lines to detect spectral biomarkers of pathology', *Infrared Phys. Technol.*, vol. 120, no. November 2021, p. 103976, 2022.

[52] M. Meurens, J. Wallon, J. Tong, H. Noël, and J. Haot, 'Breast cancer detection by Fourier transform infrared spectrometry', *Vib. Spectrosc.*, vol. 10, no. 2, pp. 341–346, 1996.

[53] Y. X. Ci, T. Y. Gao, J. Feng, and Z. Q. Guo, 'Fourier transform infrared spectroscopic characterisation of human breast tissue: implications for breast cancer diagnosis', *Appl. Spectrosc.*, vol. 53, no. 3, pp. 312–315, 1999.

[54] M. W. Kissin, G. Q. Della Rovere, D. Easton, and G. Westbury, 'Risk of lymphoedema following the treatment of breast cancer', *Br. J. Surg.*, vol. 73, no. 7, pp. 580–584, 1986.

[55] J. G. Elmore, K. Armstrong, C. D. Lehman, and S. W. Fletcher, 'Screening for breast cancer' Jama, vol. 293, no. 10, pp. 1245–1256, 2005.

[56] R. E. Mansel *et al.*, 'Randomised multicenter trial of sentinel node biopsy versus standard axillary treatment in operable breast cancer: The ALMANAC trial', *J. Natl. Cancer Inst.*, vol. 98, no. 9, pp. 599–609, 2006.

[57] R. Crane-Okada, R. A. Wascher, D. Elashoff, and A. E. Giuliano, 'Long-term morbidity of sentinel node biopsy versus complete axillary dissection for unilateral breast cancer', *Ann. Surg. Oncol.*, vol. 15, no. 7, pp. 1996–2005, 2008.

[58] B. Bird, K. Bedrossian, N. Laver, M. Miljković, M. J. Romeo, and M. Diem,

'Detection of breast micro-metastases in axillary lymph nodes by infrared micro-spectral imaging.', *Analyst*, vol. 134, no. 6, pp. 1067–76, 2009.

[59] I. U. Rehman, R. S. Khan, and S. Rehman, 'Role of artificial intelligence and vibrational spectroscopy in cancer diagnostics', *Expert Rev. Mol. Diagn.*, vol. 20, no. 8, pp. 749–755, 2020.

[60] M. Pilling and P. Gardner, 'Fundamental developments in infrared spectroscopic imaging for biomedical applications', *Chem. Soc. Rev.*, vol. 45, no. 7, pp. 1935–1957, 2016.

[61] A. Akalin *et al.*, 'Classification of malignant and benign tumors of the lung by infrared spectral histopathology (SHP).', *Lab. Invest.*, vol. 95, no. 4, pp. 406–21, 2015.

[62] N. Bergner, B. F. M. Romeike, R. Reichart, R. Kalff, C. Krafft, and J. Popp, 'Tumor margin identification and prediction of the primary tumor from brain metastases using FTIR imaging and support vector machines', *Analyst*, vol. 138, no. 14, p. 3983, 2013.

[63] I. Petersen and A. Warth, 'Lung cancer: developments, concepts, and specific aspects of the new WHO classification', *J. Cancer Res. Clin. Oncol.*, vol. 142, no. 5, pp. 895–904, 2016.

[64] P D. Lewis, K E. Lewis, R. Ghosal, et al., 'Evaluation of FTIR spectroscopy as a diagnostic tool for lung cancer using sputum', *BMC cancer*, vol.10, no. 1, pp. 1–10, 2010.

[65] O. Uckermann *et al.*, 'Label-free identification of the glioma stem-like cell fraction using Fourier-transform infrared spectroscopy', *Int. J. Radiat. Biol.*, vol. 90, no. 8, pp. 710–717, 2014.

[66] H. Ukkonen *et al.*, 'Changes in the microenvironment of invading melanoma and carcinoma cells identified by FTIR imaging', *Vib. Spectrosc.*, vol. 79, pp. 24–30, 2015.

[67] N. Wald and E. Goormaghtigh, 'Infrared imaging of primary melanomas reveals hints of regional and distant metastases', *Analyst*, vol. 140, no. 7, pp. 2144–2155, 2015.

[68] M. J. Pilling, A. Henderson, J. H. Shanks, M. D. Brown, N. W. Clarke, and P. Gardner, 'Infrared spectral histopathology using haematoxylin and eosin (H&E) stained glass slides: a major step forward towards clinical translation', *Analyst*, vol. 142, no. 8, pp. 1258–1268, 2017.

[69] R. a Shaw, H. H. Eysel, K. Z. Liu, and H. H. Mantsch, 'Infrared spectroscopic analysis of biomedical specimens using glass substrates.', *Anal. Biochem.*, vol. 259, no. 2, pp. 181–6, 1998.

[70] P. Bassan, J. Mellor, J. Shapiro, K. J. Williams, M. P. Lisanti, and P. Gardner, 'Transmission FT-IR chemical imaging on glass substrates: Applications in infrared spectral histopathology', *Anal. Chem.*, vol. 86, no. 3, pp. 1648–1653, 2014.

[71] J. K. Pijanka *et al.*, 'FTIR Microspectroscopy of Stained Cells and Tissues. Application in Cancer Diagnosis', *Spectroscopy*, vol. 24, no. 1–2, pp. 73–78, 2010.

[72] J. Tang, D. Kurfürstová, and P. Gardner, 'Breast cancer detection using infrared spectral pathology from H&E stained tissue on glass slides', *Clin. Spectrosc.*, vol. 3, no. March, p. 100008, 2021.

[73] J. Tang, A. Henderson, and P. Gardner, 'Exploring AdaBoost and Random Forests machine learning approaches for infrared pathology on unbalanced data sets', *Analyst*, vol. 146, no. 19, pp. 5880–5891, 2021.

[74] A. V. Rutter, J. Crees, H. Wright, D. G. Van Pittius, I. Yousef, and J. Sulé-Suso, 'Fourier transform infrared spectra of cells on glass coverslips. A further step in spectral pathology', *Analyst*, vol. 143, no. 23, pp. 5711–5717, 2018.

[75] A. V. Rutter *et al.*, 'Identification of a Glass Substrate to Study Cells Using Fourier Transform Infrared Spectroscopy: Are We Closer to Spectral Pathology?', *Appl. Spectrosc.*, vol. 74, no. 2, pp. 178–186, 2020.

[76] M. Kansiz, L. M. Dowling, I. Yousef, O. Guaitella, F. Borondics, and J. Sulé-Suso, 'Optical Photothermal Infrared Microspectroscopy Discriminates for the First Time Different Types of Lung Cells on Histopathology Glass Slides', *Anal. Chem.*, vol. 93, no. 32, pp. 11081–11088, 2021.

[77] M. J. Baker *et al.*, 'Clinical applications of infrared and Raman spectroscopy: State of play and future challenges', *Analyst*, vol. 143, no. 8, pp. 1735–1757, 2018.

[78] L. S. Leslie, A. Kadjacsy-Balla, and R. Bhargava, 'High-definition Fourier transform infrared spectroscopic imaging of breast tissue', *Med. Imaging 2015 Digit. Pathol.*, vol. 9420, no. March 2015, p. 94200I, 2015.

Chapter 3

Instrumentation & Methodology

3.1 The principle of vibrational spectroscopy

3.1.1 Molecular spectrum

Molecules consist of atoms joined by chemical bonds. They possess quantised energy and can be separated into electronic, vibrational and rotational energy levels. Electronic energy is caused by the motion of electrons associated with an atom. Vibrational energy is caused by the periodic displacement of atoms, and rotation energy is because of the rotation of the molecule. The relative energy of these levels is shown schematically for a diatomic molecule in figure 3.1. As can be seen, each electronic state contains a set of vibrational energy levels, and each vibrational level includes a set of rotational levels. Therefore, electronic energy is larger than vibration energy and significantly larger than rotation energy.

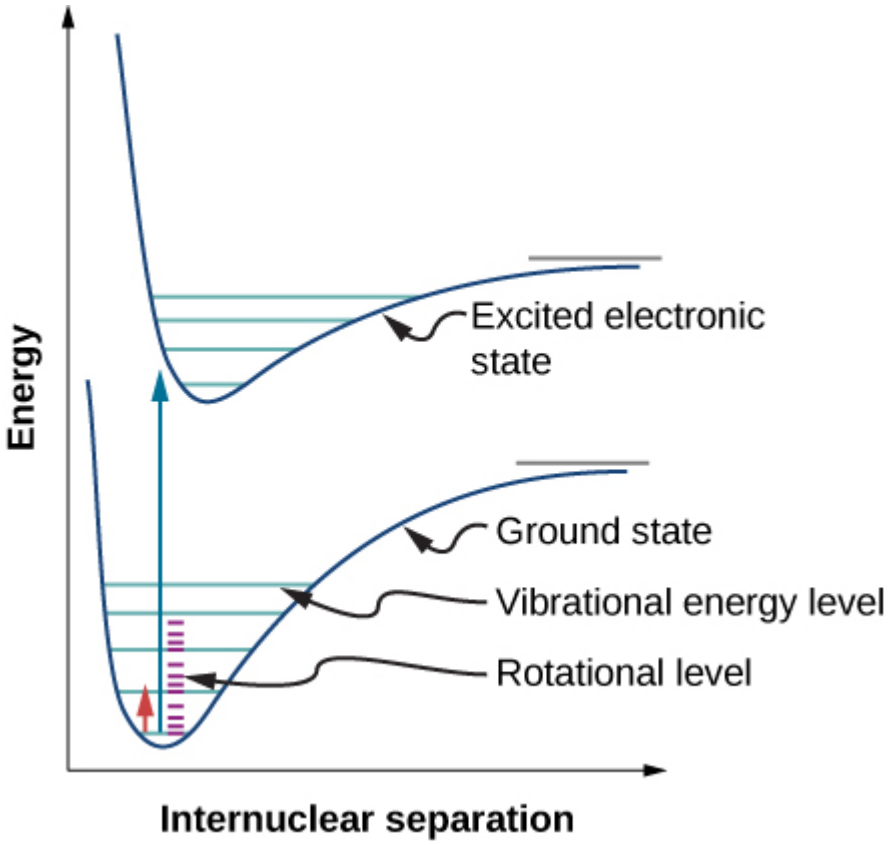

Figure3. 1 The arrangement of energy levels of a diatomic molecule.

3.1.2 Infrared spectrum

Electromagnetic radiation can be divided into radio waves, microwaves, infrared, visible light, ultraviolet, X-ray and Gamma-ray regions. The infrared light region is located between the visible light region and the microwave light region. Its wavelength range is 0.75~1000 μm, and the infrared spectrum is divided into the far-infrared region (400-10 cm^{-1}), mid-infrared region (4000-400 cm^{-1}) and near-infrared region (13300 -4000 cm^{-1}).

Figure 3.1 depicts that the rotation energy of the molecule is less than the vibration energy, which is less than electronic energy. The rotational energy level difference is relatively small, and rotational transitions can be excited using far-infrared radiation. The interval between vibrational energy levels is much larger than that of rotational energy levels, and transitions can be excited using mid-infrared radiation. The interval between electron energy levels is much larger than that between vibration energy levels, so transitions are excited using visible and ultraviolet-visible radiation.

When the natural vibrational frequency of a functional group is consistent with the frequency of the infrared light passing through the substance, the molecule can absorb the energy of the infrared light, which will lead to a transition from the ground state to the excited state [1]. As such, the intensity of the transmitted infrared light at that frequency is weakened. A plot of transmitted intensity vs wavelength (or more normally wavenumber) represents the infrared spectrum of the sample. In order for absorption to occur, however, there must be a change in the vibrational electric dipole moment of the molecules.

The most fundamental of organic and inorganic materials absorption bands will appear in the mid-infrared region for the infrared spectrum. The mid-infrared is also divided into functional group region (4000-1300 cm^{-1}) and fingerprint region (1800-400 cm^{-1}). Therefore, the peaks in the functional group region are used to identify the

functional groups of material. While in the fingerprint region, there are more complex peaks which are widely used in the study of material structure and composition. Therefore, it is beneficial for the fingerprint region to find the difference between similar compounds.

3.1.3 Molecular Vibration

In diatomic molecules, stretching vibrations occur along the connection between the two nuclei. However, in polyatomic molecules, all atoms in the molecule vibrate with different amplitudes around their equilibrium positions. Therefore, stretching vibrations are stretching between two, three or more atoms. In addition, there are various modes of deformation vibration.

In polyatomic molecules, the number of fundamental vibrations is related to the number of atoms and molecular configurations. The motion of all nuclei of molecules composed of N atoms requires N ordinary rectangular coordinate systems. The motion of each nucleus in rectangular coordinates has three degrees of freedom (X Y Z). Therefore, $3N$ degrees of freedom are required to describe the motion of N atoms. 3 degrees of freedom describe translation of the rigid molecule and 3 describe rotation of the rigid molecule. The remaining degrees of freedon must therefore describe vibrations. The number of correct vibrations of nonlinear molecules composed of N atoms is $3N$-6; for linear molecules, the number of normal vibrations is $3N$-5.

3.1.4 Vibration mode

Generally, different groups of molecules have different vibrational modes. Even if for the same group, there are several different vibration modes. In the mid-infrared spectral region, the vibrational modes can be divided into bending vibrations and stretching vibrations. The stretching vibration is the reciprocating motion of the atom along the key axis and the key length changes during the vibration. The stretching vibration is

divided into the symmetrical stretching vibration (υ_s) and asymmetrical stretching vibration (υ_{as}). The bending vibration is the atomic vibration along the perpendicular direction of the bond, which is divided into the in-plane bending vibration (δ) and out-plane bending vibration (γ). Figure 3.2 shows the vibrational modes of a CH_2 group.

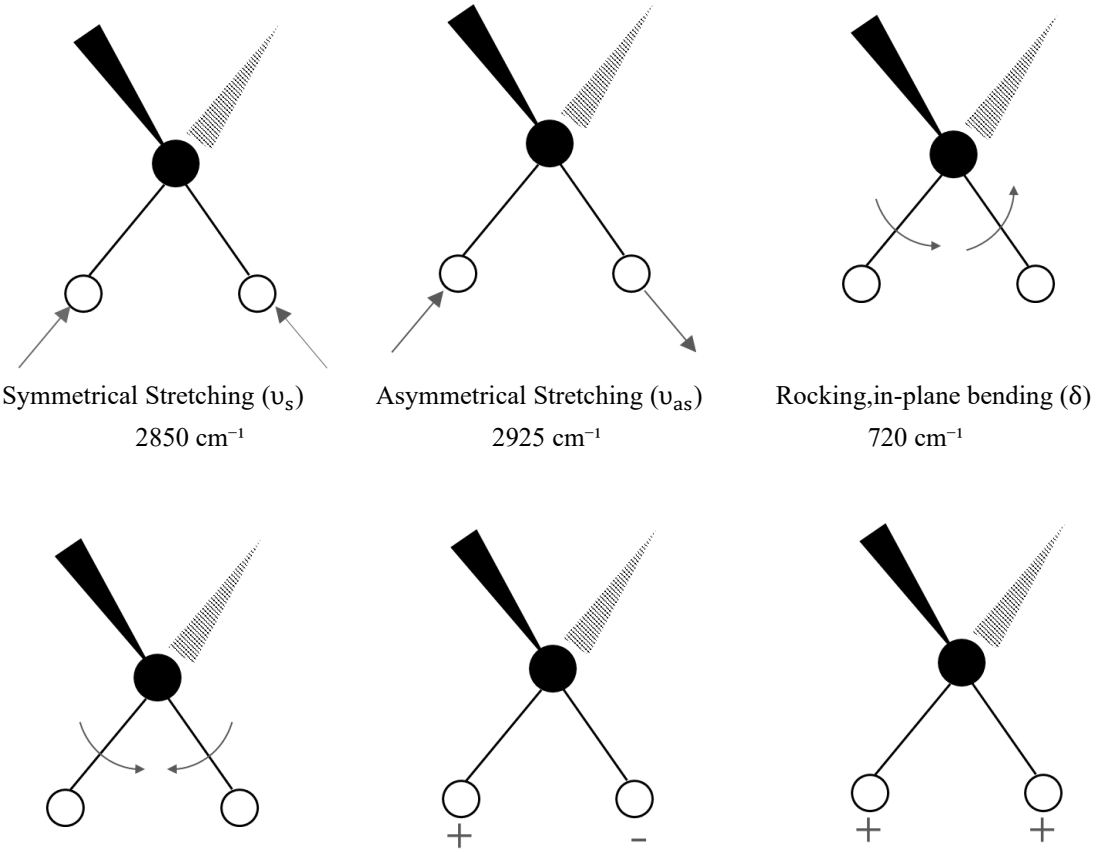

Figure3. 2 Vibrational mode for a CH_2 group

3.1.5 The Development of Infrared Spectrometer

In 1800, Herschel discovered infrared light and in 1905, Cobeltz published infrared spectra of 128 inorganic and organic compounds, demonstrating that the different functional groups have different infrared absorption. This work leads to the birth of infrared spectroscopy, and the appearance of this new analytical technology also leads to the development of infrared spectrometers.

In 1947, the prism dispersive infrared spectrometer appeared. However, the disadvantage is that the spectral resolution is low, and the spectra are slow to record. The spectrometer is more sensitively affected by the temperature and humidity of the environment.

During the 1960s, with the development of grating engraving and copying, the grating dispersive infrared spectrometer appeared. Compared with the prism dispersion infrared spectrometer, it has a high resolution, wide measuring range and was affected less by environmental conditions.

During the middle of the 1980s, the fourier transforms infrared (FTIR) spectrometer emerged with excellent spectral measurement characteristics, including a wide measuring range, high precision and resolution.

3.2. FTIR spectroscopy

3.2.1 The structure of FTIR

There are three central systems that make up the FTIR: the infrared optical system, the computer data processing system and the electronic circuit system. The most important part of the FTIR is the optical system, which is used to measure and collect data. It consists of an infrared light source, interferometer, sample chamber and detector. Computer data processing systems are used to process and store data and control the operation of the instrument.

3.2.2 The principle of FTIR

The interferometer is the core of the optical system. A high-resolution Michelson

interferometer is commonly used nowadays. The Michelson interferometer is composed of a light source, a fixed mirror, a movable mirror and a beam splitter. Figure 3.3 shows the schematic diagram of the interferometer. The beam splitter and two mirrors are normally at an angle of 45 degrees. At the beam splitter, half of the infrared light is transmitted, and the other half light is reflected. The separated transmitted beam and reflected beam are reflected by moving and fixed mirrors. Then two reflected signals return to the beamsplitter, where they recombine. Half of the recombined beam passes back to the source, but the other half is directed to pass through the sample and is detected by a detector. The changing position of the moving mirror creates an optical path difference between the two beams in the interferometer resulting in constructive and destructive interference of the combined beam[41]. The optical path difference between two reflected light beams is $\delta = 2$ (OM-OF), in which OM and OF are two beams of the optical path.

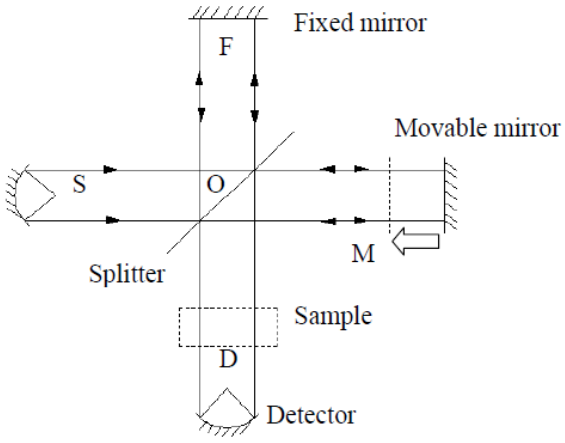

Figure3. 3 Schematic diagram of an interferometer

3.2.3 The Characteristics of FTIR

As an analytical technique, FTIR has many advantages and has been applied in a wide range of fields, including petroleum industry, polymer research, agriculture and food, biochemistry and biomedicine, environmental science[2][3]. The basic characteristics include [4]:

1) High scanning speed to reduce measurement time enabling spectra to be obtained in a few seconds.
2) High sensitivity enables small amounts of samples to be detected. In addition, because it can be scanned many times, the signal can be superimposed and the signal to noise ratio (SNR) is also improved.
3) The sample can be gas, liquid or solid.
4) High spectral resolution and high measurement accuracy.
5) Wide spectral range.
6) High precision and good reproducibility.

Besides the above features, FTIR also has a important advantage for biological applications [2]:
The measurement is non-destructive; it does not destroy the structure of the sample.
However, FTIR also has some limitations for biological application. Water is an essential component of the biological sample. And the strong absorption of water in the spectrum would disturb the detection of other functional groups.

3.3 Microscopic imaging

3.3.1 The introduction of microscopic imaging

With the continuous development of FTIR, infrared accessories are also constantly developing. At present, there are many kinds of infrared accessories, and the most important one is the infrared microscope.

The traditional infrared spectrum only gets the average composition and structure of the sample, but it cannot reflect the difference in the composition and structure of spatially heterogeneous samples. So it is mainly used for the analysis of homogeneous samples. However, when it is applied to the biological field, the complex functions of

organisms are primarily determined by the spatial structures of the biological macromolecules. For example, the functions of cells and tissues are determined by the spatial structures of protein, nucleic acid and lipids.

Infrared spectroscopic imaging successfully overcomes the above limitations. It combines the infrared spectrometer with the infrared microscope and carries on the infrared spectra measurement in a small area that is selected by the microscope[3]. Infrared spectroscopic imaging is the collection of spectral information from each point in the area of interest enabling the chemical composition to be obtained at each point.[2].

3.3.2 The development of microscopic imaging

There are three stages in the development of infrared imaging technology. The first stage is the development of the single point infrared microscope [5]. It can only provide a single point infrared spectrum of the micro region and cannot scan and image the whole sample area.

During the 1980s, single point mapping was developed. By automatic moving of the microscope stage, the sample's spectra can be measured point by point. All spectra can form a large grid, which can be combined together to create a single chemical image [6]. This instrument uses a single element detector and scans the sample point by point, which requires a long time to collect data.

The third revolution for infrared chemical imaging is the development of infrared detector technology. The linear array and the focal plane array (FPA) detector are now widely used [5]. This new method of infrared spectroscopic imaging consists of an FTIR, an infrared microscope and an array detector. The spectra of a large area of sample can be obtained simultaneously without moving the microscope stage. A large number of spectra can directly form chemical imaging. The new method can

significantly reduce the time of data collection.

There are two different types of array detectors. One is the linear array detector. A row of detector elements is distributed in a straight line, and the row of spectra can be measured simultaneously. An image is obtained by translating the sample under the array to form a two-dimensional image. The other type of detector is FPA. It has been widely used in the research field in recent years. The detector elements are distributed in a square array, such as 64×64 and 128×128. The FPA technology can significantly reduce the data collection time because a large number of spectra can be analysed at the same time [5]. For example, 128×128 FPA enable simultaneous acquisition of 16384 spectra.

3.3.3 Sampling mode for Infrared spectroscopy

In order to get the chemical imaging of the sample, there are several different modes of operation. And the most common modes are transmission, transflection and attenuated total reflection (ATR) [5]. And each mode has convenience and challenges for different kinds of samples. Therefore, it is very important for sample measurement to select a suitable sampling mode.

3.3.3.1 Transmission

The transmission mode is the primary method to measure samples, which can provide the best SNR and high spatial resolution [5]. It is suitable for the sample with good transmittance and thin thickness, such as thin biological specimens with less than 20 μm.

The transmission mode principle is that the infrared light passes the sample with the substrate, the sample absorbs some light, and the transmitted light is measured by the

detector. Substrates suitable for transmission mode are infrared transparent slides and commonly CaF_2 and BaF_2.

A significant limitation of the transmission mode is that since the infrared has to pass through the sample, and most biological samples are strong absorbers, the sample but be very thin. Ideally, the sample to be of a thickness that will give a good signal to noise ratio but not too thick such that absorption deviates from Beer-Lambert behaviour[7]. In addition, the substrate itself is a barrier for mass clinical application because of the high price and fragility of the CaF_2 and BaF_2 slides [8]. The fragility of the slide leads to them being unsuitable for handling in automated sample preparation equipment.

3.3.3.2 Transflection

In transflection mode, the infrared light passes through the sample and then is reflected by the reflective layer surface of the substrate. The reflected infrared light goes through the sample a second time and then is measured by an infrared detector [5].

The substrate and sample thickness are two critical factors for the transflection mode. The substrate should have an infrared reflecting surface, which is commonly a glass slide with IR-reflecting coating. The infrared reflective coating can be a highly reflecting metal layer such as silver or gold, but for biological samples a low-emissivity (Low-E) material is used, which is also transparent in the visible region allowing the sample to be viewed under a standard optical microscope. The commonly used coating is a tin oxide film with a buried silver layer [5][9]. Compared with transmission mode substrates, infrared reflecting substrates are cheaper and more robust. In addition, the spectra for the transflection mode has higher SNR because the infrared light passes twice through the sample. Therefore, the sample thickness for transflection mode can be ~1–4μm, whereas for transmission mode, it needs to be ~2–8μm [7].

In recent years, some doubt has been cast on the application of transflection mode for applications involving biomedical studies. This is due to the electric field standing wave (EFSW) effect [5][9][13]. Great care has to be taken with data analysis due to scattering effects (such as Mie scattering) and spectral standing wave artefacts with IR-reflective substrates when the thickness of samples is less than 2μm [7]

The EFSW effect could lead to spectral distortions which are wavelength dependant[10]–[12], [14]. There are many studies to find a method to reduce the effect of EFSW to reduce spectral distortion[15]. EFSW is affected by the range of incidence angles, the degree of coherence of the incident light and the sample thickness[16]. The influence of these distortions can be eliminated by the sufficient thickness of the sample (~5μm)[16].

Mie scattering in reflection mode is more intense than in transmission mode and would lead to the sloping of baselines [7]. There are two methods to reduce the effect, which are termed 'physics based' and 'model based', respectively. The 'physics based' method uses the optical image–formation from the first principles modelling to do the data correction. The 'model based' method uses a model to explain all sample effects. Spectra could be the correction by including extended multiplicative scattering correction (EMSC), resonant Mie scattering correction (RMieSC) and rubber band baseline correction [7] [13].

3.4 Data analysis method

MATLAB achieves all data processing in this project. The principal theory for data analysis is the machine learning algorithm, and this section describes the common learning machine algorithm methods which are used for the SHP.

3.4.1 Machine learning Algorithm

Machine learning refers to the computer science in which computers use the experience to "learn" and improve the system's performance. In short, machine learning refers to the acquisition of new experience and knowledge through computer learning the inherent regular information in the data.

Machine learning is divided into unsupervised and supervised classification algorithms. The major unsupervised classification algorithm includes principal component analysis (PCA) and hierarchical cluster analysis (HCA). In comparison, the main supervised classification algorithm involves linear discriminant analysis (LDA), Random Forest, support vector machines (SVM) and Artificial Neural Network (ANN) [17]. Typical machine learning training is mainly divided into the following processes:

1) The acquisition of data sets. In this thesis, the data are the information from all spectra by FTIR.

2) Data regularisation. The information in the collected data set is very complex, including a large number of redundant features. Therefore, data pre-processing is carried out.

3) Define the training set. After standardising the sample data, data sets are divided into a training set, validation set and test set. The training set is used to establish the model. The validation set tests the model structure and complexity and enhances the model's classification precision. The test set is used to test the performance of an algorithm and evaluate the accuracy of the model[18]. In cancer detection research, the pixels of the chemical image in training sets are identified by corresponding areas of histological classes using the conventional cancer diagnosis approach.

4) Selection of classification algorithms. According to previous SHP research[8][19], the major classification algorithm is random forest based on decision trees.

5) Classifier training. All of the samples are trained by a classification algorithm. In work related to cancer detection, the sample used for classifier training should contain the same number of spectra for different histological classes [3].

6) Performance evaluation of classifier. The ability of the classifier is evaluated by error and accuracy.

3.4.2 data pre-processing

In order to obtain optimum classification results, it is very important for collected spectra to carry out data pre-processing, which involves quality testing, noise reduction, vector normalisation and derivatisation [20].

Quality testing is used to remove the spectra obtained from areas that are without any tissue or have high levels of scattering, thus retaining the just useful diagnosis information region. Noise reduction based on PCA is applied to improve the SNR. Usually, the spectra are decomposed into principal components (PCs), and only the first 40 PCs are retained. Vector normalisation is used to eliminate the variation of the band intensity, which is caused by the different thicknesses of tissue [20].

3.4.3 PCA

A large number of variables and the inter-correlation between variables always lead to a practical problem that is complicated to solve. Therefore, the complexity of the problem can be simplified by substituting a few representative variables for the many previous variables. These new variables are independent of each other and represent the majority of the information of the original variables[21]. PCA is a statistical analysis method that replaces original variables with a few new independent variables, and the small number of new variables can reflect the maximum extent of the original data information. The new uncorrelated variables are called principal components (PC) [21].

In other words, PCA can reduce the dimensionality and overcome the fact that a single index cannot reflect the previous data information. Although a large number of

variables can reflect enough original information, it is easy to cause information redundancy. As a dimensionality reduction algorithm, PCA can significantly improve the learning speed of unsupervised classification algorithms.

In general, PCA is often used to pre-process data, eliminate noise, eliminate the correlation between variables, reduce the dimension of data, reduce the amount of calculation and improve the machine learning speed [20]. When PCA is applied to FTIR microscopic imaging data, the information contained in thousands of infrared spectra can be compressed into a small number of PCs. Generally, only the first few PCs are related to the chemical composition in the infrared microscopic image. The rest of the PCs are mainly attributable to noise.

The loading and score of the PCs can be obtained by PCA [22]. The characteristic peak position and peak shape in the loading diagram are similar to that in the original spectrum. Therefore, a loading diagram can be regarded as an abstract spectrum. The positive and negative in the loading diagram can indicate the change of the substance contained in the corresponding position. The score displays the proportion of spectral changes by each PC.

3.4.4 Random Forest

The random forest is essentially a set of decision trees. It is necessary to have a certain understanding of the decision tree.

3.4.4.1 Decision Tree

The decision tree is supervised classification learning and a kind of prediction model. It is called a decision tree because of its tree structure. The path from the root to the leaf represents classification rules. Each internal node represents a test in characteristic

attribute, each branch is the outcome of the test, and the end leaf node represents a prediction result, which is a class label [23]. The decision tree model can be used to analyse the data and also be used for prediction. There are some advantages for the decision trees:

1. Decision tree is easy to understand and implement and directly reflects the data's characteristics.
2. This classification algorithm is able to handle both data and regular attributes.
3. It is easy to evaluate the model by static test.

However, when the data is complex and noisy, the decision tree may over-divide the sample space in the classification process and conduct a too complex final decision tree, which leads to the over-fitting problem [23].

3.4.4.2 Random Forest

Random forest is an extension of the decision tree. "Forests" consists of many "trees". The final classification result is based on the proportion of trees voting [24]. In order to reduce error and improve reliability, every tree in the random forest relies on a set of random vectors, and each set of vectors is independently and uniformly distributed. Therefore, the decision trees in the forest should be randomly selected using completely different training data and different characteristics.

The construction of random forest has the following steps:

(1) Establishment of a sample training set

Training samples are selected in the original training set using the Bootstrap method [25], and each group of the training sample is used to train a decision tree. For example, in order to construct a random forest formed by K decision trees, K groups of training samples need to be selected.

(2) Training every decision tree

For a single decision tree corresponding to each group of training samples, if the total number of characteristics in the training samples is *M*, in which *S* characteristics are

randomly extracted ($S \leq M$), a single decision tree would be trained using *S* characteristics.

(3) Building a random forest

The samples of the test set are classified by several trained decision trees, and the final classification result is based on the proportion of decision trees voting.

Random forest is an integrated learning method based on Bagging [26]. The random forest has a better classification effect than a single decision tree, which makes this method widely used. Random forests have the following advantages [26]:

a) It can significantly reduce the possibility of overfitting;

b) It can be adapted to data with partially missing values.

c) It has good resistance to data noise.

d) The efficiency of the algorithm is high because it can train each tree in parallel.

3.4.4.3 Classifier performance evaluation

Classification accuracy is often used to evaluate the performance of a classifier, but for training a set with an unbalanced data number of each class, classification accuracy is unreliable to judge the classifier's performance. Therefore, some other evaluation indicators based on the confusion matrix are widely used to evaluate classifier performance[8]. The confusion matrix (Table 3.1) is used in supervised classification algorithms and indicates the accuracy of the prediction of every class.

Table3. 1 Confusion matrix

	Real Positive (P)	Real Negative (N)
Predict Positive	True positive (TP)	False positive (FP)
Predict Negative	False negative (FN)	True negative (TN)

According to the above indices in the confusion matrix, some evaluation indicators are applied:

1) $\text{Accuracy} = \frac{\text{TP+TN}}{\text{TP+FP+TN+FN}}$ (3-1)

2) ROC curves

The receiver operating characteristic (ROC) curve has been widely used in the fields of biology and medical imaging. In recent years, ROC curves have been applied to machine learning. The performance of the algorithms is evaluated and compared by the ROC curve. The true positive rate is taken as the y-axis and the false positive rate as the x-axis. By setting a series of different thresholds for a classifier, many different values of true positive rate and false positive rate can be obtained, which are used to produce the ROC curve [27].

$$\text{True positive rate} = \frac{\text{positive correctly classified}}{\text{total positive}} = \frac{\text{TP}}{\text{P}} \quad (3\text{-}2)$$

$$\text{False positive rate} = \frac{\text{negatives incorrectly classified}}{\text{total negatives}} = \frac{\text{FP}}{\text{N}} \quad (3\text{-}3)$$

$$\text{Sensitivity} = \frac{\text{TP}}{\text{P}} \quad (3\text{-}4)$$

$$\text{Specificity}\frac{\text{TN}}{\text{FP+TN}} = 1 - \frac{\text{FP}}{\text{N}} \quad (3\text{-}5)$$

3) AUC

When comparing different classifiers, ROC curves for each classifier need to be drawn. The area under the curve (AUC) is the area under the ROC curve, which can quantitatively compare different classifiers. The larger the AUC value, the better the classification performance [27].

3.4.5 Matlab

Because thousands of spectra are in one infrared image, and many images are required

to achieve cancer diagnosis using SHP. A large amount of data needs to be processed using suitable algorithms and software. Matlab is one of the most widely used scientific computing software and has been used for the analysis in this thesis.

Compared with other computer languages, it has a simple grammar structure, high speed and efficiency of mathematical computation and a friendly and brief human-machine interface. In the aspect of image processing, Matlab has abundant functions and a toolbox, which can efficiently complete the geometric and module operation of images and can carry out the free transformation of images [28].

3.5 Experimental design

The key objective of the project is to study the influence of glass type on cancer detection by SHP. Three main studies make up the whole project. The first study is to compare the spectral difference on the different blank glass slides. The second study is to study the impact of different glass slides on tissue classification. And the last study is to research the influence of different glass slides on cancer detection. The results of these three studies are displayed in chapter 4, chapter 6 and chapter 7, respectively. All experimental design details of these three studies are shown in the following sections.

3.5.1 Study 1:Spectral comparison on different blank glass slides

Glass slides have strong absorption in the infrared region, and the exact nature of this absorption could affect the spectrum of tissue samples. There are many kinds of glass sides used in clinical practices. It is possible that the different kinds of glass slides have different absorption spectra. Therefore, it is essential to study whether the different types of glass slides could affect the infrared spectra and then affect the results of cancer detection.

This study investigates the effect of the different kinds of glass slides on infrared spectra. 12 different types of glass slides are used in the experiment. And the spectra of the different types of blank glass slides will be compared.

3.5.1.1 Sample preparation

There are 12 different kinds of glass slides in the whole project. The details of these 12 glass slides are shown in table 3.2, and in order to easily comparison and description, each glass slide is labelled with a letter, such as A, B, C…, L.

The slides with a charged surface are most suitable for histopathology because the charged surface enables the tissue to adhere to slides. While the non-charged glass slides need to be coated or charged before the clinical application. Therefore, according to the charge of the interface, the glass slide can be divided into charged and non-charged glass slides. The charged glass slides include D, E, F, G, J, K, L, and the non-charged glass slides include A, B, C, H, I.

Table3. 2 The information of 12 glass slide

Label	Brand	Glass quality	Edge	Dimensions	Thickness
A	Fisherbrand	Washed and polished plain glass	ground edges 90°	26 x 76 mm	1~1.2mm
B	Academy	Pre-washed clear glass	ground edges 45°	26 x 76 mm	1~1.2mm
C	VWR International	Clear white glass	Cut edges	26 x 76 mm	1mm
D	O.Kindler SuperFrost	Extra white soda lime silicate glass with very low iron content	ground edges 45°	26 x 76 mm	1mm
E	Citoglas	Extra white glass Single frosted	ground edges 45°	25 x 75 mm	1~1.2mm
F	Citoglas	Float glass Single frosted	ground edges 45°	25 x 75 mm	1~1.2mm
G	Citoglas	Standard glass Single frosted	ground edges 45°	25 x 75 mm	1~1.2mm
H	Sail brand	Clear glass frosted	ground edges	25 x 76 mm	1~1.2mm
I	Sail brand	Clear glass	ground edges	25 x 76 mm	1~1.2mm
J	Marienfeld HistoBond	Made of soda-lime glass of 3rd hydrolytic class	ground edges	26 x 76 mm	1±0.05mm
K	Marienfeld HistoBond +	Frosted soda-lime glass of 3rd hydrolytic class Adhesive surface	ground edges	26 x 76 mm	1±0.05mm
L	Marienfeld HistoBond +s	Frosted soda-lime glass of 3rd hydrolytic class Adhesive surface (plus higher intensity of positive charge)	ground edges	26 x 76 mm	1±0.05mm

3.5.1.2 Instrument system

Infrared chemical images were collected by a Varian 620 FTIR imaging microscope coupled to a 128 × 128 FPA mercury cadmium telluride (MCT) detector with Cary 670 bench. The detector was required to be cooled using liquid nitrogen every 3 hours. Chemical imaging was collected in transmission mode. The infrared microscope used ×15 Cassegrain optics, and the pixel size was 5.5μm with a resultant field of view of 704 × 704 μm. The spectral range was from 900 to 3800 $cm^{-1}$and the resolution was 5 cm^{-1}. Because the 5 cm^{-1} resolution for tissue work could obtain good-quality spectra fastly.

The chemical images of glass slides were obtained at the same temperature and humidity to eliminate environmental interference factors. Especially the humidity of

the air was an important factor because of the strong infrared absorption of water vapour. Therefore, the dry air is continually purged into a sealed purge box to control the environmental humidity to reduce to zero during the measurement. Figure 3.4 shows the instrument in Gardner lab.

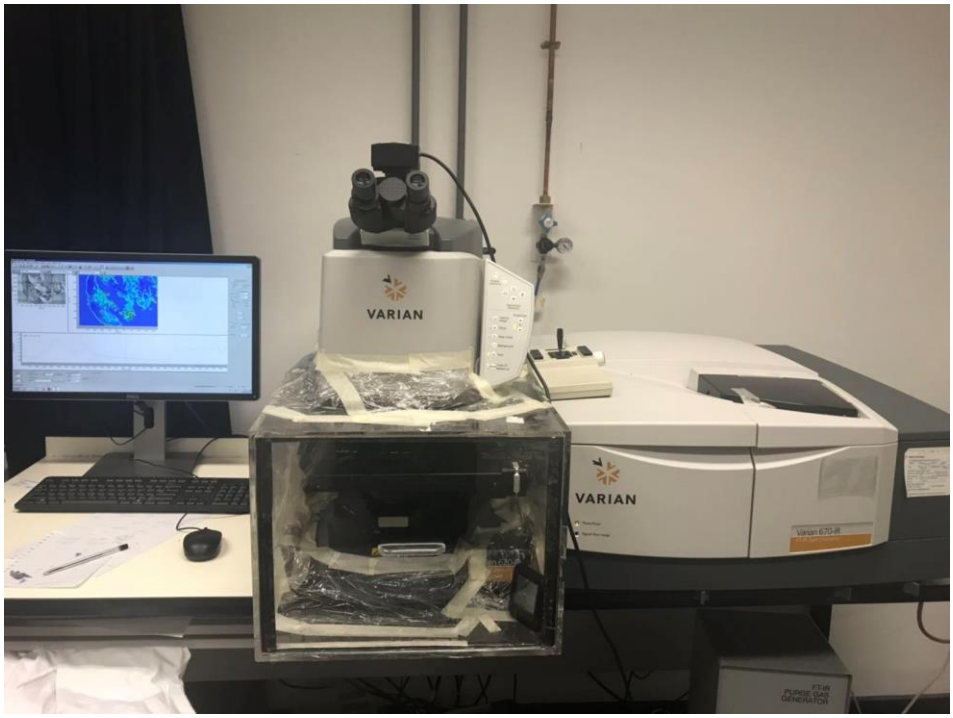

Figure3. 4 The instrument system for measurement in Gardner lab

3.5.1.3 Setting of measurement

12 glass slides are selected as samples, and the air is chosen as the background to obtain the images of blank glass slides. Co-addition scans of infrared spectra for the background and sample are128 and 16, respectively. Every glass slide is randomly selected in three different positions and collected three images at these places. Every image contains 16384 spectra. Therefore, every glass slide has 49152 spectra and takes approximately 15 min to collect.

3.5.1.4 Data processing

All data are pre-processed using Matlab 2017a and CHIToolbox. Infrared images from each glass slide are stitched together by Matlab to form a single data cube (3 ×16384 × 1506). Every type of glass slide consists of 49152 individual spectra with 1506 wavenumber data points.

Data pre-processing is a crucial step, and it usually includes quality testing, noise reduction and vector normalisation. All of these steps are used for tissue samples. However, there is no tissue sample on the glass slides, and all spectra of chemical images are from the blank glass. Therefore, the quality test of spectra is unnecessary for this study. In addition, based on the information of the 12 glass slides, the thickness of each glass slide may be different. Thus, vector normalisation is required and also achieved by CHIToolbox. To compare the spectra of 12 glass slides, the mean spectra of every glass slide are very important.

PCA is a vital data process to get a valid figure to indicate the influence of glass types on the infrared spectra. There are too many spectra of every glass slide (49152 spectra). Every glass slide randomly selected 200 spectra to do the PCA to get a better result for presentation. The loading and score are plotted, and the relationship between the different types of glass can be analysed.

All glass slides could be divided into charged and non-charged based on the charge of the surface. PCA between the charged and non-charged glass slides is done to find the effect of charge on infrared spectra. Every type of glass slide is randomly selected for 200 spectra. And then, all of the selected spectra are divided into charged and non-charged groups.

3.5.2 Study 2:The tissue classification on different glass slides

3.5.2.1 Sample preparation

The 12 glass slides used in this study are consistent with the first study (section 3.5.1), and the information of these glass slides is shown in table 3.2. The purpose of this study is to determine whether glass types could affect tissue classification. The prostate tissue used in this study is from a patient with benign prostatic hyperplasia (BPH). Figure 3.5 shows that a series of adjacent tissue sections are mounted on the 12 glass slides and stained with Haematoxylin and Eosin (H&E). To reduce the difference of every tissue section on 12 glass slides, the thickness of every tissue section is only 4μm. In order to fix and protect the tissue sections, all of them are fixed by mounting media and coverslips.

Figure3. 5 A series of prostate tissue sections from the same BPH patient are mounted on 12 different types of glass slides.

3.5.2.2 Instrumentation & experiment procedure

The composition of the whole instrument system and the primary instrumental setting have been shown in section 3.5.1.2. The specific procedures for this study are shown in this section.

Two regions (region 1 & region 2) are selected for 12 tissue slides to obtain enough spectra, which is shown in figure 3.6. For the 12 glass slides, the two regions should be located on the tissue section at the same place. Tissue sections in region 1 are imaged as a 2 × 2 mosaic and in region 2 are imaged as a 4 × 2 mosaic. All of the spectra are collected in transmission mode, and the spectral range is from 900 to 3800 cm^{-1}. The resolution of infrared spectra is $5 cm^{-1}$ and co-addition scans for background and sample are 96 and 96, respectively. In general, the collection time for region 1 and region 2 are 20 min and 40 min, respectively.

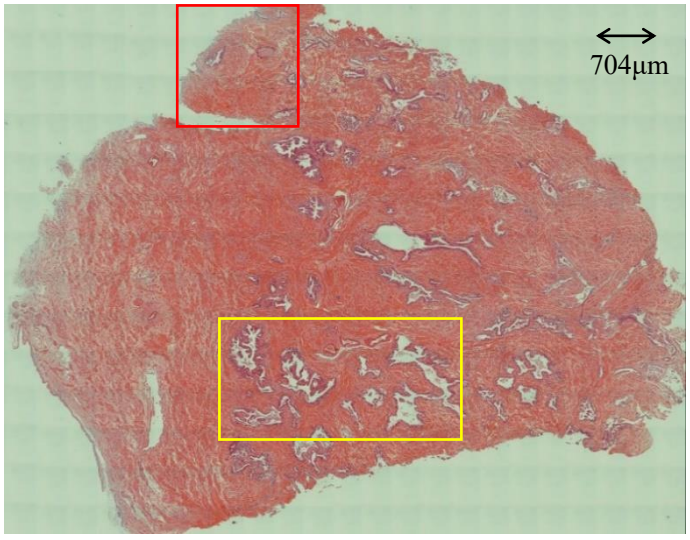

Figure3. 6 Brightfield image of the whole tissue on glass A. The area used for measurement is marked in squares, and region 1 in the red square and region 2 in the yellow square.

3.5.2.3 Two experimental methods

There are two different experimental methods, and finding the best method to achieve automated histological classification is significant. The comparison between the two

experiments is shown in table 3.3. The background in experiment 1 is measured from a clean area of the tissue glass slide, while the background in experiment 2 is the same type of blank glass slide. According to table 3.3, the final spectral information of both experiment 1 and 2 have tissue information and are affected by glue and coverslip. Therefore, to obtain the pure spectra of tissue and eliminate the influence of glue & coverslip, glue removal is necessary.

Table3. 3 Comparison between two methods of measurement.

	Background Scan	**Sample scan**	**Spectra information**
Experiment 1	Glass + coverslip + glue	Tissue + coverslip + glass + less glue	Tissue ± some glue
Experiment 2	Glass	Tissue + coverslip + glass + less glue	Tissue + coverslip + less glue

3.5.2.4 Annotation & registration

Because of the large proportion of epithelium and stroma in all histological classes of prostate tissue, they are annotated for further histological tissue classification. The annotations are done on the H&E brightfield images to keep the identical annotated spectra on the chemical images of the two experiments. The different types of tissue are annotated with different colours. Green is used to annotate epithelium, and red is used to annotate stroma. In addition, the blank and broken tissue areas are annotated in blue to eliminate the spectra with bad quality. All of the annotation work is done using GNU Image Manipulation Program (GIMP). A Nikon microscope measures the brightfield visible images with ×10 optics, and the pixel size of the brightfield image is 0.85μm.

Because the annotations are done on H&E stained images, they still need to correspond with the chemical images. The code named "registerto" in Chitoolbox could achieve it by selecting some typical points.

3.5.2.5 Data pre-processing

All spectral data are processed by Matlab, and there are many valid codes to process the spectra data in ChiToolbox. Infrared spectra are measured at 1506 points in the range of 900 - 3800cm^{-1}. Infrared tiles for region 1 included 2 × 2 mosaics. A data cube consists of 65536 individual spectra with 1506 data points each, so a data cube contains 256 × 256 ×1506 data. As for region 2, infrared tiles are made of 4 × 2 mosaics. The data cube (512 × 256 ×1506) consists of 131072 spectra with 1506 data points. To sum up, 12 adjacent tissue sections are mounted on 12 different types of glass, and 196608 spectra per tissue slide are measured.

Data pre-processing is essential to get high-quality spectra for analysis, including spectral quality testing, region selection, noise reduction and vector normalisation [20].

Because the spectra of broken tissue would have high levels of scattering, quality testing is used to remove the spectra of the area without tissue and the spectra of broken tissue. Quality testing in this study is based on the intensity of amide A (3298cm^{-1}). The blank area and damaged tissue area are annotated in blue. The highest intensity of these spectra at amide A is selected as a threshold. The threshold is the same for all tissue slides to ensure the unity of the 12 tissue slides in the subsequent comparison.

Amide A peak (3298 cm^{-1}) and three lipid peaks (2958 cm^{-1}, 2935 cm^{-1}, 2873 cm^{-1}) are all the peaks related to the tissue in the glass transparent infrared range. However, the mounting media (glue) has a significant impact on the lipid region. Therefore, amide A is the only reliable peak related to the tissue, and the spectral region is selected in 3125-3700 cm^{-1}.

Noise reduction based on PCA is applied to improve the spectral signal to noise (SNR). The largest variation in spectral data is generally contributed by chemical information rather than noise. Usually, the spectral data are decomposed into principal components

(PCs), and only the first 40 PCs are retained. 20 PCs are used for denoising in the project. Due to the heterogeneity of tissue and cutting error, the thickness of tissue is not uniform, which would lead to the variation of the band intensity. Vector normalisation is used to eliminate it.

3.5.2.6 Data processing

PCA and random forest are two crucial data process methods. PCA uses a few new independent variables to replace the original variables, and the small number of new variables can reflect the maximum extent of the original spectral data. This study's PCA results show the spectral difference between stroma and epithelium. 200 spectra of stroma and epithelium on 12 glass slides are randomly selected, and the PCA is based on these random spectra.

The random forest is used to study the effect of glass types on tissue classification. A classifier is constructed using the random forest classification algorithm to differentiate between stroma and epithelium. Classifier performance evaluation usually depends on accuracy. In order to look at whether the glass type would affect tissue classification, the classifier model could be built by the spectra from one glass slide, and the model could be tested by the tissue spectra from the other glass slides.

3.5.3 Study 3:The cancer detection on different glass slides

3.5.3.1 Sample preparation

There are 12 different brands of glass slides in the previous two studys, but only glass D, E, F, J, K, and L are widely used for tissue work and potentially for clinical application. Therefore, 6 different brands of glass slides are used in this study, and the information of the 6 glass slides is shown in table 3.4.

Table3. 4 The information of 6 glass slides for cancer detection

Label	Brand	Glass quality	Edge	Dimensions	Thickness
D	O.Kindler SuperFrost	Extra white soda lime silicate glass with very low iron content	ground edges 45 °	26 x 76 mm	1mm
E	Citoglas	Extra white glass Single frosted	ground edges 45 °	25 x 75 mm	1~1.2mm
F	Citoglas	Float glass Single frosted	ground edges 45 °	25 x 75 mm	1~1.2mm
J	Marienfeld HistoBond	Made of a soda-lime glass of 3rd hydrolytic class	ground edges	26 x 76 mm	1±0.05mm
K	Marienfeld HistoBond+	A frosted soda-lime glass of 3rd hydrolytic class Adhesive surface	ground edges	26 x 76 mm	1±0.05mm
L	Marienfeld HistoBond+s	A frosted soda-lime glass of 3rd hydrolytic class Adhesive surface (plus the higher intensity of positive charge)	ground edges	26 x 76 mm	1±0.05mm

A series of adjacent tissue slices mounted on the 6 glass slides are from 4 patients. Figure 3.7(a) shows all of the tissue samples mounted on the glass slides. Two patients have benign prostate hyperplasia (BPH), and the other two patients have prostate cancer (CaP). To easily describe, P1(BPH), P2(BPH) stand for the two BPH patients, and P3(CaP), P4(CaP) stand for the two CaP patients, respectively. The details of the 4 tissue blocks are shown in table 3.5. Four tissue slices with paraffin from 4 patients are also mounted on CaF2 slides (figure 3.7(b)) as a control experiment.

(a) (b)

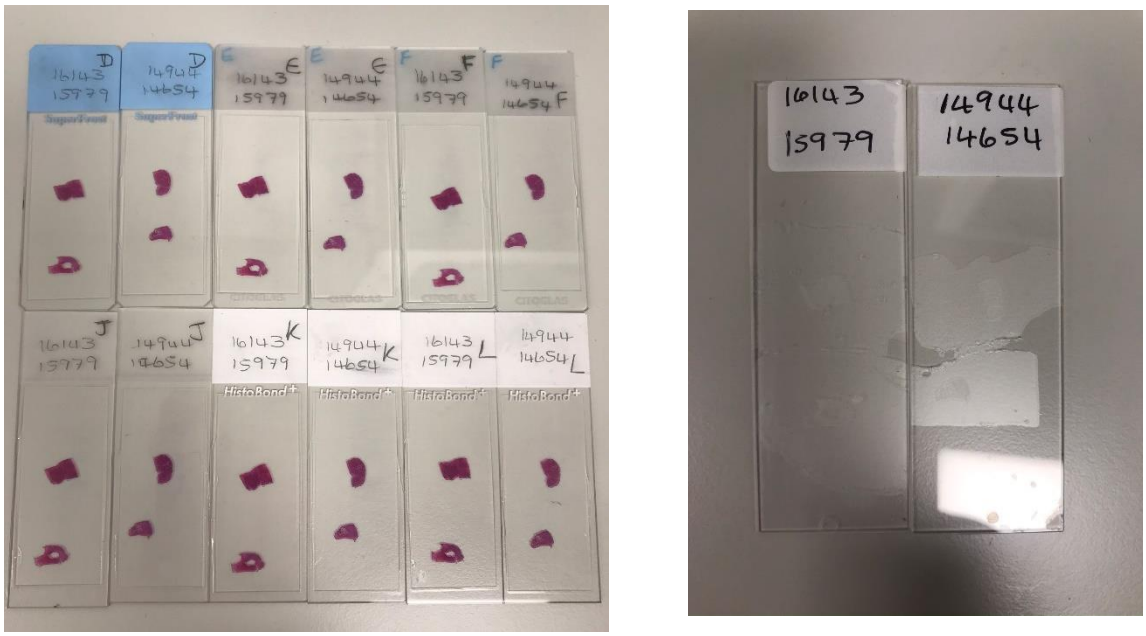

Figure3. 7 (a) A series of prostate tissue sections from the four patients mounted on 6 different types of glass slides. (b) The prostate tissue sections from the four patients mounted on CaF2 slides

Table3. 5 The information of four patients

Label	Sample ID	Disease	Thickness (μm)
P1(BPH)	14654	BPH	8
P2(BPH)	14944	BPH	8
P3(CaP)	16143	CaP	8
P4(CaP)	15979	CaP	8

3.5.3.2 Instrumentation & experiment procedure

In this study, all of the spectra are collected on the Agilent FTIR microscope in transmission mode (see section 3.5.1.2). The measurement set is also the same with study 2. The spectral range was from 900 to 3800 cm^{-1}. The resolution of infrared spectra was 5 cm^{-1} and co-addiction scans for background and sample were 96 and 96, respectively.

The study has compared two experimental methods, and the main difference between the two methods is the background selection. The comparison of the two experimental methods is shown in Table 3.3

Because scanning the whole tissue section is a very time-consuming process (around 8 hours), just two regions of every tissue section were for FTIR scanning. This still enabled enough spectra for further data processing to be collected and could save measurement time. Figure 3.8 shows the two regions of each tissue section on glass D. According to figure 3.8, regions 1 & 2 of P1(BPH) are 5 × 5 and 3 × 5 mosaics, respectively. Region 1 & 2 of P2(BPH) are 4 × 4 and 5 × 5 mosaics, respectively. Region 1 & 2 of P3(CaP) are 5 × 5 and 5 × 5 mosaics, respectively. Region 1 & 2 of P4(CaP) are 6 × 3 and 6 × 4 mosaics, respectively.

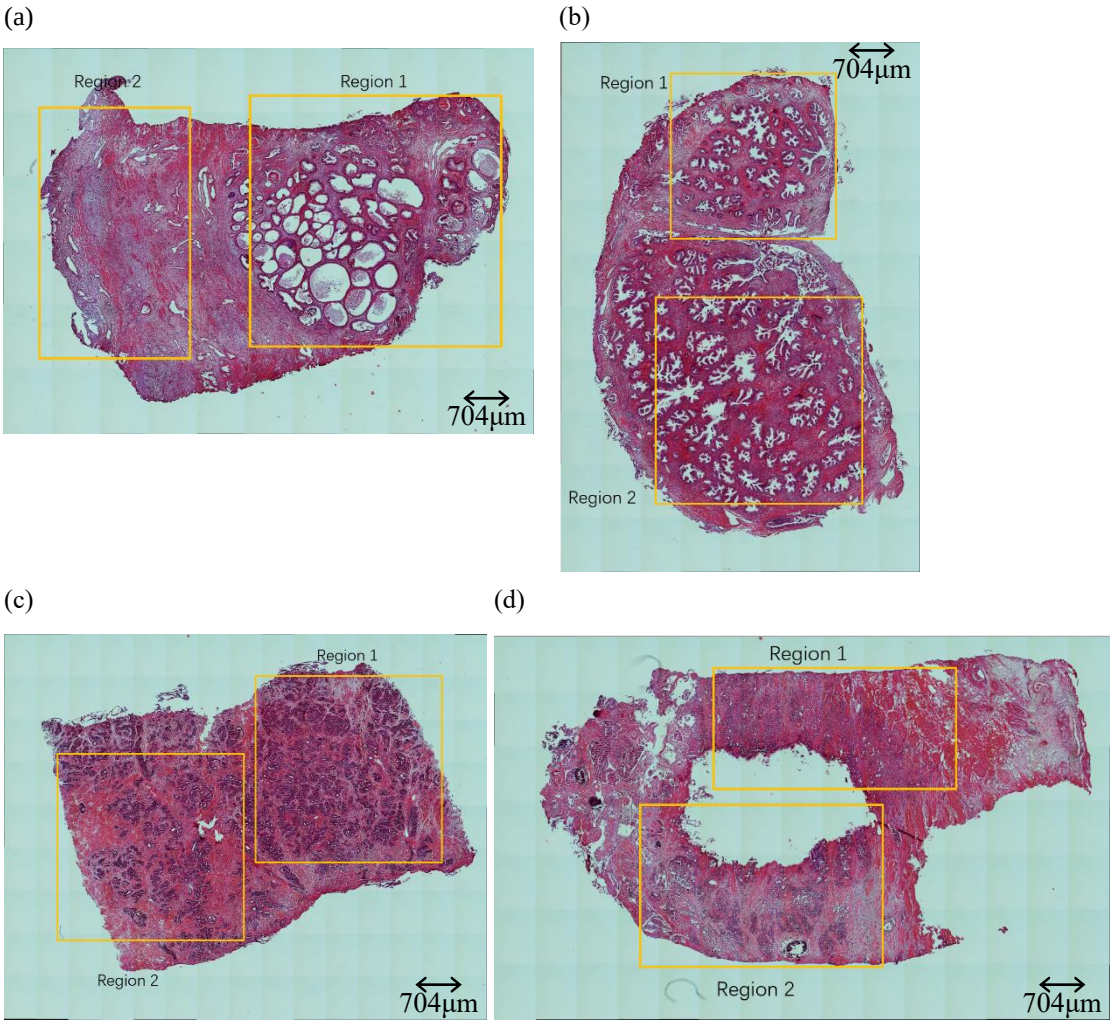

Figure3. 8 (a) Two regions of P1(BPH) on glass D for scanning. (b) Two regions of P2(BPH) on glass D for scanning. (c) Two regions of P3(CaP) on glass D for scanning. (d) Two regions of P4(CaP) on glass

D for scanning.

3.5.3.3 Annotation & registration

There are 4 tissue blocks from different patients, and the tissue slices are mounted on 6 different glass slides. A Nikon microscope measured the brightfield visible images with ×10 optics. Therefore, there are 24 H&E stained images for annotation.

The epithelium and stroma account for a large proportion of the prostate tissue. Therefore, only epithelium and stroma are used for histological tissue classification in study 2. The epithelium and stroma are still used for cancer detection to keep the consistency of the study. In addition, it is significant to look at which histological classes of prostate tissue are more suitable for cancer detection.

The GIMP image editor is used for annotation, and all the annotation work is done on the H&E stained brightfield visible image. The different types of tissue are annotated in different colours. The detail of the annotation of study 3 is the same with study 2 (see section 3.5.2.4).

3.5.3.4 data pre-processing

All of the spectral data are processed by Matlab, Chitoolbox. In the range of 900 - 3800 cm^{-1}, infrared spectra contain 1506 points. According to figure 3.8, P1(BPH), P2(BPH), P3(CaP) and P4(CaP) totally have 40 tiles, 41tiles, 50 tiles and 42 tiles, respectively. Every tile contains 128 × 128 spectra.

The data pre-processing in this study includes quality test, region selection, noise reduction, and vector normalisation. The process on the glass slide is similar to study 2 (see section 3.5.2.5). While the process on the CaF_2 is slightly different. The quality test

for tissue on CaF_2 is based on the intensity of amide I (1654 cm^{-1}). And the spectral region is 1000-3700 cm^{-1}.

3.5.3.5 Data processing

Glue removal is the main process after obtaining the high-quality spectra of epithelium and stroma. According to table 3.2, the glue influences the spectra for both experiments 1 and 2. The comparison of the results of cancer detection before and after removing glue is one of the aims of this study.

Similar to study 2, PCA and random forest are also critical processes for cancer detection. 200 spectra are randomly selected for the PCA, and the results show the spectral difference between cancer and non-cancer tissue on the same glass slides.

Random forest could be used to classify spectra of cancer and non-cancer. 80% of cancerous and non-cancerous spectral data are used to train the classifier, and the rest 20% of spectral data are used to test the classifier. The classifier can be evaluated by the accuracy of cancer detection. In order to find the influence of glass types on cancer detection, the classifier model could be built based on the spectra from one glass slide, and the model could be tested by the tissue spectra from the other glass slides.

3.6 Reference

[1] E. B. Wilson, J. C. Decius, P. C. Cross, and B. R. Sundheim, 'Molecular Vibrations: The Theory of Infrared and Raman Vibrational Spectra', *J. Electrochem. Soc.*, vol. 102, no. 9, p. 235C, 1955.

[2] J. Dubois and R. A. Shaw, 'Peer Reviewed: IR Spectroscopy in Clinical and Diagnostic Applications', *Anal. Chem.*, vol. 76, no. 19, pp. 360 A-367 A, 2004.

[3] P. Chaurand, J. L. Norris, D. S. Cornett, J. A. Mobley, and R. M. Caprioli, 'New developments in profiling and imaging of proteins from tissue sections by MALDI mass spectrometry', *Journal of Proteome Research*, vol. 5, no. 11. pp. 2889–2900, 2006.

[4] P. R. Griffiths and J. A. De Haseth, *Fourier Transform Infrared Spectrometry*. 2007.

[5] M. Pilling and P. Gardner, 'Fundamental developments in infrared spectroscopic imaging for biomedical applications', *Chem. Soc. Rev.*, vol. 45, no. 7, pp. 1935–1957, 2016.

[6] J. M. Schubert, A. I. Mazur, B. Bird, M. Miljković, and M. Diem, 'Single point vs. mapping approach for spectral cytopathology (SCP)', *J. Biophotonics*, vol. 3, no. 8–9, pp. 588–596, 2010.

[7] M. J. Baker *et al.*, 'Using Fourier transform IR spectroscopy to analyse biological materials', *Nat. Protoc.*, vol. 9, no. 8, pp. 1771–1791, 2014.

[8] M. J. Pilling, A. Henderson, J. H. Shanks, M. D. Brown, N. W. Clarke, and P. Gardner, 'Infrared spectral histopathology using haematoxylin and eosin (H&E) stained glass slides: a major step forward towards clinical translation', *Analyst*, vol. 142, no. 8, pp. 1258–1268, 2017.

[9] E. Staniszewska-Slezak, A. Rygula, K. Malek, and M. Baranska, 'Transmission versus transflection mode in FTIR analysis of blood plasma: Is the electric field standing wave effect the only reason for observed spectral distortions?', *Analyst*, vol. 140, no. 7, pp. 2412–2421, 2015.

[10] J. Filik, M. D. Frogley, J. K. Pijanka, K. Wehbe, and G. Cinque, 'Electric field

standing wave artefacts in FTIR micro-spectroscopy of biological materials'.

[11] J. G. Elmore, K. Armstrong, C. D. Lehman, and S. W. Fletcher, 'CLINICIAN ' S CORNER Screening for Breast Cancer', vol. 293, no. 10, pp. 1245–1256, 2005.

[12] E. Staniszewska-Slezak, A. Rygula, K. Malek, and M. Baranska, 'Transmission versus transflection mode in FTIR analysis of blood plasma: is the electric field standing wave effect the only reason for observed spectral distortions?', 2015.

[13] M. J. Baker *et al.*, 'Clinical applications of infrared and Raman spectroscopy: State of play and future challenges', *Analyst*, vol. 143, no. 8, pp. 1735–1757, 2018.

[14] T. G. Mayerhöfer and J. Popp, 'The electric field standing wave effect in infrared transflection spectroscopy', *Spectrochim. Acta Part A Mol. Biomol. Spectrosc.*, vol. 191, pp. 283–289, Feb. 2018.

[15] M. J. Pilling, P. Bassan, and P. Gardner, 'Comparison of transmission and transflectance mode FTIR imaging of biological tissue', *Analyst*, vol. 140, no. 7, pp. 2383–2392, 2015.

[16] T. P. Wrobel, B. Wajnchold, H. J. Byrne, and M. Baranska, 'Electric field standing wave effects in FT-IR transflection spectra of biological tissue sections: Simulated models of experimental variability', *Vib. Spectrosc.*, vol. 69, pp. 84–92, Nov. 2013.

[17] G. Monjardez, 'The feasibility of Fourier transform infrared imaging spectroscopy in discriminating benign prostatic hyperplasia from prostate cancer in blood serum samples', 2012.

[18] S. B. Kotsiantis, 'Supervised Machine Learning: A Review of Classification Techniques', *Informatica*, vol. 31, pp. 249–268, 2007.

[19] J. Tang, D. Kurfürstová, and P. Gardner, 'Breast cancer detection using infrared spectral pathology from H&E stained tissue on glass slides', *Clin. Spectrosc.*, vol. 3, p. 100008, Dec. 2021.

[20] M. J. Pilling, A. Henderson, and P. Gardner, 'Quantum Cascade Laser Spectral Histopathology: Breast Cancer Diagnostics Using High Throughput Chemical

Imaging', *Anal. Chem.*, vol. 89, no. 14, pp. 7348–7355, 2017.

[21] H. Abdi and L. J. Williams, 'Principal component analysis', *Wiley Interdisciplinary Reviews: Computational Statistics*, vol. 2, no. 4. pp. 433–459, 2010.

[22] B. Worley and R. Powers, 'Multivariate Analysis in Metabolomics', *Curr. Metabolomics*, vol. 1, no. 1, pp. 92–107, 2012.

[23] L. Rokach and O. Maimon, 'Decision Tree', *Data Min. Knowl. Discov. Handb.*, p. pp 165-192, 2005.

[24] L. Breiman, 'Random forests', *Mach. Learn.*, vol. 45, no. 1, pp. 5–32, 2001.

[25] T. Hesterberg, 'Bootstrap', *Wiley Interdiscip. Rev. Comput. Stat.*, vol. 3, no. 6, pp. 497–526, 2011.

[26] G. Biau, 'Analysis of a Random Forests Model', *J. Mach. Learn. Res.*, vol. 13, pp. 1063–1095, 2012.

[27] T. Fawcett, 'An introduction to ROC analysis', *Pattern Recognit. Lett.*, vol. 27, no. 8, pp. 861–874, 2006.

[28] M. Grant and S. Boyd, 'CVX: Matlab software for disciplined convex programming', *Available at http://cvxr.com/cvx/*. 2008.

Chapter 4

Study 1: The spectral comparison of different blank glass slide

4.1 Results and Discussion

4.1.1 Mean spectra of 12 glass slides

Blank glass slides were the samples used in this chapter. To eliminate the errors of the instrument itself and the external environment, it was necessary to take the background spectrum (figure 4.1), which was obtained by directly measuring the air spectrum.

The main compositions of the dry unpolluted air are nitrogen (N_2), oxygen (O_2), argon (Ar), carbon dioxide (CO_2) and other rare gas [1]. However, there is also a small amount of water vapour (H_2O) in natural air dependent upon ambient humidity. Only CO_2 and H_2O can produce an infrared absorption spectrum since the vibration of the molecule results in a change of dipole moment [2]. To control the variable parameters of the environment, all spectra were measured in a closed transparent box surrounding the microscope, which was purged with dry air. The dry air would remove the water vapour and CO_2 and decrease the effect of these on the infrared spectrum. Due to the fixed window size of the sample stage, up to 6 glass slides were measured at a time. 12 glass slides were randomly divided into two groups and were separately measured with the same temperature (23°C) and humidity (0% RH). The mean background spectrum was from two background images including $2 \times 128 \times 128$ spectra, and every background spectrum was obtained using the co-addition of 128 scans.

Figure 4.1 is a mean spectrum of two background spectra, the main peak which at 2349 cm^{-1} is s caused by carbon dioxide (CO_2) in air, and the noise around 1500 cm^{-1} and 3600 cm^{-1}, is from the sharp rotational fine structure of water (H_2O). The other peaks are be caused by the inherent influence of the instrument. Because the air relative humidity is 0 in the sample compartment of the microscope, water absorption shown in figure 4.1 may come from the body of the instrument.

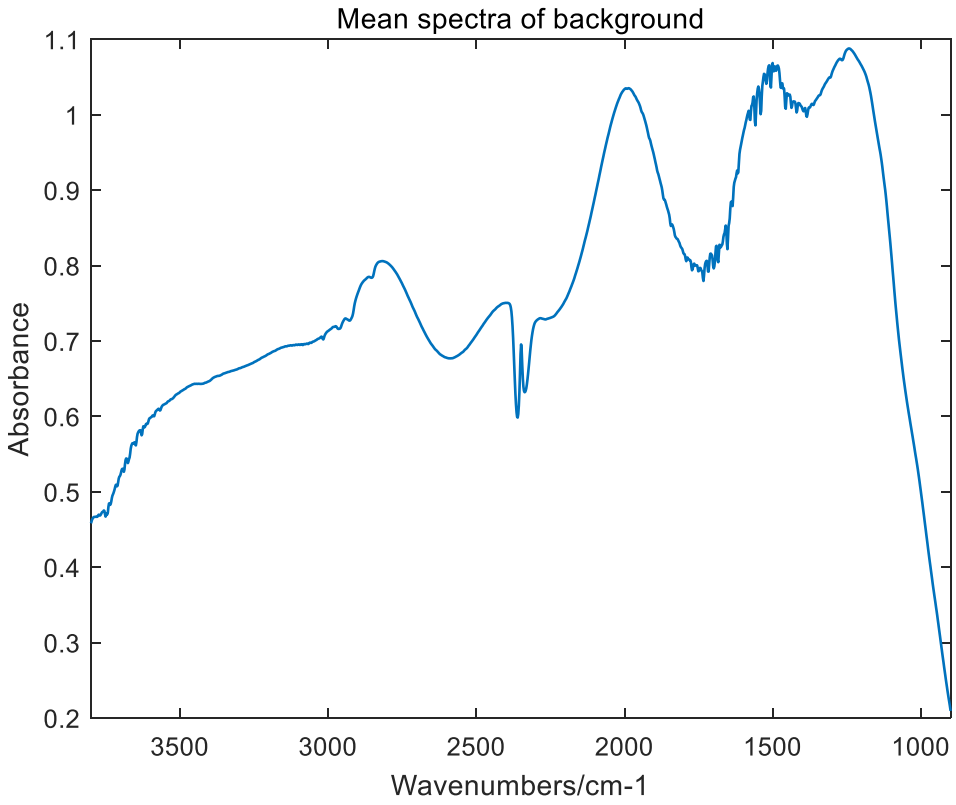

Figure4. 1 Background spectrum of air

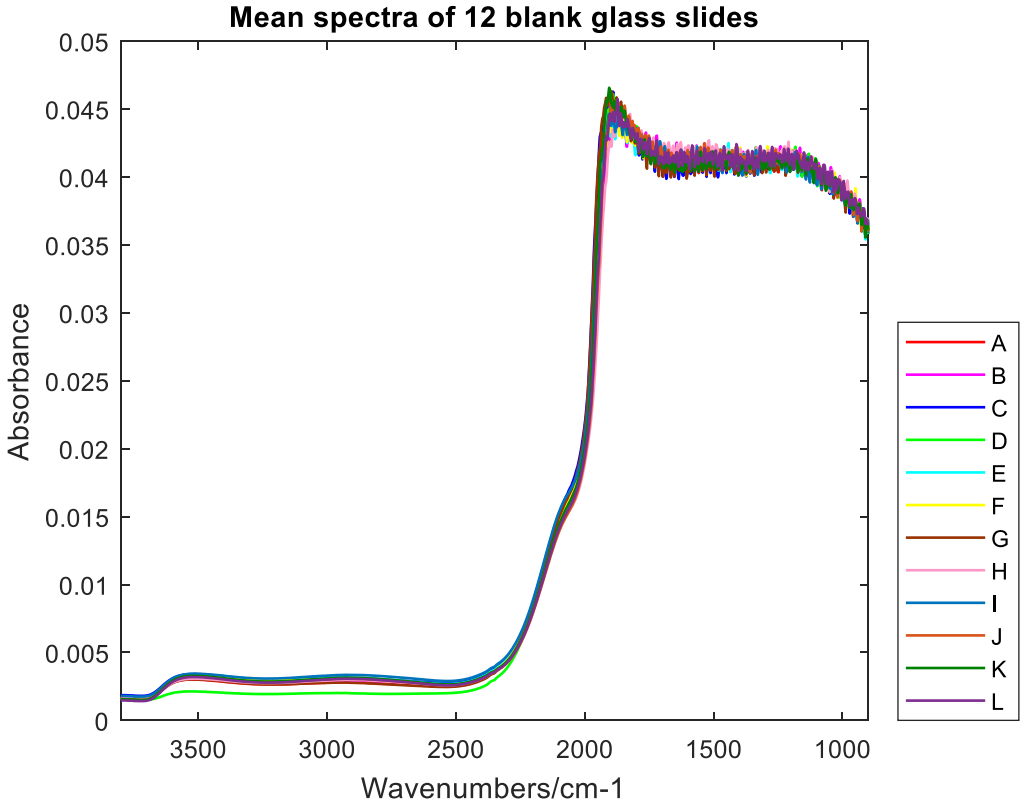

Figure4. 2 The mean spectra of 12 glass slides with the infrared range 900 - 3800 cm^{-1}

The mean spectra of 12 glass slides with the infrared range 900 - 3800 cm^{-1} are shown in figure 4.2. Every type of glass slide was measured three times and included $3 \times 128 \times 128$ spectra in total.

Figure 4.2 shows that glass slides have very high absorption in the range of 900 - 2000 cm^{-1} and it proves that the glass is not transparent in this infrared range. In addition, above 2000 cm^{-1} also was a typical infrared range for the previous SHP studies using glass substrate [12]. Therefore, infrared range between 900 - 2000 cm^{-1} should be cut. For a more precise comparison, the mean spectra in this study only remain 2500 - 3700cm^{-1}, and the mean spectra in this range are shown in figure 4.3.

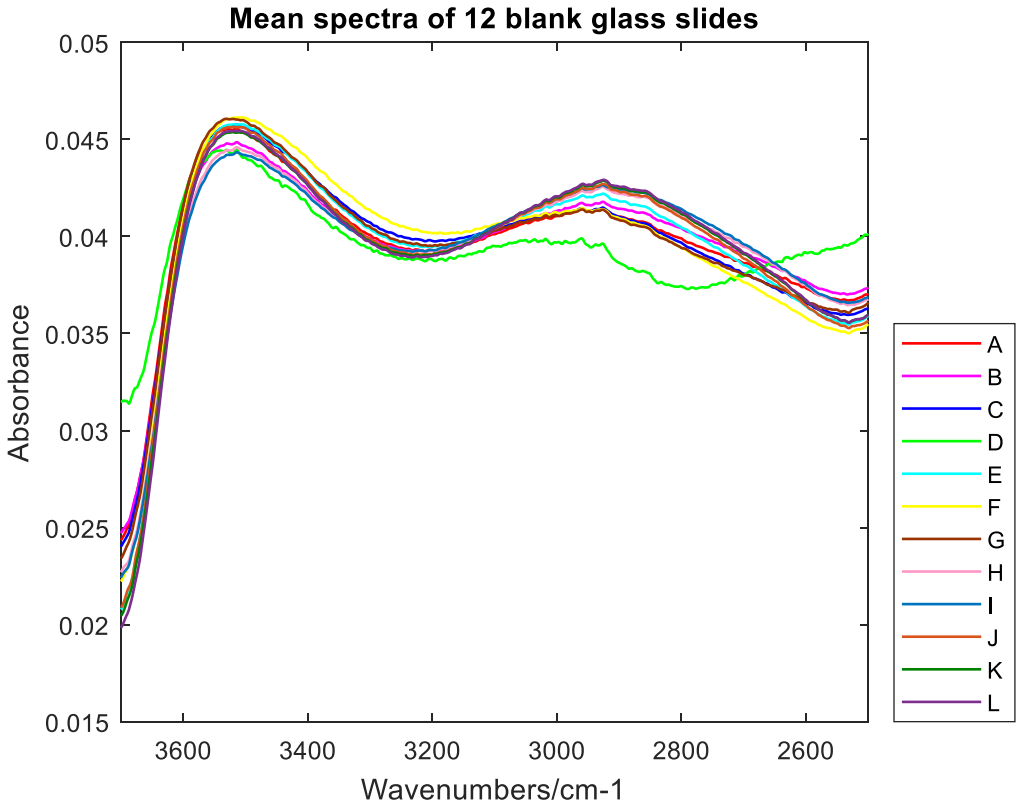

Figure4. 3 The mean spectra of 12 glass slides with the infrared range 2500 – 3700 cm^{-1}

Table4. 1 Assignment of hydroxyl infrared bands

Active groups	Information	wavenumber (cm^{-1})
$Si-OH$	Free hydroxyl in the glass $Si-OH$ stretching in different modes[3][4][5] [6] [7]	2542, 2750, 3524, 3595[5][6] 3571-3704[4] 3600-3750[3] 3600-3950[7]
H_2O	Asymmetric and symmetric stretching modes of interstitial water molecular[3][5][7]	2910, 2959, 3200, 3393[5] 2800-2980, 3400-3500[7] 3200-3500[3]
$\equiv Si-OH \ldots O-Si$	Hydrogen bonded Si-OH[3][5]	2381-2778[4] 2800±150[5] 2700-3000[3]

Generally, the composition of the glass consists of SiO_2, Al_2O_3, Fe_2O_3, MgO, K_2O, Na_2O, CaO and TiO_2 [8]. According to the glass manufacturing process, hydrogen (H_2) and water (H_2O) are the main substances to form hydroxyl [3]. H_2 is used for melting SiO_2 during the production process and H_2O is formed by the reaction between H_2 and oxygen (O_2). The vibrational peaks of the main silicate network groups should be located in the fingerprint region, which is located at 400-1400 cm^{-1} [8]. However, it is not transparent below 2000 cm^{-1} the cut-off for the glass slide. While in the range of 2000-3800 cm^{-1}, only the groups related to hydroxyl, water or similar groups have infrared absorption. The band assignment is shown in table 4.1[3][4][5][7][6].

According to figure 4.3, there are two wide bands for all blank glass slides, and the two bands for most of the glass slides are around 2926 cm^{-1} and 3526 cm^{-1}, respectively. However, the absorption intensity is different for different kinds of glass slides. Based on table 4.1, the peak at 3526 cm^{-1} is caused by isolated hydroxyl $Si-OH$ groups in different stretching modes. The peak at around 2926 cm^{-1} is wide, and the peak ranges from 2700 to 3100 cm^{-1}, which is caused by overlap peaks of hydrogen bonding ($\equiv Si-OH \ldots O-Si$) with different bond distances.

However, for glass D, the two peaks have a certain "blue shift", and the intensity of the peak about hydrogen bonds is also lower than that of the other glass slides. This is caused by the lower content of iron (Fe) in glass D. Adams [9] and Mcmillan [10]

studied the infrared spectra of the hydroxyl group in the glass. They proved that there is no hydrogen bonding for quartz glass and the absorption peak of the free hydroxyl group ($Si-OH$) at 3676 cm^{-1}. With the addition of some oxides (Al_2O_3, Fe_2O_3), the glass structure is disorderly, and the hydroxyl group readily form hydrogen bonds ($\equiv Si-OH \ldots O-Si$). Under the action of hydrogen bonds, the vibration frequency becomes lower, and the absorption peak is "red shifted". In addition, the greater the strength and binding form of hydrogen bonds, the greater the peak width. Therefore, the much lower iron content in glass D caused fewer hydrogen bonds, and the peak is more "blue shifted" [11]. The band intensity of hydrogen bonds is also lower than the others glass slides. However, the isolated hydroxyl Si−OH groups' band intensity is slightly lower than the other glass slides, which means the difference of content of isolated hydroxyl $Si-OH$ groups among 12 glass slides is small.

The forms of hydroxyl existing in glass include isolated hydroxyl ($Si-OH$), interstitial water molecules and hydrogen bonding ($\equiv Si-OH \ldots O-Si$) [4] [12]. Figure 4.3 only indicates that the spectra of glass D have a significant difference from the other glass slides. To explore the more specific factors of the difference among the 12 glass slides, the PCA of the 12 glass slides is necessary.

4.1.2 Principal component analysis (PCA) of 12 glass slides

According to the mean spectra of 12 glass slides, the apparent difference between glass D and the other glass slides is located at hydrogen bonding peaks. The infrared range of PCA in this study is selected to be 2500 – 3700cm^{-1}. Since there are too many individual spectra of each type of glass slide, 200 spectra from each type are randomly selected and used in the PCA.

(a)

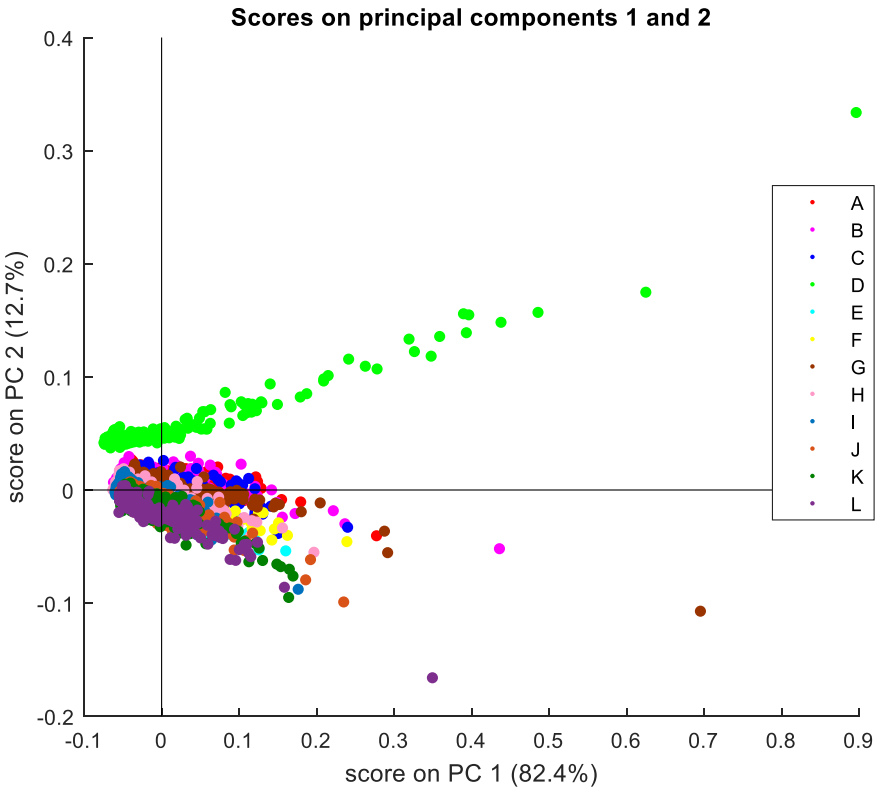
Scores on principal components 1 and 2
score on PC 2 (12.7%)
score on PC 1 (82.4%)
A
B
C
D
E
F
G
H
I
J
K
L

(b)

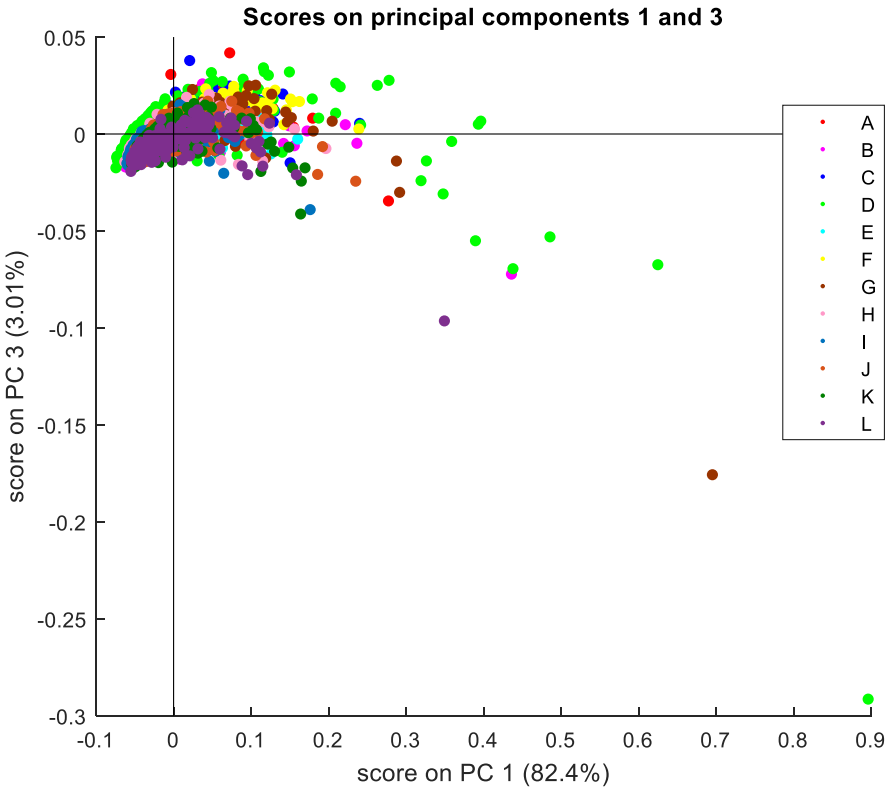
Scores on principal components 1 and 3
score on PC 3 (3.01%)
score on PC 1 (82.4%)
A
B
C
D
E
F
G
H
I
J
K
L

(c)

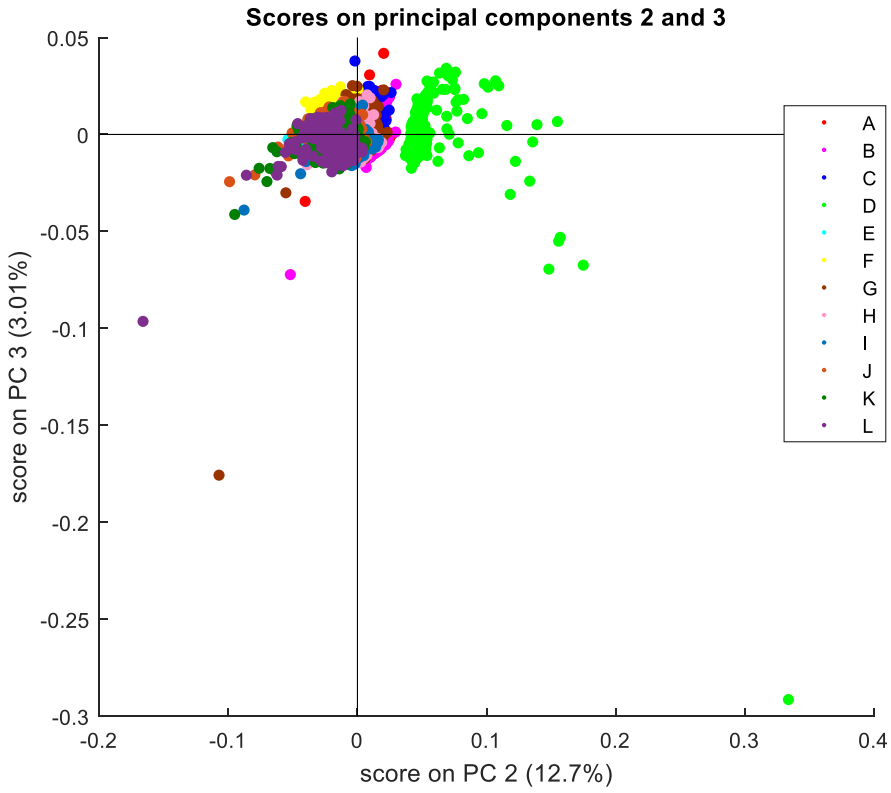

Figure4. 4 (a) The score plots of PC1 and PC2 of 12 glass slides (b) The score plots of PC1 and PC3 of 12 glass slides. (c)The score plots of PC2 and PC3 of 12 glass slides

Figure 4.4 (a), (b), (c) shows two – dimensional PCA scatter plots to analyse the e 12 glass slides, with t (a), (b), and (c) representing the score plots of PC1 vs PC2, PC1 vs PC3, PC2 vs PC3, respectively. The variance explained by PC1, PC2 and PC3 are 82.4%, 12.7% and 3.01%, respectively. The PC1 is the major component to describe the information of spectra. According to figures 4.4 (a), (b), (c), it is easy to find that there is a clear separation between glass D and the other 11 glass slides. However, there is no visual separation among the other 11 glass slides. Therefore, there is no noticeable difference among the infrared spectra of the 11 glass slides. Furthermore, figure 4.1 (a) and (c) show that PC2 is the major component to separate the glass D.

To find the major factors which lead to separating the glass D, loading figures of three components are necessary, and these are shown in figure 4.5 (a), (b), (c), respectively. The loading figures indicate the spectral absorption characteristics of every component.

PC1 is the major component, its loading is shown in figure 4.5 (a). The figure shows that PC1 is made of positive and negative peaks. According to table 4.1, the positive peak at 3560 cm^{-1} is related to the absorption of the free $Si-OH$ stretching. Therefore, there is a very positive correlation between the loading of PC1 and the content of isolate hydroxyl ($Si-OH$). While the negative peaks at 2800 cm^{-1} are related to hydrogen bonds ($\equiv Si-OH \ldots O-Si$). The PC1 is negatively related to the content of hydrogen bonds. Although there is no separation on PC1 for all glass slides, the distribution of all glass slides is similar. Most spectra of each type glass slide are located in the negative area. It means the hydrogen bonds ($\equiv$Si–OH…O–Si) content is higher than the isolated hydroxyl ($Si-OH$) for most spectra.

Figure 4.4 shows an apparent separation between glass D and the rest glass slides on the PC2. The loading of PC2 is shown in figure 4.5 (b). Two negative peaks constitute PC2. One peak is located at 3505 cm^{-1} , which is related to the isolated hydroxyl ($Si-OH$). The other peaks at 2850 cm^{-1} is related to hydrogen bonds ($\equiv Si-OH \ldots O-Si$). As for PC2, figure 4.4 (a) and (c) show that all spectra of glass D locate at the positive area of PC2, while the spectra of other glass slides distribute both positive and negative areas. Therefore, glass D could be separated because the content of isolated hydroxyl ($Si-OH$) and hydrogen bonds ($\equiv Si-OH \ldots O-Si$) in glass is much lower.

Figure 4.5 (c) shows the loading of PC3. PC3 loading has two positive peaks and a negative peak in the range of $2500-3700\ cm^{-1}$. The positive peak at 3200 cm^{-1} and 2800 cm^{-1} are related to the absorption of interstitial water molecules and hydrogen bonds ($\equiv Si-OH \ldots O-Si$), respectively. and the negative prak at 2574 cm^{-1}, is related to the isolated hydroxyl ($Si-OH$)[5]. But the score of PC3 is also very low (3.01%). Therefore, the PC3 is not an important component and can be ignored.

(a)

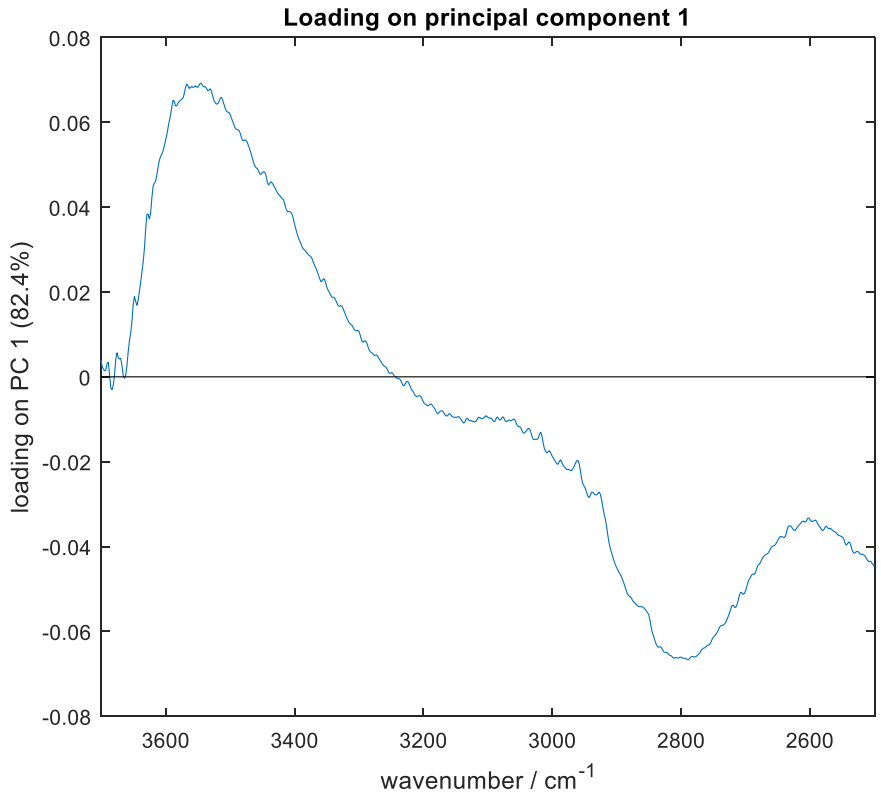
Loading on principal component 1
loading on PC 1 (82.4%)
0.08
0.06
0.04
0.02
0
-0.02
-0.04
-0.06
-0.08
3600
3400
3200
3000
2800
2600
wavenumber / cm-1

(b)

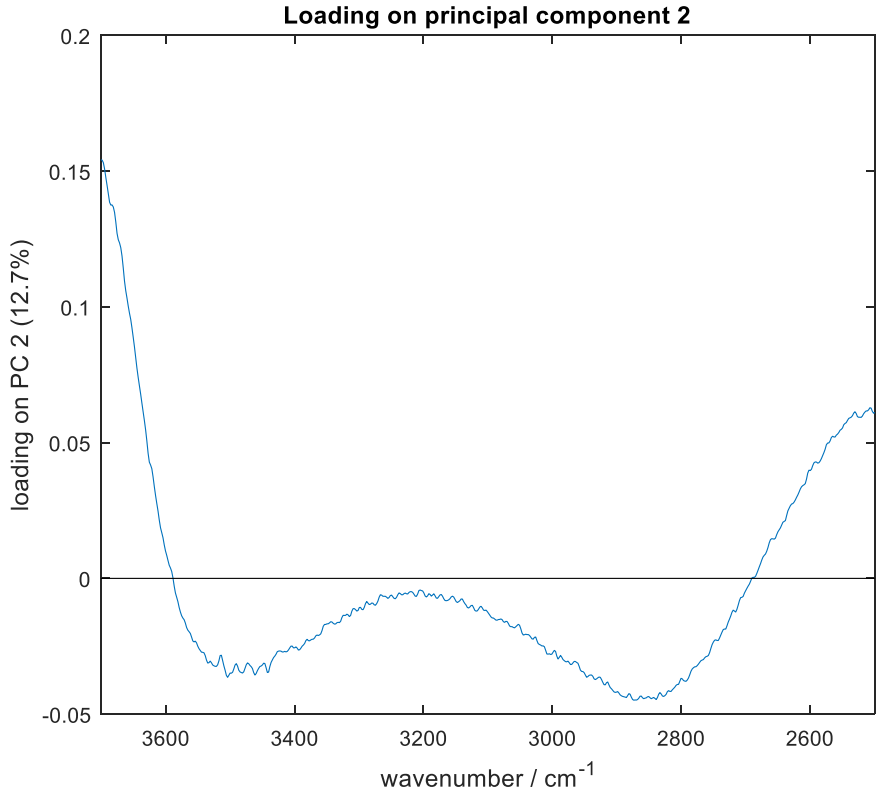
Loading on principal component 2
loading on PC 2 (12.7%)
0.2
0.15
0.1
0.05
0
-0.05
3600
3400
3200
3000
2800
2600
wavenumber / cm-1

(c)

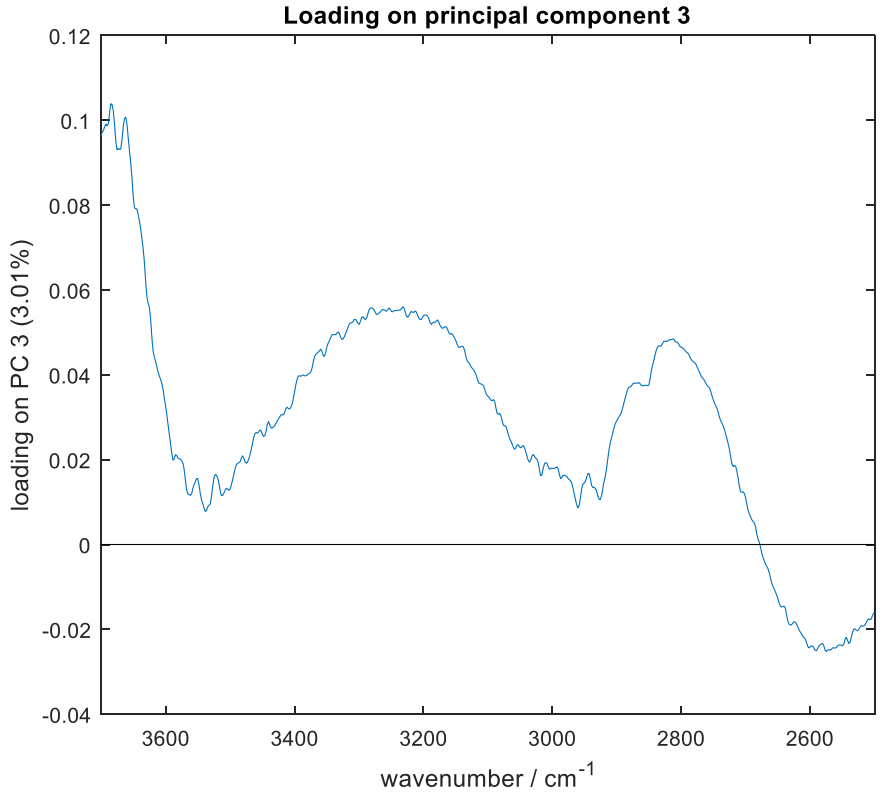

Figure4. 5 (a) The PC1 loading for PCA of 12 glass slides. (b) The PC2 loading for PCA for 12 glass slides. (c) The PC3 loading for PCA of 12 glass slides.

Within the infrared range of measurement (2500 – 3700 cm^{-1}), hydroxyl groups are present in three forms in the glass: different stretching modes of free $Si-OH$, symmetric and symmetric stretching modes of the interstitial water molecule and hydrogen-bonded $Si-OH$ ($\equiv Si-OH \ldots O-Si$). According to the PCA results of 12 glass slides, the spectral difference between glass D and the other glass slides is caused by the lower hydrogen bonds and interstitial water content.

In summary, according to the mean spectra of 12 glass slides and the PCA results, it can be concluded that glass D has slightly lower content of isolated free hydroxyl ($Si-OH$), and much lower content of hydrogen bonds ($\equiv Si-OH \ldots O-Si$) than the other 11 glass slides. In addition, hydrogen bonds decrease the vibration frequency and "red shift" of the peak. The red shift is an increase in the wavelength and a decrease in the frequency. The content of hydrogen bonds is related to the oxide. Glass D has a

lower content of iron. Therefore, compared with the other 11 glass slides, the lower hydrogen bonds of glass D leads to the peak being lower intensity and blue shifted.

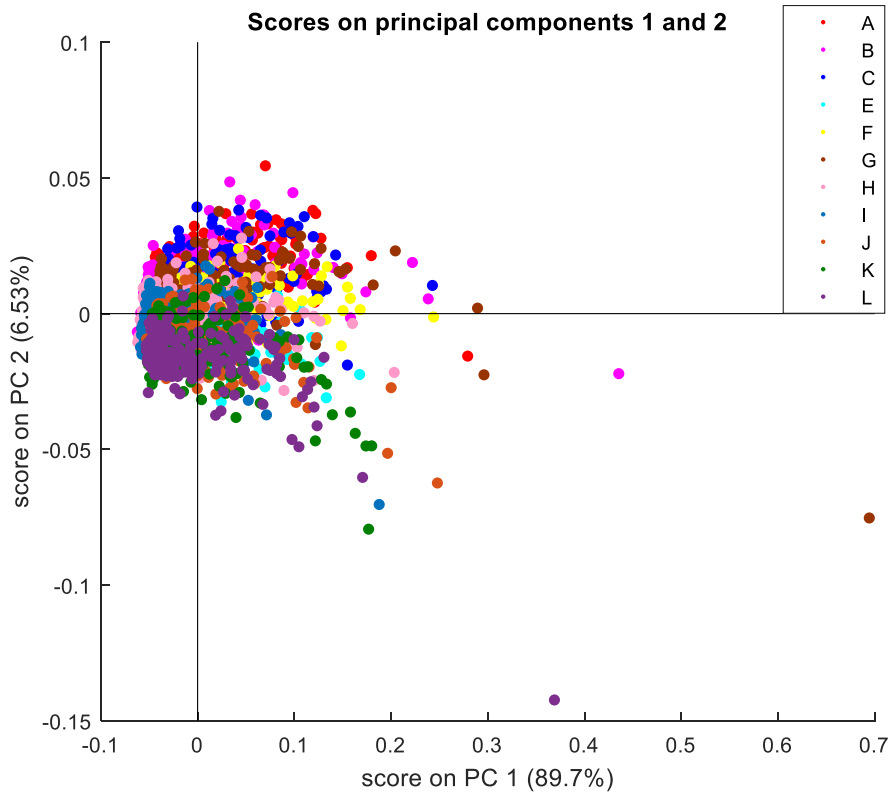

Figure4. 6 The score plots of PC1 and PC2 of 11 glass slides (remove glass D)

Figure 4.6 shows the score plots of PCA of the other 11 glass slides. The plot is only of PC1 and PC2, and the variance explained of PC1 and PC2 are 89.7% and 6.53%, respectively. Figure 4.6 indicates that except for glass D, the mean spectra of the other 11 glass slides are similar, and there is no clear separation between them. It means the type of glass slide has little effect on the infrared spectra. Glass D is not used in the next section.

4.1.3 PCA of charged and non-charged glass slides

The other 11 glass slides (remove glass D) are divided into non-charged glass slides (A, B, C, H, I) and charged glass slides (E, F, G, J, K, L). Adhesion of the glass slide is

from the positively charged surface. The surface of the glass slide has a permanent cationic charge, which can adsorb tissue or cells by electrostatic action[13]. Subsequently, a covalent bond can form between glass and a slice of tissue. Therefore, adhesive glass slides are more suitable for tissue work.

In order to study whether spectra could separate non-charged and charged glass slides, PCA between them is carried out, and the results are shown in figure 4.6. Due to the massive amount of spectra, 200 spectra are randomly selected from each type of glass, and the infrared range is 2500 – 3700cm^{-1}.

(a)

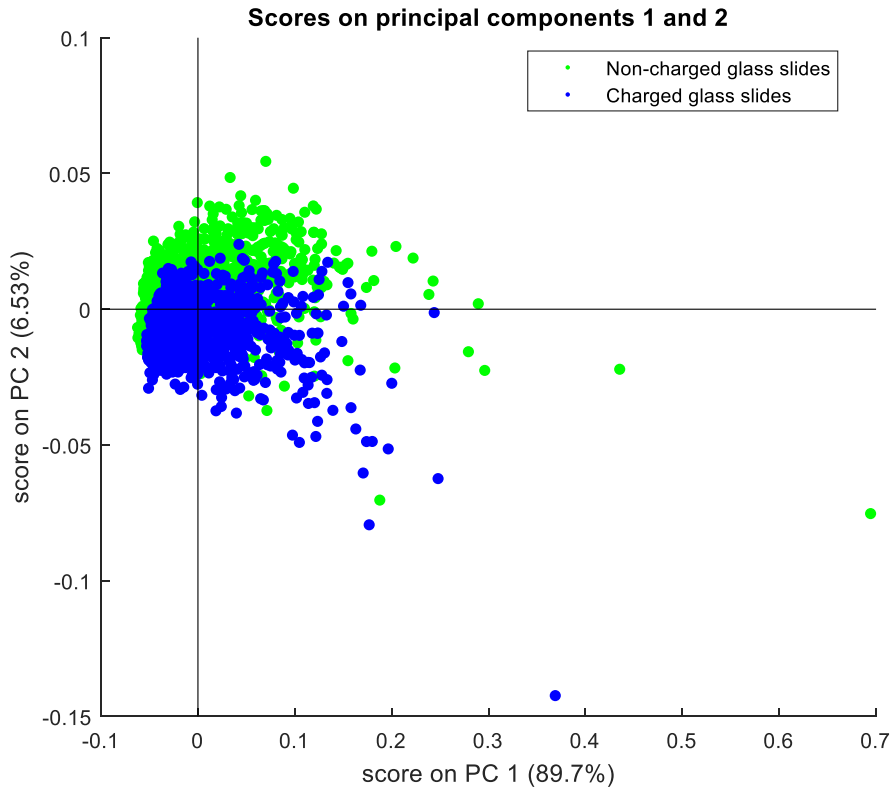

(b)

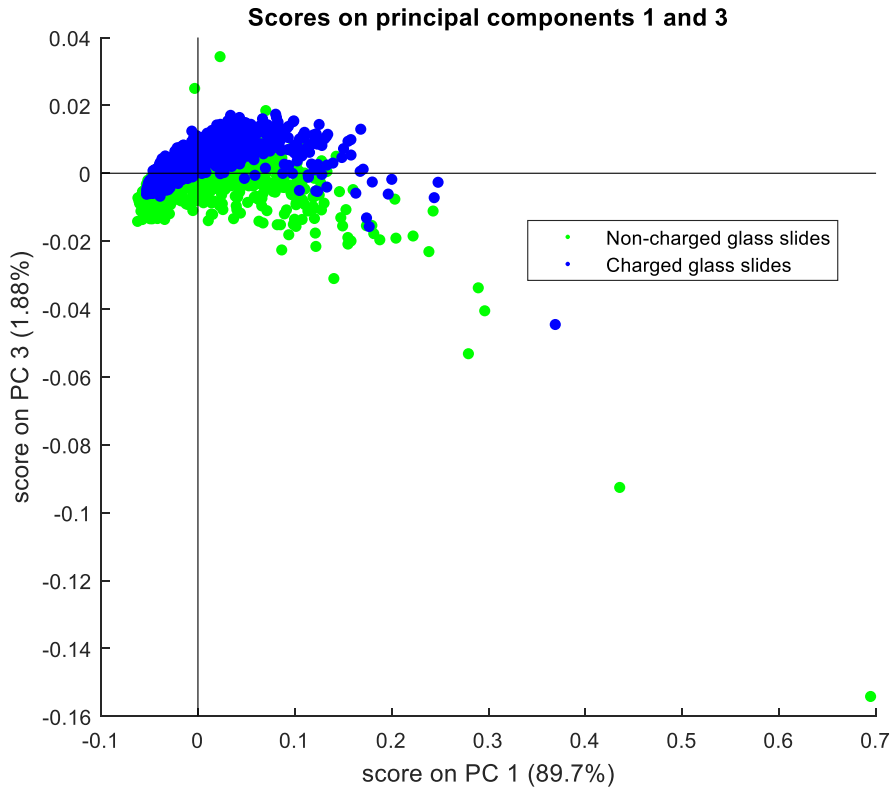

(c)

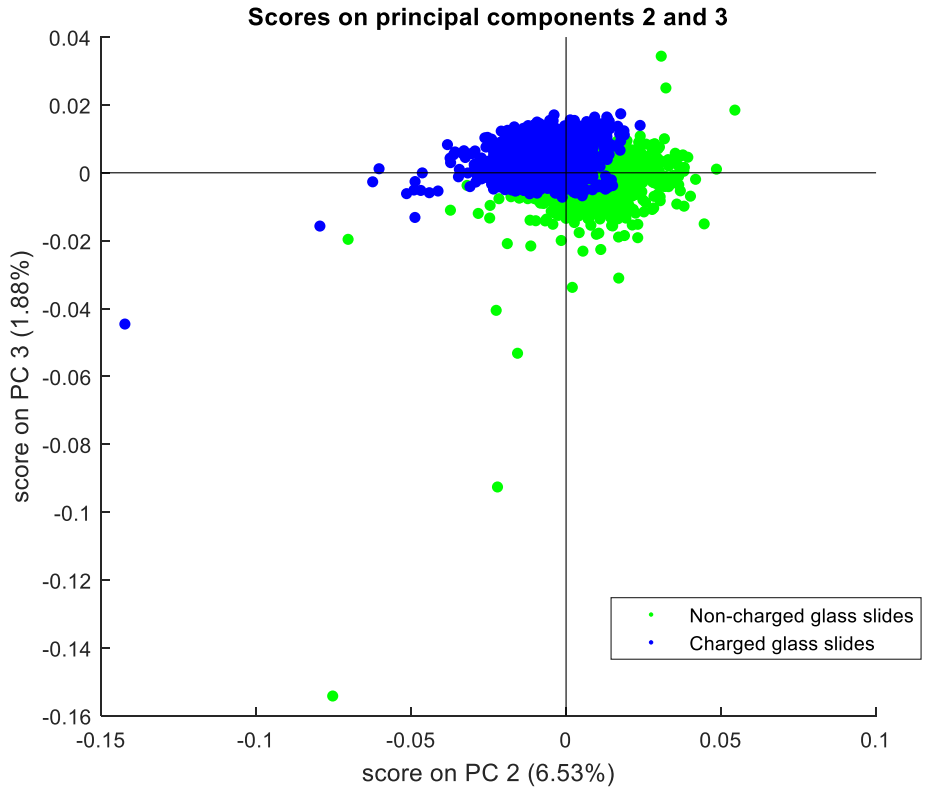

Figure4. 7 (a) The score plots of PC1 and PC2 of charged and non-charged glass slides. (b) The score

plots of PC1 and PC3 of charged and non-charged glass slides. (c)The score plots of PC2 and PC3 of charged and non-charged glass slides

Figure 4.7 (a), (b), (c) show the PCA scatter plots to separate non-charged (green) and charged (blue) glass slides. The variance explained by PC1, PC2, and PC3 are 89.7 %, 6.53 % and 1.88 %, respectively.

Figure 4.7 shows a separation trend between charged and non-charged glass slides by PC2 and PC3. Most spectra of charged glass slides are located in the negative area of PC2 and the positive area of PC3. While most spectra of the non-charged glass slides are located in the positive area of PC2. The loadings of each component are shown in figure 4.8.

(a)

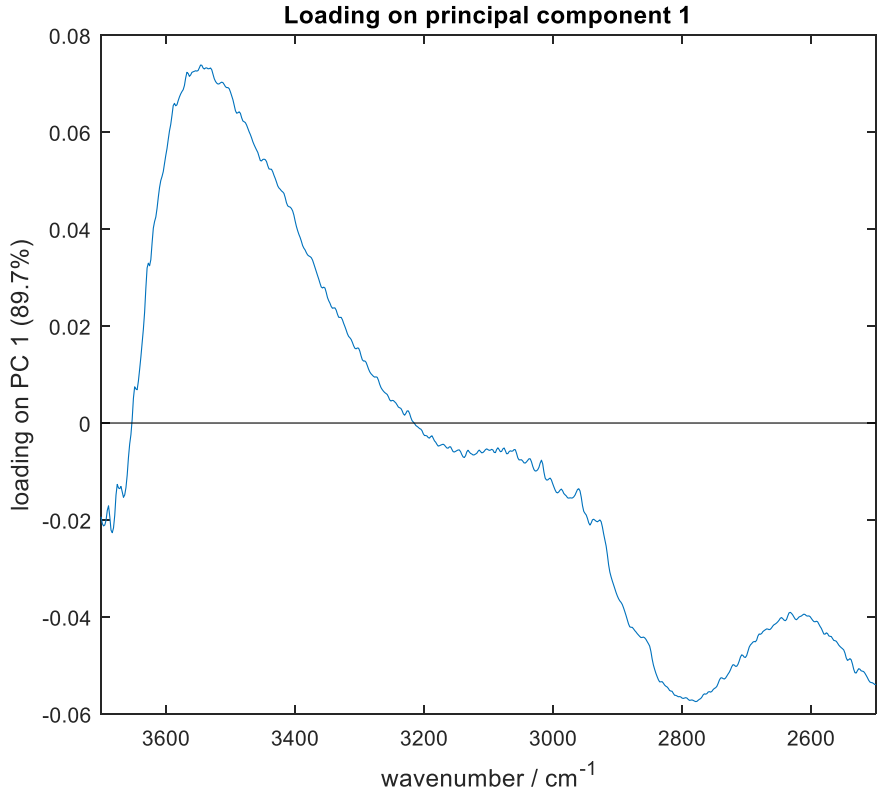

(b)

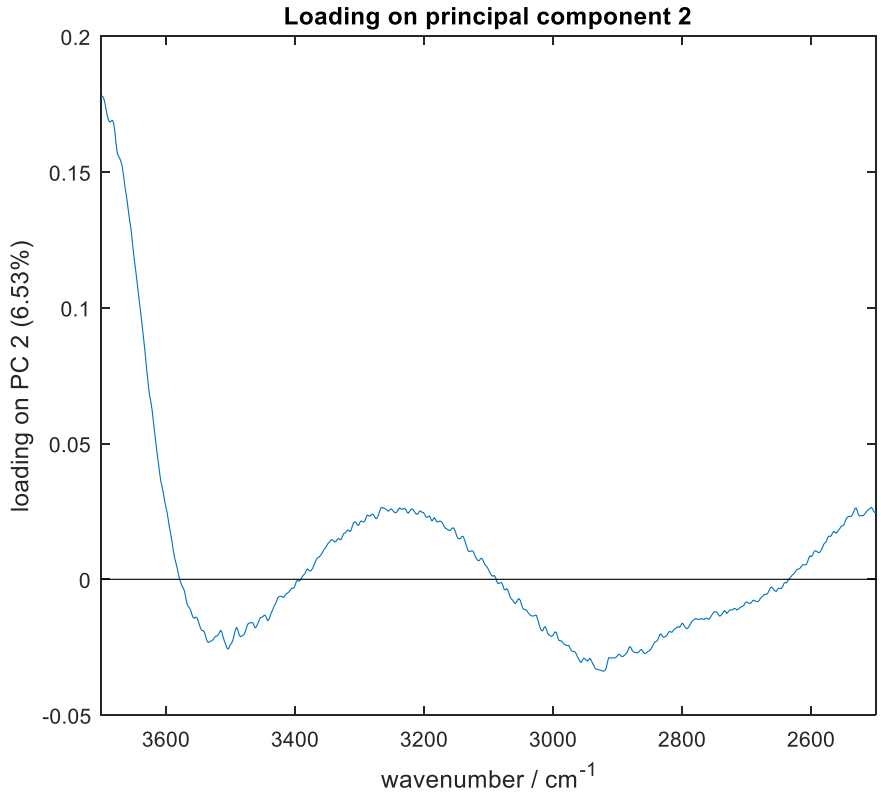

(c)

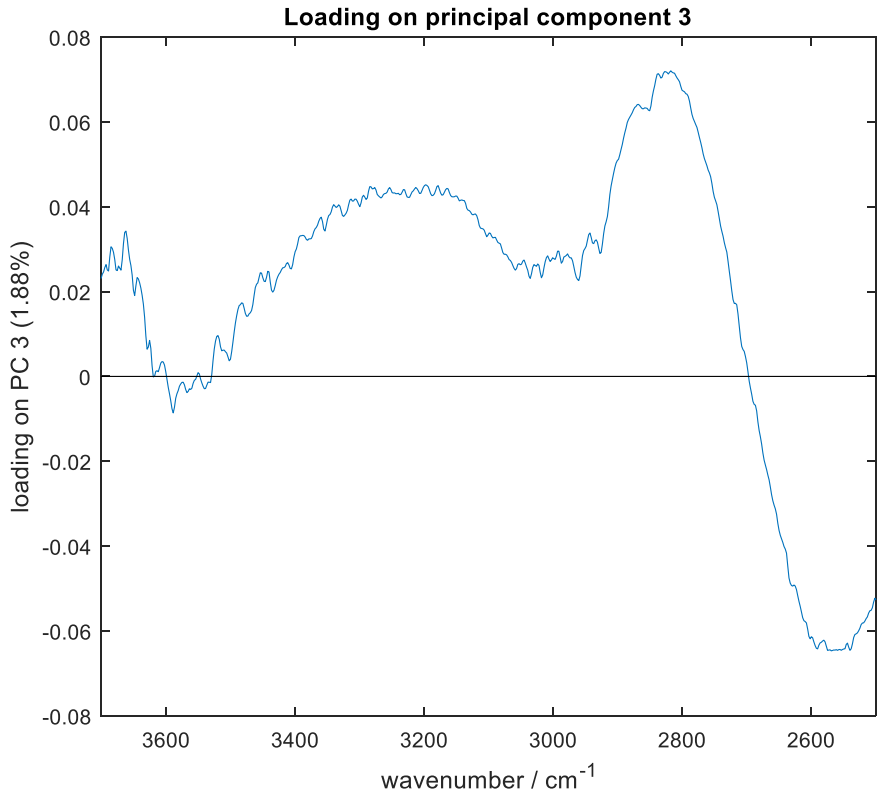

Figure4. 8 (a) The loading of PC1 in PCA of charged and non-charged glass slides. (b) The loading of

PC2 in PCA of charged and non-charged glass slides. (c) The loading of PC3 in PCA of charged and non-charged glass slides.

PC1 is the major component and contains most of the information of the spectra. Therefore, the loading plot of PC1 (figure 4.8 (a)) is essential to find which wavenumbers have an enormous influence on PC1. There are a positive band and a negative band in PC1 loading, which located at 3550 cm^{-1} and 2798 cm^{-1}, respectively. According to table 4.1, the positive band in the PC1 loading should belong to the free $Si-OH$ in different stretching modes and asymmetric and symmetric stretching of interstitial water molecular. The negative band is caused by hydrogen bonds ($\equiv Si-OH \ldots O-Si$). In addition, the loading value of stretching of free $Si-OH$ and interstitial water molecular higher than hydrogen bonds ($\equiv Si-OH \ldots O-Si$). Therefore, PC1 combines the absorption information of free $Si-OH$ and interstitial water molecular and hydrogen bonding ($\equiv Si-OH \ldots O-Si$), but is more related to the stretching of free $Si-OH$ and interstitial water molecular.

According to figure 4.7, spectra of the charged glass slide and non-charged glass slide have a slightly different distribution on PC2.The loading of PC2 contains two negative bands and a positive band. Two negative peaks locate at 3504 cm^{-1} and 2921 cm^{-1}, which are related to free $Si-OH$ and hydrogen bonds ($\equiv Si-OH \ldots O-Si$), respectively. The positive peak, located at 3237 cm^{-1} also related to the interstitial water molecular. Therefore, the PC2 is negatively associated with the spectral information of free $Si-OH$ and hydrogen bonds ($\equiv Si-OH \ldots O-Si$), and positively related to the interstitial water molecular.

Although there is no obvious separation between the charged and non-charged glass slides, most spectra of charged glass slides are distributed in the negative area of PC2, and most spectra of non-charged glass slides are located in the positive area. Because the PC2 is negatively related to the free $Si-OH$ and hydrogen bonds ($\equiv Si-OH \ldots O-Si$), most charged glass slides have more free $Si-OH$ and hydrogen bonds

than non-charged glass slides.

Figures 4.6 (b) and (c) show that most spectra of charged glass slides are distributed at the positive area of PC3. From the loading of PC3 (figure 4.8(c)), the two whole positive bands, which located at 3232 cm^{-1} and 2817 cm^{-1}, are related to the interstitial water molecular and hydrogen bonds, respectively. Therefore, most charged glass slides have more interstitial water molecular and hydrogen bonds than non-charged glass slides.

According to the PCA results, the charged glass slides have slightly more hydrogen bonds than non-charged glass slides. But the difference of hydrogen bonds is minimal, so there is no apparent red shift and influence on the infrared spectra. Therefore, whether the glass slide is charged or not, it has no impact on the infrared spectra.

4.2 Error discussion

The spectra for every type of glass slide are from three different locations on the slides to capture any local variation and thus eliminate the error. But some errors or artefacts could still exist. One such artefact relates to the presence of water vapour. The sealed box around the microscope stage was purged with dry air to reduce the relative the humidity to 0, so that it eliminates water vapour interference., It takes around one hour for the humidity to go down to zero after putting the samples on the sample stage and closing the box. However, the window size of the sample stage is limited, and only 6 glass slides could be measured at once. The measurement for the 12 blank glass slides needs to carry out twice. Although the temperature and humidity are normally the same for the two measurements, it is still possible that this introduces minor differences in the spectra.. In addition, the PCA has not used all the spectra available from 12 glass slides because each type of glass slide has associated with it 49152 spectra. 200 spectra per type of glass slide are randomly selected and be analysis. Therefore, once the 200

× 12 spectra are seleted, the PCA results would not change. I have tried many times to select the spectra randomly, and the separation of the PCA plot and the composition of loading for every PC is not changed. Only the scores have changed a little (±3%). Because the PCA is a statistical approach to finding critical bands, which caused the spectral difference of 12 glass slides. It will not affect the data analysis because loadings for every PC are not changed. Therefore, the error for the PCA is minimal and could be ignored.

4.3 Conclusion

The use of glass slides is an essential condition for the clinical application of SHP. Although previous studies have shown that SHP on glass substrates is a promising method for prostate and breast cancer detection [14][15][16]. In order to achieve clinical application, it is necessary to study the effect of glass type on cancer detection. This chapter only explores the influence of glass type on infrared spectra.

This chapter compared the infrared spectra of 12 different types of blank glass slides. Because the transmission window of glass slides at 2000 – 3800 cm^{-1}. The infrared absorption of blank glass slides at this range is caused by hydroxyl and its related groups. The groups associated with hydroxyl include isolated hydroxyl ($Si-OH$), interstitial water molecular and hydrogen bondings ($\equiv Si-OH \ldots O-Si$). Therefore, the spectral difference of glass is caused by the different content of three types of hydroxyl related groups. And a lot of factors could affect the content, such as raw materials, processing technique and so on.

According to the mean spectra and principal component analysis of 12 glass slides, except for glass D, the spectra of 11 glass slides have a similar peak position and intensity, which means the major components of the glass slide is similar. But the peak position of glass D is a little "blue shifted", and the peak intensity is much lower than

that of the other 11 glass slides. Combined with the loading of principal component, the results indicate that glass D has a much lower content of hydrogen bonds ($\equiv Si - OH \ldots O - Si$), which may be caused by the very low iron content. Because the more metal oxide would form more hydrogen bonds ($\equiv Si - OH \ldots O - Si$), and then reduce the vibration frequency and lead to the "red shift" of the band. The very low iron content of glass D caused to fewer hydrogen bonds, so the peak intensity at 2925 cm^{-1} is lower than the other glass slides, and the "blue shift" of the peak position on glass D.

The other 11 glass slides have similar mean spectra and cannot be discriminated by PCA. In conclusion, the type of most glass slides has no effect on the infrared spectra. Furthermore, the rest of 11 glass slides can be grouped as charged and non-charged glass slides. Because of the adhesive surface, the charged glass slide is more suitable for tissue work. The two groups cannot be clearly separated, but they have a separation trend, which means there is a slight difference between the two groups of glass slides on PC2 and PC3. According to the loading of PC2 and PC3, they indicate that the charged glass slides have slightly more interstitial water molecular and hydrogen bonds ($\equiv Si - OH \ldots O - Si$) than non-charged glass slides. However, the difference is too small to affect the infrared spectra.

4.4 Reference

[1] Brimblecombe P. Air composition and chemistry[M]. Cambridge University Press, 1996.

[2] P. R. Griffiths and J. A. De Haseth, *Fourier Transform Infrared Spectrometry*. 2007.

[3] H. Dunken and R. H. Doremus, 'Short time reactions of a na2o-cao-sio2 glass with water and salt solutions', *J. Non. Cryst. Solids*, vol. 92, no. 1, pp. 61–72, 1987.

[4] R. F. Bartholomew, B. L. Butler, H. L. Hoover, and C. K. Wu, 'Infrared Spectra of a Water-Containing Glass', vol. 63, no. 9, pp. 481–485, 1980.

[5] G. Navarra, I. Iliopoulos, V. Militello, S. G. Rotolo, and M. Leone, 'OH-related infrared absorption bands in oxide glasses', *J. Non. Cryst. Solids*, vol. 351, no. 21–23, pp. 1796–1800, Jul. 2005.

[6] A. M. Efimov, V. G. Pogareva, and A. V. Shashkin, 'Water-related bands in the IR absorption spectra of silicate glasses', *J. Non. Cryst. Solids*, vol. 332, no. 1–3, pp. 93–114, Dec. 2003.

[7] E. M. A. Khalil, F. H. ElBatal, Y. M. Hamdy, H. M. Zidan, M. S. Aziz, and A. M. Abdelghany, 'Infrared absorption spectra of transition metals-doped soda lime silica glasses', *Phys. B Condens. Matter*, vol. 405, no. 5, pp. 1294–1300, 2010.

[8] 'Faulques Fritsch 2001 Raman natural glasses tektites.pdf'.

[9] Adams, R. V. "Infrared absorption due to water in glasses." Physics and Chemistry of Glasses 2 (1961): 39-49.

[10] Paul F. McMillan, Richard L. Remmele; Hydroxyl sites in SiO2 glass: A note on infrared and Raman spectra. *American Mineralogist* 1986; 71 (5-6): 772–778. doi:

[11] E. Faulques, E. Fritsch, and M. Ostroumov, 'Spectroscopy of natural silica-rich glasses', *J. Mineral. Petrol. Sci.*, vol. 96, no. 3, pp. 120–128, 2001.

[12] J. E. Shelby, 'Protonic species in vitreous silica', *J. Non. Cryst. Solids*, vol.

179, no. C, pp. 138–147, 1994.

[13] B. Gottenbos, D. W. Grijpma, H. C. van der Mei, J. Feijen, and H. J. Busscher, ‘Antimicrobial effects of positively charged surfaces on adhering Gram-positive and Gram-negative bacteria’, *J. Antimicrob. Chemother.*, vol. 48, no. 1, pp. 7–13, 2001.

[14] M. J. Pilling, A. Henderson, J. H. Shanks, M. D. Brown, N. W. Clarke, and P. Gardner, ‘Infrared spectral histopathology using haematoxylin and eosin (H&E) stained glass slides: a major step forward towards clinical translation’, *Analyst*, vol. 142, no. 8, pp. 1258–1268, 2017.

[15] R. a Shaw, H. H. Eysel, K. Z. Liu, and H. H. Mantsch, ‘Infrared spectroscopic analysis of biomedical specimens using glass substrates.’, *Anal. Biochem.*, vol. 259, no. 2, pp. 181–6, 1998.

[16] J. Tang, D. Kurfürstová, and P. Gardner, ‘Breast cancer detection using infrared spectral pathology from H&E stained tissue on glass slides’, *Clin. Spectrosc.*, vol. 3, p. 100008, Dec. 2021.

Chapter 5

Glue removal

After a biopsy is removed from the patient, the samples are preserved either by flash freezing or by formalin fixation followed by being embedded in paraffin to produce a formalin-fixed paraffin embedded (FFPE) block. Both types of samples can be preserved for extended periods of time, the former obviously requiring low temperature storage conditions, while the latter has essentially no special storage requirements and can be kept for 10s of years or longer. Frozen samples are often used under intraoperative conditions where a surgeon requires results as quickly as possible (normally 15-20 min) before continuing with an operation. However, FFPE blocks are the standard used for more routine biopsies and are generally of higher quality leading to better diagnostic accuracy [1].

In order to prepare FFPE tissue samples, tissue needs to be preserved in formalin and processed by additional solutions, typically a series of successive immersions in 70%, 80%, 90%, 95% and 100% ethanol, followed by Xylene. Then the tissue is placed in paraffin wax and be cut into thin slices after the wax has hardened. When a sample is to be analysed, the tissues are dewaxed in Xylene (or suitable xylene substitute). The thin tissue slices are put on glass slides and stained with dyes. Haematoxylin and Eosin (H&E) are the common dyes in clinical applications[2]. A thin layer of mounting media is applied, followed by a glass coverslip. If the stain and subsequent steps have been properly performed, the slide will be stable for many years.

The mounting media is used to keep the tissue sample in a fixed place, prevent the sample from drying, prevent photobleaching and preserve the tissue sample for long-term storage. There are many kinds of mounting media, and they are mainly divided into aqueous mounting media and non-aqueous mounting media. Aqueous mounting media are based on distilled water. They could mount tissue sections directly after staining, and the dye usually could be dissolved in alcohol, Xylene or other organic solvents such as lipid dyes. Syrups, gelatin-based media and gum arabic media are the main types of aqueous mounting media.

Non-aqueous mounting media based on organic solvents, natural or synthetic resins dissolved in contain toluene, Xylene or benzene, and they are also called anhydrous or organic mounting media. They could protect the tissue sample and provide optical brilliance of the dye. However, dehydration is necessary after staining for non-aqueous mounting media compared with the aqueous mounting media. This step could avoid water on the tissue section that could interfere with the mounting medium. H&E are used for tissue stain and are soluble in water, so the mounting media must be water-free. The anhydrous mounting media are generally permanent and can be used for the long-term storage of stained tissue sections. Therefore, the anhydrous mounting media is widely used in clinical preparation. For easy expression, the mounting medium is called the glue for short in the project. In addition, because the tissue has been dewaxed before dying. So this project assumes there is no paraffin in the H&E stained tissue.

There are two different experimental methods in the project, and the comparison between the two experiments is shown in table 3.3. According to table 3.3, the final spectral information of both experiments 1&2 not only has tissue information but is also affected by glue and coverslip. Therefore, digital glue removal is necessary to obtain pure IR information from the tissue and eliminate the influence of glue & coverslip.

In addition, the “less glue” shown in table 3.3 is mainly caused by the structure difference between epithelium and stroma. The normal epithelium has more holes. Thus epithelium will contain more glue than stroma (see figure 5.6). But the content of glue at the epithelium area is less than that at tissue free area. So using “less glue” to tell the different glue content.

5.1 The principle of glue removal

5.1.1 Spectral subtraction

Matlab processes the glue removal in this project. The method is based on the principle of spectral subtraction. Spectral subtraction is one of the essential quantitative analysis methods. Bouguer-Lambert-Beer law (Beer's law) is the basic principle of the relationship between absorbance and concentration [3]. Beer's law is

$$\mathrm{A_i}(\tilde{\nu}) = \mathrm{a_i}(\tilde{\nu})\mathrm{bc_i} \tag{5-1}$$

where $A_i(\tilde{\nu})$ is the absorbance of species *i* at wavenumber $\tilde{\nu}$, $a_i(\tilde{\nu})$ the absorptivity of the species at that wavenumber (in units of $concentration^{-1} \cdot distance^{-1}$) and the proportionality constant is a function of the wavenumber $\tilde{\nu}$, b the pathlength, c_i the concentration of species *i*.

For a mixed component sample, when the infrared light passes through the sample, each component in the mixture absorbs the corresponding infrared light, and the total absorbance $M(\tilde{\upsilon})$ at the wavenumber $\tilde{\nu}$ is the sum of each component's absorbance,

$$M(\tilde{\upsilon}) = A_1(\tilde{\upsilon}) + A_2(\tilde{\upsilon}) + A_3(\tilde{\upsilon}) + \cdots \tag{5-2}$$

For example, the total absorbance $M(\tilde{\upsilon})$ at the wavenumber $\tilde{\nu}$ in the spectrum of the two-component system is the sum of the absorbance $A_1(\tilde{\upsilon})$ and $A_2(\tilde{\upsilon})$ produced by component 1 and component 2 at the wavenumber $\tilde{\nu}$, respectively.

$$M(\tilde{\upsilon}) = A_1(\tilde{\upsilon}) + A_2(\tilde{\upsilon}) \tag{5-3}$$

If component 1 is known and component 2 is unknown, the spectrum of unknown component 2 can be obtained by spectral subtraction of absorbance. The specific method is as follows: take a spectrum of pure component 1 as the reference spectrum and the $A'_1(\tilde{\upsilon})$ is the absorbance of the reference spectrum. The same composition of the sample, but of different concentration or pathlength (thickness), then,

$$\mathrm{A_1}(\tilde{\upsilon}) = \mathrm{kA'_1}(\tilde{\upsilon}) \tag{5-4}$$

where k is a scaling factor. Therefore, the absorbance of the unknown component 2

$$\mathrm{A}_2(\tilde{\upsilon}) = M(\tilde{\upsilon}) - \mathrm{kA'}_1(\tilde{\upsilon}) \quad (5\text{-}5)$$

5.1.2 The function of glue removal

The tissue sample consists of tissue, coverslip, glass and glue. The spectra of Matrigel, glue, and coverslip could be reference spectra. Matrigel is a gelatinous protein mixture extracted from Englebreth-Holm-Swarm mouse tumour cells. The growth and proliferation of many cells type require an attached surface. Matrigel primarily consists of laminin, collagen IV, and entactin and is commonly used as a basement membrane matrix for stem cells [4]. Matrigel could promote cell differentiation [5] and is widely used to mimic the extracellular matrix (ECM) in cancer and stem cell culture, presumably by replicating cell–ECM interactions. The shape of Matrigel spectrum is similar to the spectra of cell and tissue. Therefore, the spectrum of Matrigel could be used as a reference spectrum of tissue for glue removal. Therefore, the absorbance of the sample can be replaced as

$$M_{sample}(\tilde{\upsilon}) = \mathrm{k}_1\mathrm{A'}_{\mathrm{glue}}(\tilde{\upsilon}) + \mathrm{k}_2\mathrm{A'}_{\mathrm{matrigel}}(\tilde{\upsilon}) + \mathrm{k}_3\mathrm{A'}_{\mathrm{coverslip}}(\tilde{\upsilon}) \quad (5\text{-}6)$$

According to function 5.5, the absorbance of the tissue is,

$$\mathrm{A}_{\mathrm{tissue}}(\tilde{\upsilon}) = M_{sample}(\tilde{\upsilon}) - \mathrm{k}_1\mathrm{A'}_{\mathrm{glue}}(\tilde{\upsilon}) - \mathrm{k}_3\mathrm{A'}_{\mathrm{coverslip}}(\tilde{\upsilon}) \quad (5\text{-}7)$$

And the absorbance of the residual is,

$$\mathrm{A}_{\mathrm{residual}}(\tilde{\upsilon}) = M_{sample}(\tilde{\upsilon}) - \mathrm{k}_1\mathrm{A'}_{\mathrm{glue}}(\tilde{\upsilon}) - \mathrm{k}_2\mathrm{A'}_{\mathrm{matrigel}}(\tilde{\upsilon}) - \mathrm{k}_3\mathrm{A'}_{\mathrm{coverslip}}(\tilde{\upsilon}) \quad (5\text{-}8)$$

Where $\mathrm{A}_{\mathrm{tissue}}(\tilde{\upsilon})$: absorbance of tissue, which is the result after removing glue. $M_{sample}(\tilde{\upsilon})$: absorbance of the sample, which is the result of FTIR measurement.

$\mathrm{A'}_{\mathrm{glue}}(\tilde{\upsilon})$, $\mathrm{A'}_{\mathrm{coverslip}}(\tilde{\upsilon})$: absorbance of the pure glue and clear coverslip, respectively.

$\mathrm{A'}_{\mathrm{matrigel}}(\tilde{\upsilon})$ *:* absorbace of standard Matrigel. $\mathrm{k}_1, \mathrm{k}_2, \mathrm{k}_3$: scaling factors of glue, Matrigel and coverslip, respectively.

Because the absorbance of the sample, glue, coverslip and Matrigel are known, according to the function (5-7) and (5-8), the real tissue spectrum with glue removal could be obtained if three scaling factors are calculated. Therefore, the key to glue removal is to calculate the scaling factors of glue and coverslip. The function for getting the scaling factors is the least-squares with known covariance (LSCOV) in Matlab, and it is the critical function of glue removal code.

5.1.3 Fitting range

Because the absorbance is a function of wavenumber, the scaling factors would change with the fitting range. It is essential to find suitable fit ranges for glue removal. For a more intuitive presentation, the tissue sample, which is from a BPH patient and mounted on glass K, is used as an example to discover the impact of the fitting range changes on the glue removal results in order to find the most appropriate fitting range.

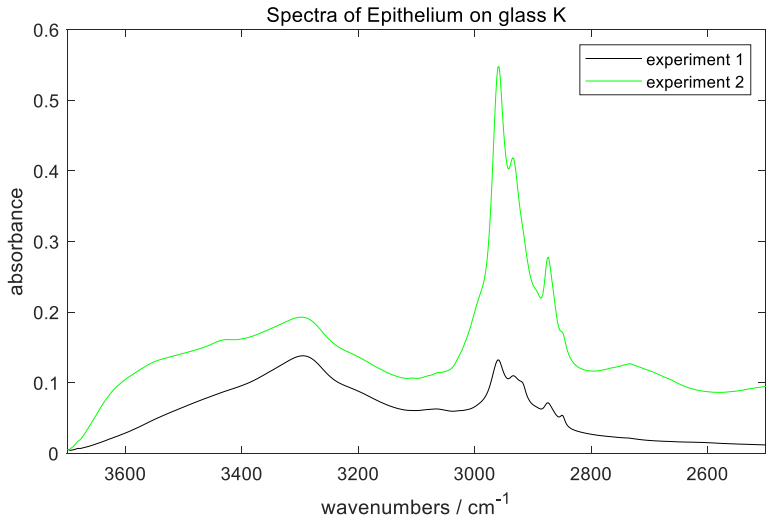

Figure5. 1 Mean spectra of epithelium on glass K from the BPH patient for experiments 1&2

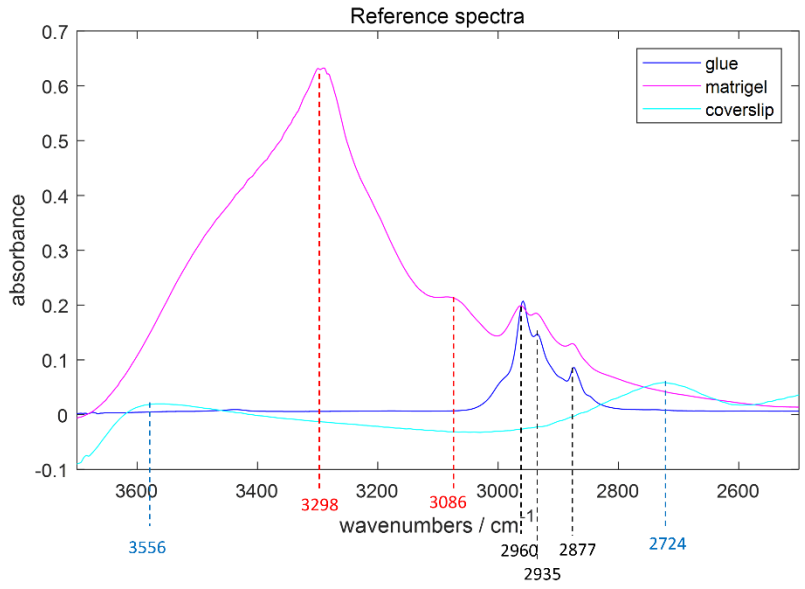

Figure5. 2 All kinds of reference mean spectra

Figure 5.1 shows the mean spectra of epithelium on glass K for Experiment 1 & 2. 196608 spectra are obtained in total for BPH tissue on glass K, and 4551 spectra are annotated as epithelium. After the quality test, there are 4041 and 4245 spectra for experiment 1 and experiment 2, respectively (see table 5.2). Figure 5.2 shows the reference spectra of Matrigel, glue, and coverslip. The glue and coverslip are from Christie hospital and keep consistent for preparing all of the tissue samples. The glue and coverslip each be measured with 32768 spectra. According to Figures 5.1 & 5.2, it is easy to see that glue has a more significant effect on experiment 2. Therefore, the mean spectra of glass K in experiment 2 are used as an example for testing the results of glue removal.

The fit range is a continuous range, which are used for calculating the most suitable scaling factors of every reference spectrum to fit the tissue spectra by LSCOV. If the fit range is too small, the errors of scaling factors of every reference spectrum are large. If the fit range is too big, it could lead to overfitting. In addition, not all spectral ranges are suitable for fitting the tissue spectra. There is some noise on the whole spectral range (2500-3700 cm^{-1}), it would lead to the significant deviation of scaling factors of every reference spectrum at every wavenumber.

To eliminate the effect of noise and reduce the error of scaling factors, a few small range of every significant peak in all reference spectra are selected simultaneously as several fit ranges. The small range is selected up and down 10 or 20 wavenumbers centred around every significant peak. Therefore, the fit ranges are divided into four types:
Fit range 1, where the tissue spectra are mainly contributed by absorption of Matrigel (3278-3318 cm^{-1}, 3066-3106 cm^{-1});
Fit range 2, where the tissue spectra are mainly contributed by absorption glue and Matrigel peak (2848-2852 cm^{-1}, 3415-3455 cm^{-1});
Fit range 3, where the tissue spectra are mainly contributed by glue and Matrigel peak (2950-2970 cm^{-1}, 2925-2945 cm^{-1}, 2867-2887 cm^{-1});
Fit range 4, where the tissue spectra are mainly contributed by absorption of coverslip & Matrigel peak (3536-3576cm^{-1}, 2704-2744cm^{-1}).

For ease of presentation, fit ranges 1, 2, 3, or 4 is marked to represent the four types of fit range, respectively. The corresponding coefficients of every reference spectrum can be calculated based on the LSCOV function in every small fit range. The final scaling factors of every reference spectrum at every wavenumber are the mean coefficients of all small fit ranges.

To find the suitable fit range, figure 5.3 (a), (b), (c), (d) show the spectra of epithelium and stroma with glue removal in 4 different fitness ranges. And to observe clear spectral results with glue removal, figure 5.4 (a), (b), (c), (d) show the zoom in of tissue spectral results with glue removal in 4 different fit ranges.

(a)

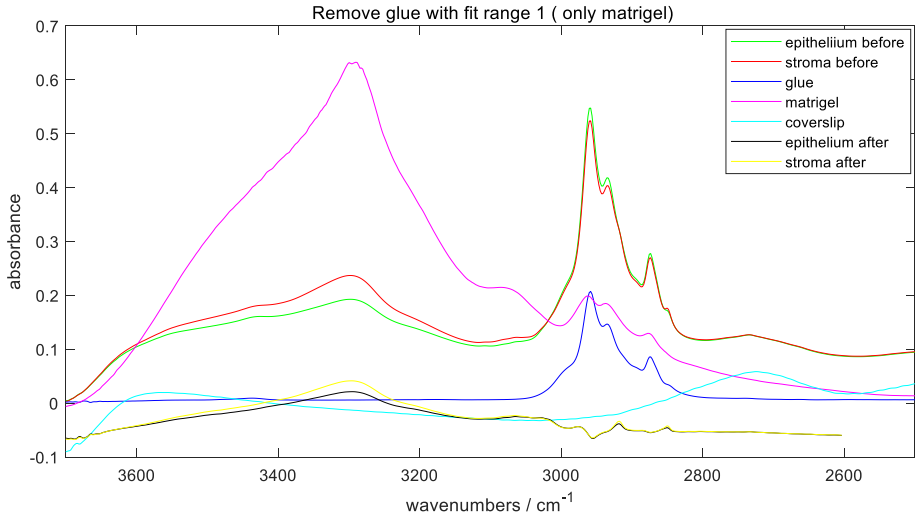
Remove glue with fit range 1 (only matrigel)
epitheliium before
stroma before
glue
matrigel
coverslip
epithelium after
stroma after
absorbance
wavenumbers / cm-1

(b)

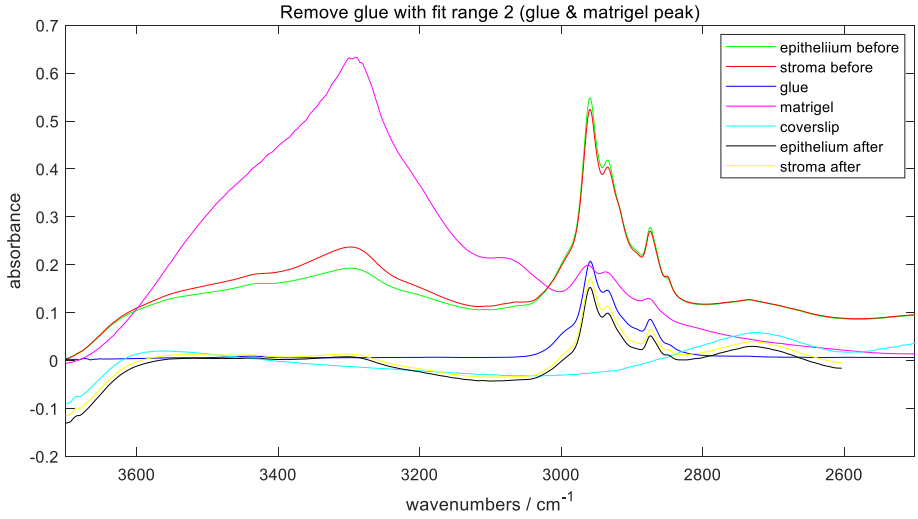
Remove glue with fit range 2 (glue & matrigel peak)
epitheliium before
stroma before
glue
matrigel
coverslip
epithelium after
stroma after
absorbance
wavenumbers / cm-1

(c)

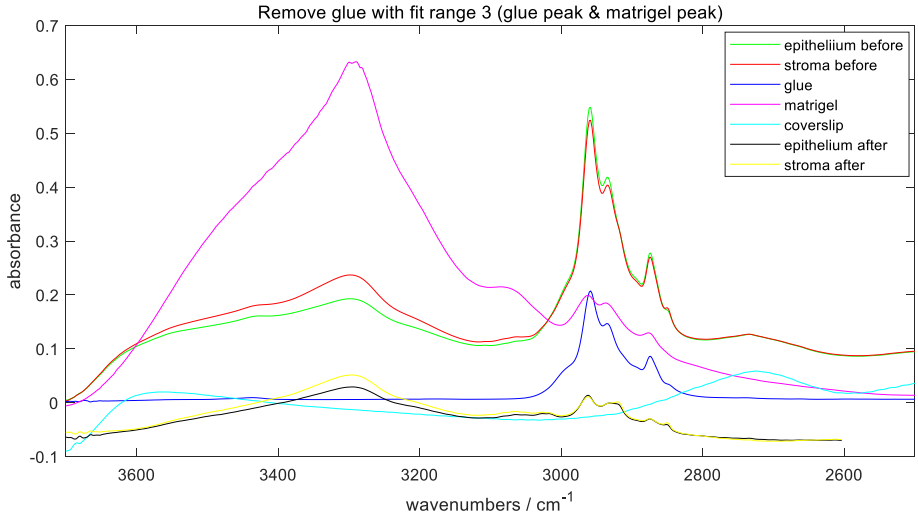
Remove glue with fit range 3 (glue peak & matrigel peak)
epitheliium before
stroma before
glue
matrigel
coverslip
epithelium after
stroma after
absorbance
wavenumbers / cm-1

(d)

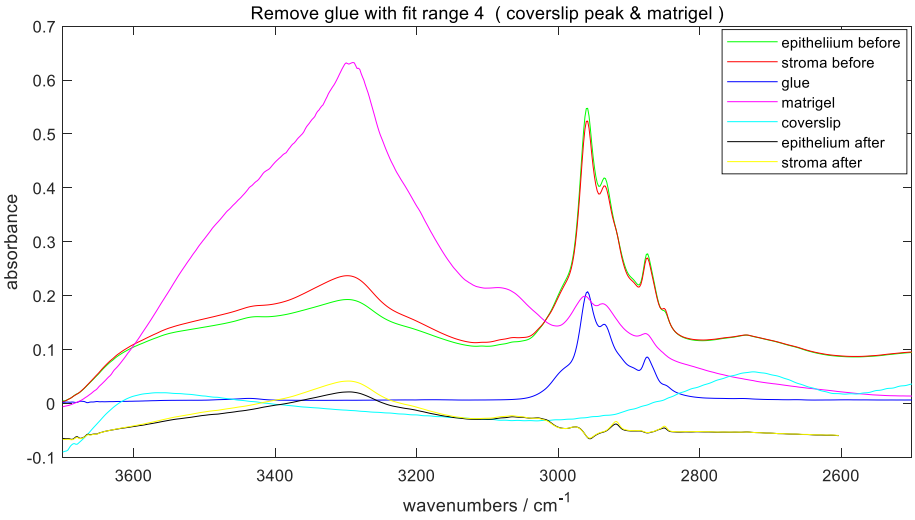

Figure5. 3(a)The spectral results of glue removal in the fit range 1 (3278-3318 cm^{-1}, 3066-3106 cm^{-1}); (b) The spectral results of glue removal in fit range 2 (2848-2852 cm^{-1}, 3415-3455 cm^{-1}); (c) The spectral results of glue removal in the fit range 3 (2950-2970 cm^{-1} 2925-2945cm^{-1}, 2867-2887 cm^{-1}); (d) The spectral results of glue removal in the fit range 4 (3536-3576 cm^{-1}, 2704-2744 cm^{-1}).

(a)

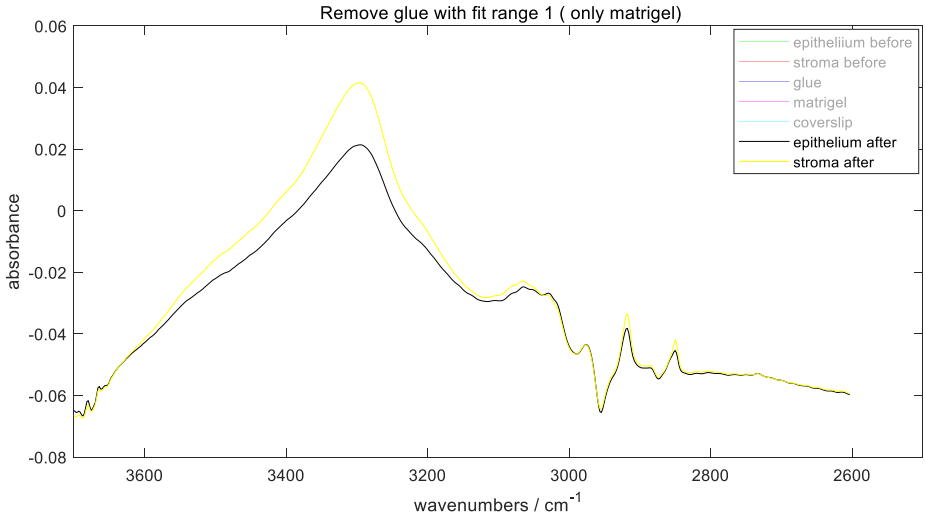
Remove glue with fit range 1 (only matrigel)
epitheliium before
stroma before
glue
matrigel
coverslip
epithelium after
stroma after
absorbance
wavenumbers / cm-1

(b)

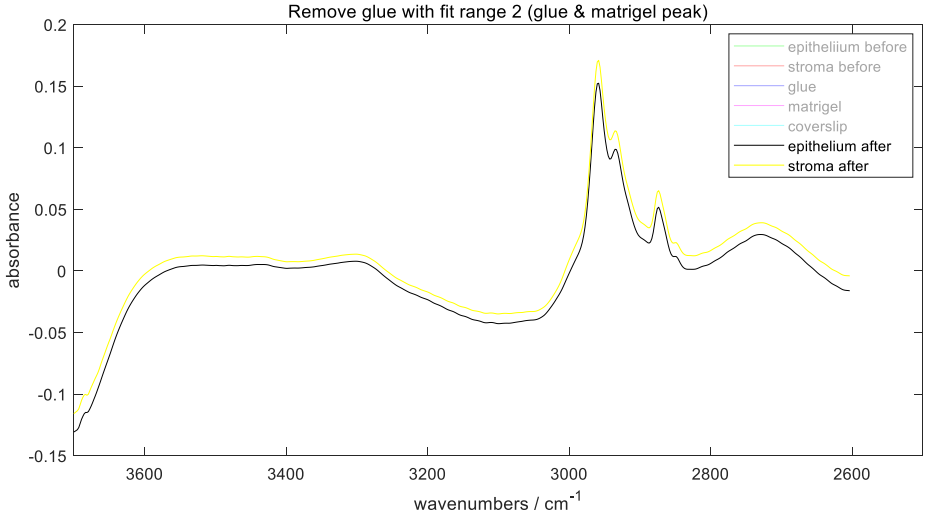
Remove glue with fit range 2 (glue & matrigel peak)
epitheliium before
stroma before
glue
matrigel
coverslip
epithelium after
stroma after
absorbance
wavenumbers / cm-1

(c)

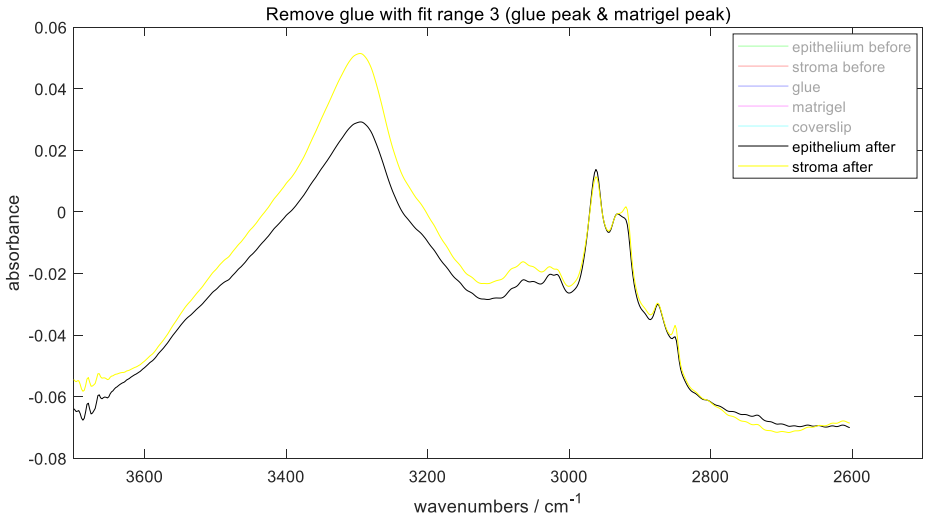
Remove glue with fit range 3 (glue peak & matrigel peak)
epitheliium before
stroma before
glue
matrigel
coverslip
epithelium after
stroma after
absorbance
wavenumbers / cm-1

(d)

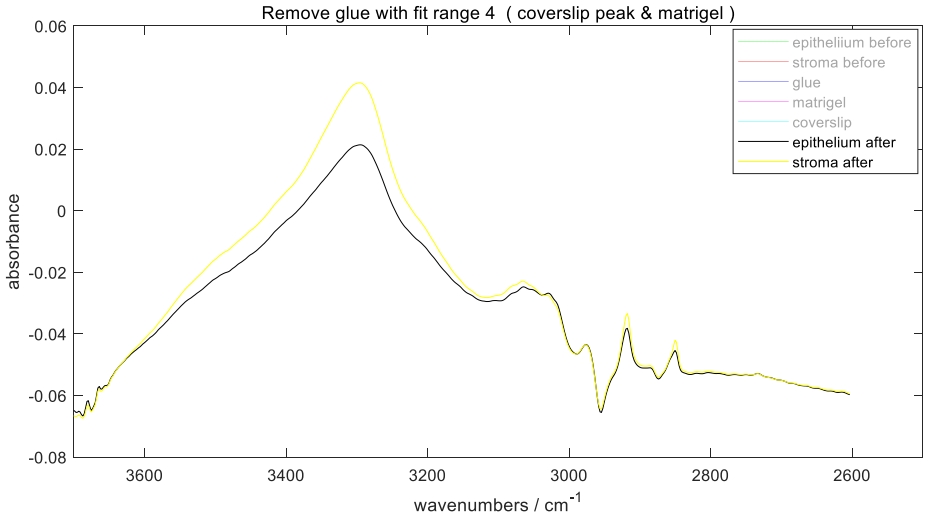

Figure5. 4 (a)The spectra of epithelium and stroma in experiment 2 with glue removal in the fit range 1 (3278-3318 cm^{-1}, 3066-3106 cm^{-1}); (b) The spectra of epithelium and stroma in experiment 2 with glue removal in the fit range 2 (2848-2852 cm^{-1}, 3415-3455 cm^{-1}); (c) The spectra of epithelium and stroma in experiment 2 with glue removal in the fit range 3 (2950-2970 cm^{-1}, 2925-2945 cm^{-1}, 2867-2887 cm^{-1}); (d) The spectra of epithelium and stroma in experiment 2 with glue removal in the fit range 4 (3536-3576 cm^{-1}, 2704-2744 cm^{-1}).

According to figure 5.3 and 5.4, comparing the spectra of epithelium and stroma before and after the glue removal, it is easy to see that in fit ranges 1, 3, 4, the shape of spectra after glue removal are similar to the Matrigel spectrum and the intensity on lipid range is also reduced. Therefore, the code of glue removal is working. While in fit range 2, the shape of spectra is totally distorted. Hence, the fit range 2 (2848-2852 cm^{-1}, 3415-3455 cm^{-1}) are not suitable for glue removal. The spectral results of glue removal in all fit ranges 1, 3, 4 are shown in figure 5.5.

(a)

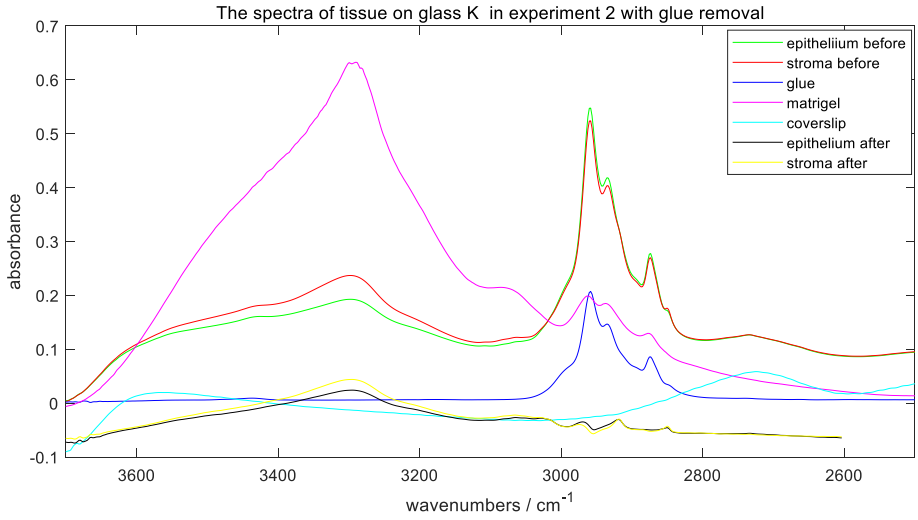

(b)

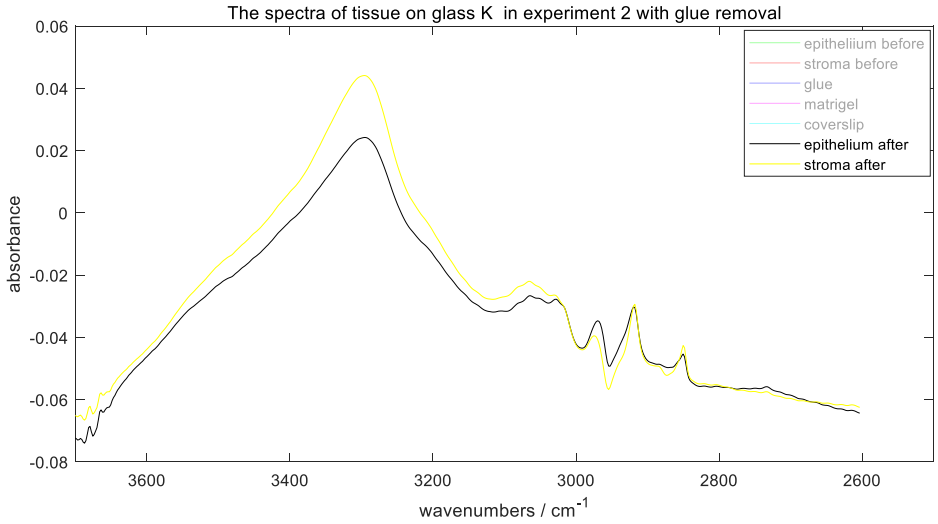

Figure5. 5 (a) The spectral results of glue removal in experiment 2 in the fit range 1, 3, 4. (b) The spectra of epithelium and stroma in experiment 2 with glue removal in the fit range 1, 3, 4.

For experiment 2, there is a significant effect in 3400 – 3600 cm^{-1} caused by coverslip and small positive peak, located at in 3400 – 3450 cm^{-1} is caused by glue. According to figure 5.5, it could be found that after removing glue, the two bands are removed, and the intensity of lipid range is also reduced. After removing glue, the final shape of the spectra is similar to the Matrigel spectrum. Therefore, the fit range 1(3278-3318 cm^{-1}, 3066-3106 cm^{-1}), fit range 3 (2950-2970 cm^{-1}, 2925-2945 cm^{-1}, 2867-2887 cm^{-1}), fit range 4 (3536-3576cm^{-1}, 2704-2744cm^{-1}) are reasonably reliable and could be used for glue removal.

5.2 Glue removal with different reference spectra

Two different glue removal methods are tested to obtain the best spectral results, with the main difference between them being the reference spectra. The spectrum of Matrigel is used as reference spectrum in method 1, and the spectra of sample in experiment 1 are used as reference spectra in method 2. The comparison of the two methods is shown in table 5.1.

Table5. 1 Comparison between two methods of glue removal.

	Reference spectra
Method 1	Matrigel (M), Glue (G), Coverslip (C)
Method 2	Spectra in Experiment 1, Glue (G), Coverslip (C)

The spectrum of Matrigel is regarded as the standard spectrum of the tissue sample, and however, it is not the real standard spectrum of tissue. According to table 3.3, the spectral information in experiment 1 is tissue plus or minus some glue. Although the spectra in experiment 1 are not precise tissue spectra, it is feasible to remove the glue by calculation.

5.2.1 The function of method 2

Figure 5.6 is a schematic diagram of measuring tissue samples in two experimental methods. And the comparison of spectral information in two experiments is shown in table 3.3. Ideally, the thickness of the tissue sample is consistent. But the normal prostate tissue has cylindrical epithelium, the thickness of the sample tissue is varied.

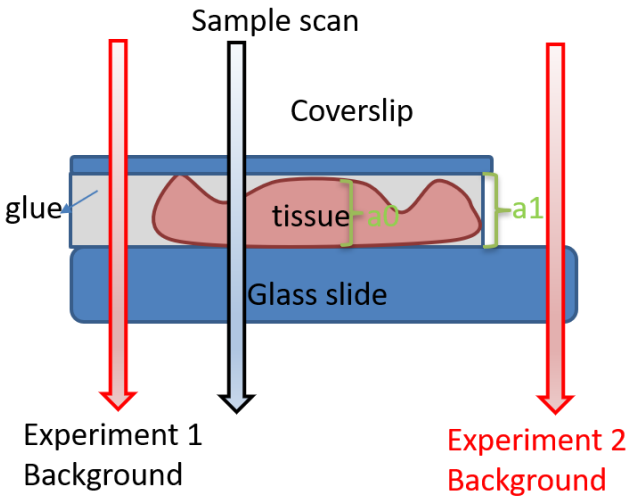

Figure5. 6 Schematic diagram of measuring tissue samples in different experimental methods

According to figure 5.6 and table 3.3, the absorbance of background spectra for experiment 1 is,

$$A_{bkg1}(\tilde{\upsilon}) = \mathrm{a}_1\, \mathrm{A'}_{\mathrm{glue}}(\tilde{\upsilon}) + \mathrm{A'}_{\mathrm{coverslip}}(\tilde{\upsilon}) + D(\tilde{\upsilon}) \quad (5\text{-}9)$$

And the absorbance of background spectra for experiment 2 is,

$$A_{bkg2}(\tilde{\upsilon}) = D(\tilde{\upsilon}) \quad (5\text{-}10)$$

While the absorbance of the sample scan,

$$A_{sample}(\tilde{\upsilon}) = (\mathrm{a}_1 - \mathrm{a}_0)\, \mathrm{A'}_{\mathrm{glue}}(\tilde{\upsilon}) + \mathrm{a}_0\, \mathrm{A'}_{\mathrm{tissue}}(\tilde{\upsilon}) + \mathrm{A'}_{\mathrm{coverslip}}(\tilde{\upsilon}) + D(\tilde{\upsilon}) \quad (5\text{-}11)$$

Where a_0 and a_1 are the thickness of the tissue and glue layer on blank area, respectively. $\mathrm{A'}_{\mathrm{glue}}(\tilde{\upsilon})$ and $\mathrm{A'}_{\mathrm{coverslip}}(\tilde{\upsilon})$ are the absorbance of the pure glue and clear coverslip, respectively. $\mathrm{A'}_{\mathrm{tissue}}(\tilde{\upsilon})$ is the absorbance of tissue. $D(\tilde{\upsilon})$ is the absorbance of glass slide.

The spectral result is the absorbance of the sample scan to remove the background. Therefore, the absorbance of spectra in experiment 1 is,

$$A_{exp1}(\tilde{\upsilon}) = \mathrm{a}_0\, \mathrm{A'}_{\mathrm{tissue}}(\tilde{\upsilon}) - \mathrm{a}_0\, \mathrm{A'}_{\mathrm{glue}}(\tilde{\upsilon}) \quad (5\text{-}12)$$

While the absorbance of spectra in experiment 2 is,

$$A_{exp2}(\tilde{\upsilon}) = (a_1 - a_0)\, A'_{glue}(\tilde{\upsilon}) + a_0\, A'_{tissue}(\tilde{\upsilon}) + A'_{coverslip}(\tilde{\upsilon}) \qquad (5\text{-}13)$$

There are three reference spectra in the new glue removal method: glue spectra, the spectra of a tissue sample in experiment 1 and coverslip spectra. The spectra in experiment 2 could be written as,

$$A_{exp2}(\tilde{\upsilon}) = k_1 a_1\, A'_{glue}(\tilde{\upsilon}) + k_2\, A_{exp1}(\tilde{\upsilon}) + k_3 A'_{coverslip}(\tilde{\upsilon}) \qquad (5\text{-}14)$$

Combine the function (5-12) and (5-14), the real absorbance of the tissue is

$$k_2 a_0\, A'_{tissue}(\tilde{\upsilon}) = A_{exp2}(\tilde{\upsilon}) - (a_1 k_1 - a_0 k_2)\, A'_{glue}(\tilde{\upsilon}) - k_3 A'_{coverslip}(\tilde{\upsilon}) \qquad (5\text{-}15)$$

Where k_1, k_2, and k_3 are the scaling factors for the three reference spectra, respectively.

In general, the thickness of tissue and glue vary slightly, so they can be assumed to be the same thickness ($a_1 \approx a_0$), then

$$k_2 a_0\, A'_{tissue}(\tilde{\upsilon}) = A_{exp2}(\tilde{\upsilon}) - (k_1 - k_2)\, a_0 A'_{glue}(\tilde{\upsilon}) - k_3 A'_{coverslip}(\tilde{\upsilon}) \qquad (5\text{-}16)$$

The least-squares with known covariance (LSCOV) in Matlab are used to obtain the scaling factors. The glue removal code of method 2 could be made by function (5-16).

5.3 Spectral results with two glue removal methods

The objective is to focus on the impact of glass types on cancer detection. Therefore, there are two groups of tissue samples. One group is a series of adjacent benign prostatic hyperplasia (BPH) tissue sections mounted on the 12 glass slides and stained with H&E. The information of the 12 glass slides has already be given in table 3.2. To quickly describe, the 12 glass slides are labelled (A, B, C…, L).

The other group is a series of adjacent tissue slices mounted on the 6 glass slides from 4 patients. Two patients have benign prostate hyperplasia (BPH), and the other 2 patients have prostate cancer (CaP). The charged glass slide is more suitable for tissue work, which has been explained in Chapter 4, but there is no description of the use of glass G for tissue work in the introduction. Therefore, only glass slides D, E, F, J, K, and L are selected for tissue work.

The experimental processes have been shown in chapter 3. The first group of tissue samples is to study the effect of type of glass slide on tissue classification (Study 2). While the second group is to find the influence of the type of glass slide on cancer detection (Study 3). According to the group of the tissue sample, the spectral results of glue removal are mainly shown in two sections (5.3.1 and 5.3.2).

5.3.1 Glue removal for BPH samples on 12 glass slides (Study 2).

The main objective of the BPH samples on 12 glass slides is to research the effect of glass type on tissue classification. So all spectra are divided into stromal and epithelial spectra. The prostate tissue sections are cut from the same BPH patient. The 12 tissue samples and the brightfield image of the whole tissue section on glass A are shown in figure 3.5 and figure 3.6. Because it would take a long time to measure the whole tissue section (around 7 h), only two regions are selected to measure for every sample, see figure 3.6.

Quality control is based on the intensity of amide A peak, which means the intensity of amide A for good quality spectra on tissue area must be higher than the highest intensity in the tissue-free area, which is set as a threshold. The quality control threshold for experiments 1 and 2 are 0.054 and 0.06, respectively.

The different thresholds of the two experiments are due to the different background scans. The number of annotated spectra before and after quality control for experiment 1 and experiment 2 is shown in table 5.2. According to the table, the number of epithelium spectra is more dramatically reduced than that of the stroma. The threshold has more influence on the quality of spectra of epithelium. Therefore, the number of spectra of the stroma is much more than the spectra of epithelium. All of the epithelium spectra are used in further analysis.

Table5. 2 The number of annotated spectra on 12 glass slides before threshold

	The number of annotated spectra					
Glass type	Annotated spectra before quality control		Experiment 1 after quality control with threshold is 0.054		Experiment 2 after quality control with threshold is 0.06	
	Stroma	Epithelium	Stroma	Epithelium	Stroma	Epithelium
Glass A	7526	3704	7526	3502	7526	3222
Glass B	6667	3990	6666	3643	6667	3765
Glass C	8519	4321	8519	3902	8519	3909
Glass D	6118	3612	6118	3128	6118	3232
Glass E	7156	4231	7155	3857	7155	3939
Glass F	6966	4585	6966	4320	6966	4368
Glass G	7493	4860	7493	4705	7493	4676
Glass H	9526	4751	9525	4093	9525	4139
Glass I	6362	4330	6362	3692	6362	3859
Glass J	7443	4200	7443	3779	7443	3918
Glass K	8765	4551	8765	4041	8765	4245
Glass L	7419	5164	7419	4541	7419	4693

5.3.1.1 The mean spectra of epithelium and stroma on 12 glass slides.

The mean spectra of histological classes for two experiments are shown in figure 5.7. According to figure 5.7, in both experiment 1 and experiment 2, there is one prominent peak at amide A (3298 cm^{-1}) and three lipid peaks (2958 cm^{-1}, 2935 cm^{-1}, 2873 cm^{-1}) for all of the mean spectra on 12 glass slides. But according to the spectra of glue (figure 5.2), the glue has a significant effect on the lipid region and has a minor influence at 3400 – 3450 cm^{-1}. Only the amide A peak is caused by tissue. Therefore, these infrared regions can be used to evaluate the result of glue removal.

The lipid region and the broad peak (3400 - 3600 cm^{-1}) are the differences between

experiments 1 & 2. According to table 3.3, the spectra contain coverslip, glue, and tissue information for experiment 2. While for experiment 1, the spectra only have the information from tissue minus or plus some glue. Therefore, there are some negative peaks in lipid regain and 3400 – 3450 cm^{-1}. They have come from the redundant removed glue spectra from the background. In addition, according to the spectra of coverslip and glue (figure 5.2), the broad peak (3400 – 3600 cm^{-1}) in experiment 2 is mainly from the coverslip.

Comparing the mean spectra of two experiments without glue removal, the spectral intensity in experiment 1 is higher than in experiment 2. Within the same experiment, the intensity of spectra from stroma is always higher than from epithelium.

(a) (b)

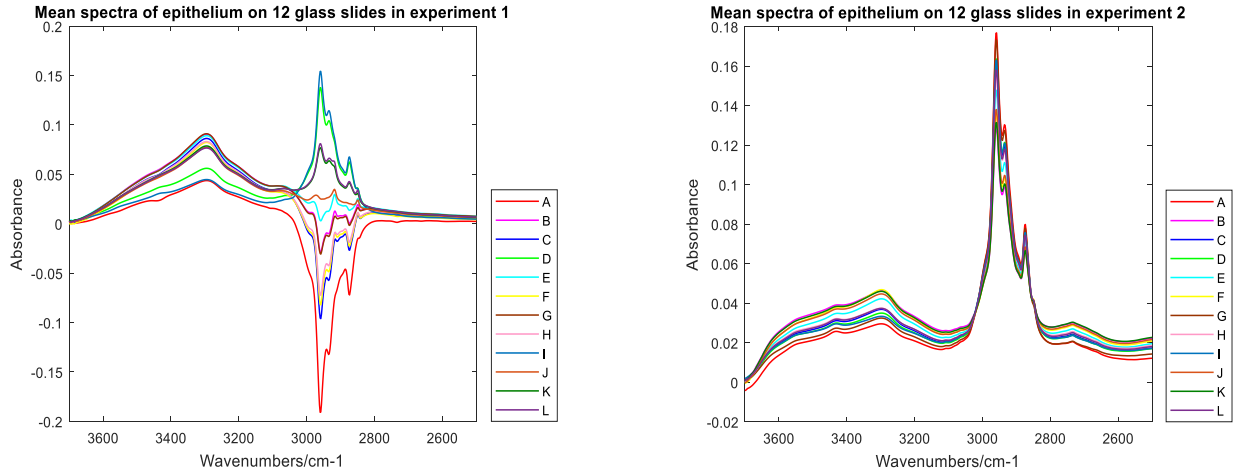

(c) (d)

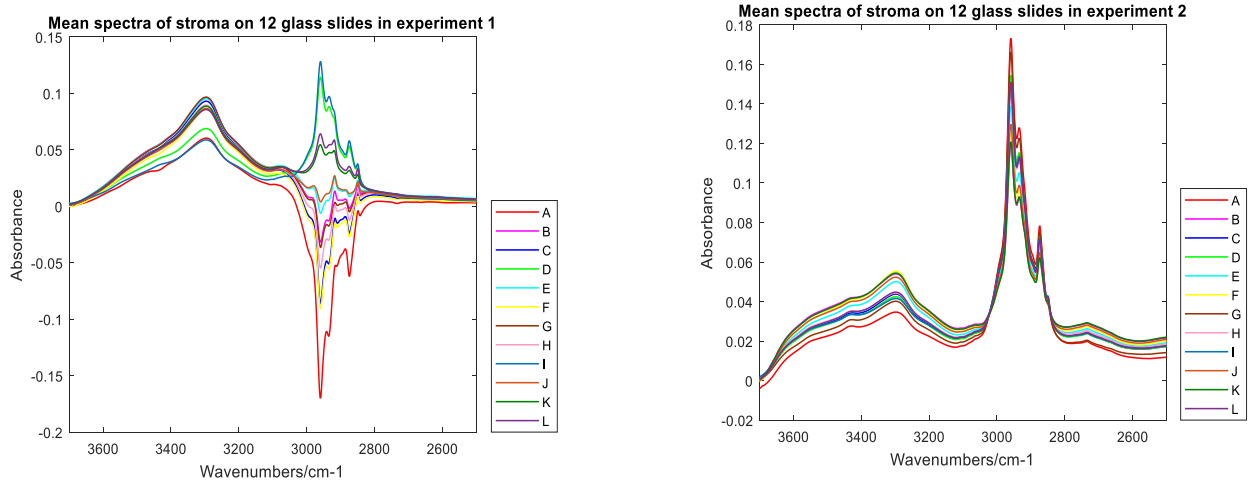

Figure5. 7 (a) Mean spectra of epithelium on 12 glass slides in 2500-3700 cm^{-1} for experiment 1. (b) Mean spectra of epithelium on 12 glass slides in 2500-3700 $cm^{-1}$for experiment 2.(c) Mean spectra of stroma on 12 glass slides in 2500-3700 cm^{-1} for experiment 1. (d) Mean spectra of stroma on 12 glass slides in 2500-3700 cm^{-1} for experiment 2.

5.3.1.2 The result of glue removal for glass F by glue removal method 1.

To indicate the results of glue removal with different methods, the spectra on glass F are used as an example for further comparison. Figure 5.8 shows the results of experiment 1 with glue removal method 1. The reference spectra of method 1 are Matrigel spectrum, glue spectra and coverslip spectra (figure 5.8(a)).

(a)

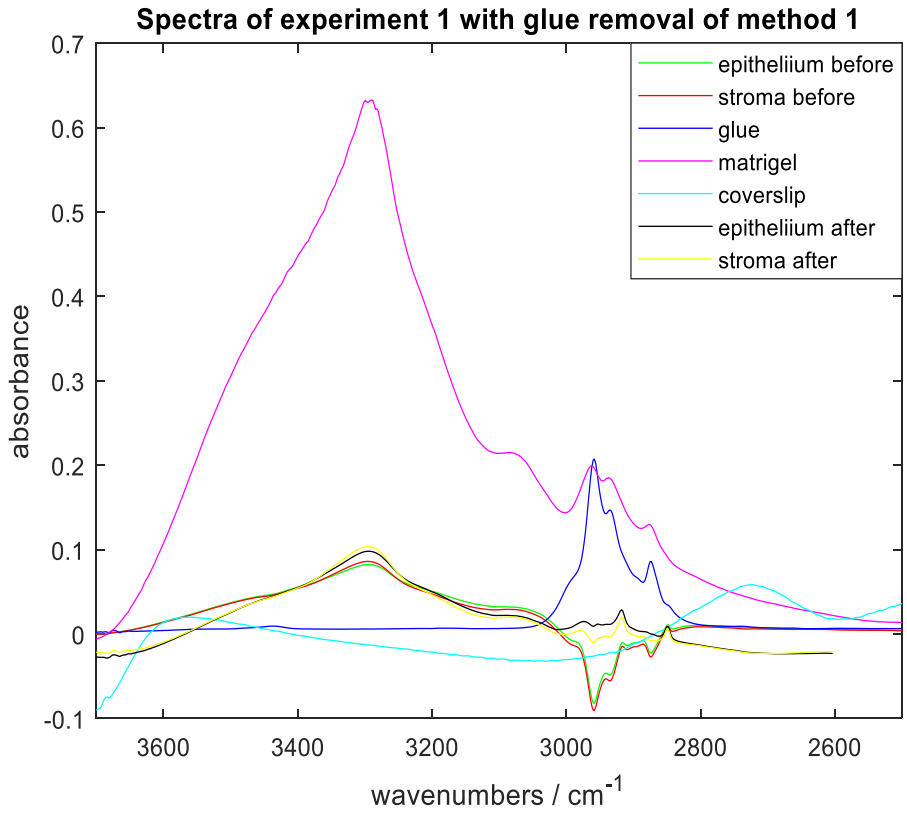
Spectra of experiment 1 with glue removal of method 1
epitheliium before
stroma before
glue
matrigel
coverslip
epitheliium after
stroma after
absorbance
0.7
0.6
0.5
0.4
0.3
0.2
0.1
0
-0.1
3600
3400
3200
3000
2800
2600
wavenumbers / cm-1

(b)

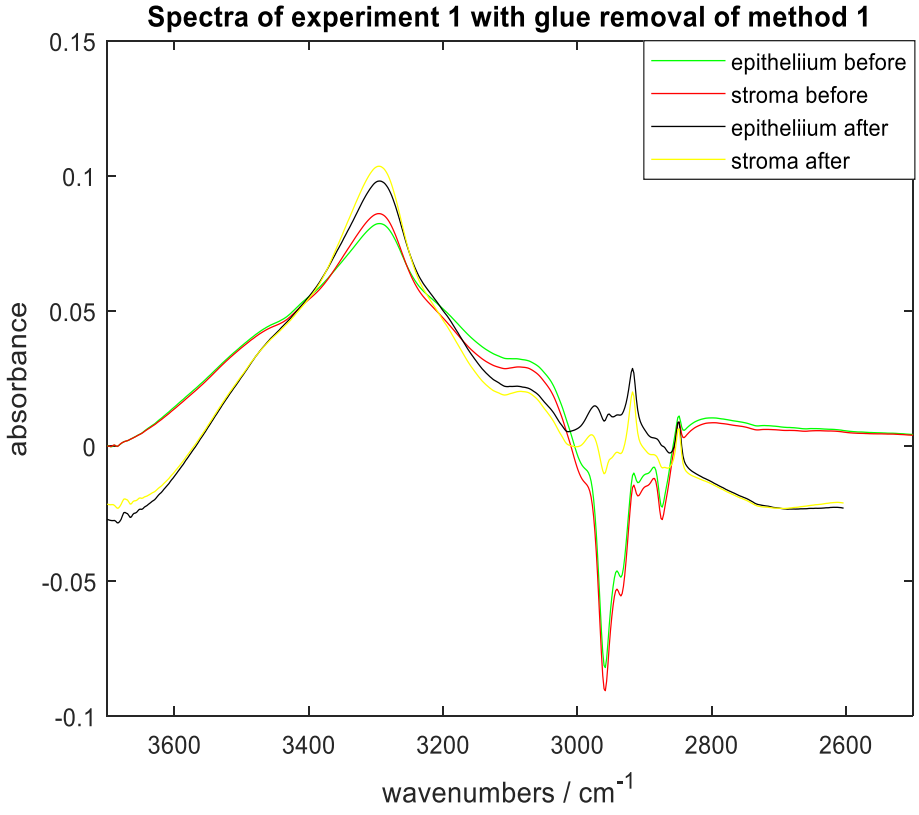
Spectra of experiment 1 with glue removal of method 1
epitheliium before
stroma before
epitheliium after
stroma after
absorbance
0.15
0.1
0.05
0
-0.05
-0.1
3600
3400
3200
3000
2800
2600
wavenumbers / cm-1

Figure5. 8 (a) shows the reference spectra and glue removal results of experiment 1 on glass F by method 1. (b) enlarge the glue removal results of experiment 1 on glass F by method 1.

Figure 5.8 compares the spectra before and after removing glue of experiment 1 by glue removal method 1. According to table 3.3, the spectra of experiment 1 contain the information of tissue minus or plus some glue. It all depends on the amount of glue in the background. According to figure 5.8, there are negative peaks in the lipid region and 3400-3450 cm^{-1}. It means the spectra are removed with more glue from the background. For glass F, the glue removal code's real objective is to eliminate the negative peaks. After glue removal, the epithelium and stroma spectra changed to the positive peak in the lipid region, and the shape of the spectra are also similar to the Matrigel spectra. The intensity of amide A is enhanced, and the intensity of stroma is still higher than epithelium.

(a)

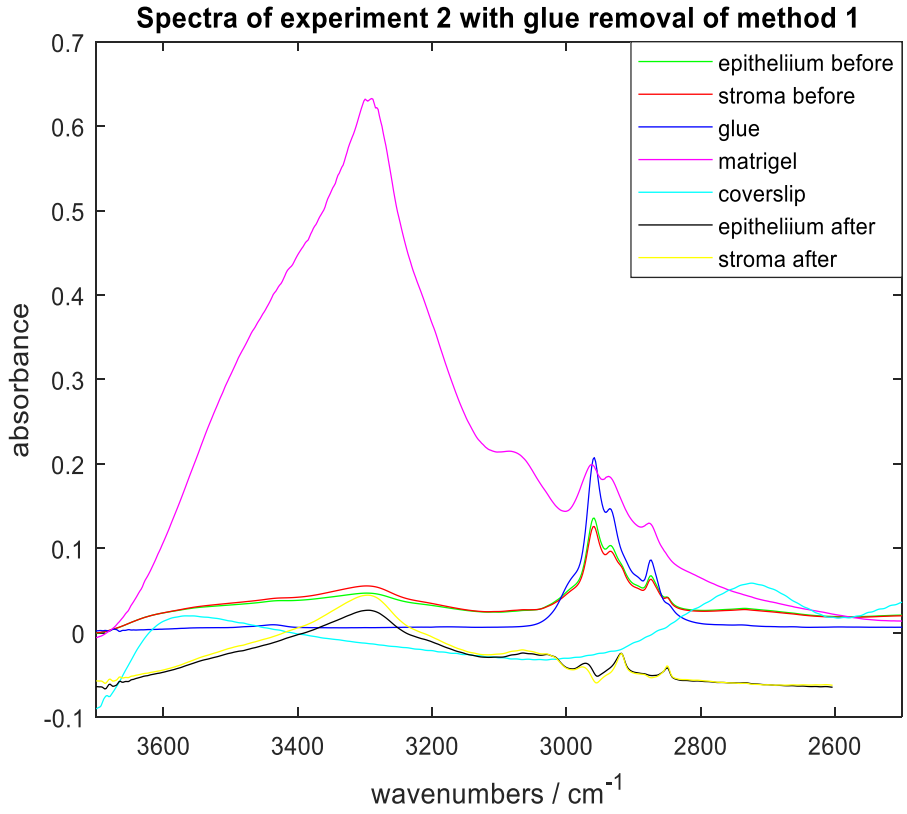

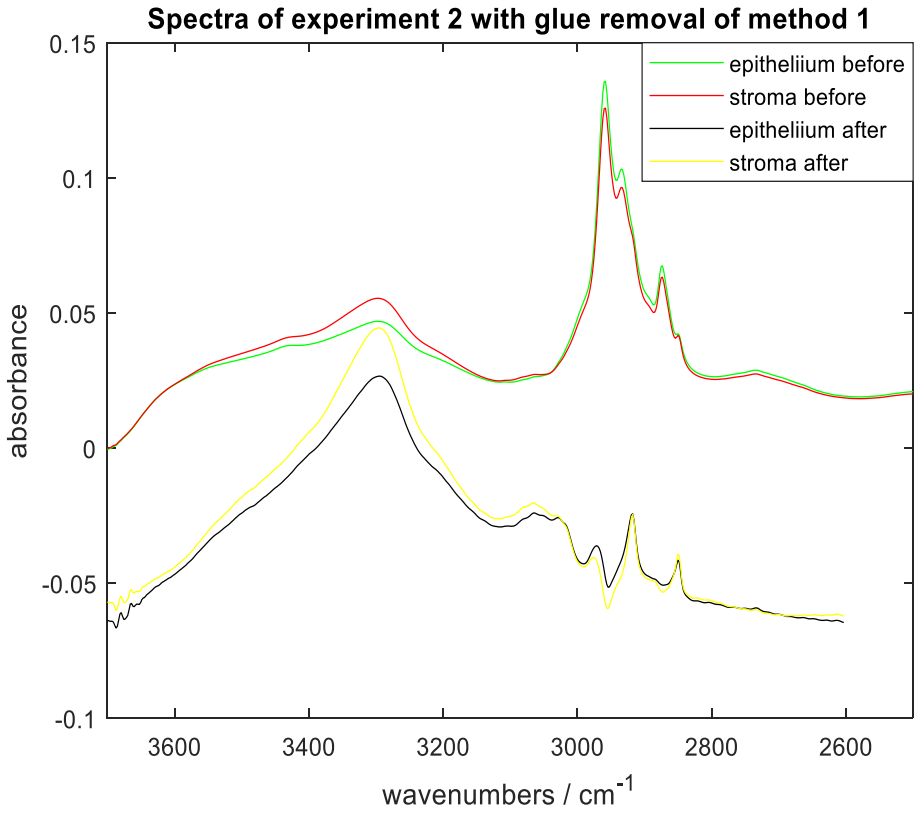

Figure5. 9 (a) shows the reference spectra and glue removal results of experiment 2 on glass F by method 1. (b) enlarge the glue removal results of experiment 2 on glass F by method 1.

According to table 3.3, the spectra of experiment 2 contain the tissue, glue, and coverslip information. Glue has a significant effect on the lipid region and 3400-3450 cm^{-1} and the coverslip has a significant impact in 3400-3600 cm^{-1} and 2700-2750 cm^{-1}. Therefore, the glue removal code for glass F in experiment 2 aims to remove the effect of the glue and the coverslip. Figure 5.9 shows the result of glue removal for experiment 2 on glass F by method 1. After removing glue, the intensity of the lipid region is reduced. The broad band (3400-3600 cm^{-1}) is disappeared, and the shape of spectra is close to Matrigel spectra, in which the intensity of amide A changes to higher than lipid. Therefore, the code of glue removal has worked in the spectra of experiment 2. In addition, after glue removal, the spectral intensities for both epithelium and stroma are lower than the original spectra.

5.3.1.3 The result of glue removal for glass F by glue removal method 2.

The references of glue removal method 2 are the spectra of the same glass in experiment 1, glue and coverslip. Figure 5.10 shows the spectra on glass F, so the reference is spectral data of glass F in experiment 1, glue and coverslip (figure 5.10 (a)). As mentioned, the objectives of the original spectra in experiment 2 are to remove the effect of glue and coverslip. According to figure 5.10 (b), after eliminating glue, the intensity of lipid has been reduced to lower than amide A, and the slight peak in 3400-3450 cm^{-1} has also disappeared. The glue could be regarded as being removed. However, the broad band in 3400-3600 cm^{-1} and small peak in 2700-2750 cm^{-1} are still existing in spectra after glue removal, which indicates that method 2 glue removal does not perform well for removing the effect of the coverslip.

(a)

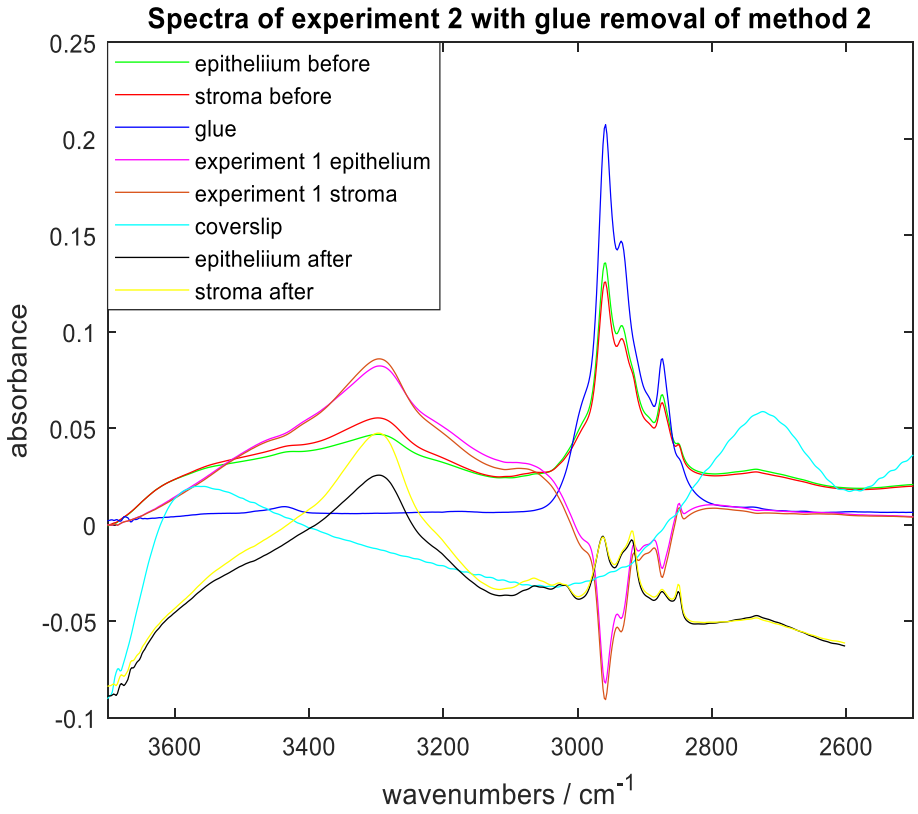

(b)

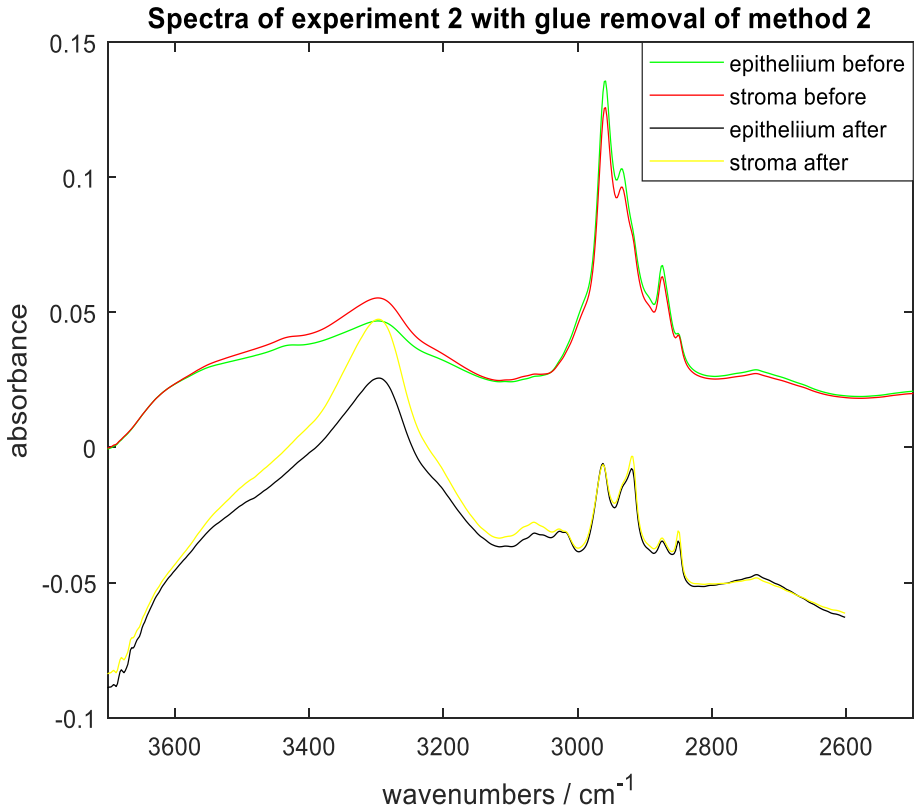

Figure5. 10 (a) shows the reference spectra and glue removal results of experiment 2 on glass F by method 2. (b) enlarge the glue removal results of experiment 2 on glass F by method 2.

The fit ranges of glue removal method 2 are the same range as method 1, but the fit ranges in method 1 are based on Matrigel, glue and coverslip. Method 2 does not use the Matrigel spectra as a reference. Therefore, new fit ranges for method 2 also is tested. Similar to the fit range in method 1, the new fit ranges are similarly divided into four types:

New fit range 1, where tissue spectra are only contributed by experiment 1's tissue spectra (3258-3338 cm^{-1}, 3050-3090 cm^{-1});

New fit range 2, where tissue spectra are contributed by the absorption of glue and experiment 1's tissue spectral peaks (2846-2854 cm^{-1}, 3422-3442 cm^{-1});

New fit range 3, where tissue spectra are contributed by the glue peak and experiment 1's tissue spectral peaks (2950-2970cm^{-1}, 2925-2945cm^{-1}, 2867-2887cm^{-1});

New fit range 4, where tissue spectra are contributed by the absorption of coverslips and experiment 1's tissue spectral peaks (3546-3586 cm^{-1}, 2704-2744 cm^{-1}).

Compared with the old four fit ranges, the new fit ranges are larger. Because the spectra of the same glass slide in experiment 1 have more overlap ranges with the spectra in experiment 2 than Matrigel. All spectral results with method 2 using the new fit range are shown in figure 5.11.

According to the results in section 5.1.3, the suitable fit ranges are fit ranges 1, 3 and 4. Therefore, figure 5.11 compares the glue removal results of the new fit ranges 1, 2, 3, 4 with new fit ranges 1, 3, 4. According to the spectral results, no matter how the fit ranges are changed, the broad bands in 3400-3600 cm^{-1}, caused by a coverslip, still exist. In addition, the intensities of lipid in some spectra are still very high, and the small peaks in 3400 -3450 cm^{-1} are not removed. It means the effects of glue in some glass slides are not totally removed. The glue removal method 2 does not perform better than method 1.

Thus, the spectral contribution of the coverslip and some glue still exists after glue

removal by method 2, and the new fit range still does not improve the glue removal results. Therefore, the old fit ranges (1, 3, and 4) will still be used in the next section.

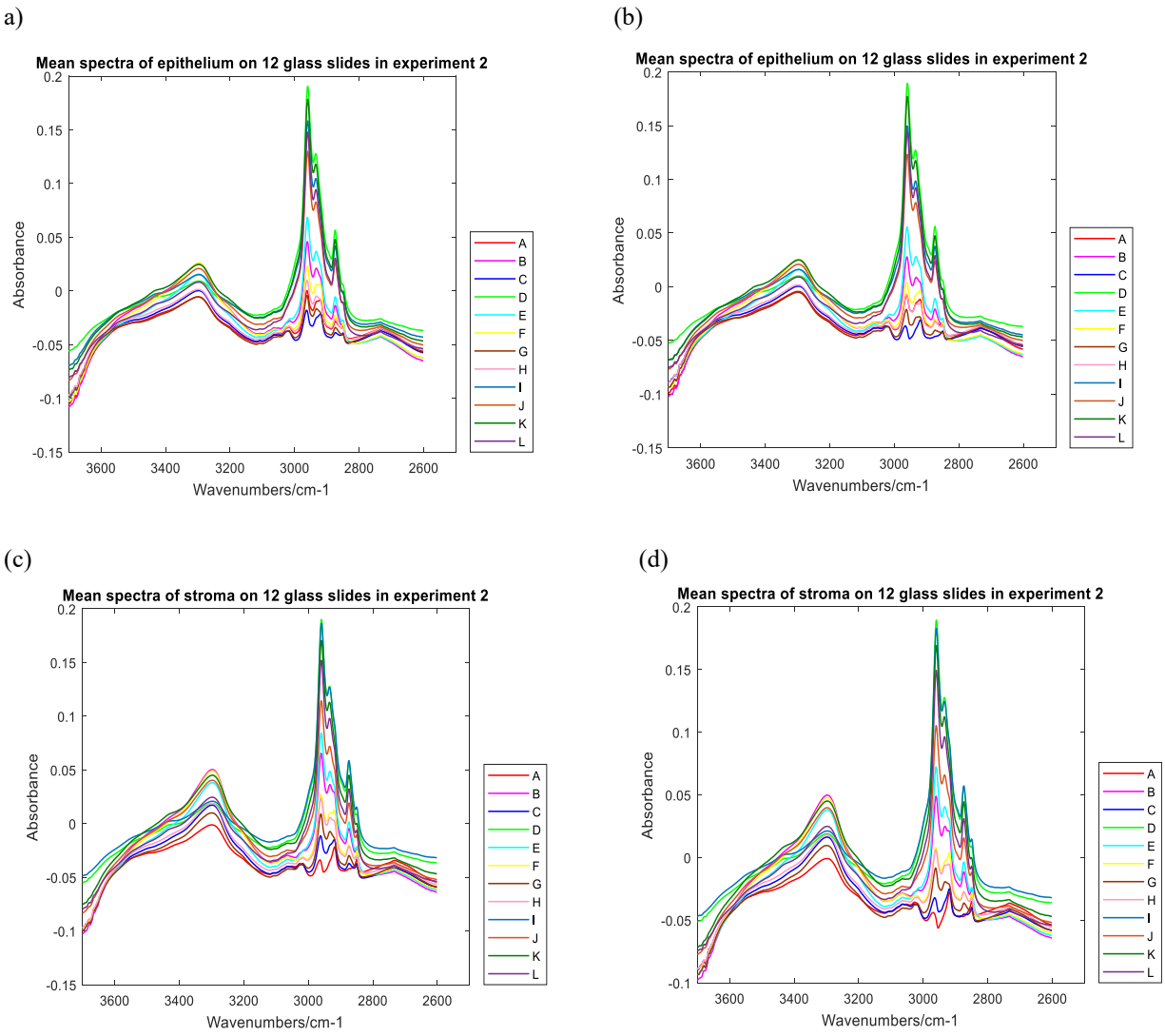

Figure5. 11 (a) Mean spectra of epithelium on 12 glass slides after glue removing with method 2 in new fit range 1, 2, 3, 4. (b) Mean spectra of epithelium on 12 glass slides after glue removing with method 2 in new fit range 1, 3, 4. (c) Mean spectra of stroma on 12 glass slides after glue removing with method 2 in new fit range 1, 2, 3, 4. (d) Mean spectra of stroma on 12 glass slides after glue removing with method 2 in new fit range 1, 3, 4.

5.3.1.4 The mean spectral result of glue removal for 12 glass slides

Comparing the spectral results of glue removal with two methods, method 1 has better performance than method 2. It means that the spectrum of Matrigel is more suitable as

the reference. For two experiments with method 1, figure 5.12 shows the glue removal result for all spectra on 12 glass slides. Compared with figure 5.7, all of the negative peaks of the original spectra in experiment 1 have changed to positive peaks. While for experiment 2, the prominent broad bands in 3400-3600 cm^{-1} in original spectra are removed. This means the glue removal code has reduced the effect of the coverslip. For experiment 2, the intensities of lipid have changed to similar to Matrigel after removing glue by method 1. However, the small peaks in 3400-3450 cm^{-1} are not very smooth as the results in experiment 1. In addition, the spectral intensities of epithelium and stroma in experiment 1 are higher than those in experiment 2. It means the spectra with glue removal method 1 in experiment 1 are more suitable for further studies.

(a)

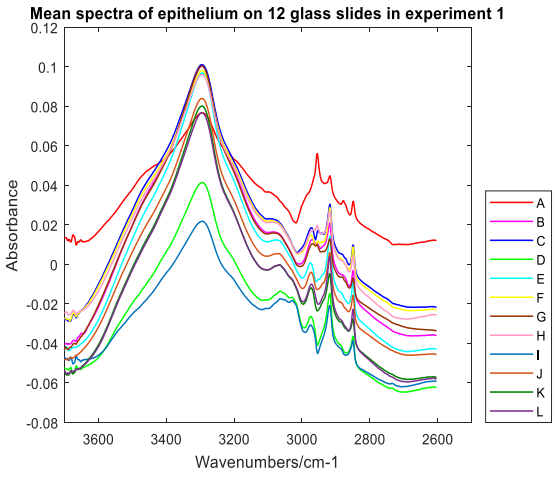

(b)

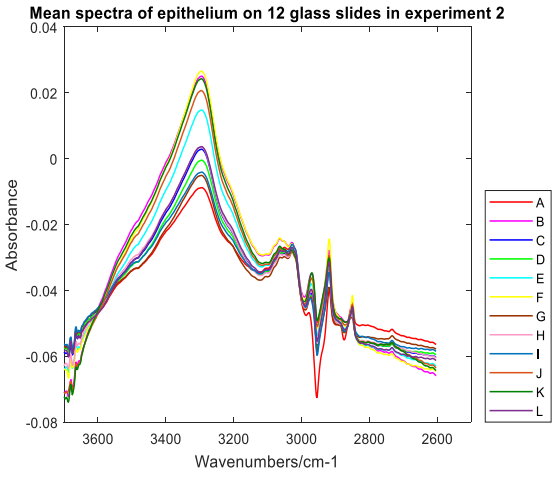

(c)

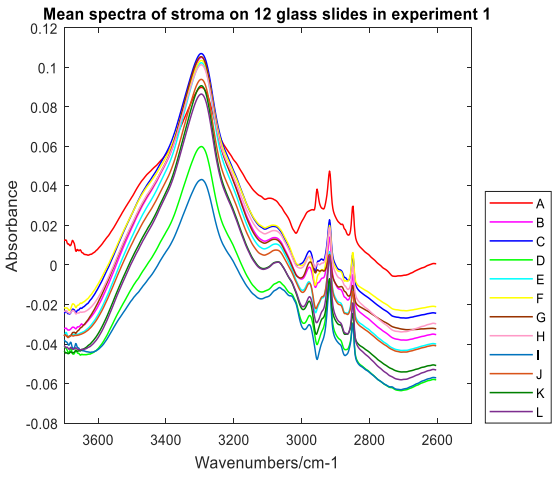

(d)

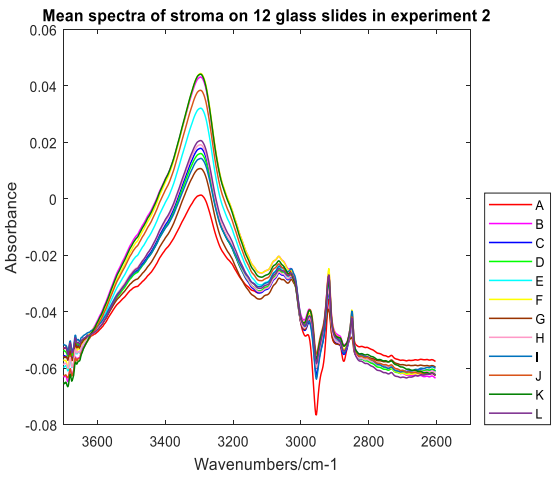

Figure5. 12 (a) Mean spectra of epithelium on 12 glass slides for experiment 1 after glue removing with method 1. (b) Mean spectra of epithelium on 12 glass slides for experiment 2 after glue removing with method 1. (c) Mean spectra of stroma on 12 glass slides for experiment 1 after glue removing with method 1. (d) Mean spectra of stroma on 12 glass slides for experiment 2 after glue removing with method 1.

5.3.2 Glue removal for BPH & CaP samples on 6 glass slides (Study 3)

The previous section shows glue removal is working for BPH samples on different types of glass slides. This section aims to test glue removal results on cancer samples.

A series of adjacent tissue slices mounted on these 6 glass slides are from 4 patients, of which two patients have benign prostate hyperplasia (BPH), and the other two patients have prostate cancer (CaP). And the information of four patients is shown in table 3.5. All of the samples are still measured by experiments 1 and 2, and the difference between the two experiments is shown in table 3.3. The experimental and data analysis processes are shown in section 3.5.3 in chapter 3.

This chapter aims to compare the different methods of glue removal and find a suitable glue removal method for further study. The previous section shows that the glue removal codes are working for the spectra of epithelium and stroma on 12 glass slides from the same BPH patient. Therefore, this section only shows the glue removal code using the spectra of epithelium on glass E from 4 patients.

The threshold is set as the highest intensity at 3298 cm^{-1} in the blank space to remove spectra from the area without tissue. The threshold of experiment 1 and experiment 2 are 0.012 and 0.050. The number of high-quality annotated epithelium spectra on glass E is shown in table 5.3. And these spectra are used in this section analysis.

Table5. 3 The number of high-quality annotated epithelium spectra on glass E

Epithelium spectra	Experiment 1	Experiment 2
P1(BPH)	8343	8316
P2(BPH)	21644	21438
P3(CaP)	17135	17100
P4(CaP)	9105	9069

5.3.2.1 The mean spectra of epithelium from 4 patients on glass E

Two types of experiments measure all spectra, and the difference between them is shown in table 3.3. Figure5.13 compares the spectra of epithelium from 4 patients before glue removal in two experiments. In 2500-3700 cm^{-1}, there is only one amide A peak and three lipid peaks from tissue, which is located at 3298 cm^{-1} and 2958 cm^{-1}, 2935 cm^{-1}, 2873 cm^{-1}, respectively. Because glue also has contribution to the lipid region, the intensity of lipid peaks is partly related to glue's content. For the spectra of experiment 1, the lipid peaks are sometimes negative, due to removing more glue from the background. While for experiment 2, the backgrounds are blank glass, and the spectra have significant effects on glue and coverslip, which mainly lead to the very high intensities of lipid peaks and a broad band in 3400-3600 cm^{-1}, respectively. In addition, the spectra of cancerous tissue are similar to the normal tissue in both experiments 1 and 2.

According to table 3.3, the glue removal code for experiment 1 is to remove or add some glue. While for experiment 2, the code is used to remove the effect of glue and coverslip. As mentioned, the glue has a particular contribution in three lipid peaks and 3400-3450 cm^{-1}. And coverslip has effects in 3400-3600 cm^{-1} and 2700-2750 cm^{-1}. Therefore, these ranges are used to evaluate the impact of glue removal.

(a) (b)

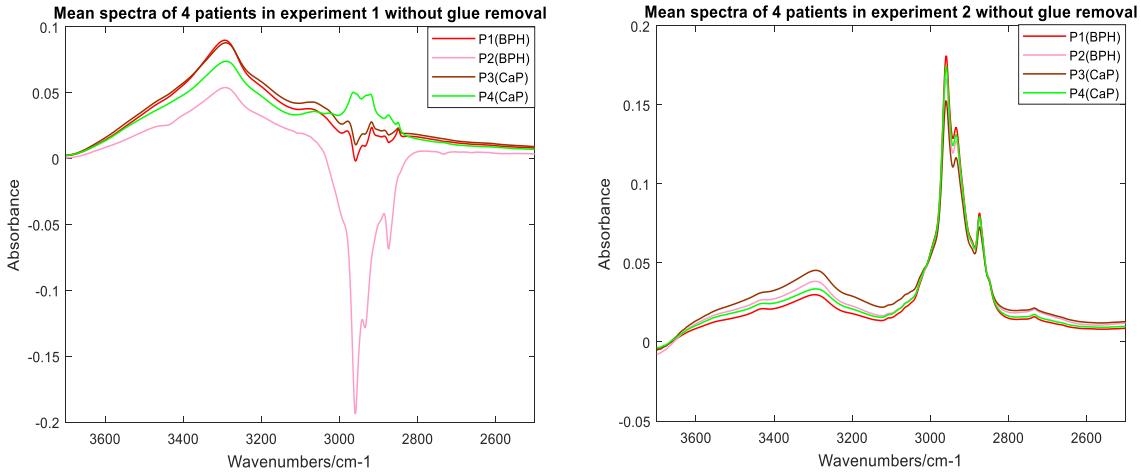

Figure5. 13 (a) Mean spectra of epithelium from 4 patients on glass E for experiment 1 before removing glue. (b) Mean spectra of epithelium from 4 patients on glass E for experiment 2 before removing glue

5.3.2.2 The result of glue removal for glass E by glue removal method 1.

Section 5.3.1 shows that two glue removal methods work for epithelium and stroma spectra on different kinds of glass slides. However, all of the tissue samples are from the same BPH patients. The objective of this section is to determine whether the two glue removal methods work in the spectra from BPH and CaP patients.

The reference of glue removal method 1 are spectra of glue, coverslip and Matrigel. And glue is removed in the fit range 1(3278-3318cm^{-1}, 3066-3106cm^{-1}), fit range 3 (2950-2970cm^{-1}, 2925-2945cm^{-1}, 2867-2887cm^{-1}), fit range 4 (3536-3576cm^{-1}, 2704-2744cm^{-1}), which are consistent with the glue removal method 1 in the previous section.

Figure 5.14 and figure 5.15 shows the mean spectra of epithelium on glass E in experiment 1 after removing glue by method 1 from two BPH patients and two CaP patients, respectively. According to figures 5.14 (a) and 5.15 (a), there is no band in 3400-3600 cm^{-1} and 2700-2750 cm^{-1} before glue removal, it means that coverslip has a more negligible effect on the original spectra of experiment 1 for both BPH and CaP

patients. But except for the P4 (CaP), all original spectra of the lipid region are negative in experiment 1 before glue removal. So the glue removal code aims to add some contribution to the glue. According to figures 5.14 (b) and 5.15 (b), the intensities of the lipid region are increasing to a certain extent. However, some of the lipid peaks are still negative, which means that method 1 does not have a stable glue removal performance. However, for these three patients, the intensity of amide A increases after removing glue, proving the glue removal method 1 is working but doesn't have a stable and great performance.

(a)

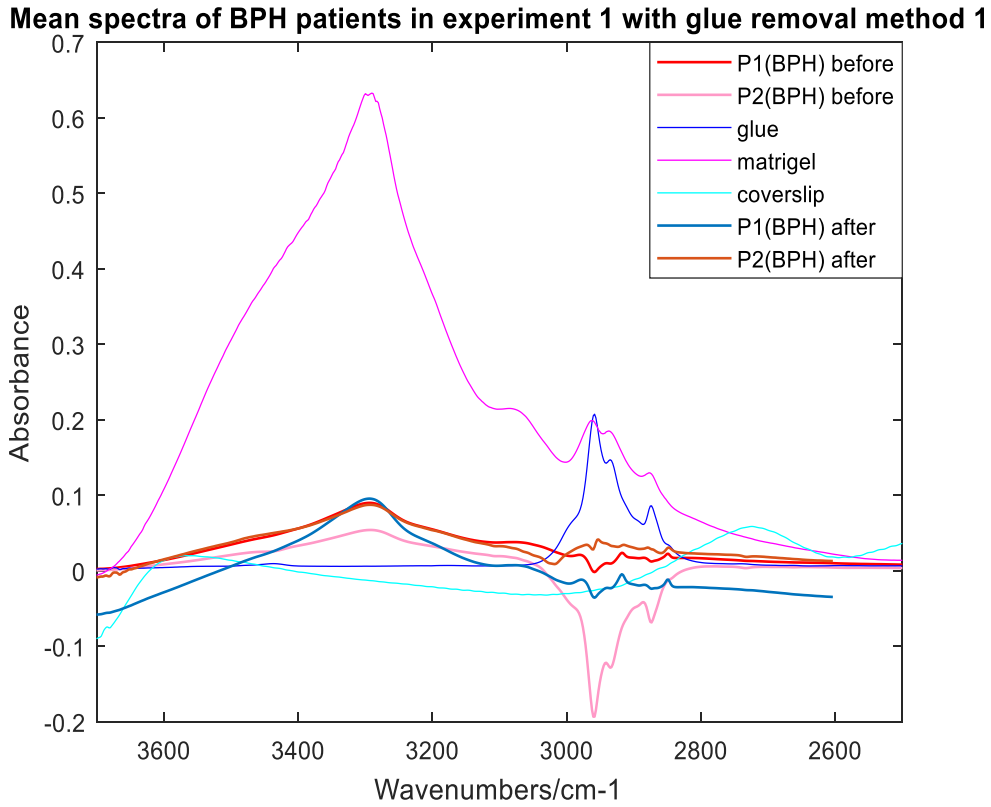

(b)

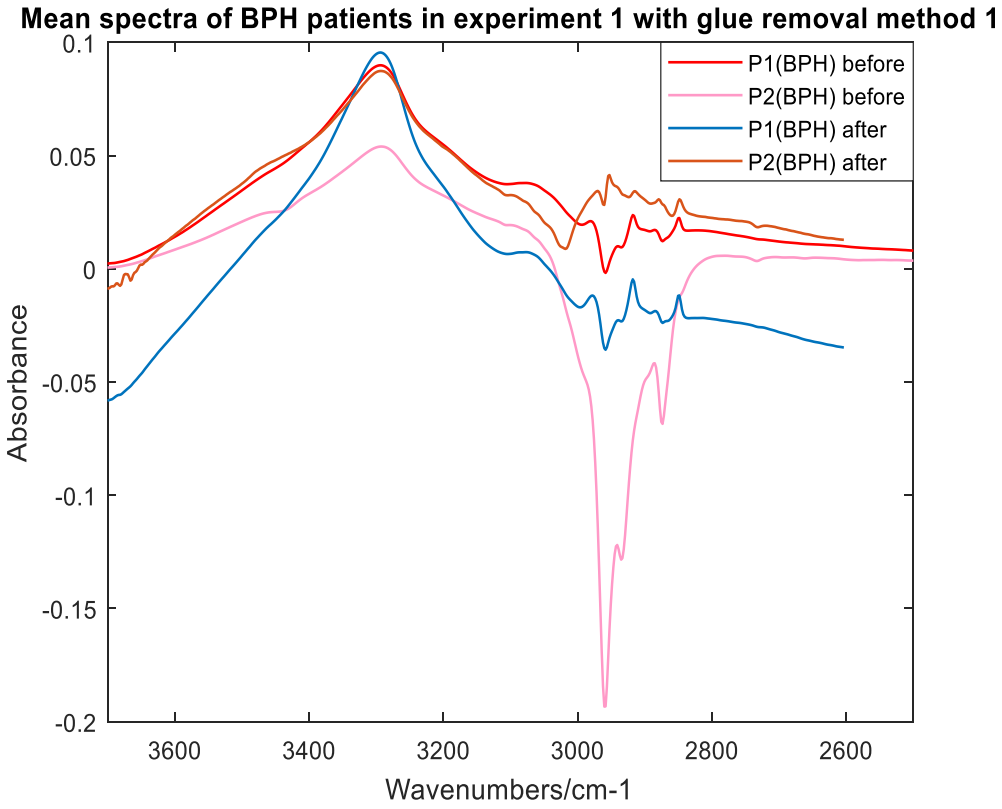

Figure5. 14 (a) shows the reference spectra and spectral results of BPH patients in experiment 1 on glass E by glue removal method 1. (b) enlarges the results of BPH patients in experiment 1 on glass E by glue

removal method 1.

(a)

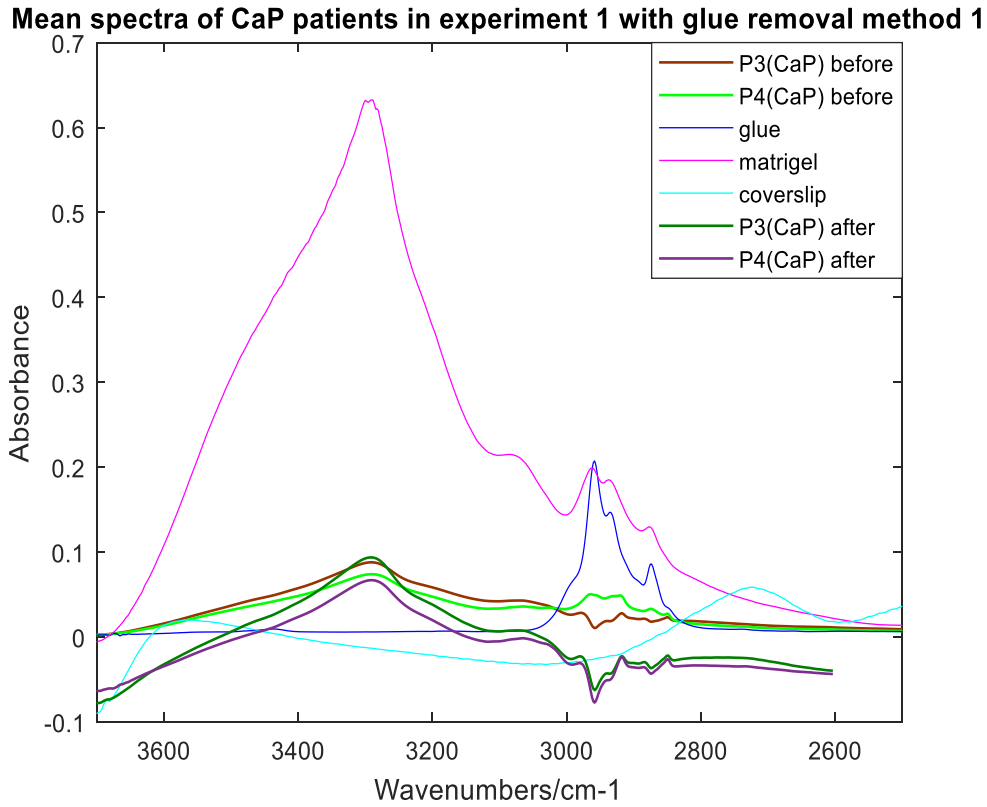

(b)

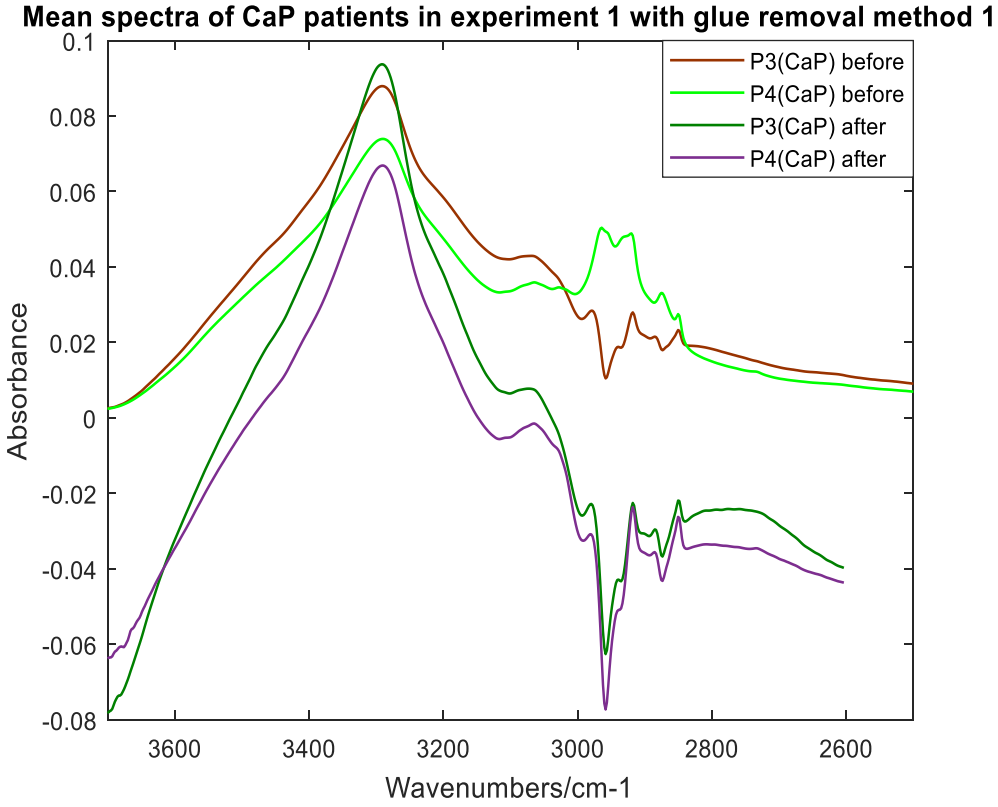

Figure5. 15 (a) shows the reference spectra and spectral results of CaP patients in experiment 1 on glass E by glue removal method 1. (b) enlarges the results of CaP patients in experiment 1 on glass E by glue removal method 1.

The lipid peaks are positive for P4(CaP) before glue removal. The glue has a much higher intensity in the lipid region than tissue, so the mean spectra of P4 still have more glue. According to figure 5.15 (b), the intensities of amide A and lipid peaks are reduced after removing glue, which means the glue removal method 1 is working in the spectra of P4 (CaP).

According to the spectra of 5.14 (b) and 5.15 (b), glue removal method 1 works in both BPH and CaP patients. However, the shape of spectra is not very similar to the Matrigel spectra, especially in the lipid region. This means method 1 does not have a particularly stable result for glue removal.

For experiment 2, the glue removal spectral results of BPH and CaP patients are shown in Figures 5.16 and 5.17, respectively. Glue and coverslip have significant effects on the original spectra in experiment 2. According to the reference spectra shown in figure 5.16 (a) and 5.17 (a), the band in 3400-3450 cm^{-1} and three very high intensity of lipid peaks (2958 cm^{-1}, 2935 cm^{-1}, 2873 cm^{-1}) are caused by glue. While the broad band in 3400-3600 cm^{-1} and a small peak at 2700-2750 cm^{-1} are caused by a coverslip. The glue removal method 1 used in the spectra of experiment 2 aims to remove these bands and reduce the intensity of lipid peaks.

According to figure 5.16 (b) and 5.17(b), for spectra of both BPH and CaP patients, the bands in 3400-3600 cm^{-1} are removed after removing glue, which means the spectra have removed the coverslip effect. However, the bands in 3400-3450 cm^{-1} and lipid region are changed to negative, which means the spectra have removed more glue. Therefore, for both BPH and CaP patients, method 1 could remove the effect of the coverslip for the spectra of experiment 2, but the impact of glue cannot totally be removed. The results may be optimised by testing the more suitable fit range.

(a)

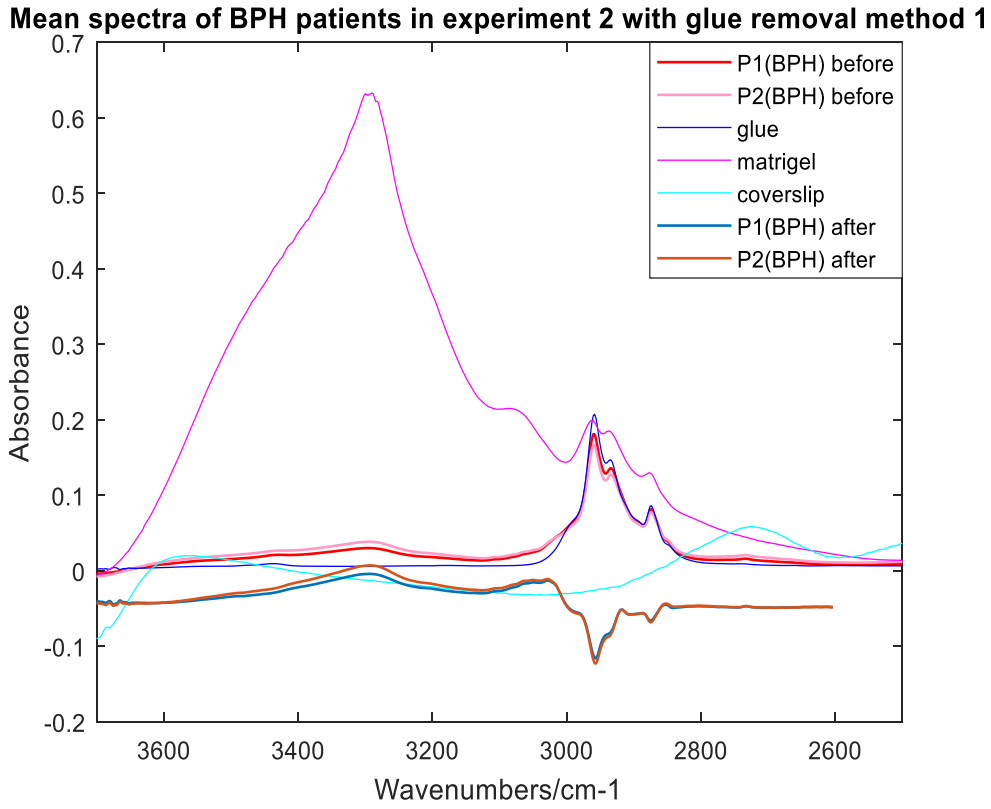
Mean spectra of BPH patients in experiment 2 with glue removal method 1
P1(BPH) before
P2(BPH) before
glue
matrigel
coverslip
P1(BPH) after
P2(BPH) after
Absorbance
0.7
0.6
0.5
0.4
0.3
0.2
0.1
0
-0.1
-0.2
3600
3400
3200
3000
2800
2600
Wavenumbers/cm-1

(b)

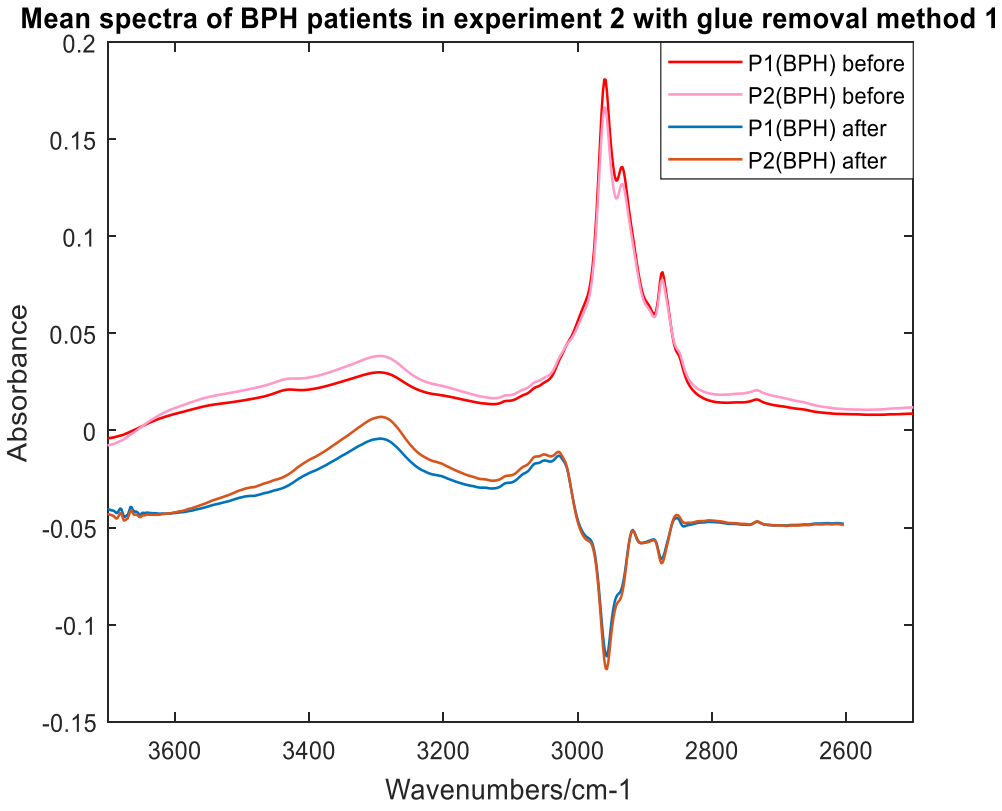
Mean spectra of BPH patients in experiment 2 with glue removal method 1
P1(BPH) before
P2(BPH) before
P1(BPH) after
P2(BPH) after
Absorbance
0.2
0.15
0.1
0.05
0
-0.05
-0.1
-0.15
3600
3400
3200
3000
2800
2600
Wavenumbers/cm-1

Figure5. 16 (a) shows the reference spectra and spectral results of BPH patients in experiment 2 on glass E by glue removal method 1. (b) enlarges the results of BPH patients in experiment 2 on glass E by glue removal method 1.

(a)

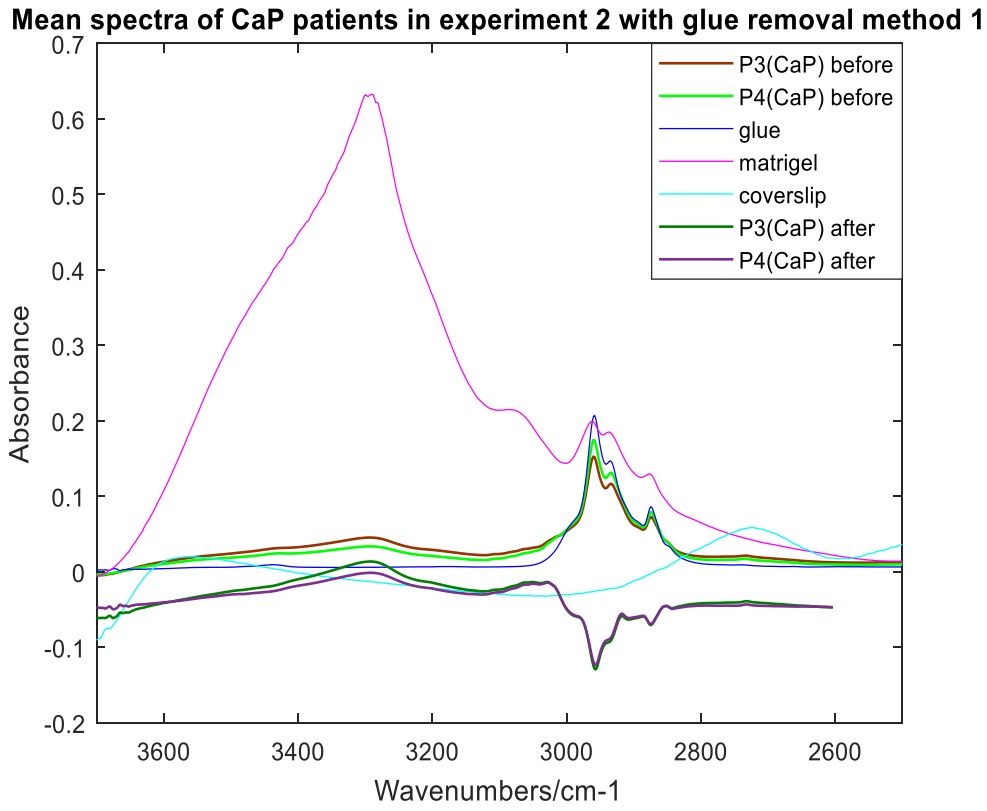

(b)

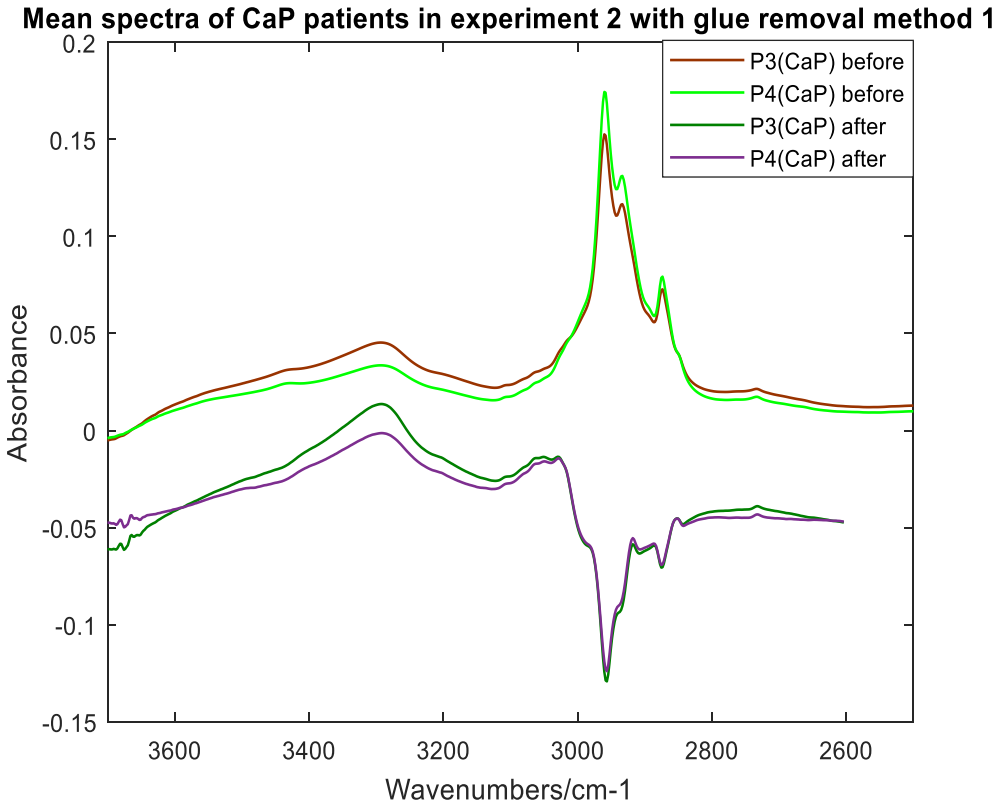

Figure5. 17 (a) shows the reference spectra and spectral results of CaP patients in experiment 2 on glass E by glue removal method 1. (b) enlarges the results of CaP patients in experiment 2 on glass E by glue removal method 1.

5.3.2.3 The result of glue removal for glass E by glue removal method 2.

Glue removal method 2 used the spectra of glue, coverslip and the spectral data in experiment 1 as the reference. The glue removal results for BPH and CaP patients are shown in Figures 5.18 and 5.19, respectively. Compared to the two figures, it is easy to see that the three lipid peaks and small bands in 3400-3450 cm^{-1} for BPH patient change to negative. Therefore, for BPH patients, glue removal method 2 works on the spectra but removes more glue. However, for the CaP patients, lipid peaks' intensities are reduced, but they are still positive. It means the glue removal method 2 also is working on CaP patients. But for spectra of P4(CaP), the intensities of lipid peaks are still higher than amide A, and the small peak in 3400-3450 cm^{-1} also is existing. It means the glue removal method 2 does not remove all of the extra glue. In addition, for

both BPH and CaP patients, there are apparent broad peaks in 3400-3600 cm^{-1} after removing glue, which is caused by the coverslip. Therefore, method 2 has a bad performance of glue removal on both spectra of BPH and CaP patients.

(a)

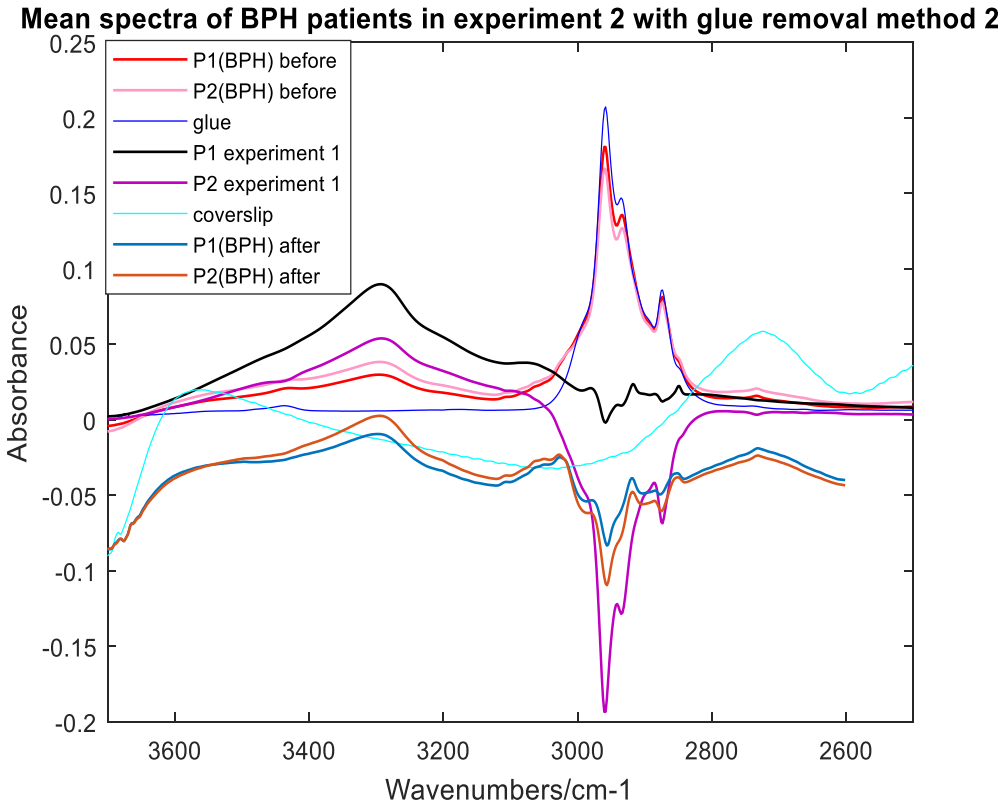

(b)

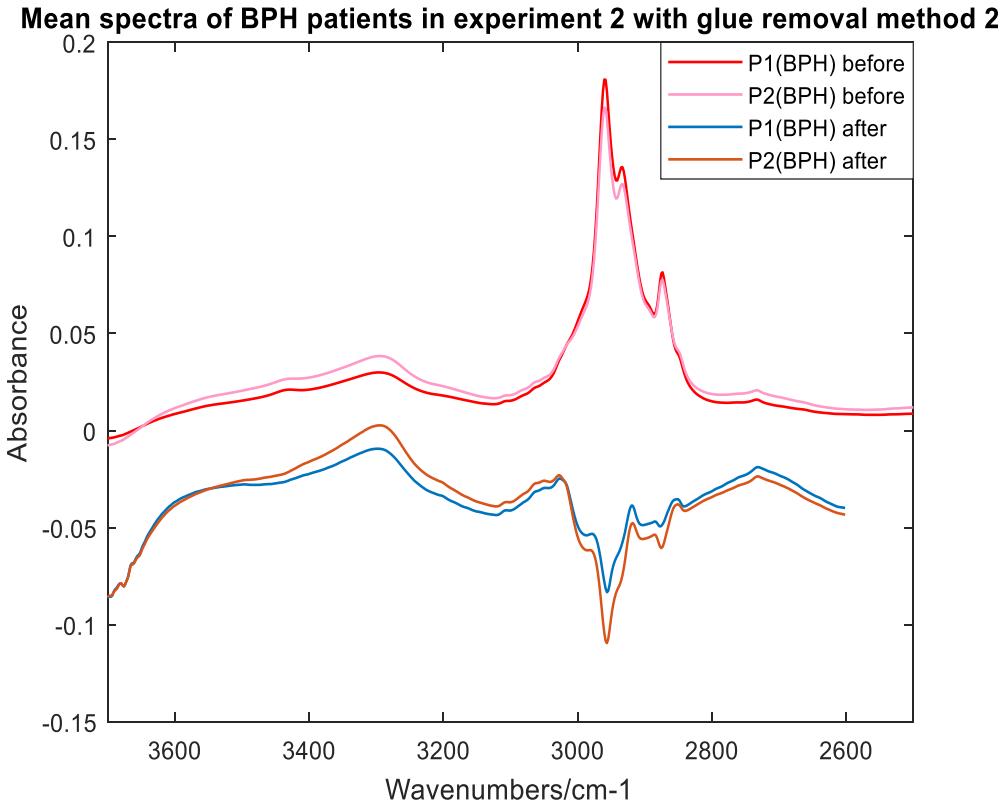

Figure5. 18 (a) shows the reference spectra and spectral results of BPH patients in experiment 2 on glass E by glue removal method 2. (b) enlarges the results of BPH patients in experiment 2 on glass E by glue removal method 2.

(a)

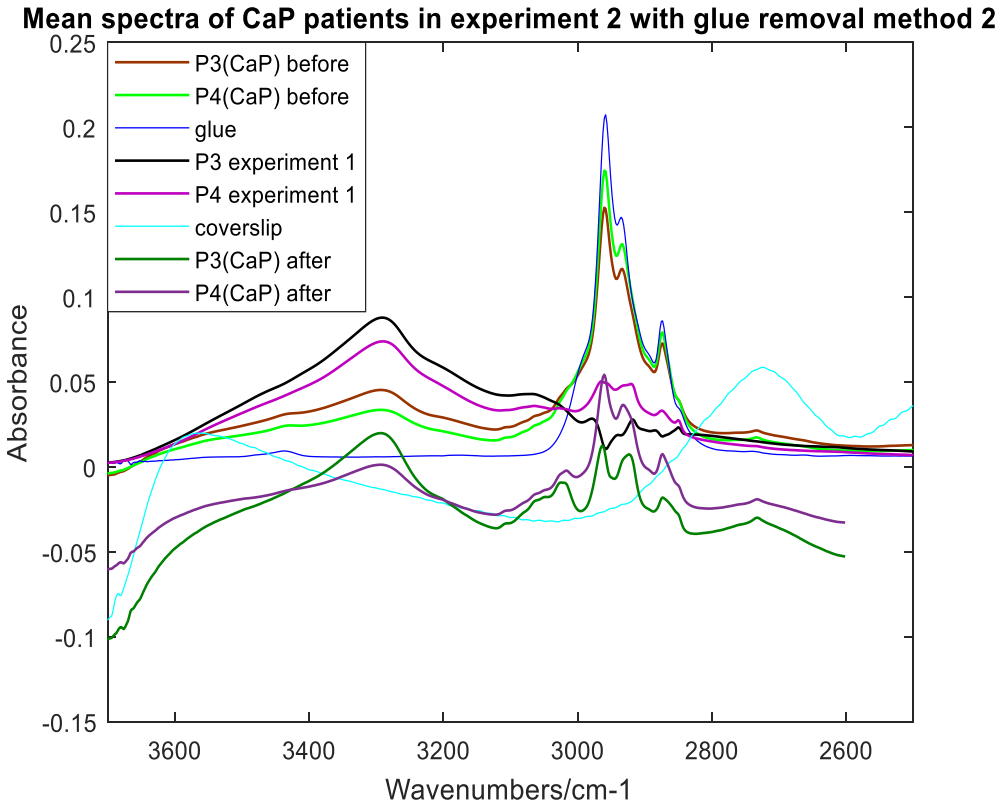
Mean spectra of CaP patients in experiment 2 with glue removal method 2
P3(CaP) before
P4(CaP) before
glue
P3 experiment 1
P4 experiment 1
coverslip
P3(CaP) after
P4(CaP) after
Absorbance
0.25
0.2
0.15
0.1
0.05
0
-0.05
-0.1
-0.15
3600
3400
3200
3000
2800
2600
Wavenumbers/cm-1

(b)

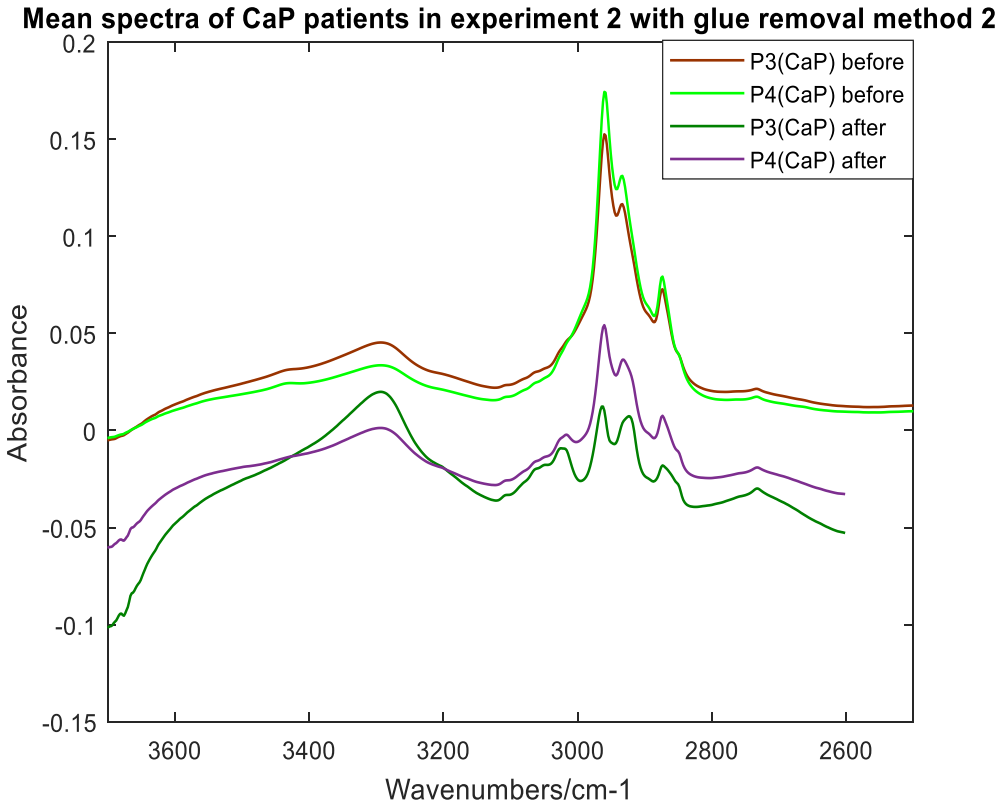
Mean spectra of CaP patients in experiment 2 with glue removal method 2
P3(CaP) before
P4(CaP) before
P3(CaP) after
P4(CaP) after
Absorbance
0.2
0.15
0.1
0.05
0
-0.05
-0.1
-0.15
3600
3400
3200
3000
2800
2600
Wavenumbers/cm-1

Figure5. 19 (a) shows the reference spectra and spectral results of CaP patients in experiment 2 on glass E by glue removal method 2. (b) enlarges the results of CaP patients in experiment 2 on glass E by glue removal method 2.

5.3.2.4 The result of glue removal for glass E by glue removal method 3.

The reference spectra of glue removal method 2 are glue spectra, coverslip spectra and the spectral data of experiment 1. The previous section has shown that the glue removal results cannot be improved even with enlarged fit ranges (figure 5.11). The fit range for method 2 would still be the same as method 1 to keep the consistency. However, the broad band in 3400-3600 cm^{-1} for BPH and CaP patients still cannot be removed and even more apparent after glue removal by method 2.

The tissue thickness from 4 patients in this section is 8 μm, which is twice the thickness of previous BPH tissue on 12 glass slides. However, the thickness of standard histological coverslips is only 0.13-0.17 mm [6][7], and it is much thinner than glass slides. The effect of the coverslip is minimal. As the thickness of tissue increases, the impact of the coverslip on the spectra is lower. Therefore, glue removal method 3 is tested in the experiment, in which the references are only the spectral data of experiment 1 and glue. Figures 5.20 and 5.21 showed the glue removal results for BPH and CaP patients with method 3.

(a)

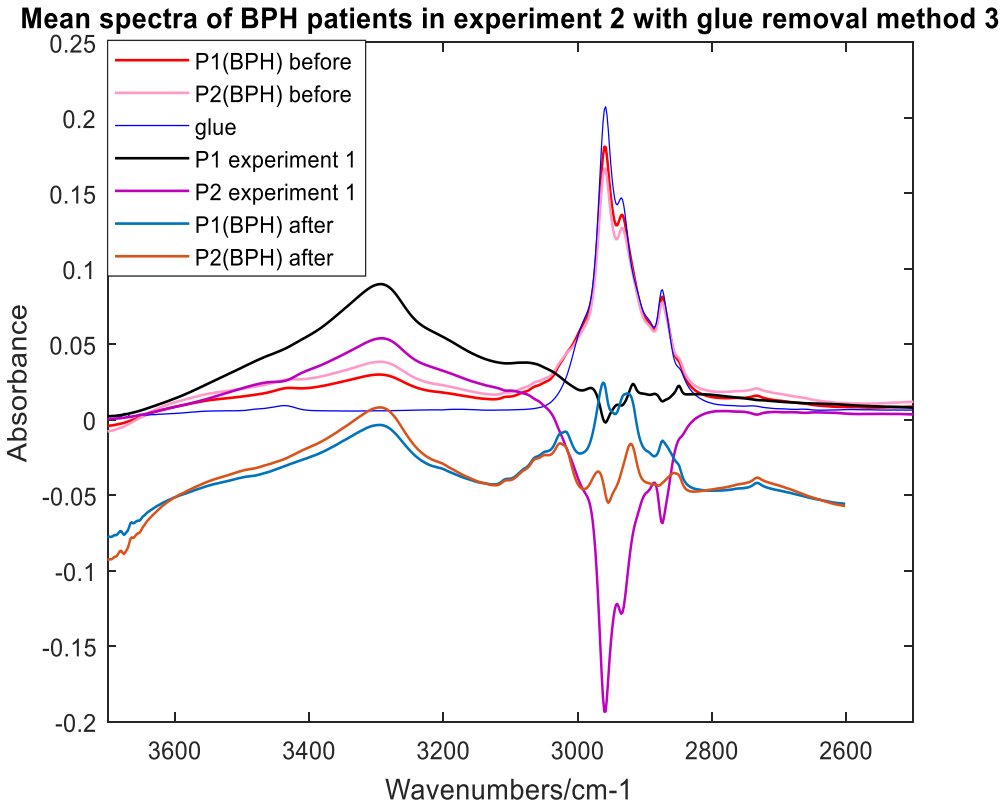
Mean spectra of BPH patients in experiment 2 with glue removal method 3
P1(BPH) before
P2(BPH) before
glue
P1 experiment 1
P2 experiment 1
P1(BPH) after
P2(BPH) after
Absorbance
0.25
0.2
0.15
0.1
0.05
0
-0.05
-0.1
-0.15
-0.2
3600
3400
3200
3000
2800
2600
Wavenumbers/cm-1

(b)

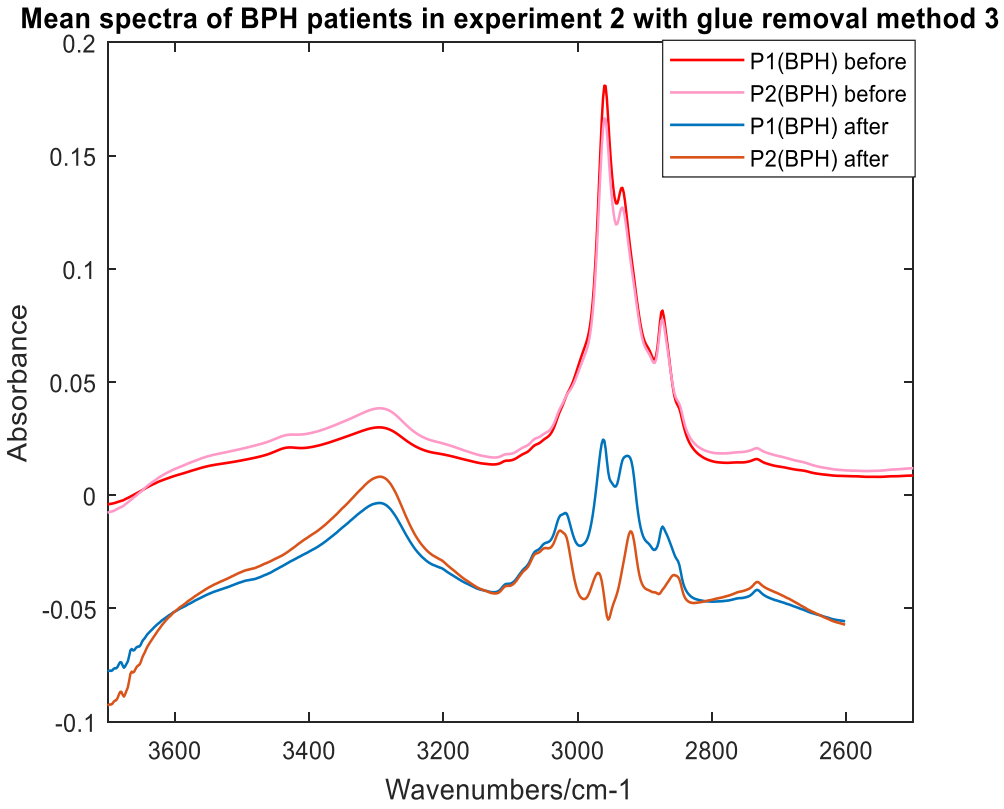
Mean spectra of BPH patients in experiment 2 with glue removal method 3
P1(BPH) before
P2(BPH) before
P1(BPH) after
P2(BPH) after
Absorbance
0.2
0.15
0.1
0.05
0
-0.05
-0.1
3600
3400
3200
3000
2800
2600
Wavenumbers/cm-1

Figure5. 20 (a) shows the reference spectra and spectral results of BPH patients in experiment 2 on glass E by glue removal method 3. (b) enlarges the results of BPH patients in experiment 2 on glass E by glue removal method 3.

According to figures 5.20 and 5.21, the intensities of lipid regions are lower than the original spectra in experiment 2, and all of the peaks are positive for both BPH and CaP patients. However, except for P2(BPH) spectra, the intensities of lipid peaks of the rest spectra are higher than amide A, and the shape of spectra is not similar to the standard tissue spectra (Matrigel). Therefore, most spectra only remove some glue, which still leaves some glue effect. In addition, compared with the glue removal result of method 2, the broad bands in 3400-3600 cm^{-1} still exist for BPH and CaP patients' spectra after glue removal by method 3. Therefore, method 3 still could not improve the glue removal performance.

(a)

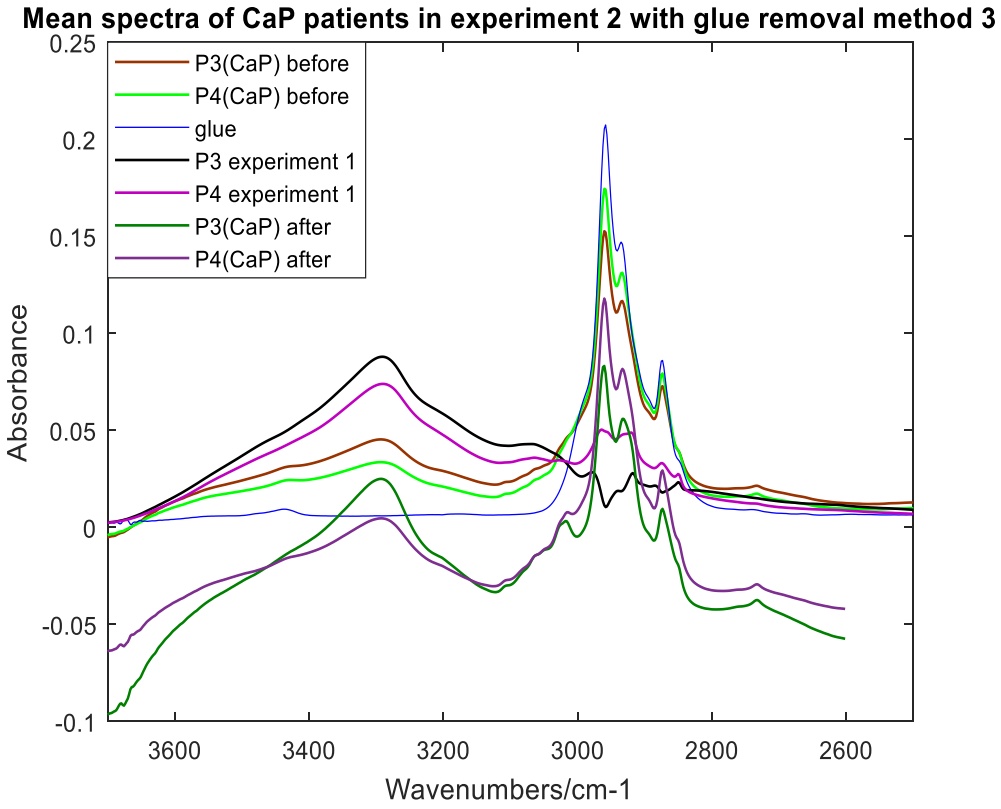
Mean spectra of CaP patients in experiment 2 with glue removal method 3
P3(CaP) before
P4(CaP) before
glue
P3 experiment 1
P4 experiment 1
P3(CaP) after
P4(CaP) after
Absorbance
0.25
0.2
0.15
0.1
0.05
0
-0.05
-0.1
3600
3400
3200
3000
2800
2600
Wavenumbers/cm-1

(b)

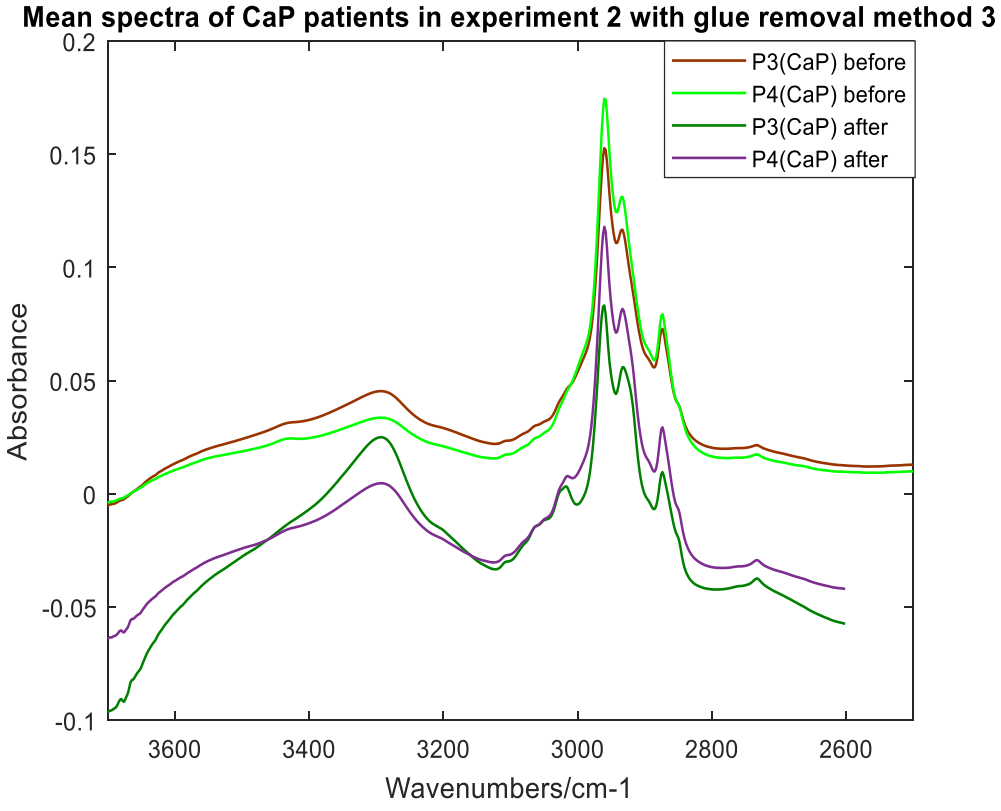
Mean spectra of CaP patients in experiment 2 with glue removal method 3
P3(CaP) before
P4(CaP) before
P3(CaP) after
P4(CaP) after
Absorbance
0.2
0.15
0.1
0.05
0
-0.05
-0.1
3600
3400
3200
3000
2800
2600
Wavenumbers/cm-1

Figure5. 21 (a) shows the reference spectra and spectral results of CaP patients in experiment 2 on glass E by glue removal method 3. (b) enlarges the results of CaP patients in experiment 2 on glass E by glue removal method 3.

5.4 Error discussion

The glue removal is the data process to remove the effect of glue. The reference spectra for glue and coverslip are the mean spectra. The main glue removal error is from the fit range selection, and the effect of removing glue is related to the fit range. The whole range (2500-3700 cm^{-1}) is not used as a fit range because it caused overfitting. The final best fit range in chapter 5 is a relatively better range of all tests. The real best fit range needs to be continuous optimization by constantly reprocessing. However, it is clear that removing glue via this algorithm actually introduces more variation in the spectra and generally results in poor performance. In addition, the paraffin was removed before the staining process for H&E stained tissue sample. But it might still contain some paraffin in actual situations. Therefore, the remained paraffin might still have a contribution to the spectra. Therefore, paraffin may need to be considered for glue removal.

5.5 Conclusion

There are contain mounting media for the clinical H&E stained tissue sample. The mounting media always affect the spectra no matter what backgrounds are used during the measurement. Glue is used to represent the mounting media in this project. Therefore, it is desirable to find a suitable glue removal method for further study.

There are two kinds of glue removal methods used and the critical difference in the reference spectra. The reference spectra of method 1 are glue, coverslip and Matrigel. The spectrum of Matrigel is regarded as the standard spectrum of tissue, but it is not a true spectrum of tissue. The reference spectra of method 2 are selected from glue,

coverslip, and spectral data of experiment 1. The original spectra applied the glue removal method 2 are all from experiment 2. Therefore, there are mainly three types of glue removal spectra for comparison: experiment 1 spectra with glue removal method 1, experiment 2 spectra with glue removal method 1 and experiment 2 spectra with glue removal method 2.

Overfitting will result if the fit range selected the whole spectral range (2500-3700 cm^{-1}) in the glue removal process. It is vital to find a suitable fit range for the glue removal. The fit ranges which are used for the test are selected by the obvious peaks of the reference spectra. According to the reference spectra and the tissue spectra without glue removal, the available range 2500-3700 cm^{-1} could be divided into four types, which are fit range 1: Matrigel (3278-3318cm^{-1}, 3066-3106cm^{-1}); fit range 2: glue & Matrigel peak (2848-2852cm^{-1}, 3415-3455cm^{-1}); fit range 3: glue peak & Matrigel peak (2950-2970cm^{-1}, 2925-2945cm^{-1}, 2867-2887cm^{-1}); fit range 4 coverslip & Matrigel peak (3536-3576cm^{-1}, 2704-2744cm^{-1}). According to the comparison of glue removal results, the more suitable fit range are 1, 3 and 4. To keep the consistency, these fit ranges are applied in both methods 1 and 2.

According to the spectral results of glue removal, both methods 1 and 2 could achieve glue removal on both epithelium and stroma spectra from both BPH and CaP patients. However, glue removal method 1 has better performance than method 2. According to the results of two section studies, method 2 still cannot remove the effect of the coverslip. In addition, experiment 1 spectra with glue removal method 1 have better performance than on experiment 2. Therefore, glue removal method 1 would be applied in further studies.

5.6 Reference

[1] K. Houck *et al.*, 'Borderline tumors of the ovary: Correlation of frozen and permanent histopathologic diagnosis', *Obstet. Gynecol.*, 2000.

[2] M. Slaoui and L. Fiette, 'Histopathology Procedures: From Tissue Sampling to Histopathological Evaluation', 2010.

[3] P. R. Griffiths and J. A. De Haseth, *Fourier Transform Infrared Spectrometry*. 2007.

[4] C. S. Hughes, L. M. Postovit, and G. A. Lajoie, 'Matrigel: a complex protein mixture required for optimal growth of cell culture.', *Proteomics*, vol. 10, no. 9, pp. 1886–1890, 2010.

[5] H. K. Kleinman and G. R. Martin, 'Matrigel: Basement membrane matrix with biological activity', *Semin. Cancer Biol.*, vol. 15, no. 5 SPEC. ISS., pp. 378–386, 2005.

[6] M. J. Pilling, A. Henderson, J. H. Shanks, M. D. Brown, N. W. Clarke, and P. Gardner, 'Infrared spectral histopathology using haematoxylin and eosin (H&E) stained glass slides: a major step forward towards clinical translation', *Analyst*, vol. 142, no. 8, pp. 1258–1268, Apr. 2017.

[7] M. Kansiz, L. M. Dowling, I. Yousef, O. Guaitella, F. Borondics, and J. Sulé-Suso, 'Optical Photothermal Infrared Microspectroscopy Discriminates for the First Time Different Types of Lung Cells on Histopathology Glass Slides', *Anal. Chem.*, vol. 93, no. 32, pp. 11081–11088, 2021.

Chapter 6

Study 2: Tissue classification of Haematoxylin and Eosin (H&E) Stained Prostate Tissue on Different Types of Glass Slides

The project aims to study the impact of glass types on cancer detection. In addition, cancer detection by SHP could be based on the spectra of different histological classes of tissue. In general, histological categories of prostate tissue include epithelium, stroma, blood and secretion. Therefore, it is necessary to study whether the glass types could affect tissue classification before cancer detection. Because the epithelium and stroma account for a large proportion of prostate tissue, only epithelium and stroma were used for automated histological tissue classification in this study.

12 different brands of glass slides (entirely from different manufacturers) are studied in this chapter. A series of adjacent prostate tissue sections from the same benign prostatic hyperplasia (BPH) patients are mounted on different glass slides. The specific experimental detail could see in section 3.5.2 in chapter 3. The objective of this chapter is to find the influence of glass types on tissue classification.

6.1 Annotation results

All of the annotation work is done using GIMP. The annotated brightfield images of glass L are examples and shown in figure 6.1. The specific pixels of H&E brightfield image are annotated for analysis. Epithelium is annotated in green; stroma is annotated in red; the blank and broken tissue areas are annotated in blue.

(a) (b)

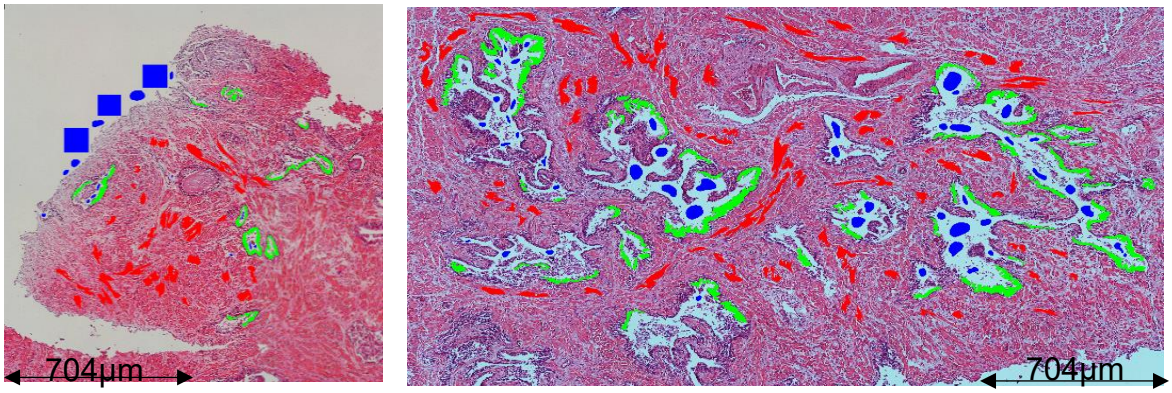

Figure6. 1 (a) the annotation of region 1 of BPH tissue on brightfield image of glass L. (b) the annotation of region 2 of BPH tissue on brightfield image of glass L. Epithelium, stroma and blank are annotated in green, red and blue, respectively.

6.2 Results and Discussion

This chapter aims to study whether different types of glass impact pathological tissue classification. All spectra on 12 glass slides are processed by PCA and random forest. The spectral data from one of the glass slides are used to train the random forest model to classify the epithelium and stroma, and the rest spectra from the other glass slides are tested using the model. If the classifier could discriminate the spectra of epithelium and stroma on different glass slides, it would indicate that the type of glass does not affect histological classification. If not, the glass type affects the classification results. However, before the primary study process, the pre-processing of raw spectra is essential as well.

6.2.1 Infrared chemical imaging

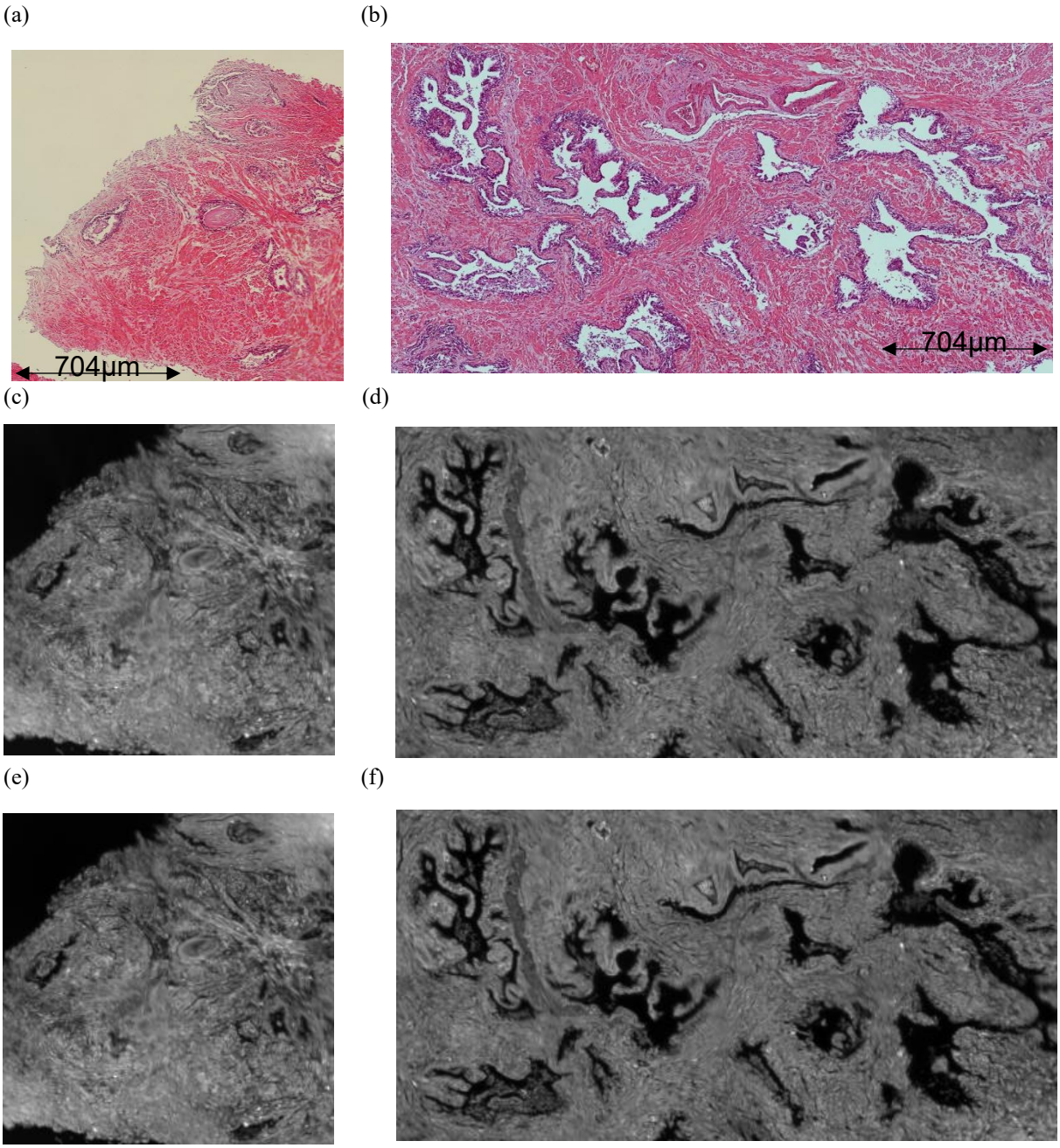

Figure6. 2 Comparison between the brightfield images and chemical images from the two experiments. (a) The brightfield image of prostate tissue on glass L in region 1. (b) The brightfield image of prostate tissue on glass L in region 2. (c) Chemical image on amide A (3298 cm^{-1}) of prostate tissue on glass L in region 1 obtained in experiment 1. (d) Chemical image of prostate tissue on glass L in region 2 obtained in experiment 1. (e) Chemical image on amide A of prostate tissue on glass L in region 1 obtained in experiment 2. (f) Chemical image of prostate tissue on glass L in region 2 obtained in experiment 2.

A series of adjacent prostate tissue is mounted on 12 different types of glass slides, and

figure 3.5 shows all of the tissue on the 12 glass slides. Figure 3.6 shows the one of the whole tissue mounted on the glass slides and the marks of the two regions measured. The chemical images are rendered by the intensity of the amide A band, which is located at 3298 cm^{-1}. Figure 6.2 compares the chemical images of prostate tissue on glass L with the brightfield image on the same glass slides.

According to figure 6.2, it is easy to see there is an excellent agreement in the morphology between the brightfield images and chemical images obtained from both experiments 1 and 2. Different experimental methods do not affect the chemical image. Since the annotation is marked on the H&E brightfield images, it has the same annotated histological epithelium and stroma spectra between the two experiments.

6.2.2 Quality control for spectra

To make every tissue section on each glass slide has the same shape and structure as possible, the 12 adjacent tissue sections are cut too thin (4μm). It caused the broken of some tissue areas, especially for epithelium. Figure 6.3 shows one of the broken tissue areas. The fractured tissue would lead to the scattering of spectra, which would significantly impact tissue classification results. Therefore, it is essential to remove the spectra from these broken areas and control quality before data processing.

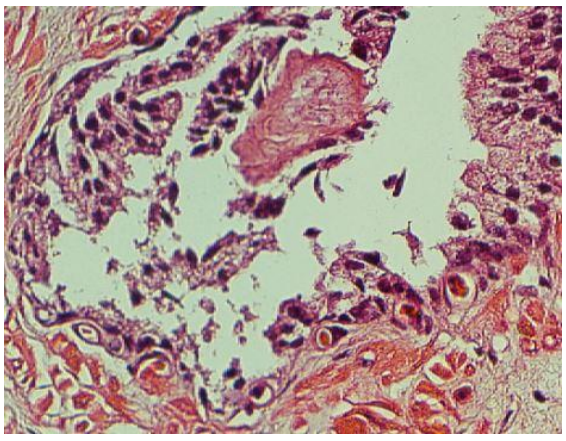

Figure6. 3 A broken epithelium of prostate tissue on glass L.

Quality control aims to remove spectra from without tissue and broken tissue area. IR transmission window for glass slides is only above 2000 cm^{-1}. Therefore, quality control is based on the intensity of amide A peak. It means the intensity of amide A for good-quality spectra in tissue area must be higher than the highest intensity in the tissue-free area. And the highest intensity at 3298 cm^{-1} in the blank space was set as a threshold.

Because annotated spectra of experiments 1 & 2 are extracted based on the same annotated H&E brightfield images, the number of original annotated spectra for every glass slide in experiments 1 & 2 is the same, shown in table 6.1.

Table6. 1 The number of annotated spectra on 12 glass slides in experiments 1 and 2

	The number of annotated spectra		
	Epithelium	Stroma	Blank & broken tissue area
Glass A	3704	7526	2889
Glass B	3990	6667	2690
Glass C	4321	8519	2492
Glass D	3612	6118	2292
Glass E	4231	7156	2240
Glass F	4585	6966	2793
Glass G	4860	7493	2871
Glass H	4751	9526	3076
Glass I	4330	6362	2673
Glass J	4200	7443	3017
Glass K	4551	8765	3792
Glass L	5164	7419	3803

According to table 6.1, there is a difference in the number of annotated spectra among 12 glass slides slides. Although the 12 tissue sections are adjacent and cut from the same patient, the structure of the tissue sections on every glass slide has a slight difference. In addition, the annotation is a subjective process, and all of the operations are done manually. Therefore, the annotation cannot keep consistency among the 12 tissue sections. In addition, because stroma accounts for the majority in every tissue section, and most of the epithelium is broken and cannot be annotated, the number of annotated epithelium spectra is much lower than stroma spectra.

The threshold of every glass slide is set as the highest intensity of amide A on the annotated blank and broken-tissue area. The thresholds of 12 glass slides in experiments 1 and 2 are shown in table 6.2. To keep the consistency for further comparison among the spectra on 12 glass slides, the highest threshold in every experiment 1 is selected and applied. According to table 6.2, the thresholds for experiments 1 and 2 are 0.054 and 0.060, respectively. Tables 6.3 and 6.4 show the number of spectra after quality control in experiments 1 and 2, separately.

Compared to table 6.3 and 6.4 with table 6.2, it is easy to see the variation in the number of spectra after quality control. There is little change in the number of stroma spectra for the two experiments. However, most of the epithelium spectra are removed, and the broken epithelium causes it in the tissue section.

Table6. 2 The thresholds of 12 glass slides in experiments 1 and 2

Glass type	Experiment 1	Experiment 2
Glass A	0.0386	0.0378
Glass B	0.0157	0.0243
Glass C	0.0240	0.0312
Glass D	0.0282	0.0374
Glass E	0.0223	0.0330
Glass F	0.0252	0.0303
Glass G	0.0232	0.0278
Glass H	0.0540	0.0600
Glass I	0.0145	0.0253
Glass J	0.0173	0.0251
Glass K	0.0237	0.0361
Glass L	0.0276	0.0370

Table6. 3 The number of annotated spectra on 12 glass slides in experiment 1 after quality control

	The number of annotated spectra	
	Stroma	Epithelium
Glass A	7526	3502
Glass B	6666	3643
Glass C	8519	3902
Glass D	6118	3128
Glass E	7155	3857
Glass F	6966	4320
Glass G	7493	4705
Glass H	9525	4093
Glass I	6362	3692
Glass J	7443	3779
Glass K	8765	4041
Glass L	7419	4541

Table6. 4 The number of annotated spectra on 12 glass slides in experiment 2 after quality control

	The number of annotated spectra	
	Stroma	Epithelium
Glass A	7526	3222
Glass B	6667	3765
Glass C	8519	3909
Glass D	6118	3232
Glass E	7155	3939
Glass F	6966	4368
Glass G	7493	4676
Glass H	9525	4139
Glass I	6362	3859
Glass J	7443	3918
Glass K	8765	4245
Glass L	7419	4693

After quality control, all good-quality spectra are processed in order of range selection, noise reduction and vector normalization. Because the three peaks related to the lipid region are highly affected by the glue. The range is only selected in 3125-3700 cm^{-1} to reduce the interference from the noise, and this range contains the most valuable biological information in a glass transmission window. The noise reduction is using the first 20 PCs.

6.2.3 Tissue classification without glue correction

6.2.3.1 Mean spectra of histological classes

6.2.3.1.1 Mean spectra in experiment 1

The mean spectra of epithelium and stroma on 12 glass slides for experiment 1 are shown in figure 6.4. According to the figure, although the tissue sections are mounted on different glass slides, the shape of spectra is similar. There is only a pronounced peak at amide A (3298 cm^{-1}) for all of the mean spectra on 12 glass slides in experiment 1, and the peak results from tissue. The intensity of amide A on 12 glass slides is also similar. Comparing the mean spectra of epithelium and stroma on 12 glass slides (figure 6.4 (a) &(b)), the intensities of stroma spectra are always higher than the epithelium spectra on the same glass slides. Because the structure of epithelium has more holes.

However, the spectral intensity and the trend of 12 glass slides are different in 3400-3450 cm^{-1}. The peak in this range is related to the O-H &N-H stretching[19]. According to the spectra of glue in figure 5.2, this difference is caused by the glue and measurement method. For experiment 1, the background is a clear area without tissue. Due to tissue thickness, the glue content on the background is variable. If the content of glue on the background is less than that in the sample, the tissue spectra would contain a little glue, and there would be a positive peak in 3400 – 3450 cm^{-1} in figure 6.4, which are indicated in the spectra on glass I and glass D. If not, the final spectra would be from tissue minus a little glue and cause a negative peak in this range, which is obviously indicated in the spectra on glass A (figure 6.4). The spectra are generated only from the tissue when the glue content on the background is exactly the same as that on tissue. However, it is tough to achieve.

(a)

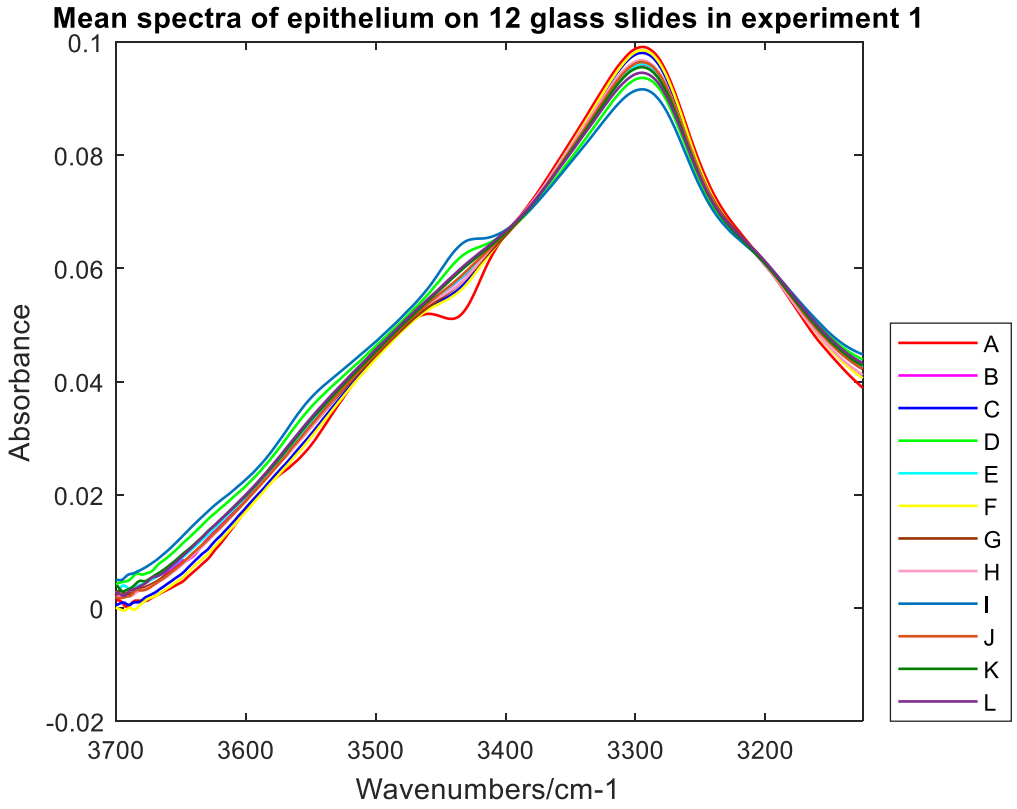
Mean spectra of epithelium on 12 glass slides in experiment 1
Absorbance
Wavenumbers/cm-1
0.1
0.08
0.06
0.04
0.02
0
-0.02
3700
3600
3500
3400
3300
3200
A
B
C
D
E
F
G
H
I
J
K
L

(b)

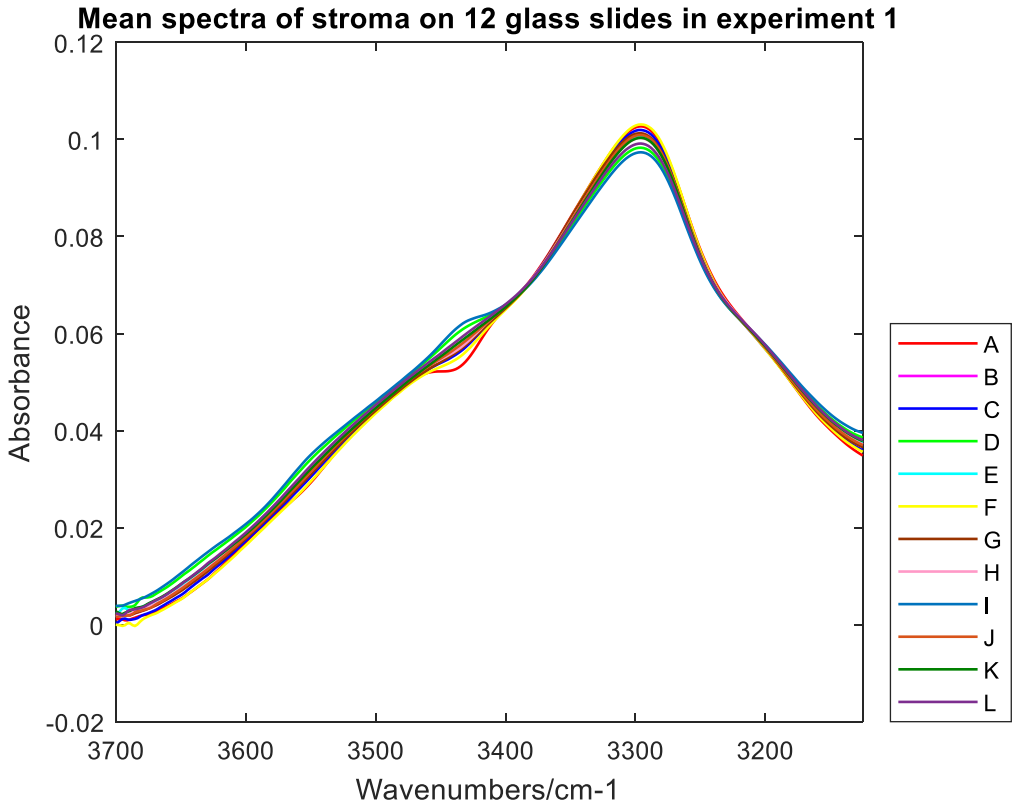
Mean spectra of stroma on 12 glass slides in experiment 1
Absorbance
Wavenumbers/cm-1
0.12
0.1
0.08
0.06
0.04
0.02
0
-0.02
3700
3600
3500
3400
3300
3200
A
B
C
D
E
F
G
H
I
J
K
L

Figure6. 4 (a) Mean spectra of epithelium on 12 glass slides in 3125 – 3700 cm^{-1} for experiment 1. (b) Mean spectra of stroma on 12 glass slides in 3125 – 3700 cm^{-1} for experiment 1.

6.2.3.1.2 Mean spectra in experiment 2

Figure 6.5 shows the mean spectra of tissue in experiment 2. Compared with the mean spectra in experiment 1 (figure 6.4), the main differences are the band in 3400-3450 cm^{-1} and 3400-3600 cm^{-1}. Because the background in experiment 2 is blank glass and sample measurement includes coverslip, glue, tissue and glass slide, so the final spectra contain the information from coverslip, glue and tissue (table 3.3). According to figure 5.2, the band in 3400-3450 cm^{-1} and 3400-3600 cm^{-1} are caused by glue and coverslip, respectively. Although the glue and coverslip significantly affect spectra, all of the mean spectra on 12 glass slides have the same shape and trend, and only the intensity of amide A is slightly different. It indicates that the type of glass has no extreme effect on spectra.

(a)

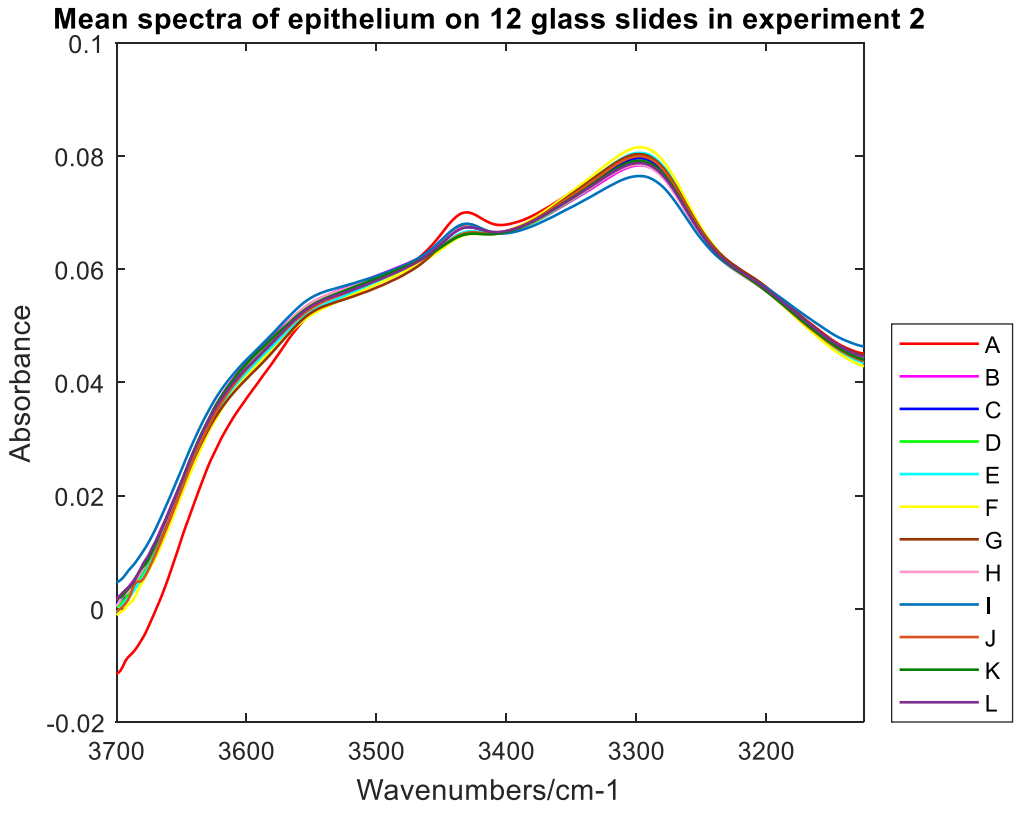

(b)

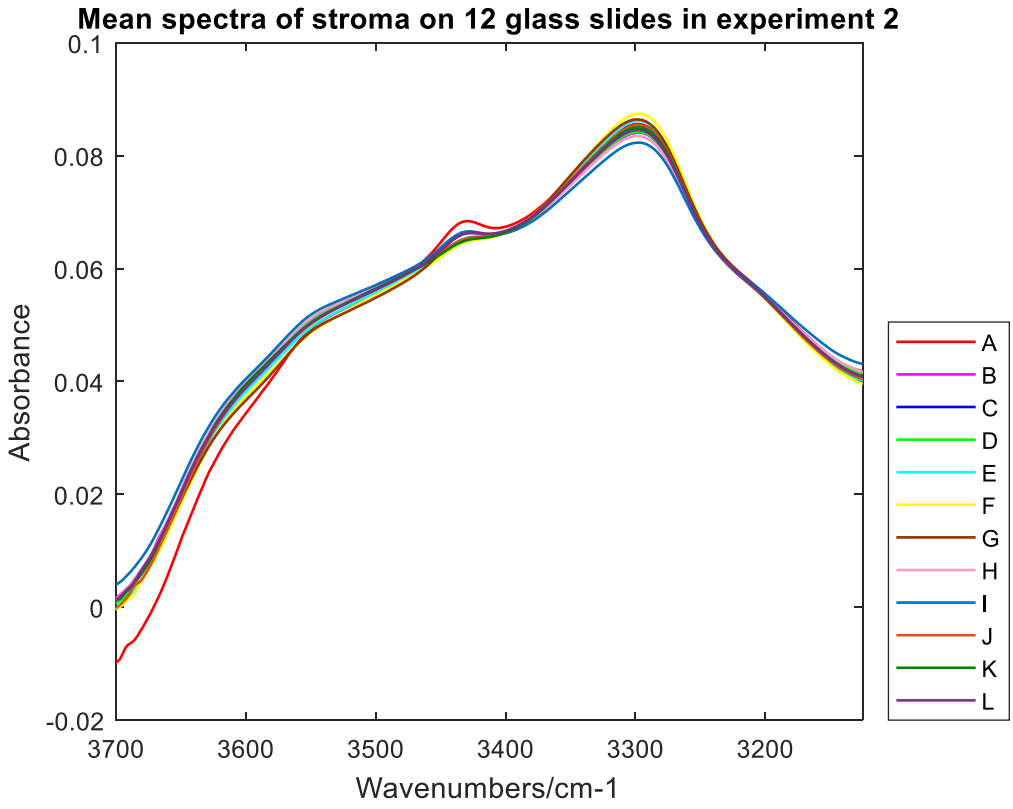

Figure6. 5 (a) Mean spectra of epithelium on 12 glass slides in 3125 – 3700 cm^{-1} for experiment 2. (b) Mean spectra of stroma on 12 glass slides in 3125 – 3700 cm^{-1} for experiment 2.

In addition, the spectra of epithelium and stroma have a similar shape for both two experiments. However, the spectral intensity of stroma is always higher than epithelium on the same glass slide due to the structure of epithelium.

6.2.3.2 The PCA of 12 glass slides

There is no noticeable difference among the mean spectra on 12 glass slides for experiments 1 and 2. Therefore, the results of PCA could indicate the difference in spectral data among different types of glass slides. Two hundred spectra of stroma and epithelium on 12 glass slides are randomly selected, and the PCA is based on these random spectra. Figure 6.6 and figure 6.8 show the PCA results of 12 glass slides for experiment 1 and experiment 2. Because the spectra of epithelium and stroma have

similar PCA distribution in both experiments 1 and 2, only the PCA results of spectra of stroma in the two experiments are shown.

6.2.3.2.1 The results of PCA of 12 glass slides in experiment 1

Figure 6.6 is PCA scatter plots to separate stroma on 12 glass slides in experiment 1, in which the (a), (b), (c) represent the score plots of PC1 vs PC2, PC1 vs PC3, and PC2 vs PC3, respectively. The scores of PC1, PC2 and PC3 are 68.8%, 22.5% and 3.69% respectively. In addition, figure 6.7 shows the loadings on the three PCs. There is no clear separation among the spectra of tissue sections on 12 glass slides in experiment 1. However, the spectra have a regular distribution on PC1.

(a)

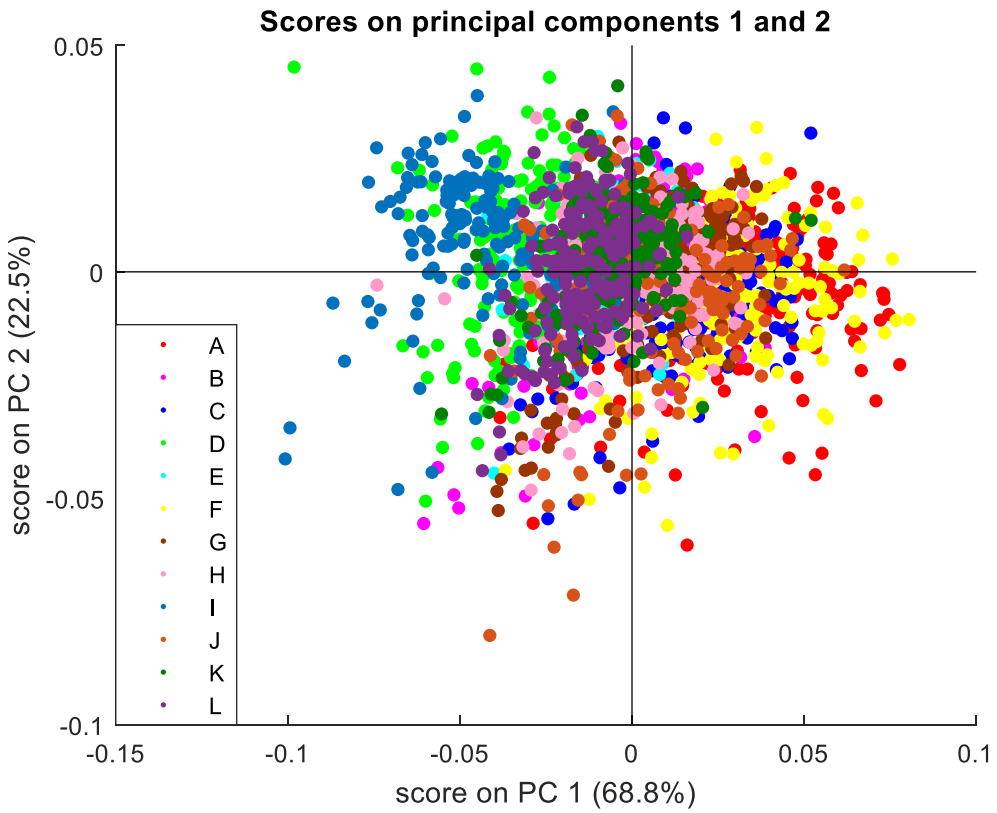

(b)

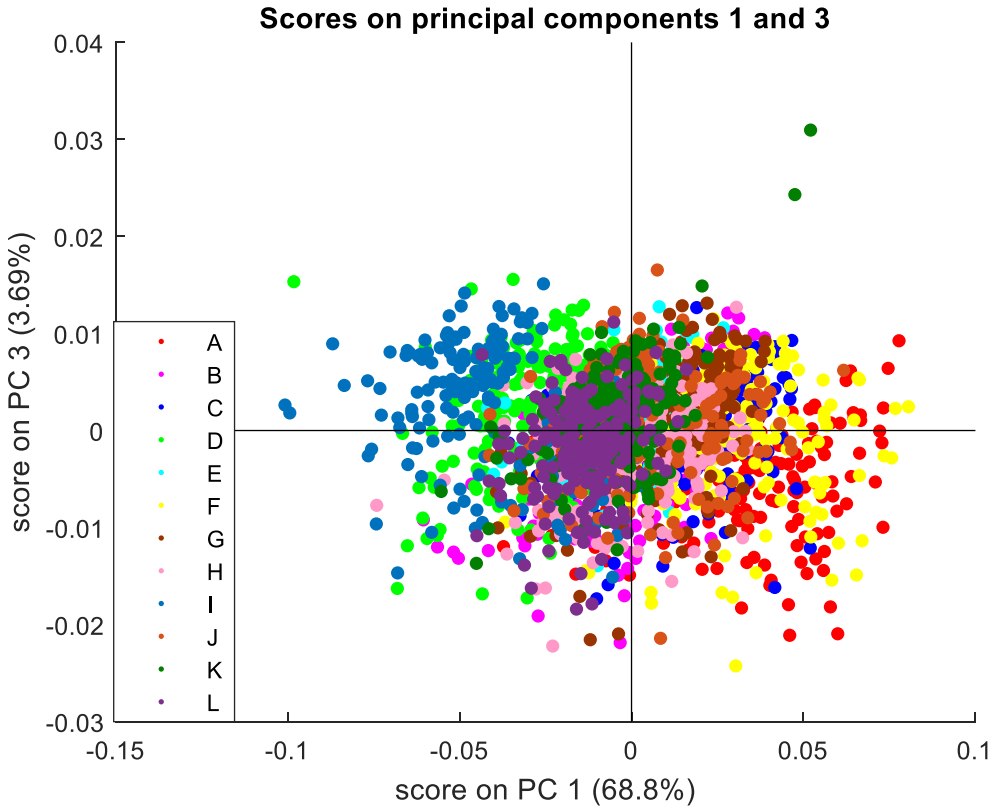
Scores on principal components 1 and 3
score on PC 3 (3.69%)
score on PC 1 (68.8%)
0.04
0.03
0.02
0.01
0
-0.01
-0.02
-0.03
-0.15
-0.1
-0.05
0
0.05
0.1
A
B
C
D
E
F
G
H
I
J
K
L

(c)

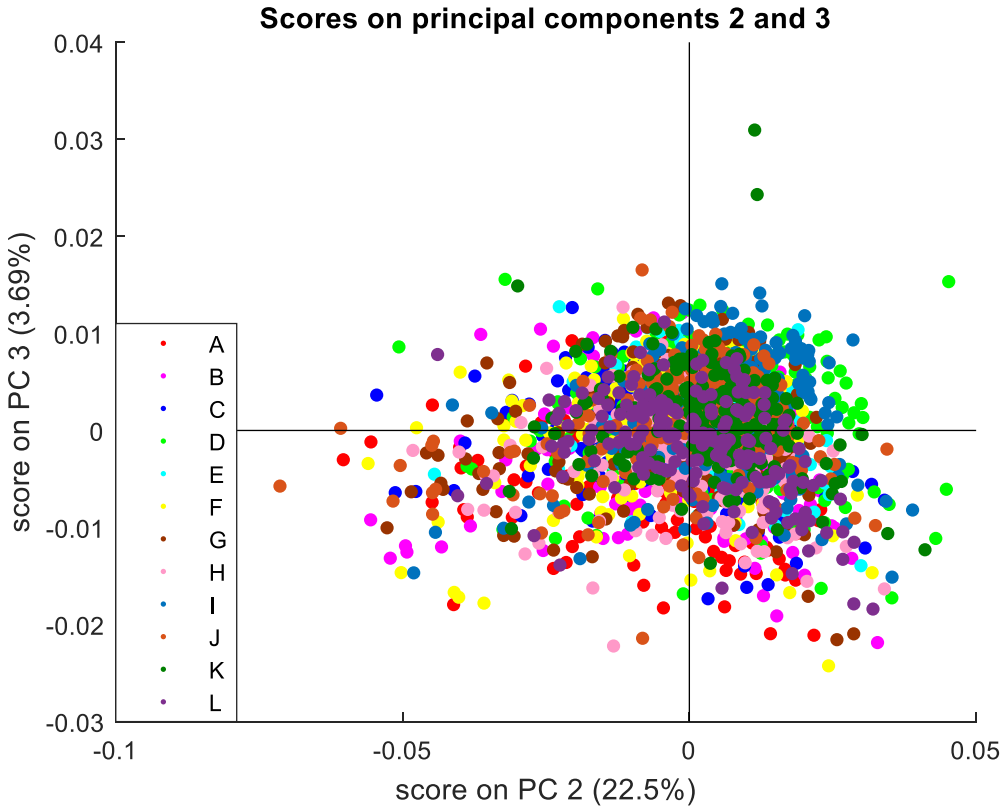
Scores on principal components 2 and 3
score on PC 3 (3.69%)
score on PC 2 (22.5%)
0.04
0.03
0.02
0.01
0
-0.01
-0.02
-0.03
-0.1
-0.05
0
0.05
A
B
C
D
E
F
G
H
I
J
K
L

Figure6. 6 (a) The score plots of PC1 and PC2 of stroma on 12 glass slides in experiment 1. (b) The score plots of PC1 and PC3 of stroma on 12 glass slides in experiment 1. (c)The score plots of PC2 and PC3 of stroma on 12 glass slides in experiment 1.

According to figure 6.7 (a), PC1 mainly has two whole peaks in the range of 3125 – 3700 cm^{-1}. The positive peak located at 3295 cm^{-1} is related to amide A. The broad negative peak located at 3437 cm^{-1} is associated with O-H asymmetric stretching[19]. According to the comparison of the mean spectra of glue (figure 5.2), the negative peak (3437 cm^{-1}) is caused by glue. According to the loading of PC1, the distribution of spectra on PC1 is nearly positively correlated with the intensity of amide A and negatively relative to the intensity of glue peak (3400-3450 cm^{-1}).

The loading on PC2 is shown in figure 6.7 (b). The positive peak located at 3274 cm^{-1} belongs to O-H symmetric stretching. The negative peaks located at 3342 and 3478 cm^{-1} are related to N-H and O-H stretching [19][20]. The spectra on every glass are distributed in both positive and negative areas, which means spectra cannot be separated based on the PC2.

According to figure 6.7 (c), many peaks are made of the PC3 loading. The two positive peaks (3295 and 3432 cm^{-1}) are related to amide A (N-H stretching) [19]. All of the negative peaks (3224, 3350 and 3486 cm^{-1}) and one positive peak (3556 cm^{-1}) are related to O-H stretching [20]. According to figure 6.6 (b) and (c), spectra on every glass slide have similar distributions on both negative and positive areas of PC3 . Therefore, the spectra cannot be separated based on the PC3.

(a)

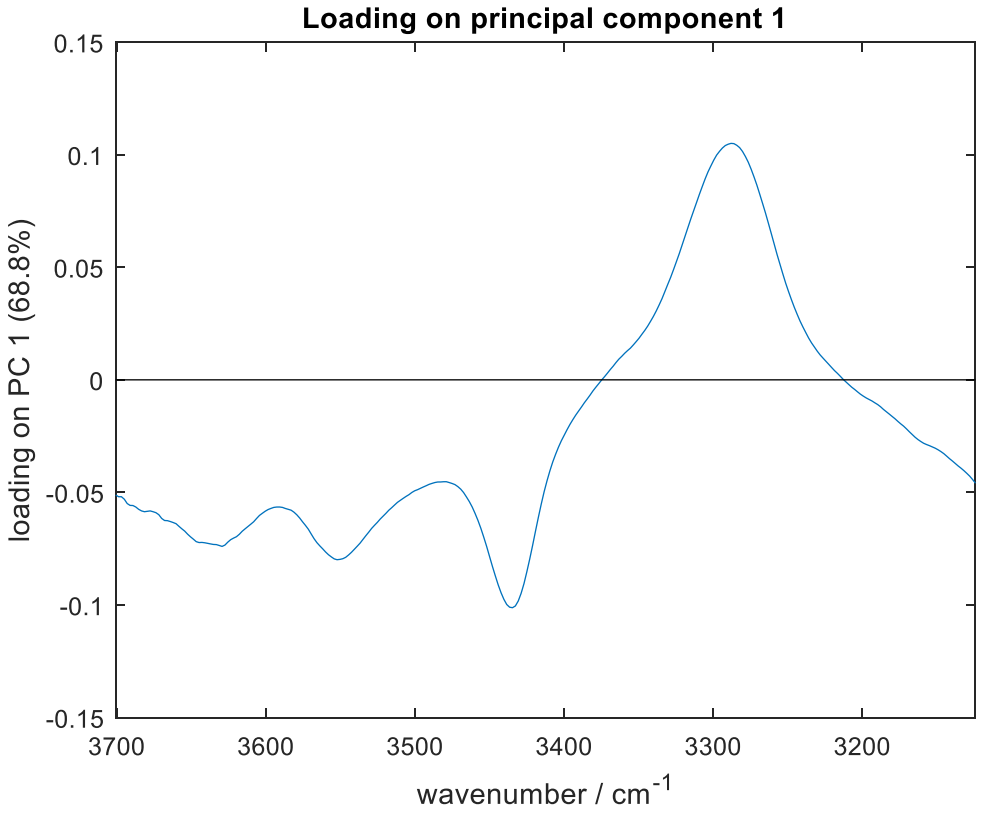
Loading on principal component 1
loading on PC 1 (68.8%)
0.15
0.1
0.05
0
-0.05
-0.1
-0.15
3700
3600
3500
3400
3300
3200
wavenumber / cm-1

(b)

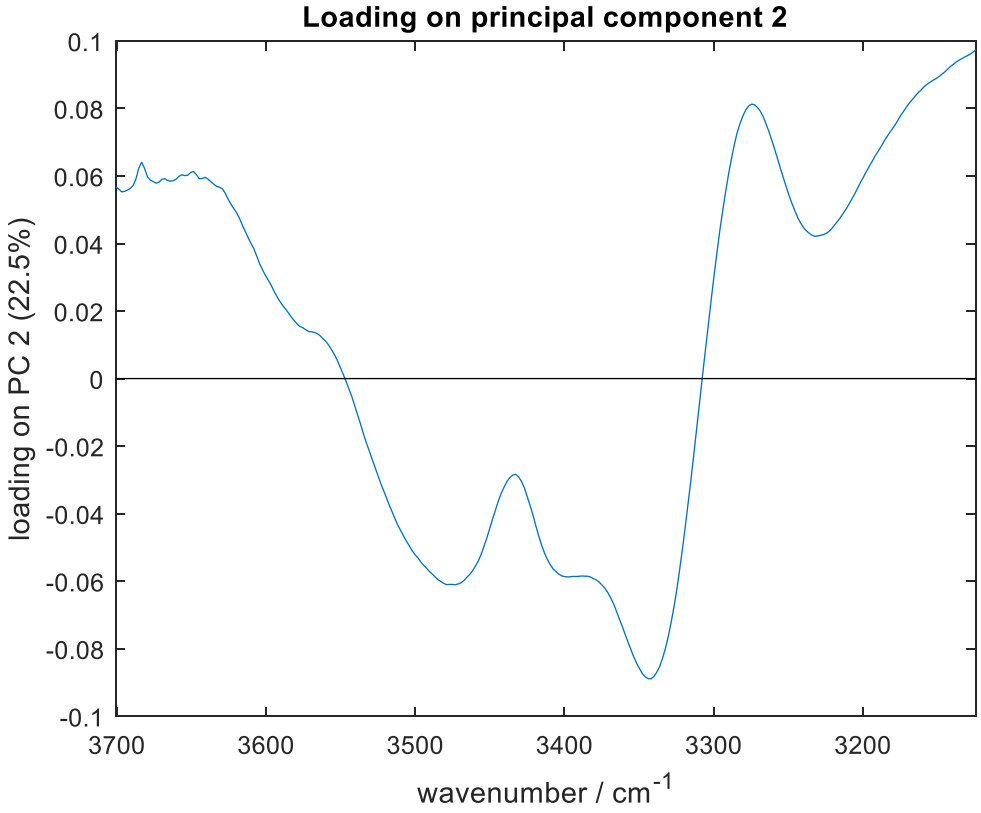
Loading on principal component 2
loading on PC 2 (22.5%)
0.1
0.08
0.06
0.04
0.02
0
-0.02
-0.04
-0.06
-0.08
-0.1
3700
3600
3500
3400
3300
3200
wavenumber / cm-1

(c)

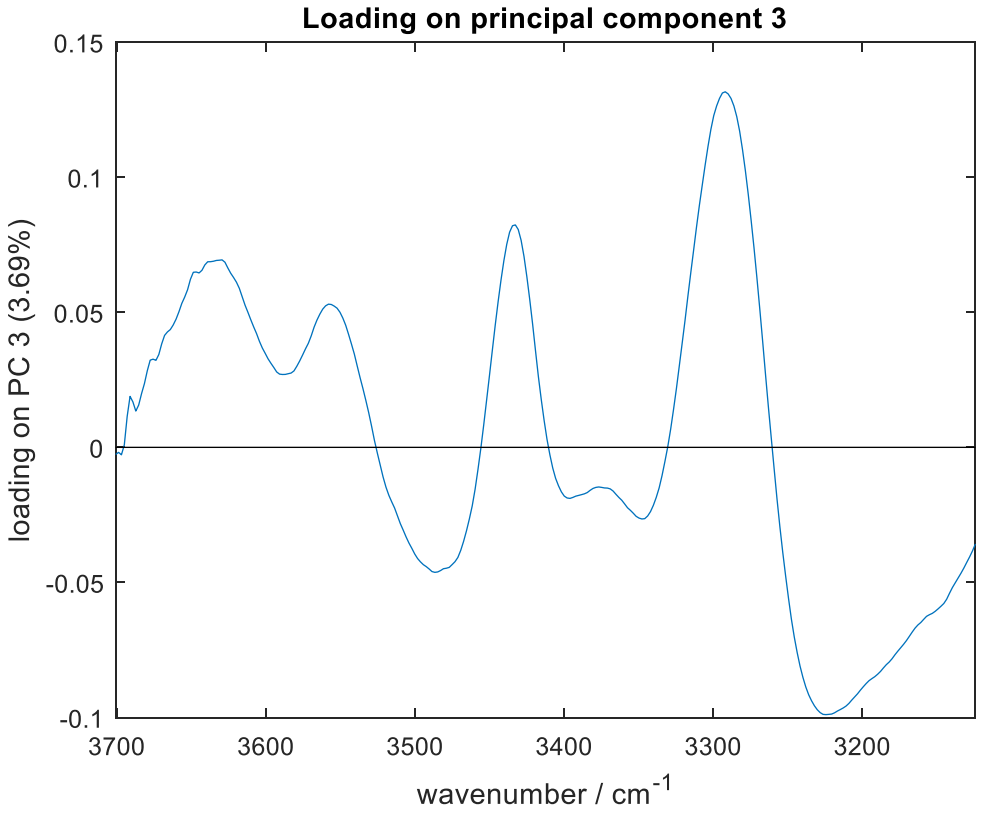

Figure6. 7 (a) The PC1 loading for PCA of stroma on 12 glass slides in experiment 1. (b) The PC2 loading for PCA stroma on 12 glass slides in experiment 1. (c) The PC3 loading for PCA of stroma on 12 glass slides in experiment 1.

6.2.3.2.2 The results of PCA of 12 glass slides in experiment 2

The scores of PC1, PC2 and PC3 in experiment 2 are 64.4%, 22.3% and 7.39%, respectively. Figure 6.8 (a) indicates a clear separation between the spectra of stroma on glass A and the other glass slides depending on PC1 and PC2. However, the spectra of stroma on the other 11 glass slides cannot be separated entirely.

The loadings of three PCs are shown in figure 6.9. The PC1 mainly results from the negative peak (3295 cm^{-1}), which is related to amide A. The distribution of spectra on PC1 should be around negatively correlated with the intensity of amide A. According to the mean spectra of stroma on glass A (figure 6.4 (b)), the intensity of amide A on glass A is relatively high than on most glass slides, so the spectra of glass A distributed on the PC1 negative area.

Figure 6.9 (b) indicates PC2 mainly includes three peaks. One positive peak, located at 3293 cm^{-1}, is related to amide A, and two negative peaks located at 3436 and 3544 cm^{-1} are both related to O-H stretching, which may be from the glue and coverslip, respectively. The distribution of spectra on PC2 is nearly positively correlated with the intensity of amide A and negatively related to the intensity of glue and coverslip. According to the mean spectra of stroma on 12 glass slides (figure 6.4 (b)), the intensity of amide A generally negatively correlates with the intensity of glue peak on most glass slides. So except for glass A, the spectra on the other 11 glass slides locate on both positive and negative areas of PC2 and cannot separate.

For the spectra on glass A, the intensity of amide A is relatively high, but the intensity of glue peak (3450 cm^{-1}) is much higher than the other glass slides. Therefore, the distribution of spectra of glass A on PC2 is more affected by the intensity of the glue peak. The spectra of stroma on glass A only distribute on the negative area of PC2.

(a)

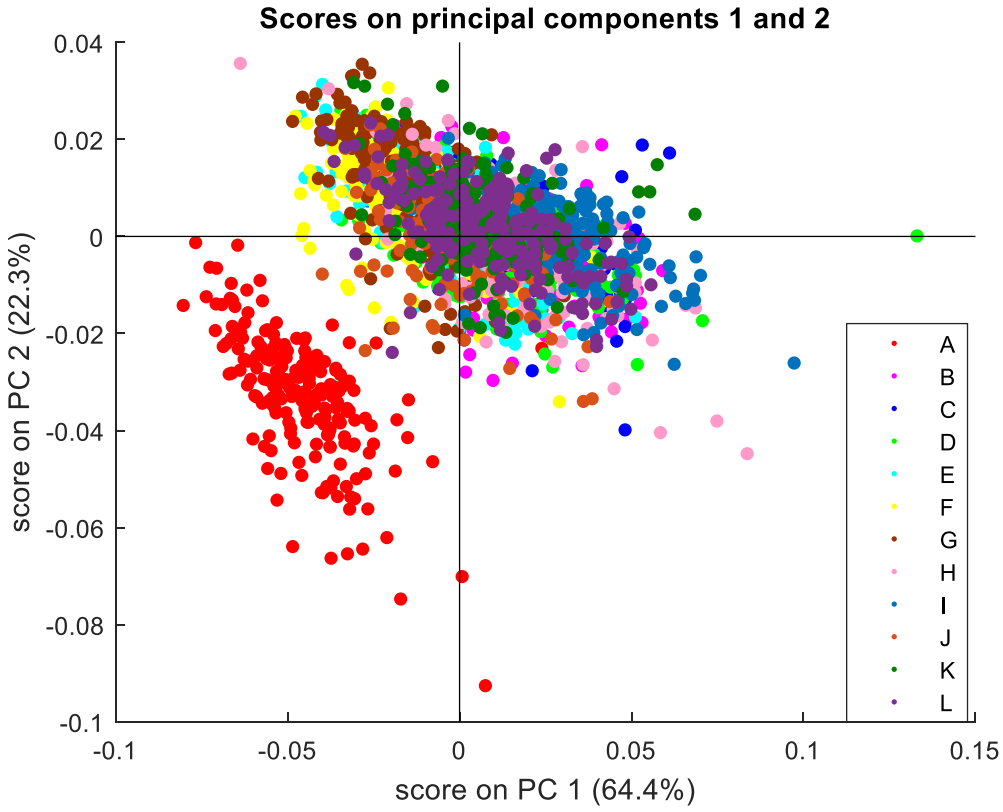
Scores on principal components 1 and 2
score on PC 2 (22.3%)
score on PC 1 (64.4%)
0.04
0.02
0
-0.02
-0.04
-0.06
-0.08
-0.1
-0.1
-0.05
0
0.05
0.1
0.15
A
B
C
D
E
F
G
H
I
J
K
L

(b)

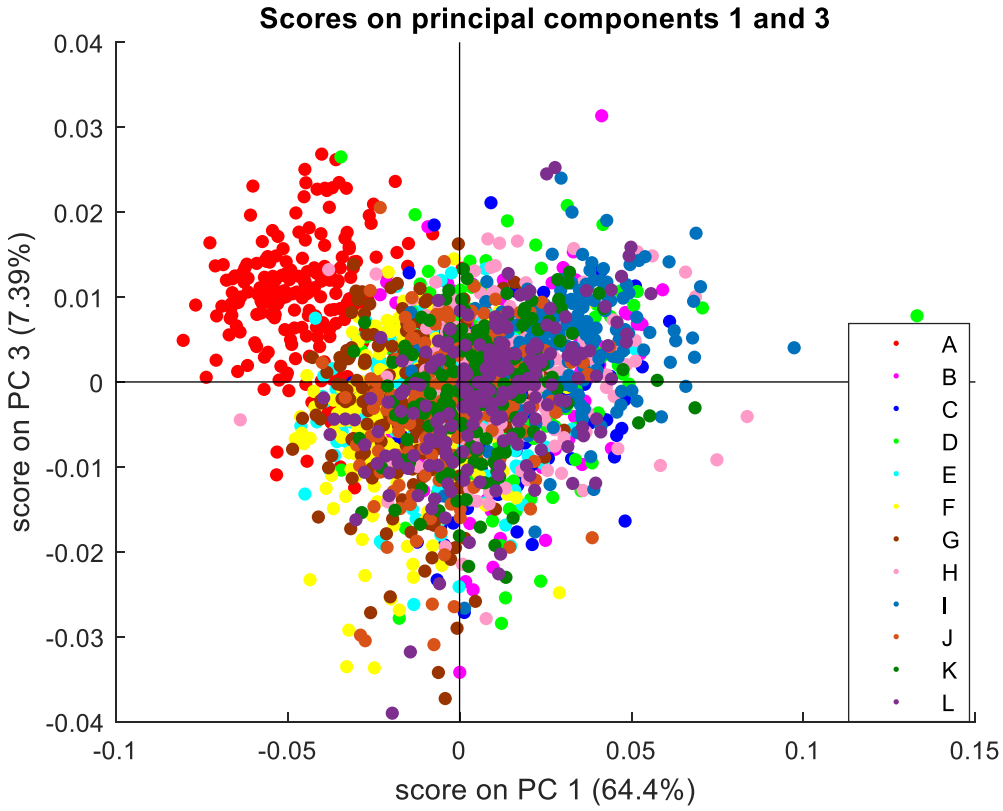
Scores on principal components 1 and 3
score on PC 3 (7.39%)
score on PC 1 (64.4%)
0.04
0.03
0.02
0.01
0
-0.01
-0.02
-0.03
-0.04
-0.1
-0.05
0
0.05
0.1
0.15
A
B
C
D
E
F
G
H
I
J
K
L

(c)

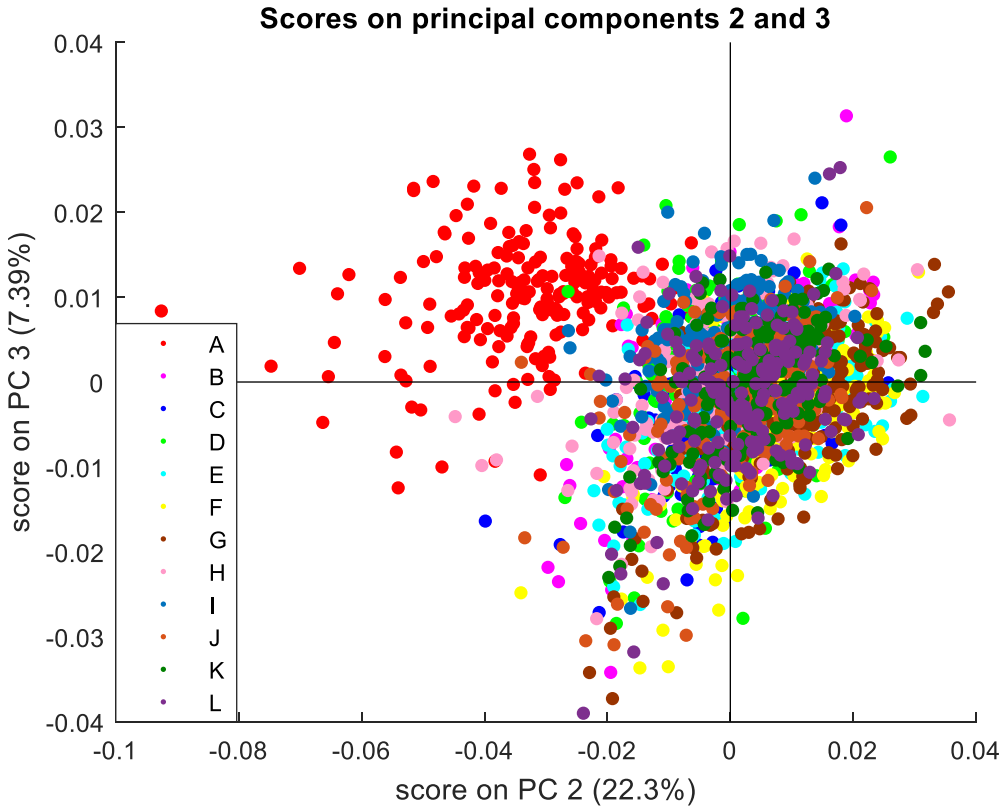

Figure6. 8 (a) The score plots of PC1 and PC2 of stroma on 12 glass slides in experiment 2. (b) The score plots of PC1 and PC3 of stroma on 12 glass slides in experiment 2. (c)The score plots of PC2 and PC3 of stroma on 12 glass slides in experiment 2.

(a)

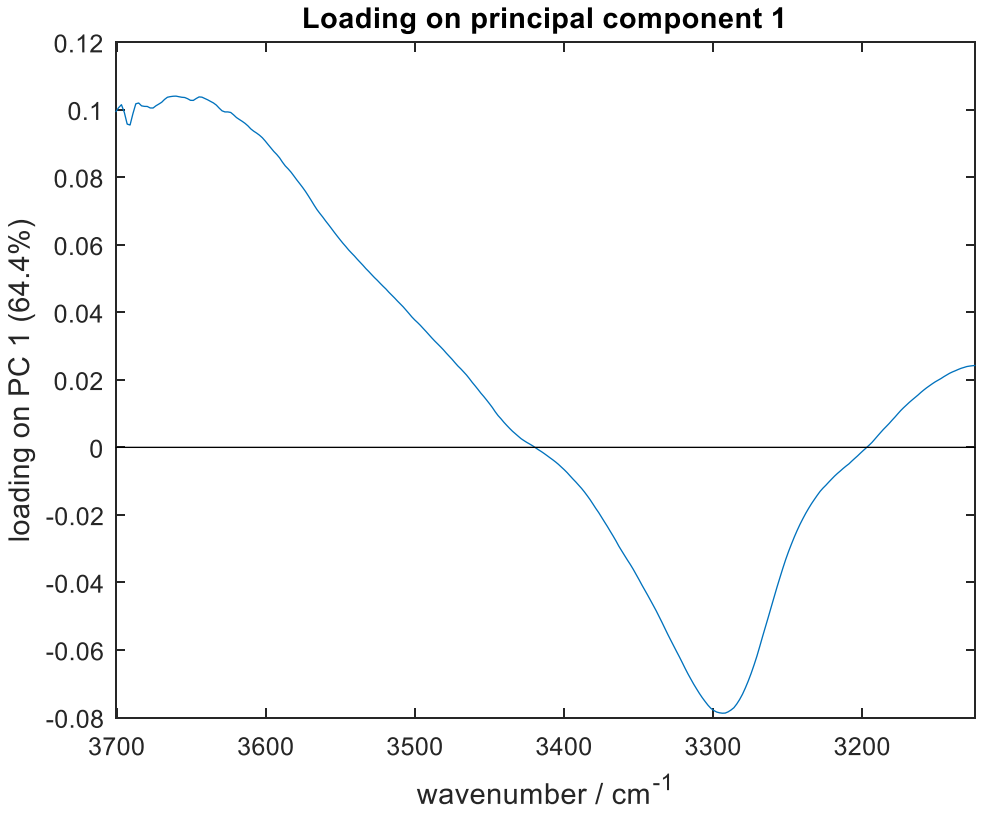
Loading on principal component 1
loading on PC 1 (64.4%)
0.12
0.1
0.08
0.06
0.04
0.02
0
-0.02
-0.04
-0.06
-0.08
3700
3600
3500
3400
3300
3200
wavenumber / cm-1

(b)

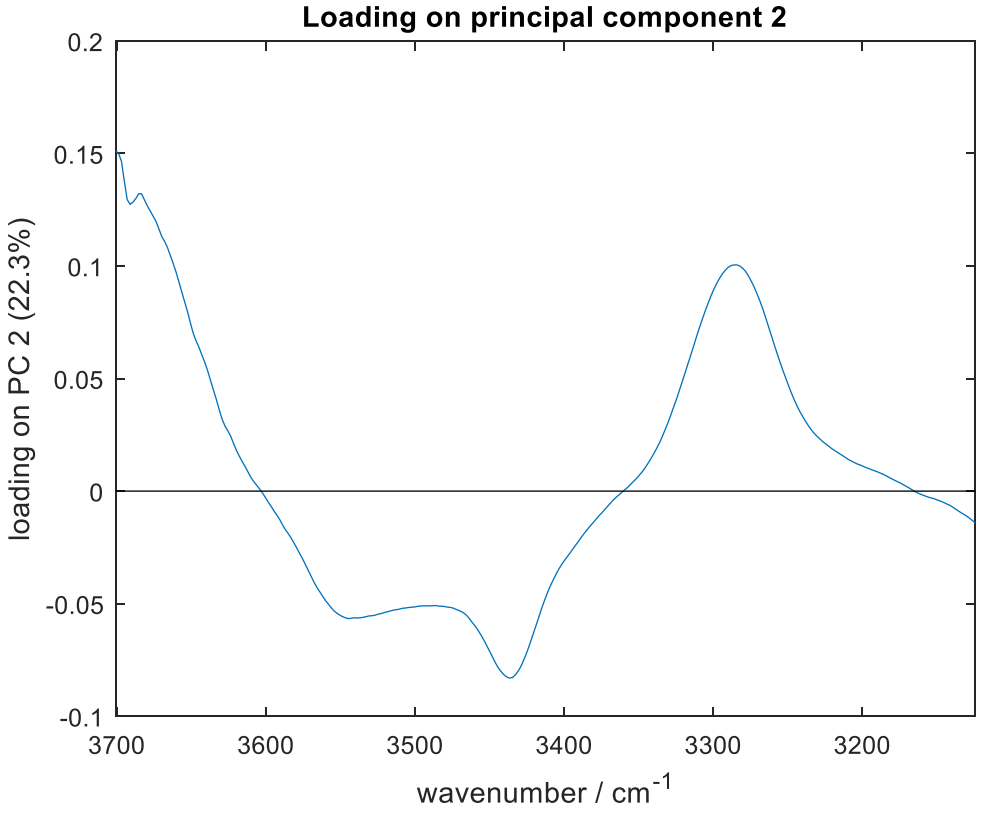
Loading on principal component 2
loading on PC 2 (22.3%)
0.2
0.15
0.1
0.05
0
-0.05
-0.1
3700
3600
3500
3400
3300
3200
wavenumber / cm-1

(c)

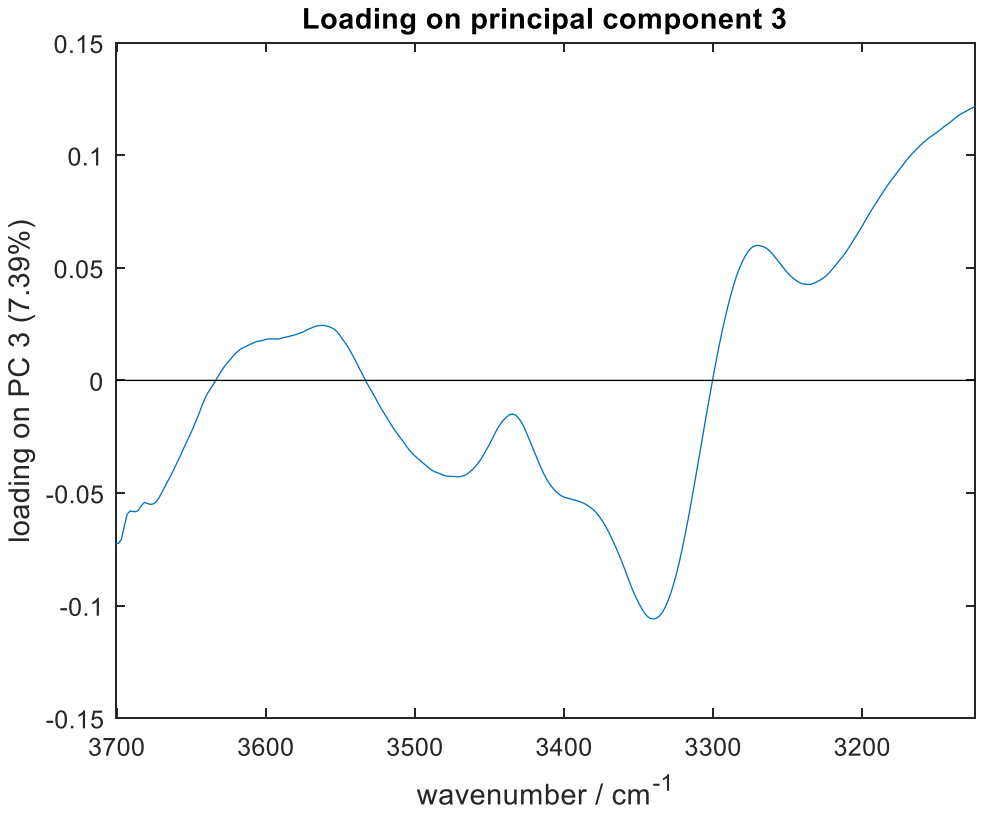

Figure6. 9 (a) The PC1 loading for PCA of stroma on 12 glass slides in experiment 2. (b) The PC2 loading for PCA stroma on 12 glass slides in experiment 2. (c) The PC3 loading for PCA of stroma on 12 glass slides in experiment 2.

6.2.3.3 The epithelium and stroma classification on every glass slide

Spectra of epithelium and stroma are compared in 3125 – 3700 cm^{-1} to find the difference between the epithelium and stroma on the same glass slides. Because the results of the spectral comparison of epithelium and stroma on the same glass are similar. The comparison of spectra of epithelium and stroma on glass L is used as an example and demonstrated. Figures 6.10 and 6.12 show the spectral comparison results on glass L for experiment 1 and experiment 2.

6.2.3.3.1 Tissue classification on same glass slides in experiment 1

(a)

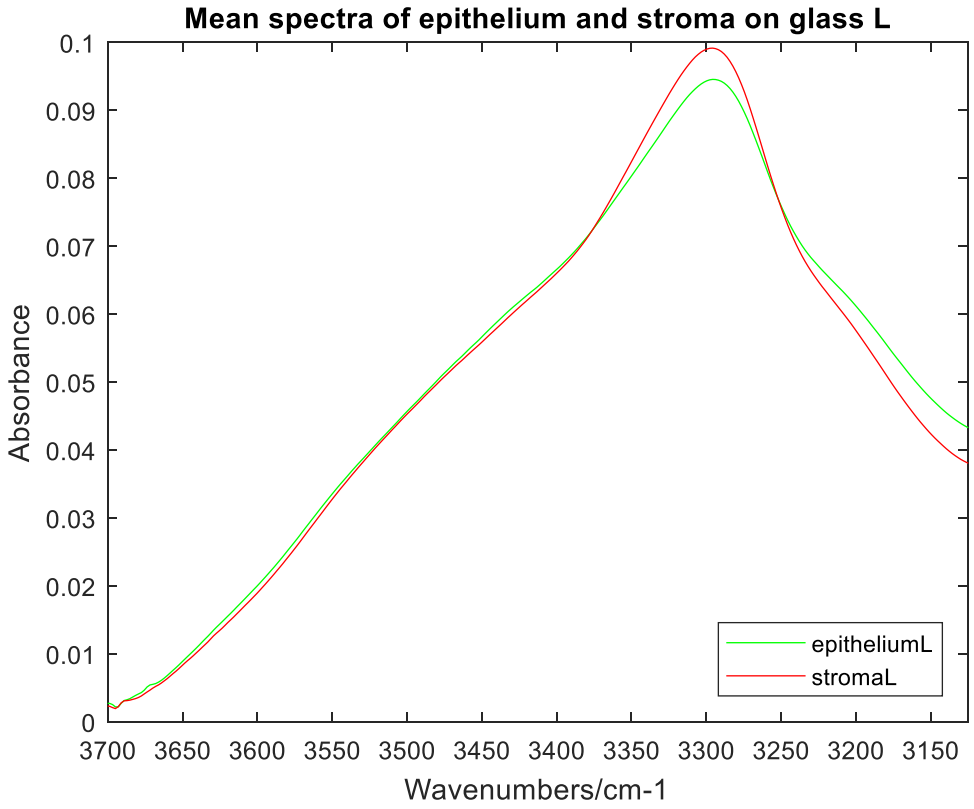
Mean spectra of epithelium and stroma on glass L
Absorbance
0.1
0.09
0.08
0.07
0.06
0.05
0.04
0.03
0.02
0.01
0
3700 3650 3600 3550 3500 3450 3400 3350 3300 3250 3200 3150
Wavenumbers/cm-1
epitheliumL
stromaL

(b)

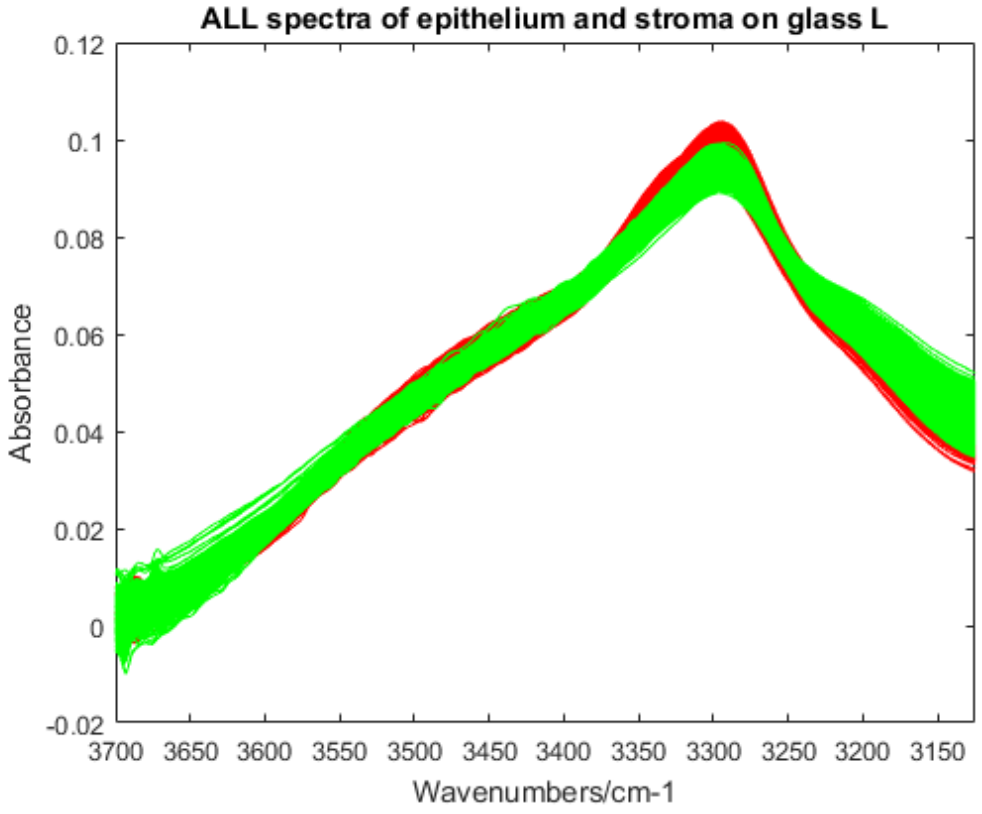
ALL spectra of epithelium and stroma on glass L
Absorbance
0.12
0.1
0.08
0.06
0.04
0.02
0
-0.02
3700 3650 3600 3550 3500 3450 3400 3350 3300 3250 3200 3150
Wavenumbers/cm-1

Figure6. 10 (a) Mean spectra of epithelium and stroma on glass L in experiment 1. (b) All of the spectra of stroma and epithelium on glass L in experiment 1 (epithelium in green and stroma in red).

Based on the mean spectra of epithelium and stroma (figure 6.10 (a)), it generally indicates that the intensity of amide A for stroma is higher than the epithelium. However, Figure 6.10 (b) shows that the stroma and epithelium spectra on glass L are nearly overlapping. It means the spectra of epithelium and stroma on the same glass slide have a minor difference. Therefore, to have an apparent separation between epithelium and stroma, PCA of spectra of stroma and epithelium is necessary to process, and 200 spectra of every type of tissue are randomly selected.

(a)

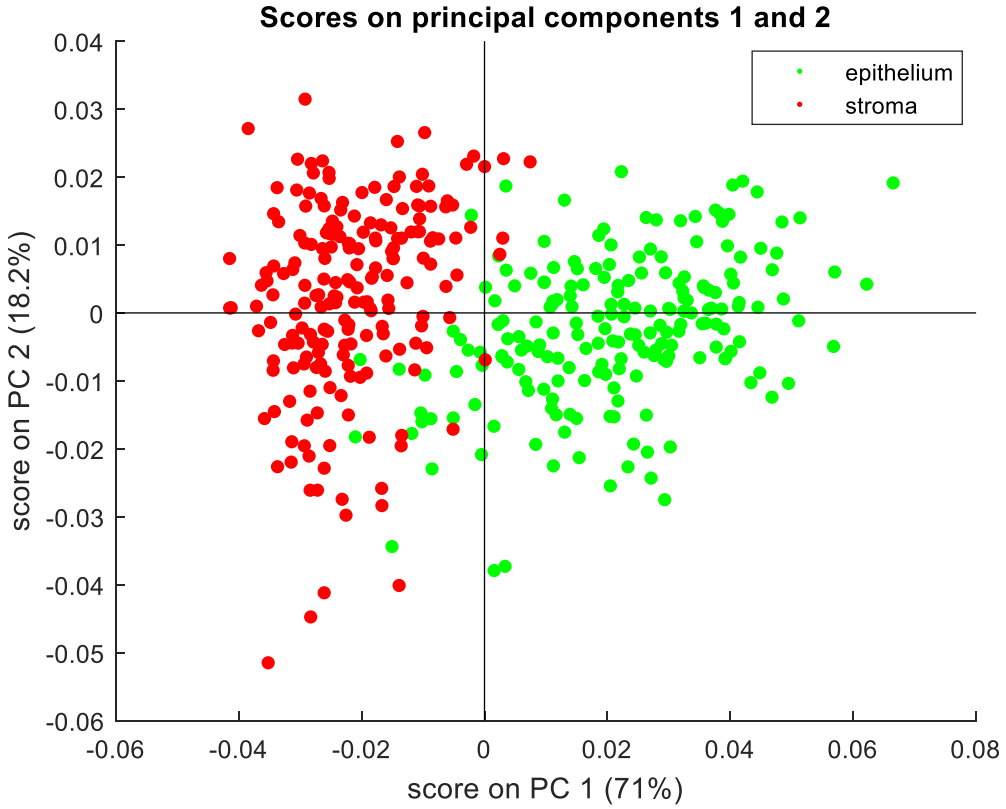

(b)

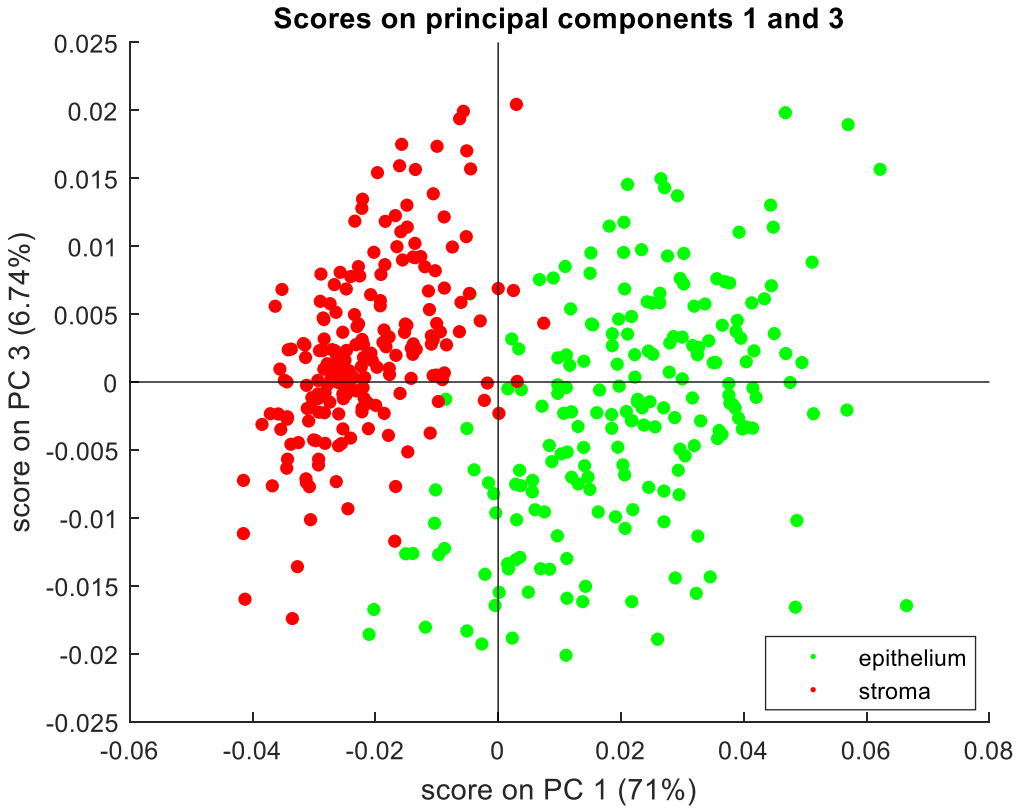
Scores on principal components 1 and 3
score on PC 3 (6.74%)
score on PC 1 (71%)
0.025
0.02
0.015
0.01
0.005
0
-0.005
-0.01
-0.015
-0.02
-0.025
-0.06
-0.04
-0.02
0
0.02
0.04
0.06
0.08
epithelium
stroma

(c)

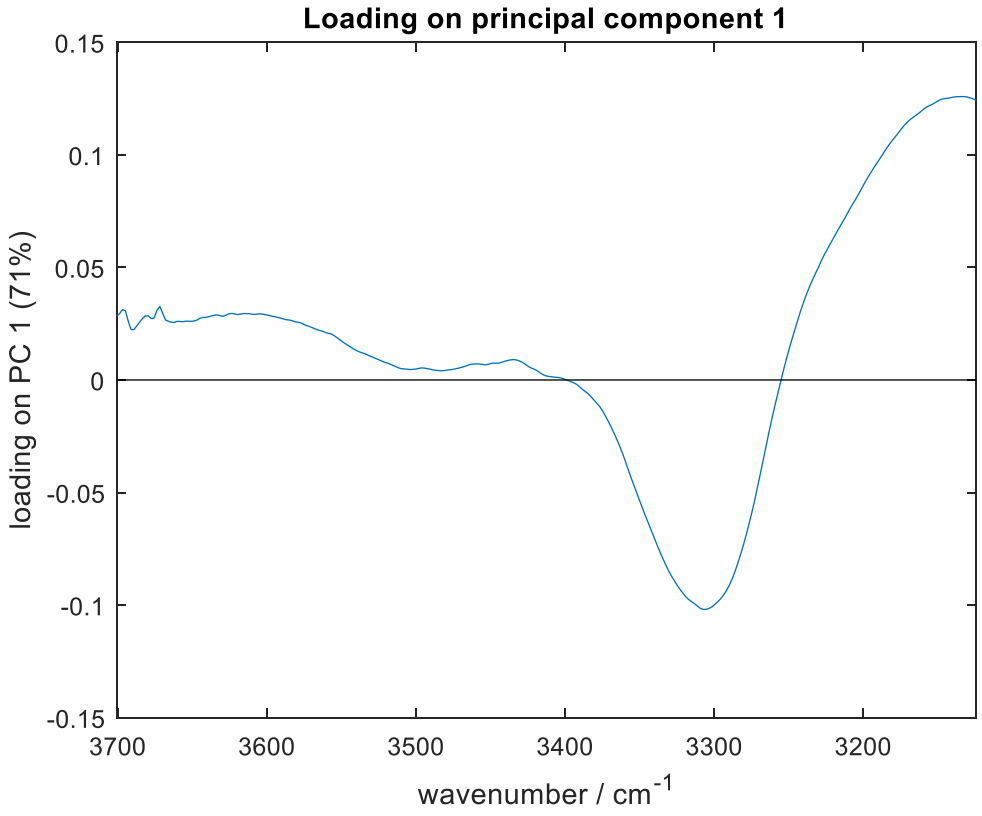
Loading on principal component 1
loading on PC 1 (71%)
wavenumber / cm-1
0.15
0.1
0.05
0
-0.05
-0.1
-0.15
3700
3600
3500
3400
3300
3200

Figure6. 11 (a) The score plots of PC1 and PC2 of epithelium and stroma on glass L in experiment 1. (b) The score plots of PC1 and PC3 of epithelium and stroma on glass L in experiment 1. (c) The PC1 loading for PCA of epithelium and stroma on glass L in experiment 1.

According to figure 6.11 (a) and (b), there is a relatively clear separation between the spectra of epithelium and stroma on glass L, and the separation is based on PC1. The loading of PC1 is shown in figure 6.11 (c). The score of PC1 is 71%, and PC1 is mainly made of the negative peak (3306 cm^{-1}), which is related to N-H asymmetric stretching [19]. N-H is from the tissue, and their intensity is positively correlated to amide A. Therefore, the distribution of spectra on PC1 is negatively correlated with the intensity of amide A. It means the spectra with higher intensity of amide A are distributed in a negative area of PC1. According to the spectra of epithelium and stroma on glass L (figure 6.10), most of the intensity of amide A of the stroma is higher than the epithelium. Thus, the spectra of the stroma are mainly located in a negative area of PC1, and most of the spectra of epithelium are distributed in a positive area of PC1.

6.2.3.3.2 Tissue classification on the same glass slides in experiment 2

Because the spectra in experiment 2 contain additional spectral information of glue and coverslip. The small peak in 3400-3450 cm^{-1} and broad peak in 3400-3600 cm^{-1} is related to glue and coverslip, respectively. For experiment 2, the mean spectra and all of the spectra of epithelium and stroma on glass L are shown in figure 6.12 (a) and (b). The mean spectra indicate that, in general, the intensity of amide A of the stroma is higher than the epithelium. While the intensity of bands (3400 – 3600 cm^{-1}) of epithelium is higher than the stroma. Figure 6.12 (b) shows that all spectra of epithelium and stroma, and most of the spectra are overlap and cannot be separated only depending on the spectra. It is necessary to separate epithelium and stroma by PCA.

(a)

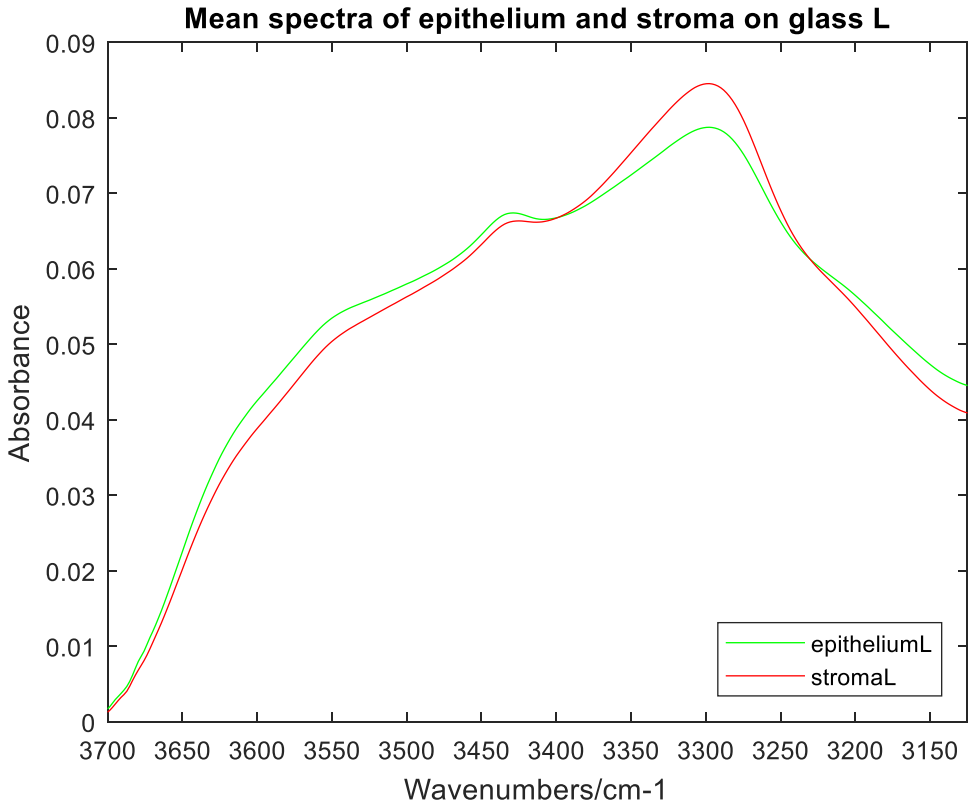
Mean spectra of epithelium and stroma on glass L
Absorbance
0.09
0.08
0.07
0.06
0.05
0.04
0.03
0.02
0.01
0
3700 3650 3600 3550 3500 3450 3400 3350 3300 3250 3200 3150
Wavenumbers/cm-1
epitheliumL
stromaL

(b)

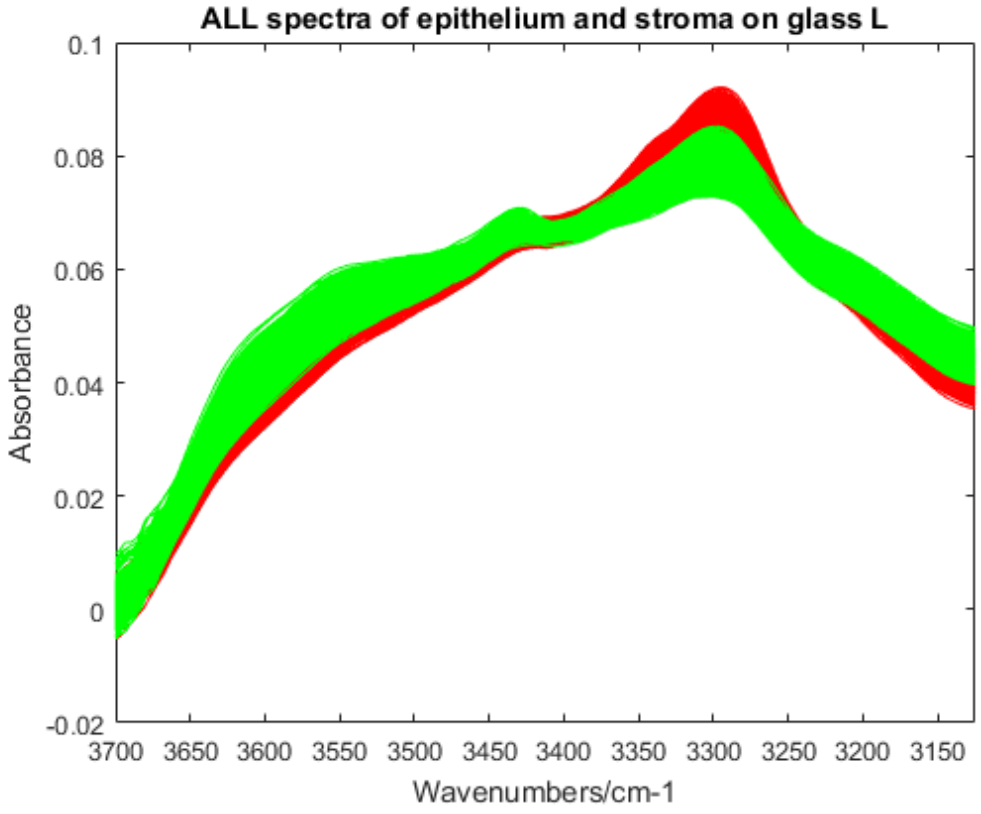
ALL spectra of epithelium and stroma on glass L
Absorbance
0.1
0.08
0.06
0.04
0.02
0
-0.02
3700 3650 3600 3550 3500 3450 3400 3350 3300 3250 3200 3150
Wavenumbers/cm-1

Figure6. 12 (a) Mean spectra of epithelium and stroma on glass L in experiment 2. (b) All of the spectra of stroma and epithelium on glass L in experiment 2 (epithelium in green and stroma in red).

Figure 6.13 (a) and (b) make it easy to see that the epithelium and stroma have a separation trend in experiment 2 based on the PC1. And the loading of PC1 is shown in figure 6.13 (c). Two whole peaks are made of PC1. One is a positive peak (3298 cm^{-1}) related to amide A and the negative abroad peak (3400 – 3700 cm^{-1}) is connected to glue and coverslip. They mean the intensity of amide A is positively correlated to PC1, and the intensity of bands related to glue and coverslip are negatively correlated to PC1. According to figure 6.12, for stroma spectra in experiment 2, the intensity at amide A is higher than epithelium, while the intensity at glue range is lower than epithelium. Therefore, most of the spectra of the stroma are located in a positive area of PC1, while most of the spectra of epithelium are located in the negative area.

(a)

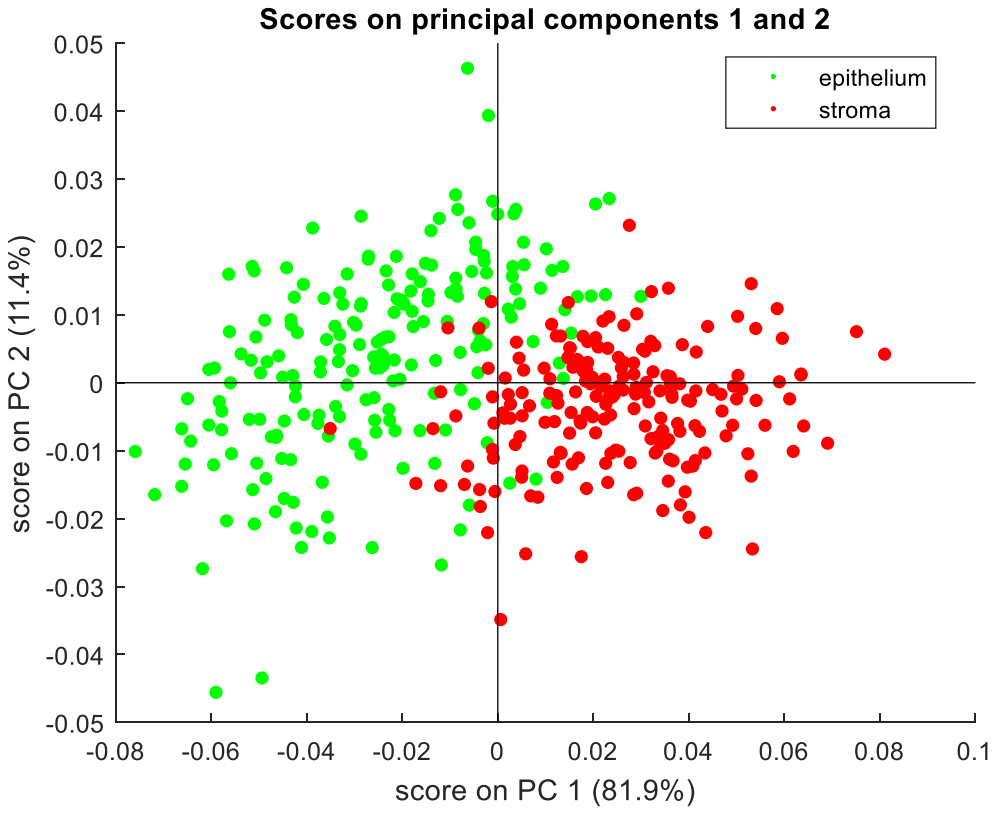

(b)

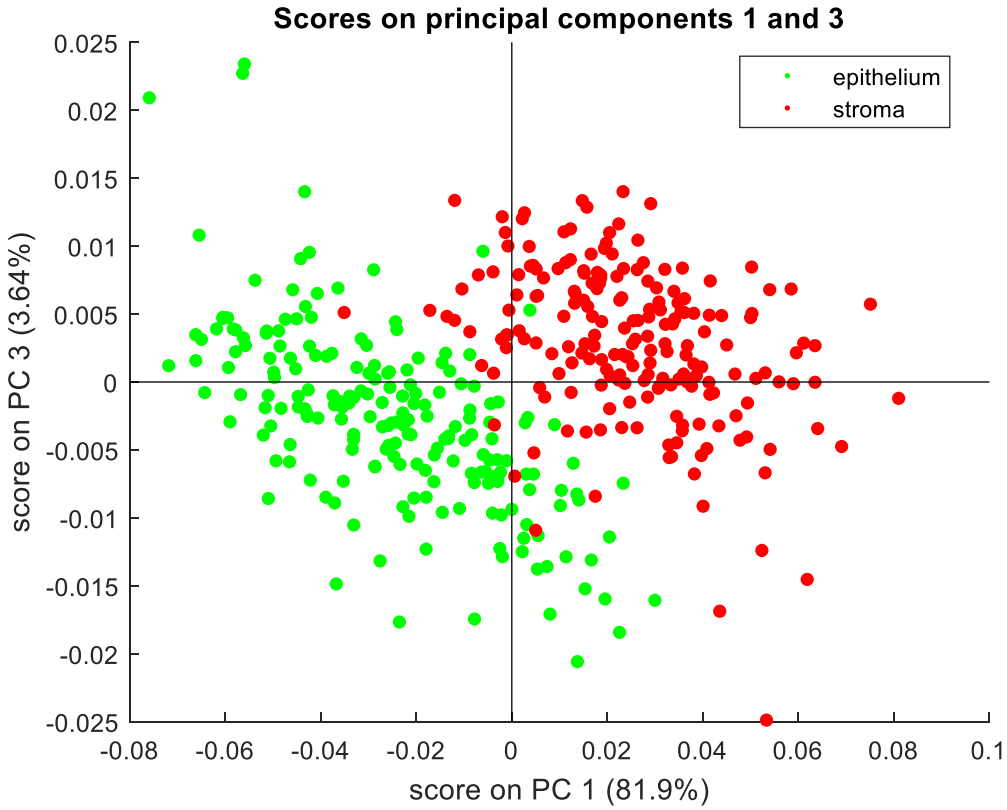
Scores on principal components 1 and 3
epithelium
stroma
score on PC 3 (3.64%)
score on PC 1 (81.9%)
0.025
0.02
0.015
0.01
0.005
0
-0.005
-0.01
-0.015
-0.02
-0.025
-0.08
-0.06
-0.04
-0.02
0
0.02
0.04
0.06
0.08
0.1

(c)

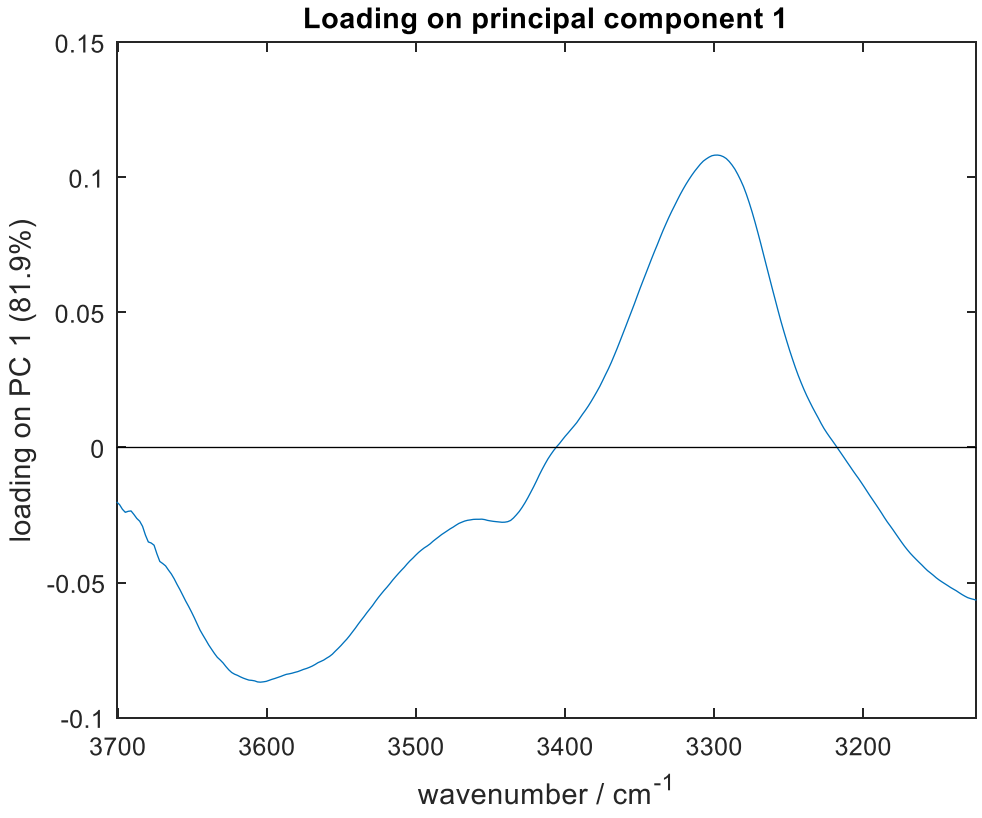
Loading on principal component 1
loading on PC 1 (81.9%)
wavenumber / cm-1
0.15
0.1
0.05
0
-0.05
-0.1
3700
3600
3500
3400
3300
3200

Figure6. 13 (a) The score plots of PC1 and PC2 of epithelium and stroma on glass L in experiment 2. (b) The score plots of PC1 and PC3 of epithelium and stroma on glass L in experiment 2. (c) The PC1 loading for PCA of epithelium and stroma on glass L in experiment 2.

In addition, comparing the PCA results of epithelium and stroma between the two experiments (figure 6.11 and 6.13), the spectra of epithelium and stroma in experiment 1 have a better separation than spectra in experiment 2.

6.2.3.4 Automated histopathological classification on the same glass slide

Random forest is a common method to classify spectra of epithelium and stroma. All of the spectra of epithelium and stroma on the same glass slides are divided into two data set. 80% of spectral data are used to train the classifier, and the rest 20% of spectral data are used to test the classifier. The classifier can be evaluated by the accuracy of histological classification.

Table6. 5 Classifier construction by random forest (Take spectra on glass L as an example.)

	Training set	Test set
Model test	80% spectra of stroma L	20% spectra of stroma L
	80% spectra of epithelium L	20% spectra of epithelium L

The accuracies of epithelium and stroma classification on the same glass for experiments 1 and 2 are shown in table 6.6. According to the exactness in the table, all of the overall accuracies are above 98.40%. It indicates the classifier has high accuracy in discriminating the epithelium and stroma on the same glass slides for experiments 1 and 2. Compared with the specific accuracies on the same glass slide, the classification results in experiment 1 are slightly better than those in experiment 2.

Table6. 6 The accuracy of histological classification on the same glass slide in experiments 1 and 2.

Model test (%)	Experiment 1	Experiment 2
Glass A	98.78	98.84
Glass B	99.37	98.80
Glass C	98.71	98.95
Glass D	99.24	98.82
Glass E	99.77	99.14
Glass F	99.47	98.99
Glass G	99.51	99.42
Glass H	98.42	98.83
Glass I	99.25	99.22
Glass J	99.55	99.38
Glass K	99.53	99.58
Glass L	99.62	99.38

6.2.3.5 Automated histopathological classification on the different glass slides

The high accuracy in the previous part has indicated that the spectra of epithelium and stroma could be easily classified on the same glass slide by random forest. Furthermore, the main aim of this chapter is to look at the influence of glass type on histological classification. It is necessary to classify the spectra of epithelium and stroma on the different glass slides.

Spectral data from one glass slide are used to train the classifier to distinguish epithelium and stroma. And the spectra from the other glass slide are used to test the classifier. If the classifier could classify the spectra of epithelium and stroma on the different glass slides, it would indicate that the type of glass does not affect histological classification. If not, the type of glass affects tissue classification.

Tables 6.7 and 6.8 show all results of tissue classification on different types of glass slides in experiments 1 and 2. According to the classification results in experiment 1 (Table 6.7), most of the tissue classification accuracy of the classifier is above 90%. The bad classification results, which classification accuracy lower than 80%, are highlighted in blue. According to the highlighting in table 6.7, it could be easier to find that the performance of classifiers, which independently tested on the spectra on glass I, are poor and the worst accuracy are only around 52%.

Table6. 7 The accuracy of histological classification on different glass slides in experiment 1

Accuracy (%)	Test on glass A	Test on glass B	Test on glass C	Test on glass D	Test on glass E	Test on glass F	Test on glass G	Test on glass H	Test on glass I	Test on glass J	Test on glass K	Test on glass L
Train on glass A		99.29	98.37	96.24	98.86	98.09	98.66	97.63	87.51	98.83	99.25	98.47
Train on glass B	92.07		96.63	92.13	98.95	96.01	96.74	96.78	67.90	98.50	99.55	97.02
Train on glass C	98.54	99.19		94.82	99.13	99.18	99.02	97.56	76.98	99.22	99.21	96.38
Train on glass D	78.29	95.19	85.14		94.39	82.05	89.34	89.43	95.75	93.13	97.01	98.09
Train on glass E	94.42	99.25	98.10	93.69		95.86	98.15	97.75	77.23	98.33	99.32	95.59
Train on glass F	97.64	96.83	98.37	80.92	97.17		98.82	93.02	63.43	96.77	95.09	83.15
Train on glass G	96.16	97.52	98.98	71.26	98.01	97.86		94.38	52.12	96.90	96.59	80.07
Train on glass H	93.70	99.46	97.69	97.49	98.81	93.09	98.55		80.13	98.89	99.47	98.81
Train on glass I	89.35	96.97	90.65	97.20	95.20	86.91	92.81	93.67		94.72	97.18	98.89
Train on glass J	97.82	99.41	98.41	97.86	98.91	98.70	98.53	97.86	90.87		99.39	98.20
Train on glass K	92.28	99.35	95.64	95.39	98.64	94.58	96.59	96.97	75.72	98.24		98.00
Train on glass L	84.61	98.26	92.10	98.57	95.82	89.39	92.32	93.66	95.67	95.96	97.81	

Table6. 8 The accuracy of histological classification on different glass slides in experiment 2

Accuracy (%)	Test on glass A	Test on glass B	Test on glass C	Test on glass D	Test on glass E	Test on glass F	Test on glass G	Test on glass H	Test on glass I	Test on glass J	Test on glass K	Test on glass L
Train on glass A		72.85	75.72	76.13	72.20	67.93	70.81	78.77	80.06	73.33	74.27	76.31
Train on glass B	56.89		98.41	97.68	96.62	92.73	98.82	97.52	93.48	98.01	98.46	99.26
Train on glass C	58.48	98.32		97.26	97.80	94.97	99.27	95.89	87.05	98.84	99.19	98.74
Train on glass D	75.76	98.06	97.98		94.48	88.50	98.74	97.61	90.64	96.05	95.78	98.89
Train on glass E	61.45	94.01	96.51	90.51		98.11	98.24	85.69	59.45	99.05	98.25	93.48
Train on glass F	48.45	89.95	94.12	84.62	97.91		97.66	75.75	57.33	96.37	95.70	89.94
Train on glass G	68.13	97.11	98.20	94.99	98.19	97.68		93.95	78.27	98.64	98.75	97.88
Train on glass H	69.42	98.14	96.93	98.45	90.72	80.75	97.47		96.01	94.16	95.18	98.63
Train on glass I	96.40	93.41	87.89	92.36	80.22	72.00	88.13	93.36		84.26	87.62	92.59
Train on glass J	54.55	96.27	97.55	93.72	98.60	96.31	99.01	90.57	65.76		99.02	95.92
Train on glass K	69.43	97.32	98.36	95.71	98.57	96.05	99.14	93.95	74.06	99.11		97.52
Train on glass L	68.33	98.59	98.30	96.91	95.97	93.55	98.45	97.01	91.29	97.80	98.35	

For experiment 2, classification accuracy is above 90% for most classifiers. However, the classifier trained by spectral data of glass A always has a poor classification performance. In addition, the other classifiers always have poor accuracy results when they are tested on glass A and glass I. It is caused by the spectral difference on glass A. According to the mean spectra (figure 6.5) and PCA results (figure 6.8) in experiment 2, the spectra of glass A have a specific difference and could be separated from the

spectra on the rest 11 glass slides. Glass A has much more glue than the other glass slide, which lead to the intensity of glue peak (3400-3450 cm^{-1}) are much higher. For glue peak, the intensity of epithelium is usually higher than stroma. Therefore, if the spectral data on glass A is used to train a model, the tested spectra of epithelium on the other 11 glass slides would be misclassified as stroma and cause low accuracy.

The high classification accuracies of the two experiments indicate that the type of glass slide has little influence on tissue classification. In addition, the spectra in experiment 1 always have better tissue classification performance than experiment 2.

6.2.4 Tissue classification with glue removal

According to the comparison between experiments 1 and 2 (tale 3.3), it is easy to see glue will have much more influence on the spectra in experiment 2. While for experiment 1, because the glue content on the background and tissue sample is variable, spectra information maybe plus or minus a little glue. It can be seen in the mean spectra of 12 glass slides (figure 6.4); some of the mean spectra have positive peaks, and some of them have negative peaks in 3400 – 3450 cm^{-1}. However, the little glue has a slight influence on spectra in experiment 1. Therefore, in both experiments 1 and 2 an attempt will be made to correct or remove glue from spectra.

Glue removal is based on the principle of spectral subtraction, and the critical function of code is least squares with known covariance (LSCOV). According to the discussion in chapter 5, the most suitable reference spectra of glue removal are the spectra of Matrigel, coverslip and glue, and the most suitable fit ranges include range 1: Matrigel (3278-3318 cm^{-1}, 3066-3106 cm^{-1}); range 3: glue peak & Matrigel peak (2950-2970 cm^{-1}, 2925-2945 cm^{-1}, 2867-2887 cm^{-1}); range 4 coverslip & Matrigel peak (3536-3576 cm^{-1}, 2704-2744 cm^{-1}). The reference spectra are shown in figure 5.2. Every mean spectrum of epithelium and stroma has had the glue removed. Figures 6.14

and 15 showed the mean spectra after correcting or removing glue on 12 glass slides in experiments 1 and 2.

6.2.4.1. Mean spectra with glue removal

6.2.4.1.1 Mean spectra with glue removal in experiment 1

(a)

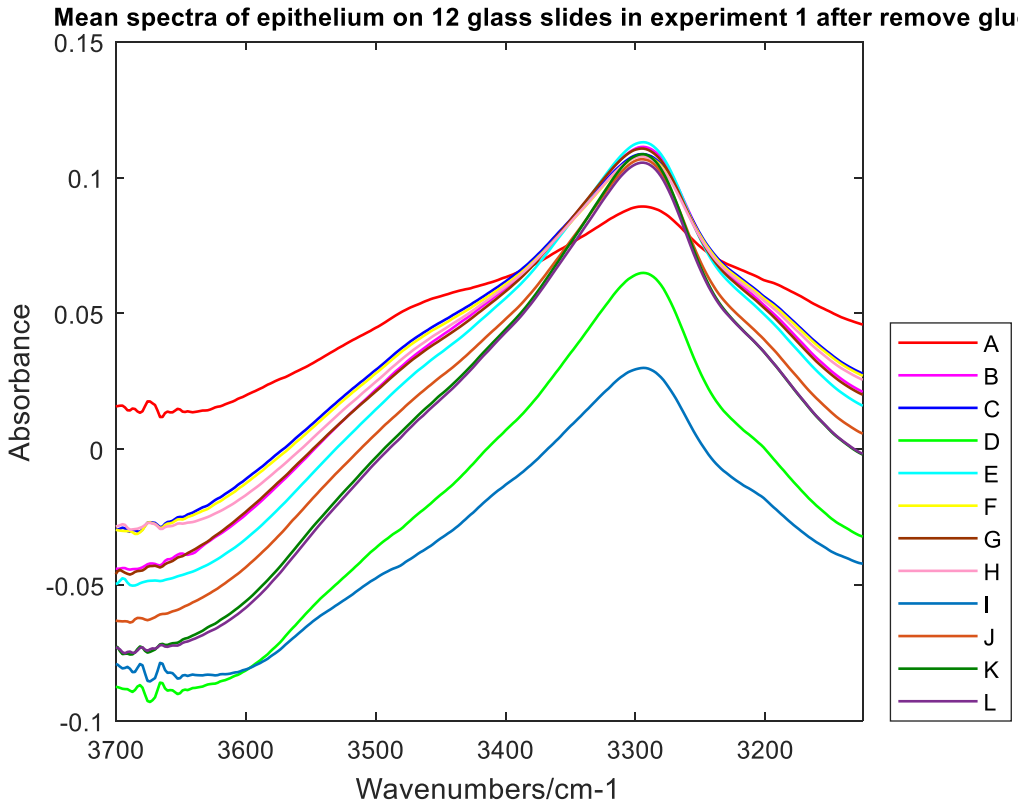

(b)

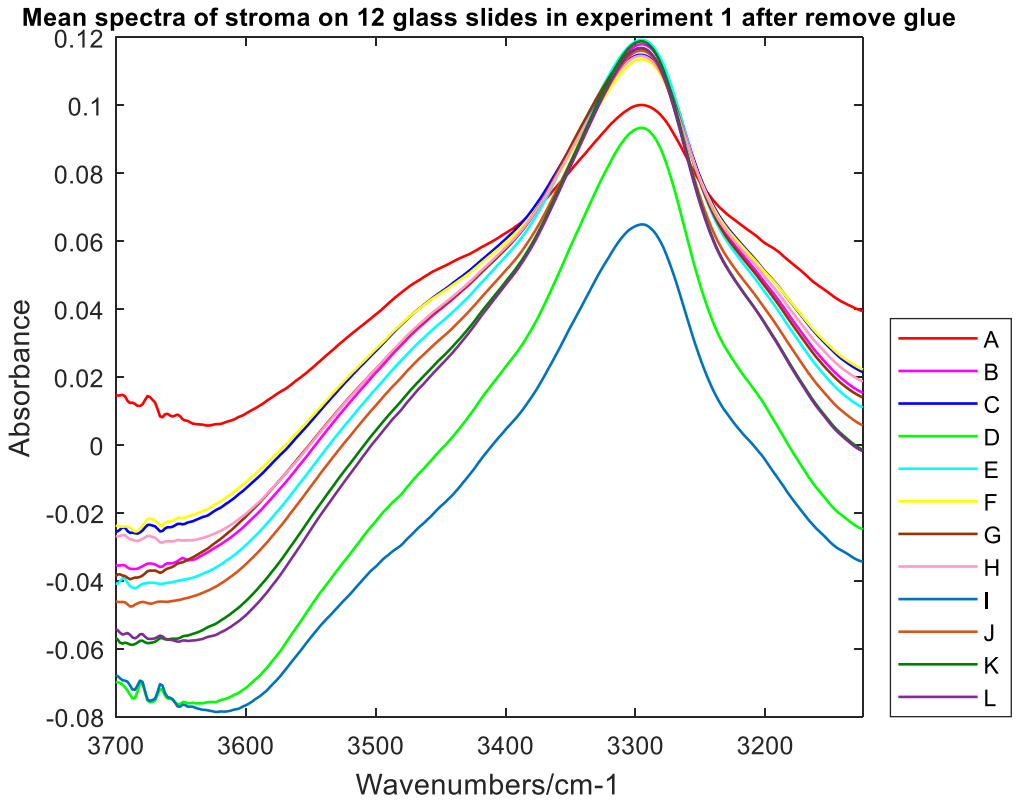

Figure6. 14 (a) the mean spectra of epithelium on 12 glass slides with glue removal in 3125 – 3700 cm^{-1} for experiment 1. (b) mean spectra of stroma on 12 glass slides with glue removal in 3125 – 3700 cm^{-1} for experiment 1

Table 3.3 shows that the spectra information in experiment 1 includes tissue plus or minus some glue. In addition, the spectral range in 3400-3450 cm^{-1} is related to glue. Therefore, the mean spectra without glue removal on 12 glass slides (figure 6.4) have different trends in the 3400-3450 cm^{-1} region. For example, the mean spectra on glass A have prominent negative peaks in 3400-3450 cm^{-1} but the mean spectra on glass I positive peaks in this range.

Figure 6.14 show that after removing glue, for mean spectra on glass A the negative peak in 3400 -3450 cm^{-1} has disappeared, indicating that some of the glue has been added to mean spectra on glass A, while for the mean spectra on glass I, there is no positive peak in the range of 3400 -3450 cm^{-1} after glue removal. It shows the glue on spectra of glass I has already been removed.

6.2.4.1.2 Mean spectra with glue removal in experiment 2

Table 3.3 indicates that spectra in experiment 2 are significantly affected by the glue and coverslip. Based on the spectra in figure 5.2, the band in 3400-3450 cm^{-1} and 3400-3600 cm^{-1} are caused by glue and coverslip, respectively. Figure 6.15 shows the mean spectra of 12 glass slides in experiment 2 after removing the glue, and it is easy to see the small peaks 3400-3450 cm^{-1} and the broad brands in 3400-3600 cm^{-1} have been removed, compared with the mean spectra of 12 glass slides without removing glue (figure 6.5).

However, the spectra in 3400-3450 cm^{-1} are not very smooth and have slightly negative trends after removing glue in figure 6.15. It is caused by over remove the glue. Therefore, there is some limitation on the code of glue removal.

(a)

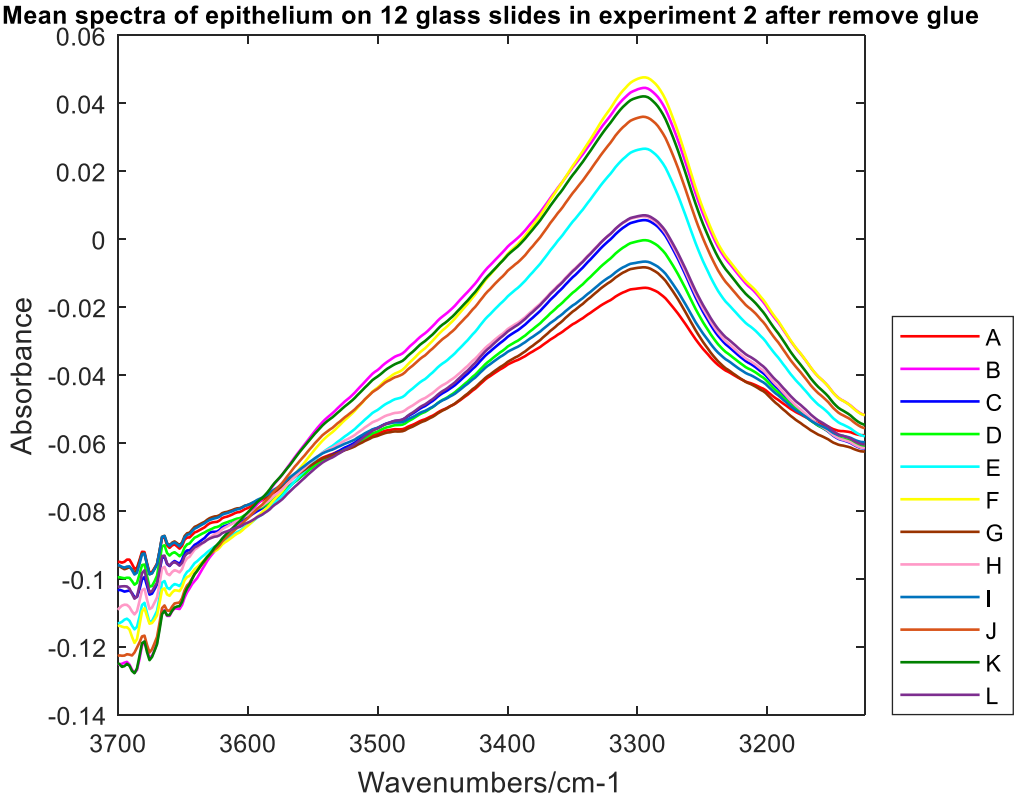

(b)

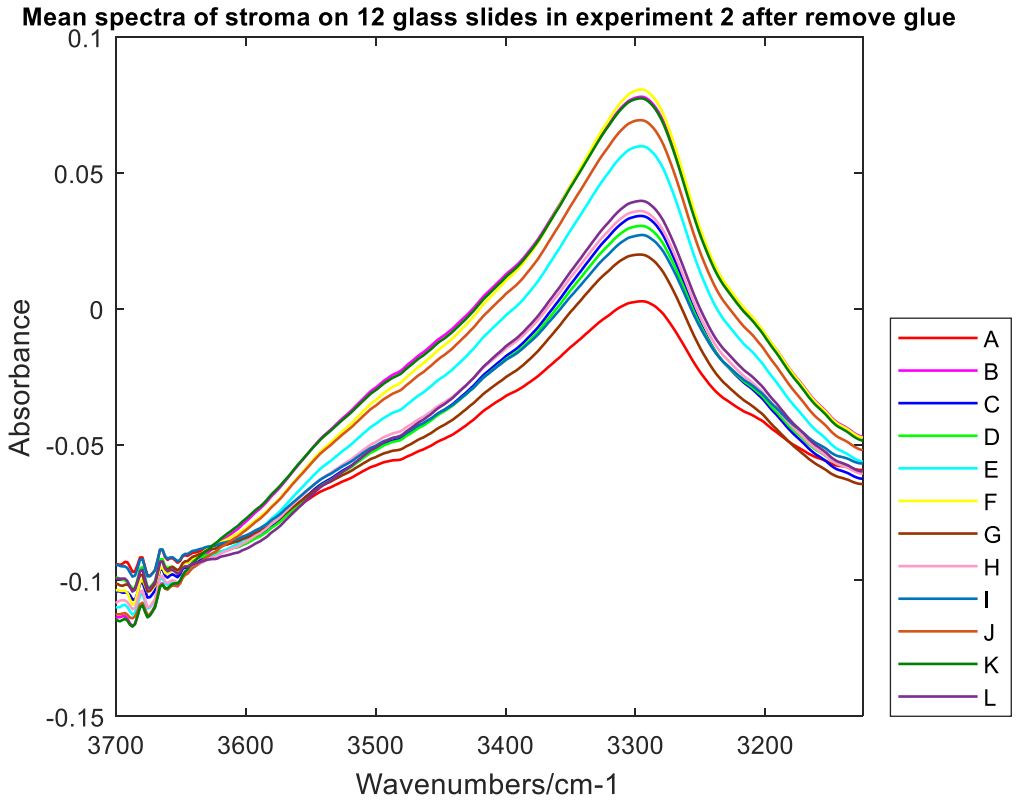

Figure6. 15 (a) the mean spectra of epithelium on 12 glass slides after removing glue in 3125-3700 cm^{-1} for experiment 2. (b) mean spectra of stroma on 12 glass slides after removing glue in 3125-3700 cm^{-1} for experiment 2

6.2.4.2. The PCA on 12 glass slides with glue removal

PCA results of spectra on 12 glass slides in experiments 1 and 2 with glue removal are shown in Figures 6.16 and 6.17, respectively. The PCA distributions of epithelium and stroma on 12 glass slides are similar, so the PCA results are shown from spectra of the stroma only.

6.2.4.2.1 The results of PCA on 12 glass slides in experiment 1 with glue removal

According to figure 6.16 (a), there is no clear separation between the spectra on 12 glass slides, but there is a regular trend in distribution on PC2. Therefore, figure 6.16 only shows the score plots of PC2 and PC3 and the loading of PC2.

(a)

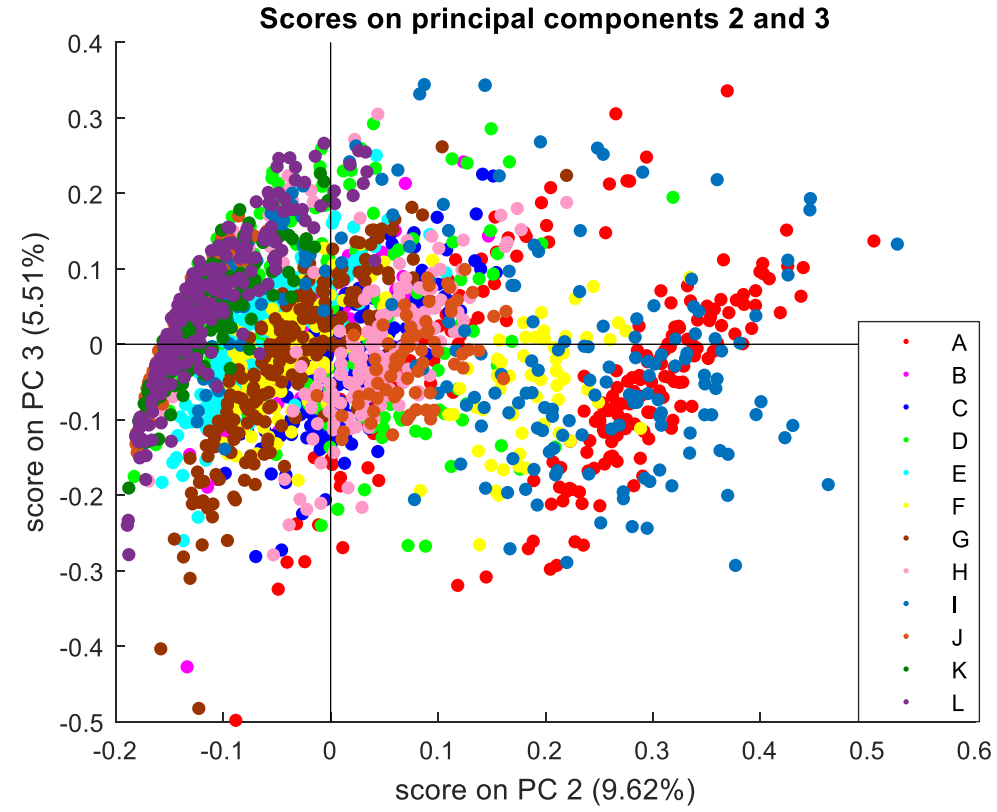
Scores on principal components 2 and 3
score on PC 3 (5.51%)
score on PC 2 (9.62%)
0.4
0.3
0.2
0.1
0
-0.1
-0.2
-0.3
-0.4
-0.5
-0.2
-0.1
0
0.1
0.2
0.3
0.4
0.5
0.6
A
B
C
D
E
F
G
H
I
J
K
L

(b)

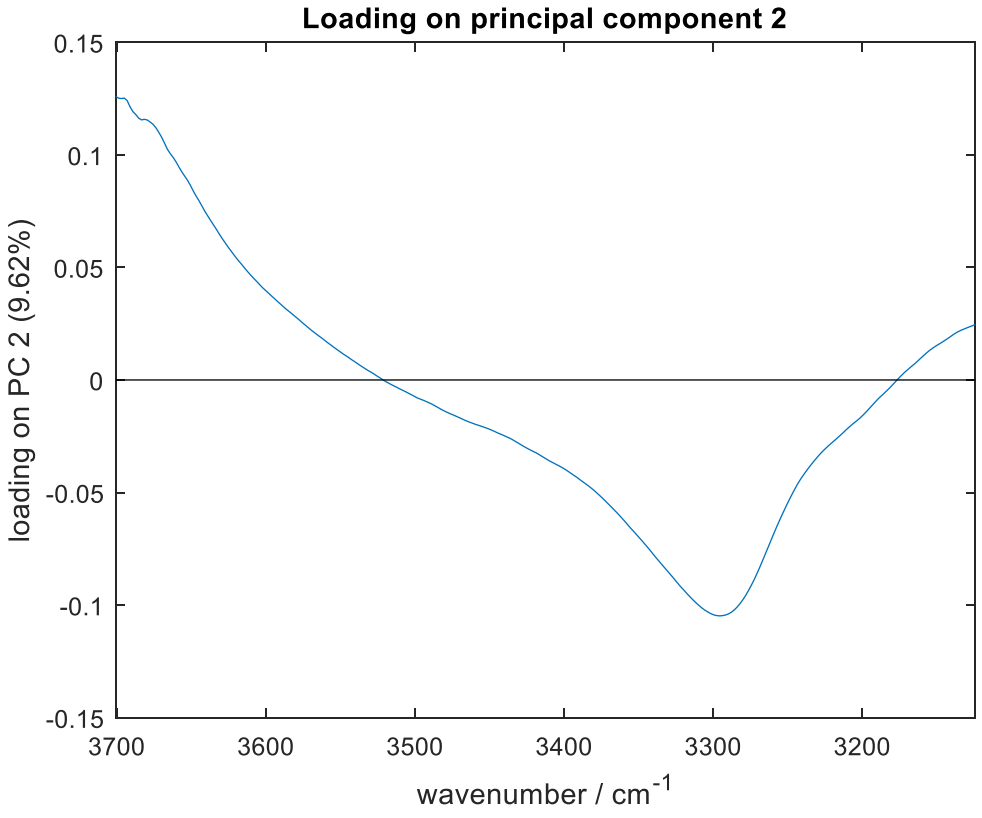
Loading on principal component 2
loading on PC 2 (9.62%)
wavenumber / cm-1
0.15
0.1
0.05
0
-0.05
-0.1
-0.15
3700
3600
3500
3400
3300
3200

Figure6. 16 (a) The score plots of PC2 and PC3 of stroma on 12 glass slides with glue removal in experiment 1. (b) The PC2 loading for PCA stroma on 12 glass slides with glue removal in experiment 1.

According to the loading of PC2 (figure 6.16 (b)), it shows that the PC2 only is made of one negative peak, which is related to amide A (3296 cm^{-1}). Therefore, the intensity of amide A is negatively correlated to PC2. It means the lower the intensity of amide A, the more spectra are distributed in the positive area of PC2.

6.2.4.2.2 The results of PCA on 12 glass slides in experiment 2 with glue removal

PCA results of spectra of stroma on 12 glass slides after removing glue are shown in figure 6.17. There is no separation among the spectra on 12 glass slides from the score plots. And according to the loading of PC1, PC1 is made of a significant positive peak at 3298 cm^{-1}, which is related to amide A. Thus, the distribution of PC1 is positively associated with the intensity of amide A. However, because the difference of intensities of amide A among 12 glass slides is tiny, the distribution of spectra on PC2 only has a regular but cannot be separated.

In addition, compared with the PCA results of spectra on 12 glass slides in experiment 2 without glue removal (figure 6.8), there is an apparent separation between glass A and the other glass slides. However, after removing the glue, the separation disappeared. Therefore, the split for spectra without glue removal is much more caused by glue rather than tissue. Furthermore, the type of glass slides has very slight effect on the infrared spectra.

(a)

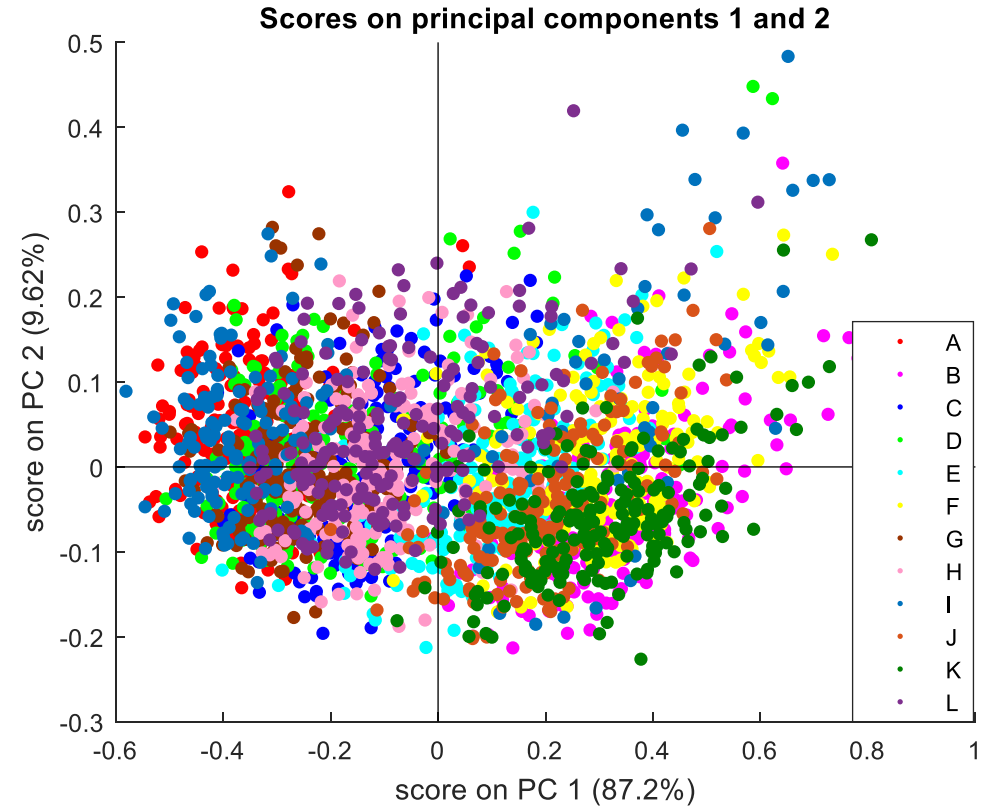

(b)

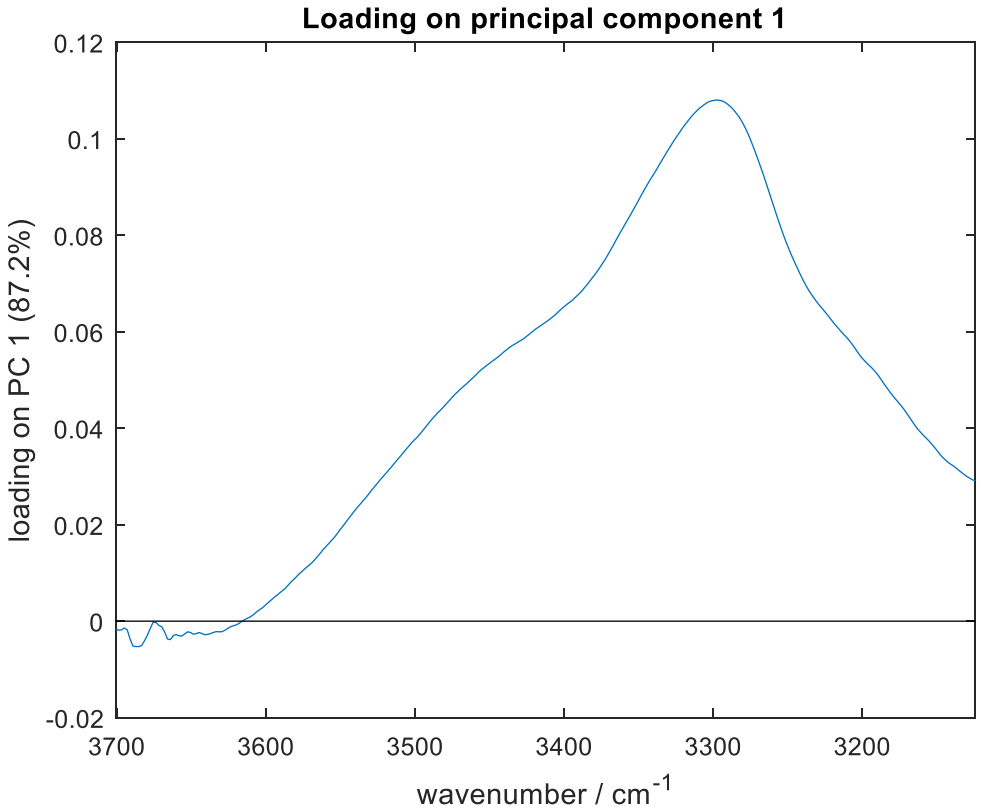

Figure6. 17 (a) The score plots of PC1 and PC2 of stroma on 12 glass slides after removing glue in experiment 2 (b) The PC1 loading for PCA stroma on 12 glass slides after removing glue in experiment

2.

6.2.4.3 The epithelium and stroma classification on every glass slide

According to the PCA results of spectra with glue removal on 12 glass slides, there is no separation in experiments 1 and 2. It indicates that the spectra with glue removal on 12 glass slides are similar. Therefore, the spectra of epithelium and stroma on glass L are used as an example.

6.2.4.3.1 The tissue classification on every glass slide in experiment 1

(a)

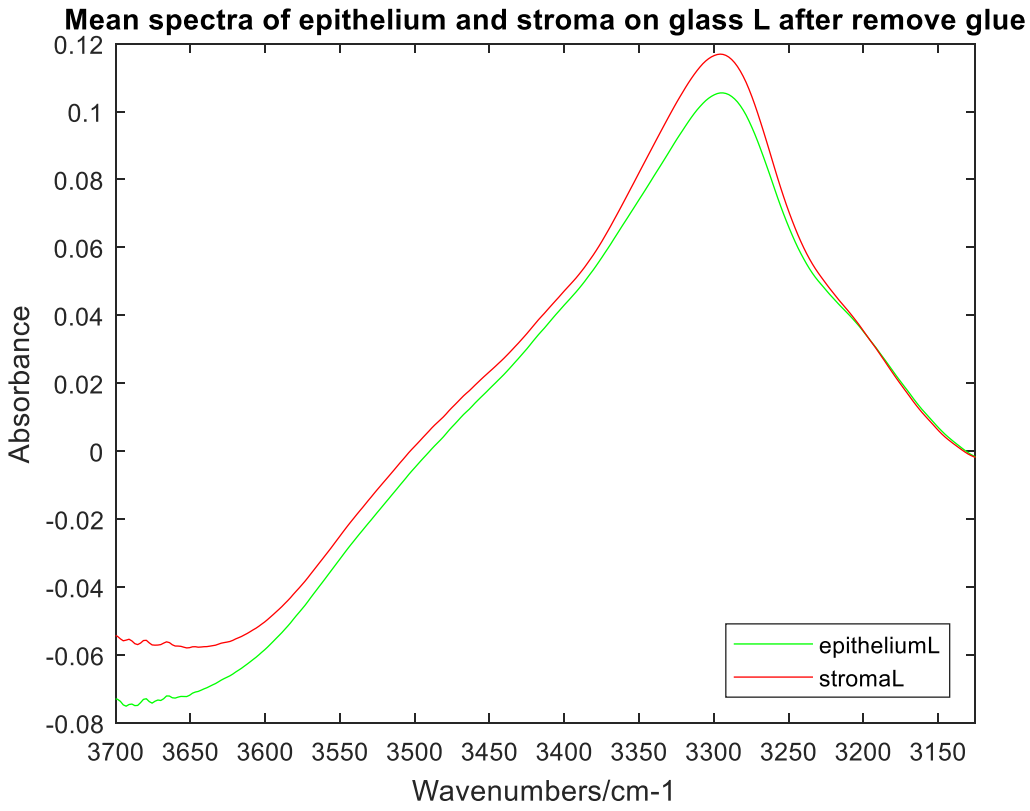

(b)

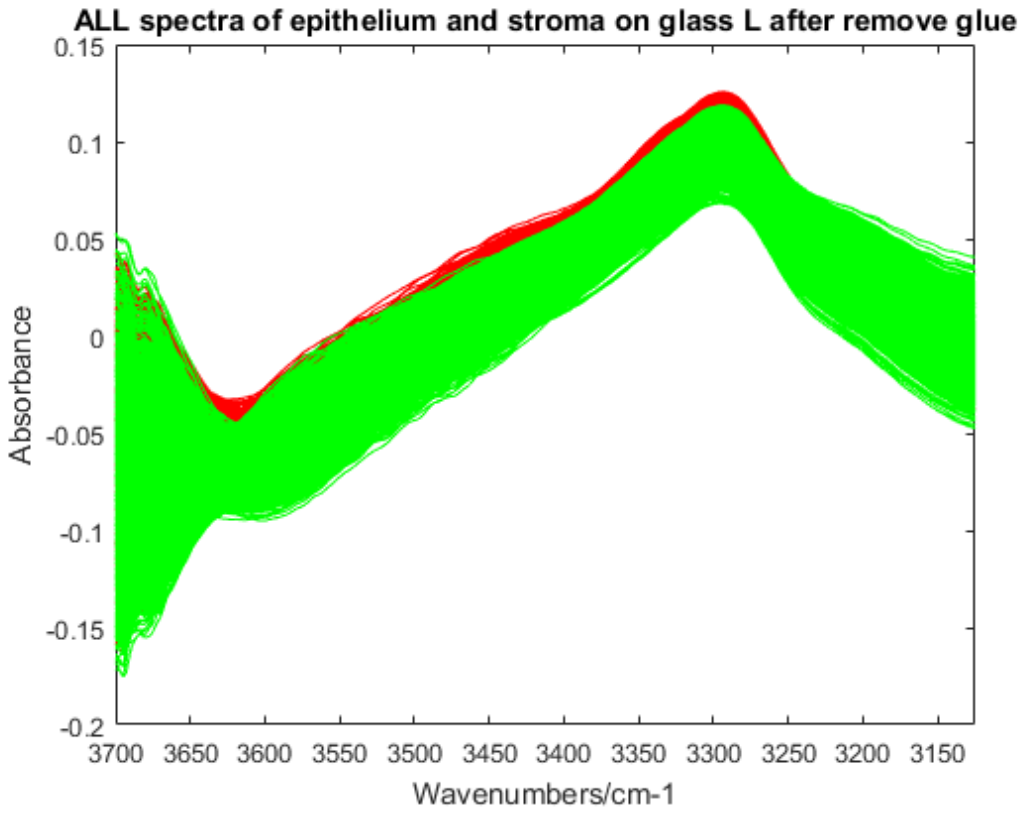

Figure6. 18 (a) Mean spectra of stroma and epithelium on glass L with glue removal in experiment 1 (b)All of the spectra of stroma and epithelium on glass L with glue removal in experiment 1 (epithelium in green and stroma in red).

According to the mean spectra of epithelium and stroma on glass L (figure 6.18 (a)), the spectral intensity of amide A of epithelium is lower than the stroma. Figure 6.18 (b) indicates all spectra of epithelium and stroma in experiment 1 after removing glue have a significant overlap. However, spectra of epithelium and stroma can be separated by PCA. And figure 6.19 shows the PCA results of stroma and epithelium on glass L.

(a)

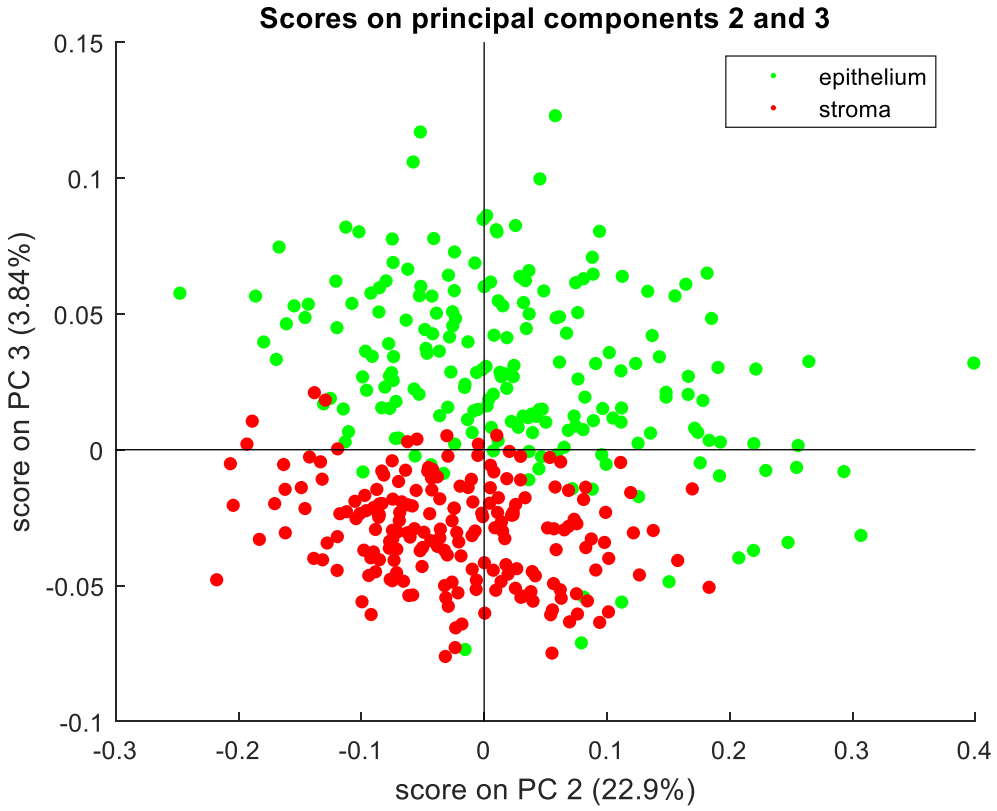

(b)

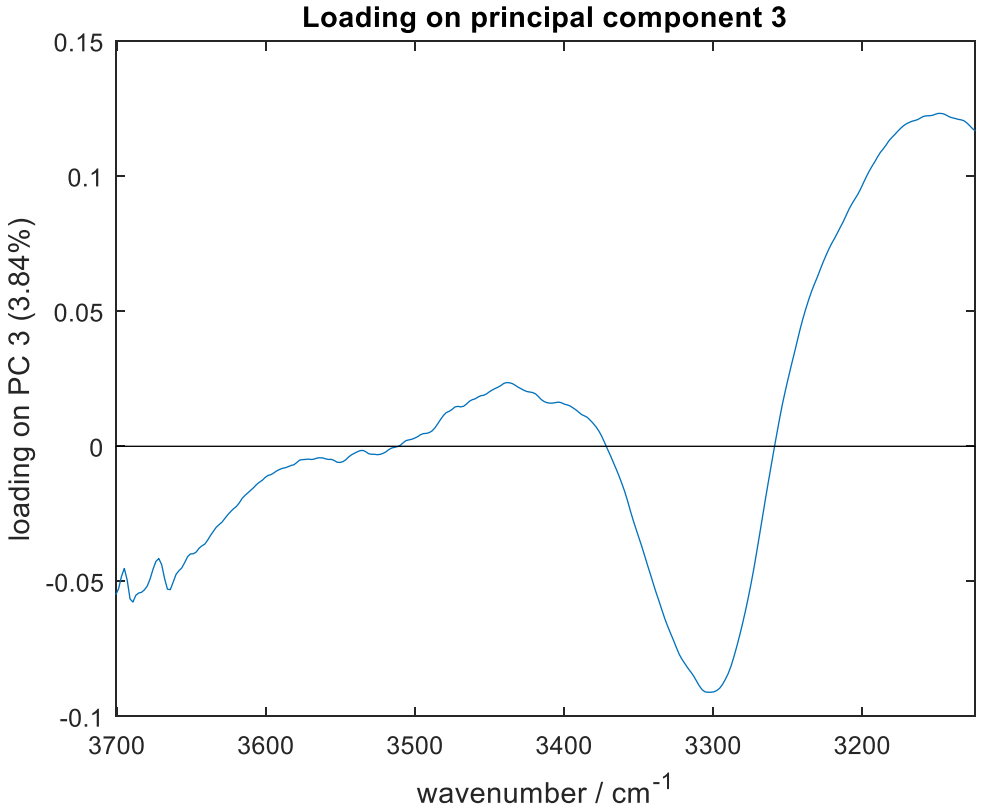

Figure6. 19 (a) The score plots of PC2 and PC3 of epithelium and stroma on glass L with glue removal in experiment 1. (b) The PC3 loading for PCA of epithelium and stroma on glass L with glue removal in

experiment 1.

According to figure 6.19 (a), there is a separation between the spectra of epithelium and stroma with glue removal on glass L. The separation mainly depends on the PC3, which only accounts for 3.84% of the full information. From the loading of PC3 (figure 6.19 (b)), it is mainly made of a negative peak, which locates at 3302 cm^{-1}. Thus, the distribution of spectra on PC3 is negatively correlated with the intensity of amide A. Figure 6.18 has indicated that most of the spectra of stroma have higher intensity at amide A than spectra of epithelium. Therefore, most of the spectra of the stroma are distributed in the negative area of PC3.

6.2.4.3.2 The tissue classification on every glass slide in experiment 2

Figure 6.20 shows the spectra of stroma and epithelium after removing glue in experiment 2. Although the spectra overlap, the difference between the stroma and epithelium is the intensity of amide A. In general, the intensity of amide A for most spectra of the stroma is higher than epithelium.

(a)

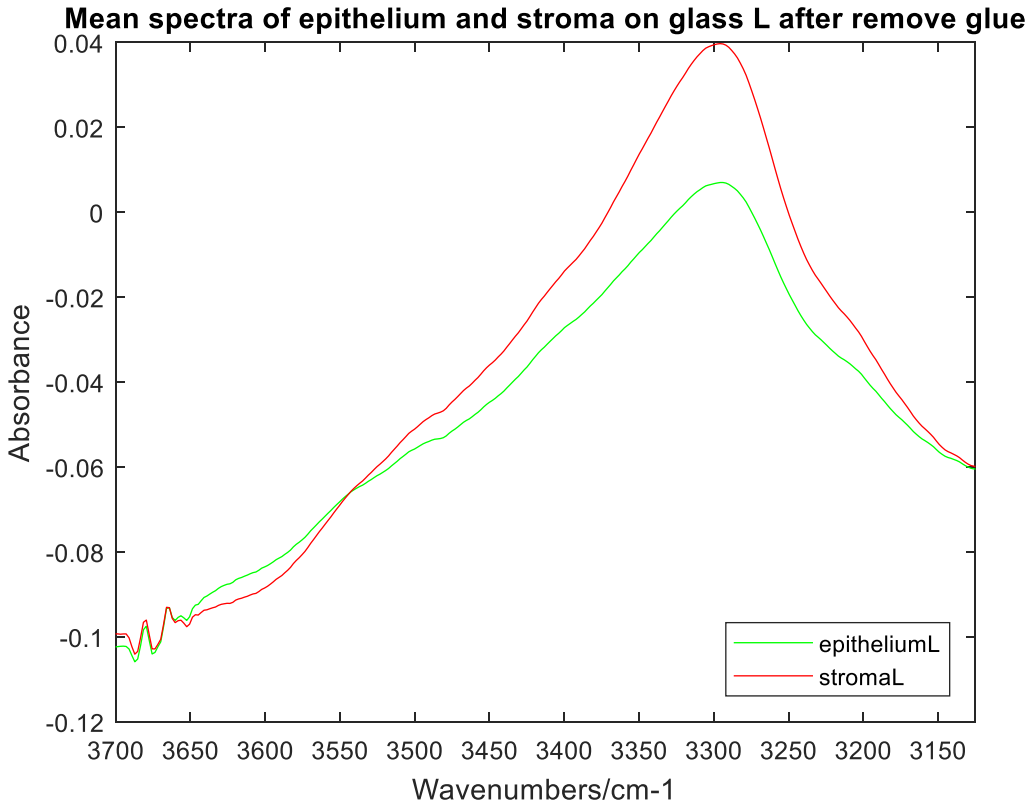

(b)

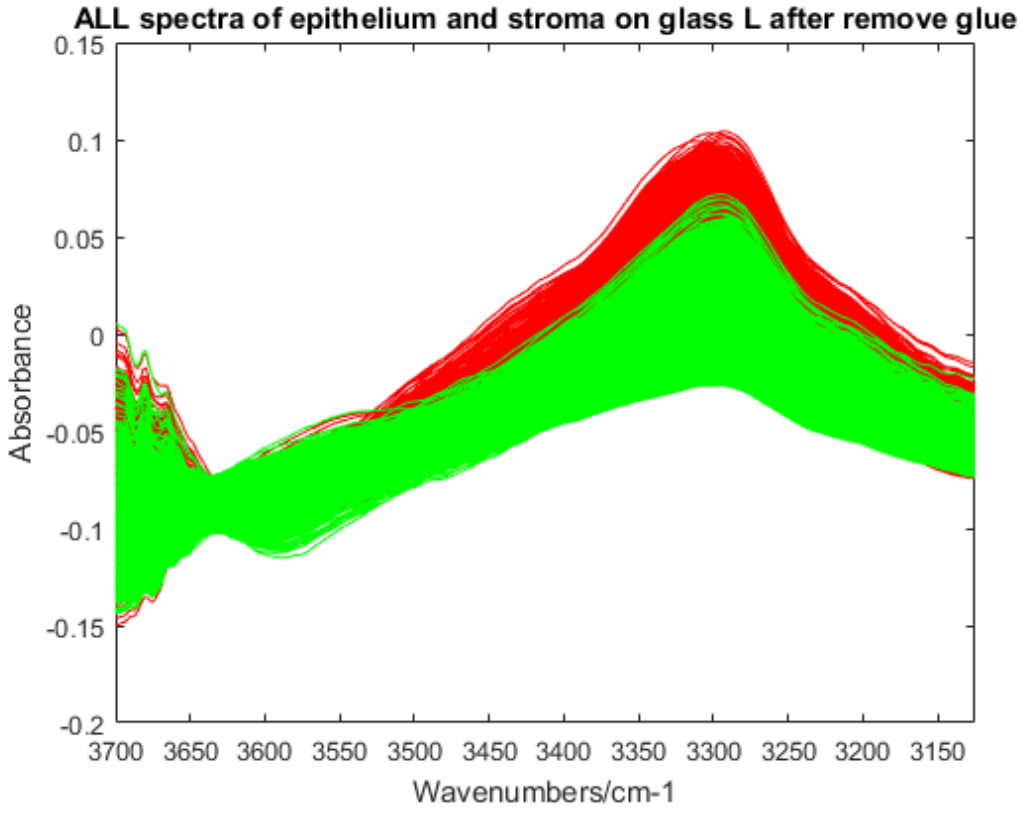

Figure6. 20 (a) Mean spectra of stroma and epithelium on glass L after removing glue in experiment 2.

(b) All of the spectra of stroma and epithelium on glass L after removing glue in experiment 2. (epithelium in green and stroma in red).

Because the epithelium and stroma cannot be distinguished,obviously, the PCA is used for discrimination. Figure 6.21 shows the PCA results of tissue classification. The score plot of PC1 and PC2 shows that the spectra of epithelium and stroma cannot be separated. But there is a separating trend on the PC1. According to the loading of PC1 (figure 6.21(b)), the positive peak at 3300 cm^{-1} and the negative peak at 3600 cm^{-1} are made PC1. In addition, the peak at 3600 is caused by O-H stretching. Therefore, the PC1 is positively related to the intensity of amide A and negatively related to the O-H stretching. According to the spectra of epithelium and stroma in figure 6.20, the intensity of amide A of the stroma is higher than the epithelium. While the intensity of peaks at 3600 cm^{-1} for stroma usually is lower than epithelium. Thus, more spectra of the stroma are distributed in the positive area of PC1.

(a)

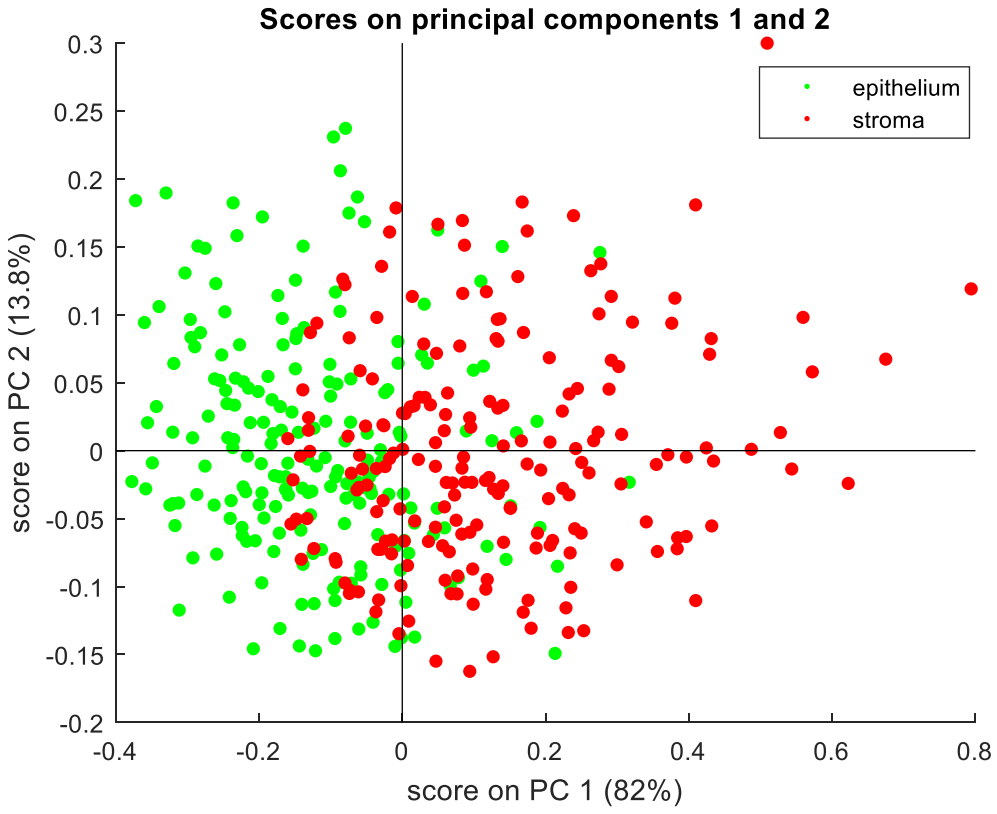

(b)

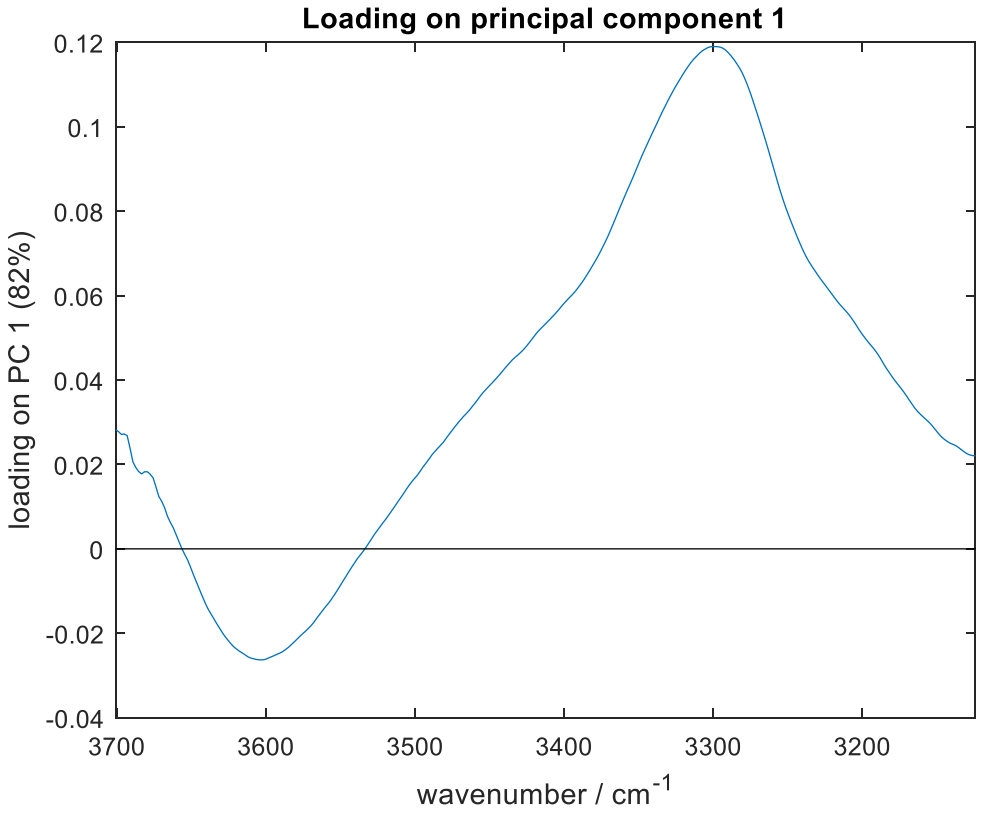

Figure6. 21 (a) The score plots of PC1 and PC2 of epithelium and stroma on glass L after removing glue in experiment 2. (b) The PC1 loading for PCA of epithelium and stroma on glass L after removing glue in experiment 2.

Comparing the PCA results before and after removing glue in both experiments 1 and 2, it is easy to find that the separation of epithelium and stroma based on PCA always has a better performance when the spectra have not been subjected to glue removal. It suggests that the glue has a specific contribution to tissue classification.

6.2.4.4 Automated histopathological classification on the same glass slide

As mentioned in the previous section, the separation of spectra of epithelium and stroma with glue removal on the same glass slide is not very clear, according to PCA. It is necessary to achieve stroma and epithelium classification by building a classifier.

Random forest based histopathological classification on the same glass slides is

achieved by training a classifier using 80% spectra of stroma and epithelium. The remaining 20% spectra are used to test whether the classifier could predict the class the spectrum belongs to (table 6.5). The accuracy is used to evaluate the performance of the classifier. The accuracy of the classifier on the same glass slides in experiments 1 and 2 with glue removal is shown in table 6.9.

Table6. 9 The accuracy of histological classification on the same glass slide in experiments 1 and 2 after removing the glue.

Model test	Experiment 1	Experiment 2
Glass A	98.14	98.05
Glass B	98.98	97.99
Glass C	98.67	98.51
Glass D	97.73	97.38
Glass E	98.68	98.69
Glass F	98.72	97.71
Glass G	98.61	98.85
Glass H	97.76	97.07
Glass I	99.01	97.99
Glass J	98.75	98.72
Glass K	99.26	98.77
Glass L	99.21	98.18

According to the accuracies in table 6.9, the overall accuracies are above 97.70% in experiments 1 and 2 after removing the glue. It indicates classifiers still have high accuracy in discriminating the epithelium and stroma on the same glass slides for both experiments with glue removal. In addition, the accuracy in experiment 1 with glue removal is slightly higher than in experiment 2 with glue removal.

Compared with the accuracy without glue removal (Table 6.6), the accuracies of experiments 1 & 2 with glue removal (97.70%) are slightly lower than those without glue removal (98.40%).

6.2.4.5 Automated histopathological classification on the different glass slides

The independent test is processed to study the effect of glass type on tissue classification. The independent test uses the spectra from one of the glass slides to test a classifier

trained by spectral data from the other glass slides. The independent test results in experiments 1 and 2 with glue removal are shown in Tables 6.10 and 6.11, respectively. In addition, the accuracies lower than 80% in the two tables are highlighted in blue. Therefore, it is easy to find that the tissue classification on the different glass slides has poor performance in two experiments with glue removal, but the accuracy in experiment 2 with glue removal is slightly higher.

Table6. 10 The accuracy of histological classification on different glass slides in experiment 1 after removing glue

Accuracy (%)	Test on glass A	Test on glass B	Test on glass C	Test on glass D	Test on glass E	Test on glass F	Test on glass G	Test on glass H	Test on glass I	Test on glass J	Test on glass K	Test on glass L
Train on glass A		67.07	82.05	66.27	65.53	68.82	62.62	83.35	63.48	74.02	68.56	62.68
Train on glass B	33.91		85.19	69.04	90.54	76.18	96.31	67.77	67.38	61.38	73.68	73.79
Train on glass C	48.23	99.19		69.37	92.39	76.88	96.72	92.92	67.78	77.37	75.22	76.25
Train on glass D	38.27	94.75	88.58		89.97	72.84	87.12	83.32	82.56	88.79	97.18	97.58
Train on glass E	32.36	97.48	71.80	48.69		76.24	97.64	53.39	50.59	46.01	61.51	56.56
Train on glass F	55.89	97.22	93.05	60.74	97.86		96.30	84.10	54.53	87.60	94.94	94.56
Train on glass G	32.52	98.25	72.35	60.69	95.39	76.24		59.13	55.16	65.29	81.38	86.91
Train on glass H	52.91	93.04	96.50	61.31	86.60	72.15	87.25		56.03	97.80	98.39	97.06
Train on glass I	37.07	97.47	74.78	87.74	93.27	74.61	93.70	68.10		75.56	91.10	86.28
Train on glass J	52.68	77.18	86.55	61.12	77.38	66.07	72.14	90.81	55.19		98.52	96.74
Train on glass K	32.43	96.05	70.73	60.71	95.55	74.51	92.63	63.22	55.40	80.20		96.20
Train on glass L	35.33	94.96	76.79	62.58	95.24	73.64	93.81	70.99	55.85	83.84	97.64	

Table6. 11 The accuracy of histological classification on different glass slides in experiment 2 after removing glue

Accuracy (%)	Test on glass A	Test on glass B	Test on glass C	Test on glass D	Test on glass E	Test on glass F	Test on glass G	Test on glass H	Test on glass I	Test on glass J	Test on glass K	Test on glass L
Train on glass A		64.36	69.30	68.28	64.95	61.65	63.60	71.09	69.52	65.87	67.50	63.65
Train on glass B	29.98		75.26	60.57	97.13	94.12	53.82	68.78	55.73	98.24	97.84	76.76
Train on glass C	30.32	89.11		94.35	92.73	78.82	96.51	95.66	75.53	92.27	87.76	97.89
Train on glass D	31.97	88.11	95.99		86.49	74.94	98.41	96.12	90.22	88.60	84.27	96.51
Train on glass E	30.00	92.12	87.90	65.25		93.13	67.61	77.13	53.47	97.89	97.52	85.12
Train on glass F	29.98	87.13	66.74	49.79	94.74		50.10	49.69	47.38	93.21	97.33	65.67
Train on glass G	33.04	72.13	94.45	95.74	78.84	66.78		94.04	84.80	76.12	73.31	93.44
Train on glass H	31.78	90.53	97.20	96.04	88.01	74.57	97.42		81.65	90.23	85.84	97.70
Train on glass I	52.70	89.69	83.76	91.14	78.12	70.49	90.13	89.53		85.04	82.52	86.49
Train on glass J	29.99	95.02	67.77	56.51	96.76	93.09	48.27	61.07	54.28		97.97	71.09
Train on glass K	29.98	92.33	43.58	46.12	91.41	95.88	40.38	45.01	50.72	97.01		55.42
Train on glass L	30.87	90.19	98.01	94.83	92.14	78.31	95.92	96.20	76.54	91.99	86.68	

However, comparing the classification accuracies between before glue removal (table 6.7 and 6.8) and after glue removal (table 6.10 and 6.11) in experiments 1 and 2, the results clearly showed that the accuracy without glue removal always is higher. Above all, the lower classification accuracy may be caused by successful glue removal. Glue removal adds variance. Because glue has a certain contribution to tissue classification. According to the mean spectra of epithelium and stroma, the intensity of epithelium is always lower than stroma at amide A. While a small peak in 3400-3450 cm^{-1}, the spectral intensity of epithelium is always higher than stroma. It is caused by the different structures between epithelium and stroma. The columnar epithelium has lots of holes in the normal prostate tissue, and the content of glue is related higher than stroma.

6.3 Error discussion

There are many reasons for the error in chapter 6. First, in terms of measurement, only two tissue slides could be tested at a time due to the limitation of the window size of the sample stage. The measurement for a tissue sample needs around 2 hours (including

waiting humidity time); Therefore, the total 12 tissue samples need to be tested in a few days. The purge box could keep the humidity at0, but the temperature has slightly changed (23.5℃±0.5℃). Slight temperature variation can be source of error related to background variations, but this is unlikely to significantly influence the results. The annotation is an important factor in error. Compared with the directly annotated IR chemical image achieved with the subjective judgement of the eyes, annotations on the H&E brightfield image are more accurate. However, there is an error in registering the annotation on H&E images into chemical images by Matlab. Because the pixel resolution of H&E images and chemical images is different (<0.5 μm compared with 5.5 μm), if the registered annotation is on the edge of one pixel of a chemical image, the corresponding spectrum cannot be used. Thus, the quality test could effectively eliminate most of these spectra, and the rest would cause an error. The error for PCA results comes from the random selection of 200 stroma and 200 epithelium spectra for every tissue sample. The PCA score will slightly change (±3%) if the selected spectra are changed. But the loading composition of the three main PC will not modify, which is more critical for the data analysis. The algorithm itself causes the error of the random forest. 80% of spectra are randomly selected to build the model, and the remaining 20% of spectra test the model. Therefore, the spectra used for the train and test model cannot be the same every time the random forest is reprocessed. But the classification accuracy only has a slight change (around ±0.35%).

6.4 Conclusion

The purpose of this chapter is to study whether the different types of glass could affect histopathological classification. In addition, to find the most suitable experiment method.

A series of prostate tissue sections from the same BPH patient are mounted on the 12 different glass slides. Because these tissue sections are adjacent, the composition and

structure of tissue on different glass slides are roundly the same. Due to the same kinds of glue and coverslip, the glass slides are the only difference between the 12 tissue samples.

Different methods measure the spectra, and the most significant difference between the two methods is from the selection of background. The background for experiment 1 is a clear and tissue-free area. While for experiment 2, the background is an empty glass. Therefore, the spectra in experiment 1 are made of tissue information minus or add a little glue information. The spectra in experiment 2 are made of tissue, coverslip and glue information. Thus, there is an obvious amide A band at 3298 cm^{-1} in every spectrum of both experiments. However, the shape of the spectrum in experiments 1 and 2 is different. The spectra in experiment 1 have slightly different trends in 3400-3450 cm^{-1}, which is related to the glue. In experiment 2, the spectra have a small peak in 3400-3450 cm^{-1} and a broad band in 3400-3600 cm^{-1}, which are related to glue and coverslip, respectively.

According to the PCA results of 12 glass slides, there is no separation for the spectra on the different glass slides in experiment 1. While in experiment 2, except for the spectra on glass A, the rest spectra on the other 11 glass slides cannot be separated. It can indicate that the type of glass slide generally does not affect the spectra. In addition, there is an obvious separation between the spectra of stroma and epithelium on the same glass slide based on PCA. It indicates that the spectra of epithelium and stroma on the same glass slides have a particular difference and could be discriminated. Combined with the mean spectra, the intensity of epithelium is always lower than stroma at amide A. While at small glue peak 3400-3450 cm^{-1}, the spectral intensity of epithelium is always higher than stroma.

The random forest looks at the effect of glass slides on histological classification. A classifier, trained by spectra on one glass slide, is used to classify the spectra of epithelium and stroma on another glass slide. If it works, it would indicate glass type

does not affect tissue classification, and if not, it would mean the type of glass influences tissue classification.

Comparing two experiments without glue removal, both have high accuracy in classifying the epithelium and stroma on the same glass slides. The classification accuracies in the two experiments are above 98.40%. There is no significant difference in accuracy on the same glass slides between the two experiments. Therefore, epithelium and stroma could be easily classified on the same glass slide in both experiments 1 and 2.

However, when the classifier is used to classify the epithelium and stroma on a different glass slide, most tissue classification accuracy is above 90% in both experiments. But spectral data in experiment 1 have a better performance than experiment 2. In experiment 1, only the accuracy of classifiers, independently tested on glass I, are poor (52%). While in experiment 2, the classifier trained by spectra on glass A always has a bad classification performance, and the other classifiers always have bad accuracy results when is tested on glass A and glass I.

Above all, tissue classification on the same glass slide has very high accuracy (above 98.40%) for the two experiments. There is also very good performance in tissue classification on different glass slides, which means that the type of glass slide has a minor influence on tissue classification. In addition, the spectra in experiment 1 always have better tissue classification performance than experiment 2.

Because spectra in both experiments are affected by the glue, it is important to see if it is possible to eliminate the influence of glue on spectra. The glue removal method has been studied in chapter 5, and the most suitable way is using spectra of glue, Matrigel and coverslip as reference spectra and fit range are range 1: Matrigel (3278-3318cm^{-1}, 3066-3106cm^{-1}); range 3: glue peak & Matrigel peak (2950-2970cm^{-1}, 2925-2945 cm^{-1}, 2867-2887 cm^{-1}); range 4 coverslip & Matrigel peak (3536-

3576cm^{-1}, 2704-2744cm^{-1}). Therefore, all of the spectra in experiments 1 and 2 are processed for glue removal. Reprocessing all of the steps using spectral data with glue removal.

The results show good accuracies (above 97.7%) for both experiments to classify epithelium and stroma on the same glass slide. But both experiments have very poor accuracy for tissue classification on different glass slides. It indicates that the type of glass greatly influences tissue classification in both experiments with glue correction.

In addition, the changes in accuracy after glue correction are also compared. For both experiments, the accuracies of tissue classification on the same glass slide decreased after glue removal. It indicates the presence of glue also has a particular contribution to tissue classification. Because the structure of epithelium is thinner than stroma, the glue content on epithelium is more than stroma. In 3400 – 3450 cm^{-1}, the spectral intensity of epithelium is higher than stroma.

In conclusion, before removing glue, the type of glass slide only has a slight influence on tissue classification, especially for experiment 1 without glue removal. However, after eliminating glue, the effect of the kind of glass slide on tissue classification increases. In addition, the performance of tissue classification on the same glass slides is always very good for both experiments before or after removing the glue.

6.5 Reference

[1] M. J. Pilling, A. Henderson, J. H. Shanks, M. D. Brown, N. W. Clarke, and P. Gardner, 'Infrared spectral histopathology using haematoxylin and eosin (H&E) stained glass slides: a major step forward towards clinical translation', *Analyst*, vol. 142, no. 8, pp. 1258–1268, 2017.

[2] A. Akalin *et al.*, 'Classification of malignant and benign tumors of the lung by infrared spectral histopathology (SHP).', *Lab. Invest.*, vol. 95, no. 4, pp. 406–21, 2015.

[3] X. Mu *et al.*, 'Statistical analysis of a lung cancer spectral histopathology (SHP) data set', *Analyst*, vol. 140, no. 7, pp. 2449–2464, 2015.

[4] F. Großerueschkamp *et al.*, 'Marker-free automated histopathological annotation of lung tumour subtypes by FTIR imaging', *Analyst*, vol. 140, no. 7, pp. 2114–2120, 2015.

[5] C. Kuepper, F. Großerueschkamp, A. Kallenbach-Thieltges, A. Mosig, A. Tannapfel, and K. Gerwert, 'Label-free classification of colon cancer grading using infrared spectral histopathology', *Faraday Discuss.*, vol. 187, pp. 105–118, 2016.

[6] A. Kallenbach-Thieltges, F. Gro??er??schkamp, A. Mosig, M. Diem, A. Tannapfel, and K. Gerwert, 'Immunohistochemistry, histopathology and infrared spectral histopathology of colon cancer tissue sections', *J. Biophotonics*, vol. 6, no. 1, pp. 88–100, 2013.

[7] J. Nallala *et al.*, 'Infrared spectral imaging as a novel approach for histopathological recognition in colon cancer diagnosis', *J. Biomed. Opt.*, 2012.

[8] S. Kumar, C. Desmedt, D. Larsimont, C. Sotiriou, and E. Goormaghtigh, 'Change in the microenvironment of breast cancer studied by FTIR imaging', *Analyst*, 2013.

[9] F. N. Pounder, R. K. Reddy, and R. Bhargava, 'Development of a practical spatial-spectral analysis protocol for breast histopathology using Fourier transform infrared spectroscopic imaging', *Faraday Discuss.*, 2016.

[10] E. Gazi *et al.*, ‘Applications of Fourier transform infrared microspectroscopy in studies of benign prostate and prostate cancer. A pilot study’, *J. Pathol.*, vol. 201, no. 1, pp. 99–108, 2003.

[11] C. Hughes *et al.*, ‘Assessment of paraffin removal from prostate FFPE sections using transmission mode FTIR-FPA imaging’, *Anal. Methods*, vol. 6, no. 4, p. 1028, 2014.

[12] M. J. Baker, E. Gazi, M. D. Brown, J. H. Shanks, N. W. Clarke, and P. Gardner, ‘Investigating FTIR based histopathology for the diagnosis of prostate cancer’, *J. Biophotonics*, vol. 2, no. 1–2, pp. 104–113, 2009.

[13] P. Bassan, J. Mellor, J. Shapiro, K. J. Williams, M. P. Lisanti, and P. Gardner, ‘Transmission FT-IR chemical imaging on glass substrates: Applications in infrared spectral histopathology’, *Anal. Chem.*, vol. 86, no. 3, pp. 1648–1653, 2014.

[14] M. Pilling and P. Gardner, ‘Fundamental developments in infrared spectroscopic imaging for biomedical applications’, *Chem. Soc. Rev.*, vol. 45, no. 7, pp. 1935–1957, 2016.

[15] M. J. Pilling, A. Henderson, and P. Gardner, ‘Quantum Cascade Laser Spectral Histopathology: Breast Cancer Diagnostics Using High Throughput Chemical Imaging’, *Anal. Chem.*, vol. 89, no. 14, pp. 7348–7355, 2017.

[16] P. R. Griffiths *et al.*, ‘Discrimination of normal and malignant gastric tissues with FTIR spectroscopy and principal component analysis’, *Guangpuxue Yu Guangpu Fenxi*, vol. 24, no. 9, pp. 1025–1027, 2004.

[17] C. Hughes *et al.*, ‘Enhanced FTIR bench-top imaging of single biological cells’, *Analyst*, vol. 140, no. 7, pp. 2080–2085, 2015.

[18] L. S. Leslie, T. P. Wrobel, D. Mayerich, S. Bindra, R. Emmadi, and R. Bhargava, ‘High definition infrared spectroscopic imaging for lymph node histopathology’, *PLoS One*, vol. 10, no. 6, pp. 1–17, 2015.

[19] Z. Movasaghi, S. Rehman, and I. U. Rehman, ‘Fourier transform infrared (FTIR) spectroscopy of biological tissues’, *Appl. Spectrosc. Rev.*, vol. 43, no. 2, pp. 134–179, 2008.

[20] G. I. Dovbeshko, N. Y. Gridina, E. B. Kruglova, and O. P. Pashchuk, ‘FTIR spectroscopy studies of nucleic acid damage’, in *Talanta,* 2000.

Chapter 7

Study 3:Cancer detection on the different type of glass slide

Although many studies have proven that SHP can distinguish normal and cancerous samples[1][2][3], this has generally been achieved in small-scale trials and is not currently in clinical practice [1]. Since in order for SHP to gain acceptance into clinical, it would be preferable that the new pre-screening SHP process should not disrupt the existing pathology workflow. Ideally, the sample preparation process should not be disturbed, and the same Haematoxylin and Eosin (H&E) stained tissue sample on the glass slide should be used for pre-screening by SHP[5]. This means that the glass sides have to be used as the substrate for SHP.

The infrared chemical images used for SHP are measured by Fourier transform infrared spectroscopy (FTIR). However, glass is partly opaque in the infrared region, and the partly transparent infrared region is from 2500 to 3800cm^{-1} [2][5]. Therefore, most of the critical biological peaks used for further data processing are completely blocked out by the glass absorption. The only useful peak in the glass transmission window is the very broad amide A band centred at ~3298cm^{-1}. The previous study by Pilling et al. has shown that SHP could distinguish prostate cancerous tissue from benign tissue on the glass substrate with high sensitivity and accuracy; similarly, Bassan et al. and Tang et al. demonstrated that it could be used to distinguish breast cancer[7][8]. Thus, SHP can discriminate between cancerous and normal tissue on the glass slides. However, the glass substrate would be measured during SHP, and there are a variety of different types of glass slides used in clinical practice. Therefore, it is essential for SHP clinical application to study whether the different types of glass could affect the detection result.

A number of these different brands of glass slides (from completely different manufacturers) are studied in the project. The whole project is divided into 3 main steps. Firstly, establish the critical infrared spectral differences of the blank glass slides. Secondly, establish whether the glass types could affect basic tissue classification. Thirdly, establish whether the glass types could affect cancer detection.

Using FTIR measure 12 blank glass slides and the data are processed by Matlab. The

results showed that except for one of the glass slides (glass D), there is no significant difference among the rest 11 types of glass slides.

In chapter 6, a series of prostate tissue sections from the same benign prostate hyperplasia (BPH) patient mounted on 12 different types of glass slides are measured in two experimental methods and annotated by GIMP. The purpose is to find the influence of glass types on tissue classification. And the results in chapter 6 have shown a good classification for epithelium and stroma spectra on different types of glass slides, especially for the spectra without glue removal. It has proved that the kind of glass slide has significantly less effect on tissue classification.

In this chapter, a series of adjacent tissue slices mounted on the 6 glass slides, which form 4 patients (2 benign prostate hyperplasia & 2 prostate cancer), are measured in two experimental methods and annotated by GIMP. The study is to find the influence of glass type on cancer detection. Due to the effect of glue, glue removal is also an important process in this project. The specific experimental design and data process are shown in section 3.5.3 in chapter 3.

7.1 Annotation results

The GIMP image editor is used for annotation, and all of the annotation work is done on the H&E stained brightfield visible image. Epithelium and stroma were used for cancer detection and are annotated in green and red, respectively. Tissue-free area are annotated in blue. Figure 7.1 shows the annotated H&E images of each tissue section on glass D.

(a)

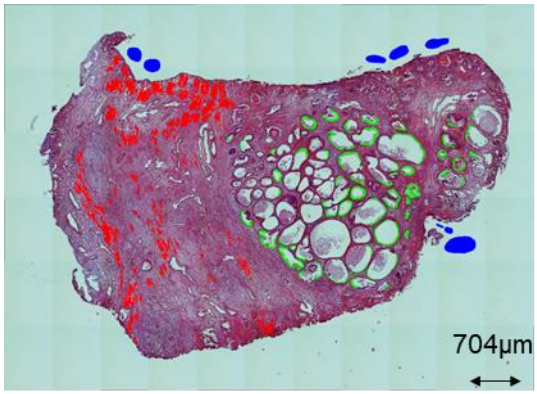

(b)

(c)

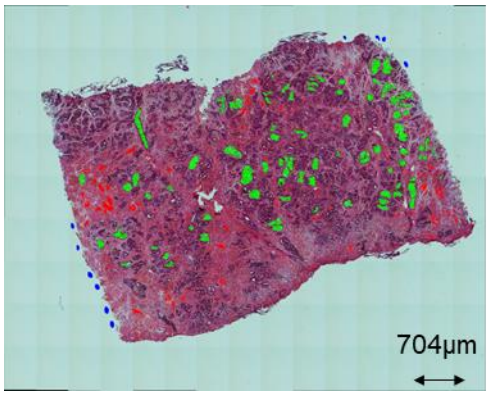

(d)

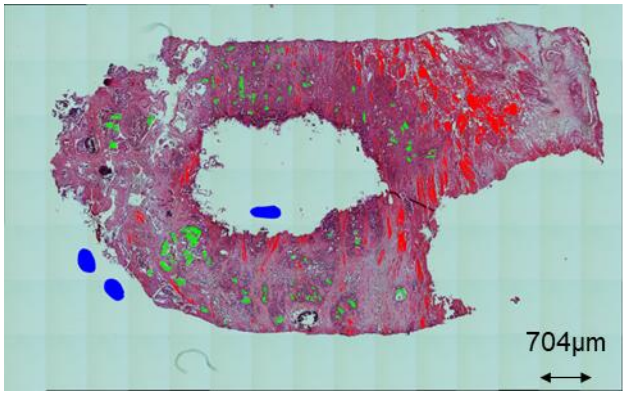

Figure7. 1 (a) The annotated H&E images of P1(BPH) on glass D. (b) The annotated H&E images of P2(BPH) on glass D. (c) The annotated H&E images of P3(CaP) on glass D. (d) The annotated H&E images of P4(CaP) on glass D.

7.2 Results and Discussion

7.2.1 Cancer detection for CaF2 slide

To evaluate whether the spectra of cancer and non-cancer tissue are different and whether infrared spectral histopathology (SHP) is a potential method for cancer detection, the tissue slices of 4 patients are mounted on CaF_2 slides. This enables the whole range spectral range to be collected, and the analysis acts as the spectral gold standard. The tissue slices are in paraffin wax and are not H&E stained.

The spectral range on the CaF_2 is 1000 - 3700 cm^{-1} and the quality control is based on the intensity of amide I, which is located at 1654 cm^{-1}. The threshold of the intensity

of amide I is 0.5-2. The number of annotated spectra of epithelium and stroma from 4 patients are shown in table 7.1.

Table7. 1 The number of annotated spectra on CaF2 slide from 4 patients

Spectra	P1(BPH)	P2(BPH)	P3(CaP)	P4(CaP)
epithelium	1662	666	8199	2567
stroma	5198	6028	7488	13313

The mean spectra of epithelium and stroma from 4 patients are shown in figure 7-3 (a) and (b), respectively. There are mainly eight peaks in 1000 - 3700 cm^{-1} and most of the bands are due to protein and lipids. Protein has three main bands, which are amide I (1658 cm^{-1}), amide II (1537 cm^{-1}) and amide A (3298 cm^{-1}). Lipid range in 2700-3000 cm^{-1} are affected by the paraffin, so it is removed. Another lipid range in 1340-1490 cm^{-1} is also affected by paraffin and removed. 2300-2400 cm^{-1} is also removed due to the CO_2 absorption. Thus, figure 7.2 shows the mean spectra of 4 patients on CaF_2 without paraffin.

(a)

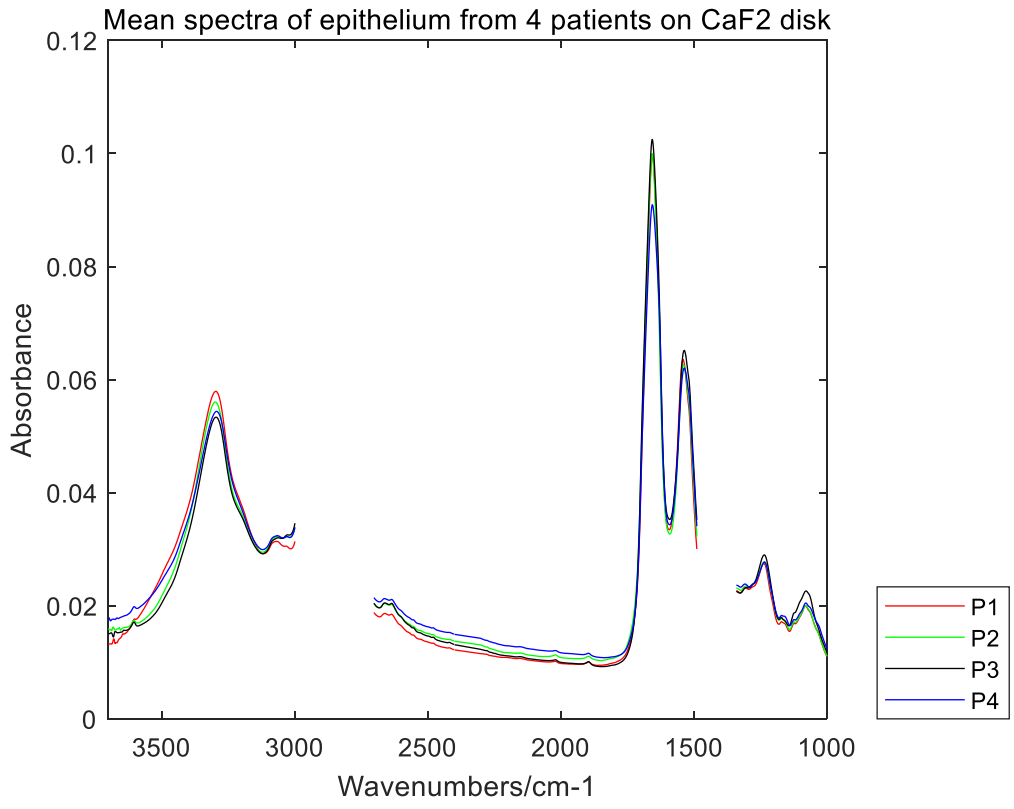

(b)

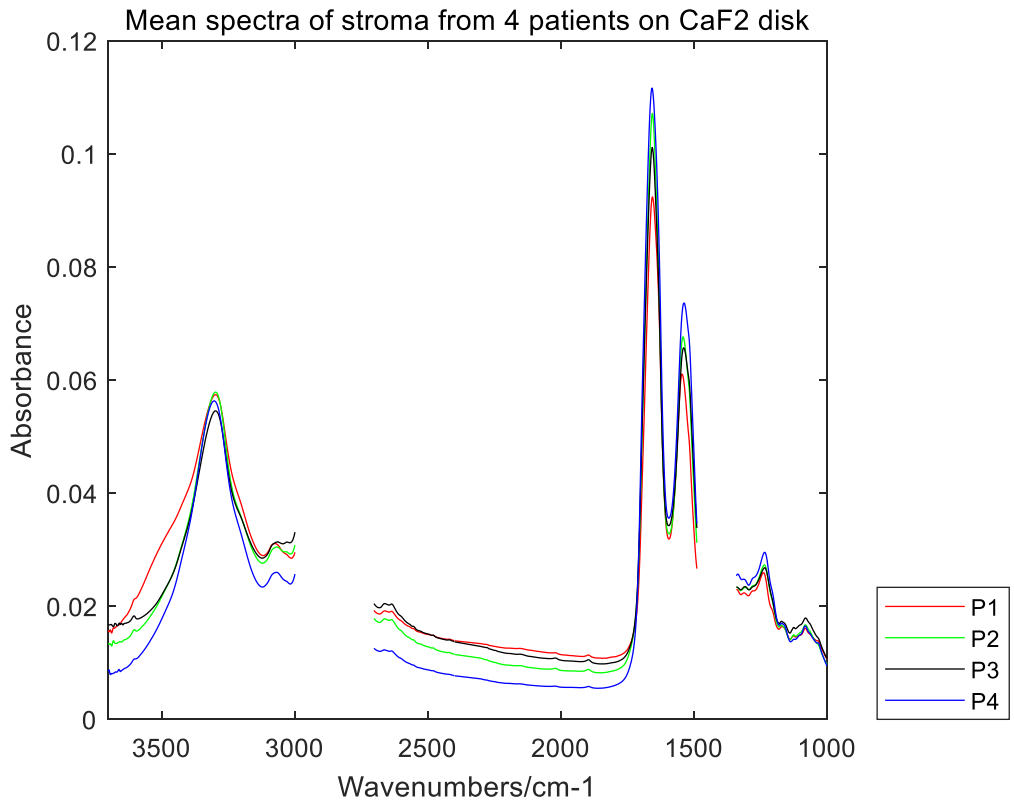

Figure7. 2 (a) The mean spectra of epithelium on CaF_2 from 4 patients in 1000 – 3700 cm^{-1} without wax. (b) The mean spectra of stroma on CaF_2 from 4 patients in 1000 – 3700 cm^{-1} without wax.

7.2.1.1 The PCA of cancer & non-cancer patients on CaF_2 slide

The 4 patients could be divided into cancer and non-cancer groups based on the disease. Therefore, P1(BPH) and P2(BPH) belong to the non-cancer group, and P3(CaP) and P4(CaP) belong to the cancer group. Randomly selecting 200 spectra from every patient and doing the PCA. The PCA results of the two groups are shown in figure 7.3.

(a)

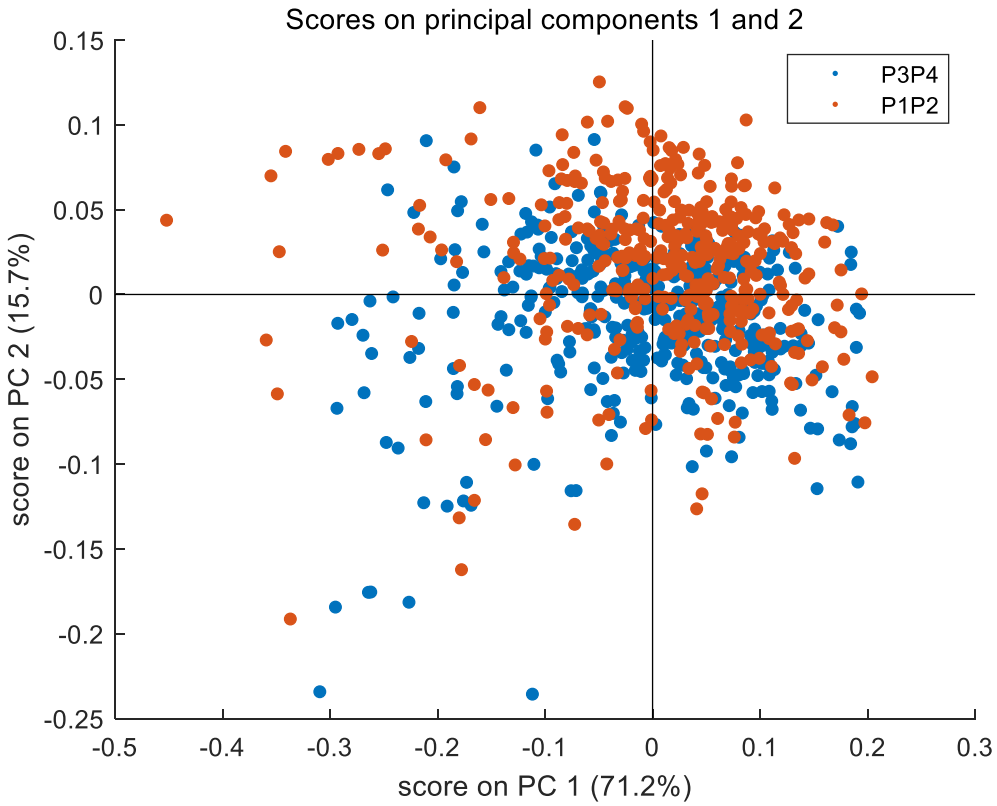
Scores on principal components 1 and 2
P3P4
P1P2
score on PC 2 (15.7%)
score on PC 1 (71.2%)
0.15
0.1
0.05
0
-0.05
-0.1
-0.15
-0.2
-0.25
-0.5
-0.4
-0.3
-0.2
-0.1
0
0.1
0.2
0.3

(b)

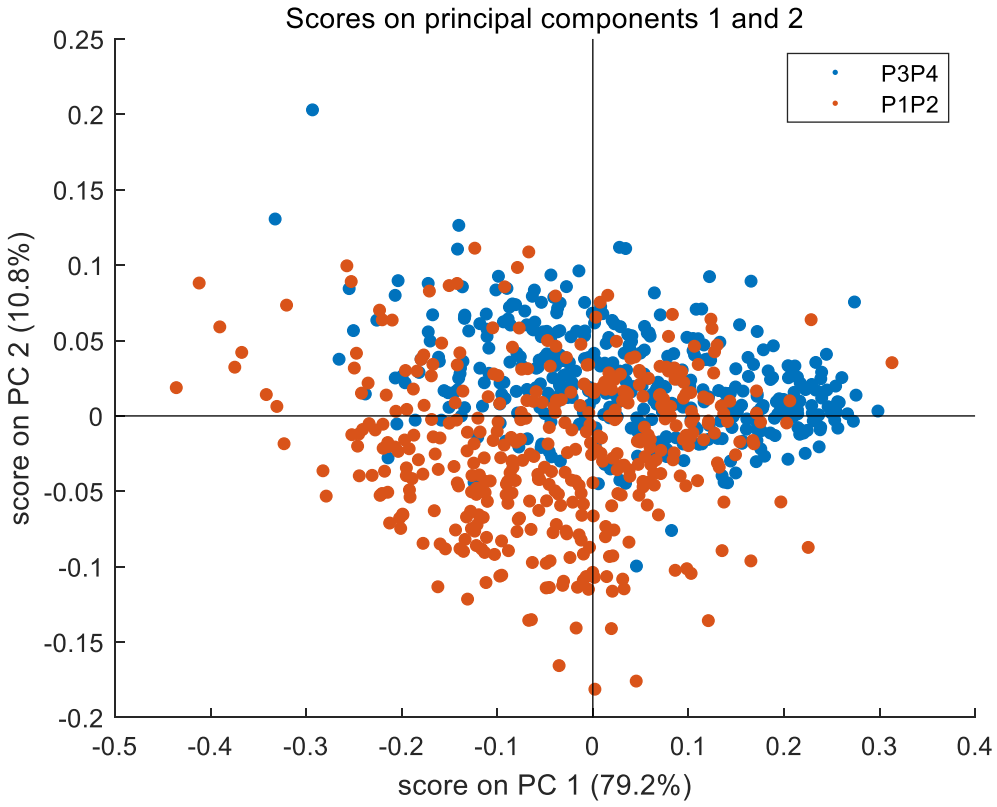
Scores on principal components 1 and 2
P3P4
P1P2
score on PC 2 (10.8%)
score on PC 1 (79.2%)
0.25
0.2
0.15
0.1
0.05
0
-0.05
-0.1
-0.15
-0.2
-0.5
-0.4
-0.3
-0.2
-0.1
0
0.1
0.2
0.3
0.4

(c)

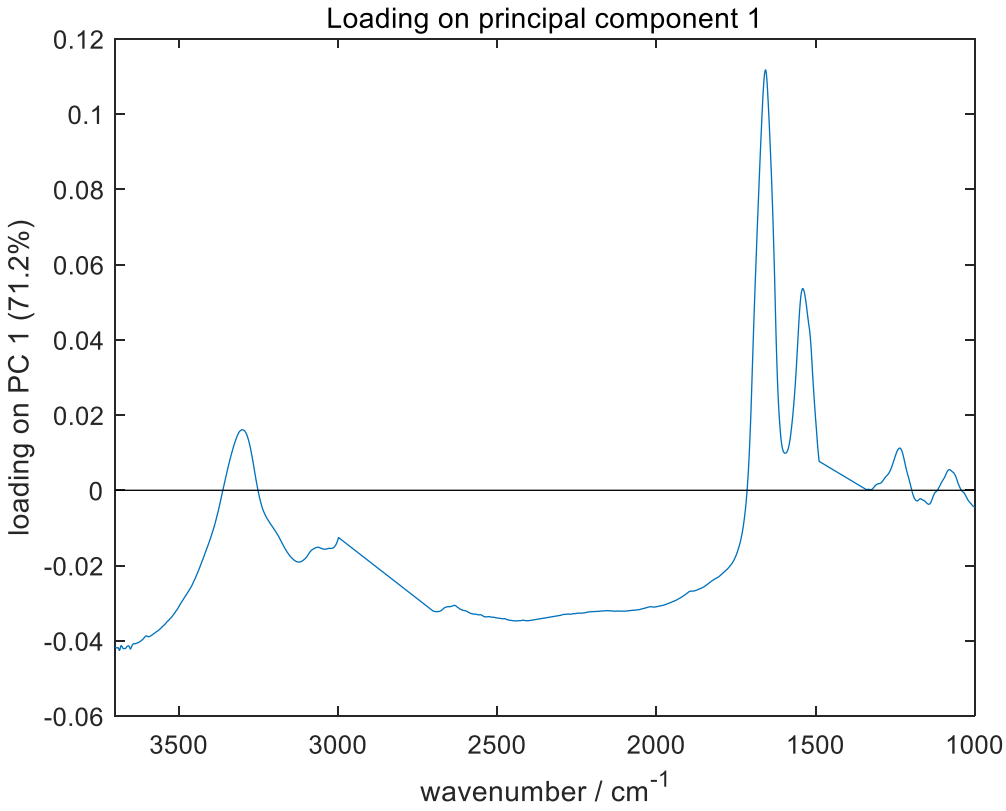

Figure7. 3 (a) The score plots of PC1 and PC2 of epithelium on CaF_2 slide for cancer and non-cancer patients. (b) The score plots of PC1 and PC2 of stroma on glass CaF_2 for cancer and non-cancer patients. (c) The loading of PC1 of epithelium on CaF_2 slide.

According to figure 7.3 (a) and (b), there is no separation between the cancer and non-cancer group for both spectra of epithelium and stroma. According to the loading of PC1 (figure 7.3 (c)), the composition of PC1 is three positive peaks, which is related to amide A, amide I and amide II. However, the spectra of cancer and non-cancer groups cannot be separated based on PC1. It means the spectral difference between the two groups is small in the absorption of protein (amide A, amide I and amide II).

7.2.1.2 Cancer detection on CaF_2 slide by random forest

As mentioned before, there is no separation of spectra of cancer and non-cancer groups on the CaF_2 slide according to PCA. It is necessary to achieve cancer and non-cancer

classification by building a classifier. 80% of spectral data are used to train the classifier, and the rest 20% of spectral data are used to test the classifier. There are 4 combinations of cancer and non-cancer groups for 4 patients, which are P3(CaP)&P1(BPH), P3(CaP)&P2(BPH), P4(CaP)&P1(BPH), P4(CaP)&P2(BPH). In addition, the cancer group is combined by the spectra of P3(CaP) & P4(CaP), while the non-cancer group is the combination of the spectra of P1(BPH) & P2(BPH). Table 7.2 shows all accuracies of cancer detection

Table7. 2 The accuracy of cancer detection on the CaF_2 slide.

Model test (%)	epithelium	stroma
Cancer group P1(BPH) P2(BPH) & Non-cancer group P3(CaP) P4(CaP)	97.79	97.50
P3(CaP) & P1(BPH)	98.99	99.92
P3(CaP) & P2(BPH)	98.28	97.52
P4(CaP) & P1(BPH)	96.93	99.59
P4(CaP) & P2(BPH)	96.13	97.67

According to table 7.2, all of the accuracies of cancer detection on CaF_2 slide are above 96.13%, and the lowest accuracy is the classification of P4(CaP) & P2(BPH) by epithelium spectra. It may be because of the fewer spectra of epithelium from P2(BPH). The high accuracy of cancer detection indicates the spectra of cancer and non-cancer tissue could be separated by random forest, and SHP could be used for cancer detection.

7.2.2 Quality control for spectra

The purpose of quality control is to remove spectra from an area without tissue. The IR transmission window on the glass slide is only above 2000 cm^{-1}. In the range of 2000 – 3700 cm^{-1}, the amide A is the only proper biological peak. Therefore, quality control is based on the intensity of amide A peak, which means the intensity of amide A for good quality spectra on tissue area must be higher than the highest intensity in the tissue-free area. And the highest intensity at 3298 cm^{-1} in the blank area was set as a threshold. The highest threshold was selected and applied in all spectra to keep the consistency for further comparison among the spectra on 6 glass slides,. Due to the

different experimental methods, the thresholds of annotated spectra from 4 patients on every glass slide threshold is different.

7.2.2.1 Experiment 1

The thresholds of annotated spectra from 4 patients on every glass slide are shown in table7.3. In order to keep the consistency for further comparison among the spectra on 6 glass slides, the highest threshold was selected and applied to all of the spectra. According to table 7.3, the threshold for all spectra is 0.0120. The number of annotated spectra of epithelium and stroma with high quality from 4 patients is shown in tables 7.4 & 7.5, respectively.

Table7. 3 The thresholds of annotated spectra on 6 glass slides

Threshold	P1(BPH)	P2(BPH)	P3(CaP)	P4(CaP)
Glass D	0.0113	0.0069	0.0081	0.0049
Glass E	0.0050	0.0120	0.0025	0.0085
Glass F	0.0043	0.0029	0.0113	0.0085
Glass J	0.0103	0.0067	0.0077	0.0119
Glass K	0.0085	0.0044	0.0107	0.0097
Glass L	0.0064	-0.0018	0.0114	0.0087

Table7. 4 The number of high-quality annotated epithelium spectra on 6 glass slides

epithelium spectra	P1(BPH)	P2(BPH)	P3(CaP)	P4(CaP)
Glass D	10442	32204	29476	7391
Glass E	8343	21644	17135	9105
Glass F	5727	14716	8975	8791
Glass J	8221	28372	9312	10953
Glass K	9103	31159	15071	9784
Glass L	8889	28064	18396	9543

Table7. 5 The number of high-quality annotated stroma spectra on 6 glass slides

stroma spectra	P1(BPH)	P2(BPH)	P3(CaP)	P4(CaP)
Glass D	16563	9770	6504	14185
Glass E	6020	8715	5610	14593
Glass F	7673	7677	5366	17449
Glass J	5828	9147	4705	13411
Glass K	3826	8853	6872	14301
Glass L	6442	8510	11921	14023

7.2.2.2 Experiment 2

Compared with experiment 1, the spectra of annotation are the same between the two experiments, but the background spectrum is different. Thus the threshold is different, and it is shown in table 7.6. The enormous threshold in table 7.6 is 0.050, and it is applied in all of the spectra in experiment 2. Tables 7.7 and 7.8 show the number of high-quality annotated spectra of epithelium and stroma.

Table7. 6 The thresholds of annotated spectra on 6 glass slides

Threshold	P1(BPH)	P2(BPH)	P3(CaP)	P4(CaP)
Glass D	0.0500	0.0389	0.0239	0.0280
Glass E	0.0431	0.0312	0.0464	0.0470
Glass F	0.0456	0.0333	0.0344	0.0424
Glass J	0.0398	0.0386	0.043	0.0485
Glass K	0.0135	0.0135	0.0408	0.0478
Glass L	0.0380	0.0388	0.0474	0.0493

Table7. 7 The number of annotated epithelium spectra on 6 glass slides

epithelium spectra	P1(BPH)	P2(BPH)	P3(CaP)	P4(CaP)
Glass D	10423	32015	29275	7352
Glass E	8316	21438	17100	9069
Glass F	5712	14585	8953	8731
Glass J	8187	27889	9282	10896
Glass K	9060	30769	15043	9764
Glass L	8804	27426	18349	9533

Table7. 8 The number of annotated stroma spectra on 6 glass slides

stroma spectra	P1(BPH)	P2(BPH)	P3(CaP)	P4(CaP)
Glass D	16562	9770	6503	14185
Glass E	6020	8714	5610	14592
Glass F	7673	7677	5366	17448
Glass J	5828	9147	4705	13411
Glass K	3826	8853	6872	14300
Glass L	6438	8508	11921	14023

According to tables 7.4, 7.5, 7.7 and 7.8, it is easy to find that the high-quality number of annotated spectra from the same patient on different glass slides has a big difference. It is because the annotation is a subjective process, and all of the processes only depend on my judgment. Although a series of tissue slices from the same patients are adjacent, they still slightly different, and the structure of the tissue slices on every glass slide is a little different.

After quality control, all good quality spectra were processed in order of range selection, noise reduction, and vector normalisation. To reduce the interference from the noise, the range was only selected in 3125-3700 cm^{-1}, which contain all of the valuable biological information in a glass transmission window.

7.2.3 Experiment 1 result

7.2.3.1 Mean spectra

The mean spectra of epithelium and stroma on 6 glass slides for 4 patients are shown in figure 7.4. According to all of the mean spectra in figure 7.4, there is only a pronounced peak at amide A (3298 cm^{-1}) in the wavenumber range. Although the tissue sections are mounted on different glass slides, the shape of spectra is the same, and the intensity of amide A is also similar. The peak in 3400 – 3450 cm^{-1} is related to the O-H &N-H stretching. However, in this range, the spectral intensity and the trend of 6 glass slides are different. The glue mainly causes this difference. The background is a clear area without a tissue in experiment 1. Although tissue thickness is 8 μm, the structure of epithelium and stroma is different. The columnar epithelium has lots of holes. Therefore, the content of glue is variable. If the content of glue on the background is less than that in the sample, the tissue spectra would contain a little glue, and there would be a positive peak in 3400-3450 cm^{-1}. If not, the final tissue spectra would be minus a bit of glue and cause a negative peak in this range. Only when the glue content on the background is precisely the same as that on the tissue do the spectra only represent the tissue. However, this perfect match is tough to achieve. The shape and trend of spectra among 6 glass slides are similar. It indicates that the type of glass has no extreme effect on spectra. Study 1 in chapter 4 has shown the spectra of blank glass D are different than the other blank glass slides. However, the difference is "disappeared" when the tissue is mounted on the glass slide. It could indicate that the tissue contributes much more to the spectra than the glass slide. The spectral influence of glass type cannot be directly told by eyes. Therefore, more specific data processes (PCA and random

forest) are necessary to explore the effect of glass type on cancer detection.

(a)

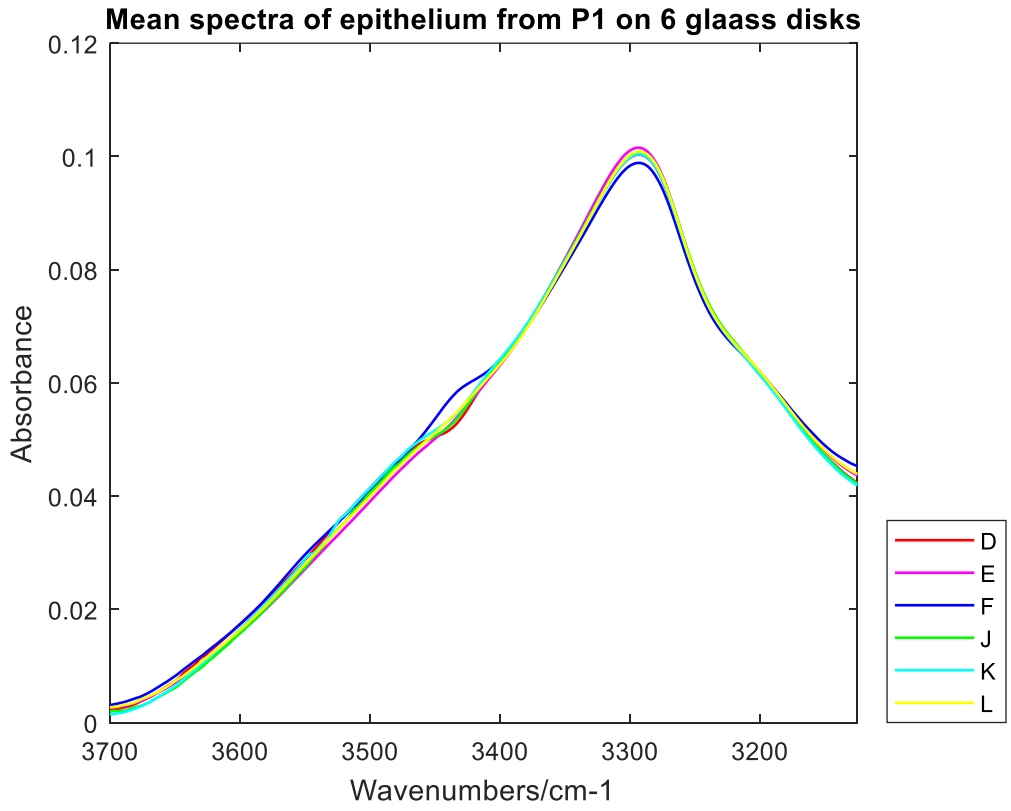

(b)

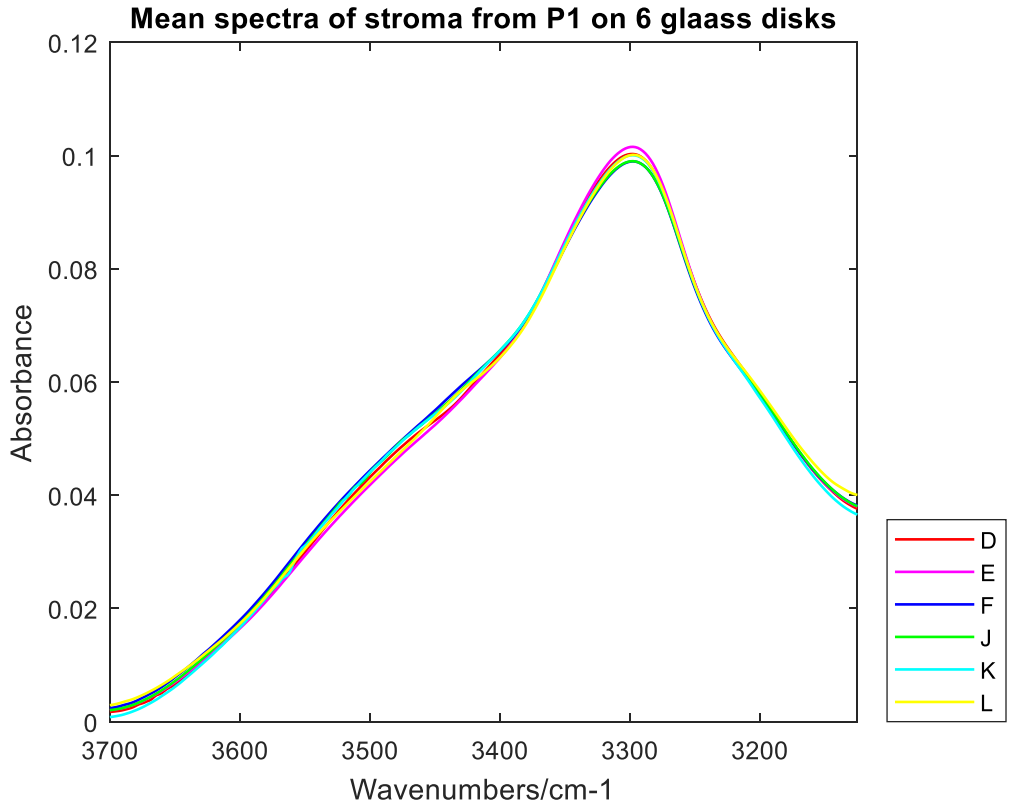
Mean spectra of stroma from P1 on 6 glaass disks
Absorbance
0.12
0.1
0.08
0.06
0.04
0.02
0
3700
3600
3500
3400
3300
3200
Wavenumbers/cm-1
D
E
F
J
K
L

(c)

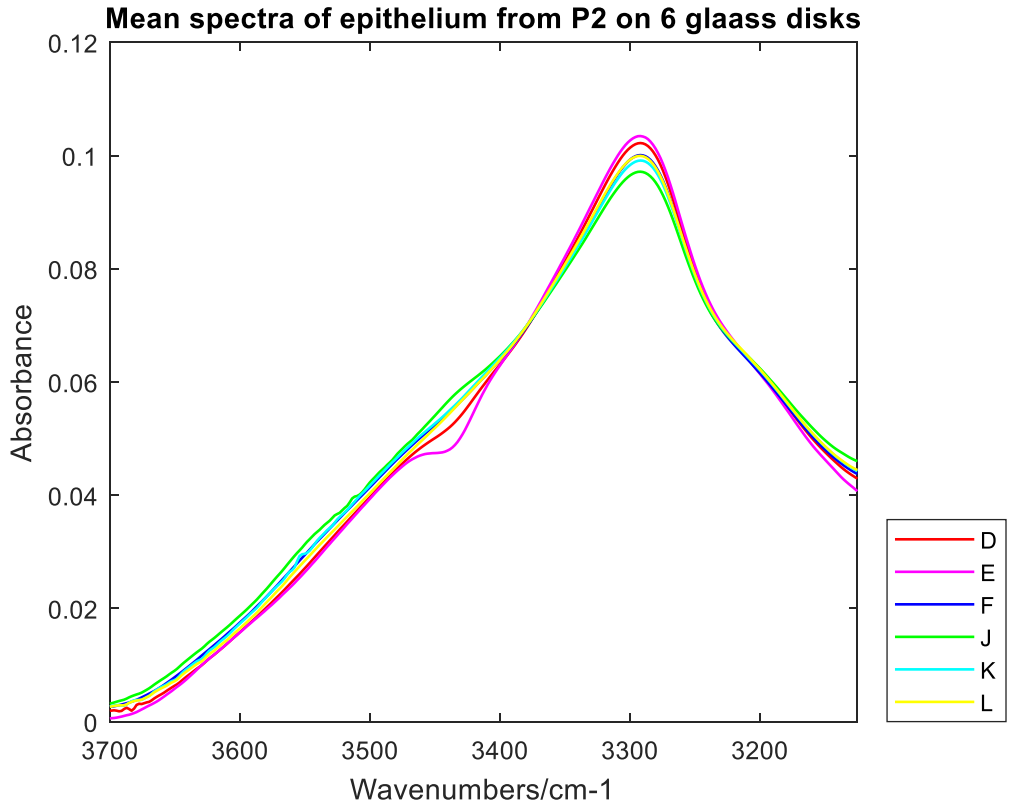
Mean spectra of epithelium from P2 on 6 glaass disks
Absorbance
0.12
0.1
0.08
0.06
0.04
0.02
0
3700
3600
3500
3400
3300
3200
Wavenumbers/cm-1
D
E
F
J
K
L

(d)

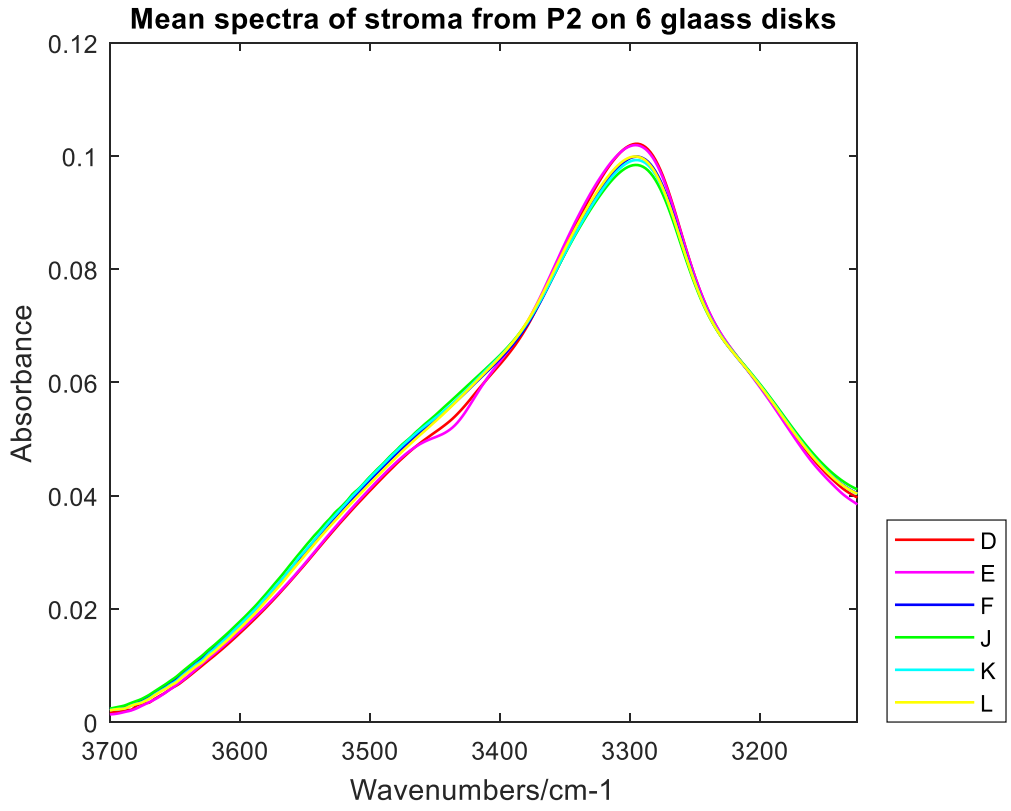
Mean spectra of stroma from P2 on 6 glaass disks
Absorbance
0.12
0.1
0.08
0.06
0.04
0.02
0
3700
3600
3500
3400
3300
3200
Wavenumbers/cm-1
D
E
F
J
K
L

(e)

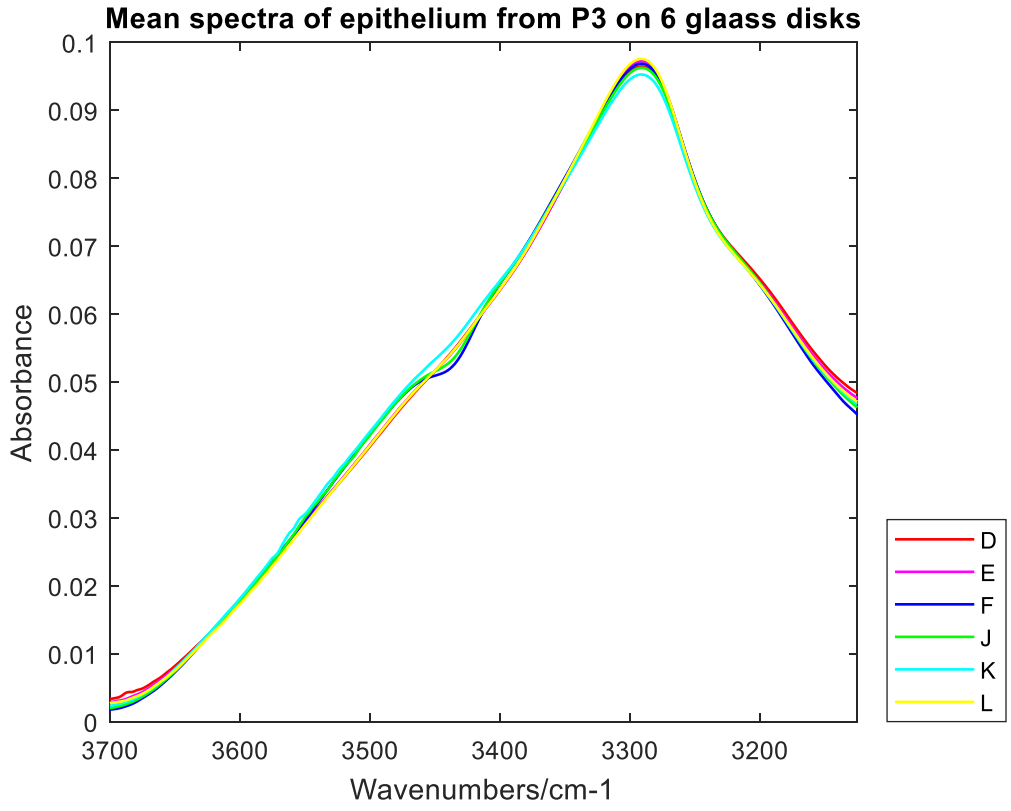
Mean spectra of epithelium from P3 on 6 glaass disks
Absorbance
0.1
0.09
0.08
0.07
0.06
0.05
0.04
0.03
0.02
0.01
0
3700
3600
3500
3400
3300
3200
Wavenumbers/cm-1
D
E
F
J
K
L

(f)

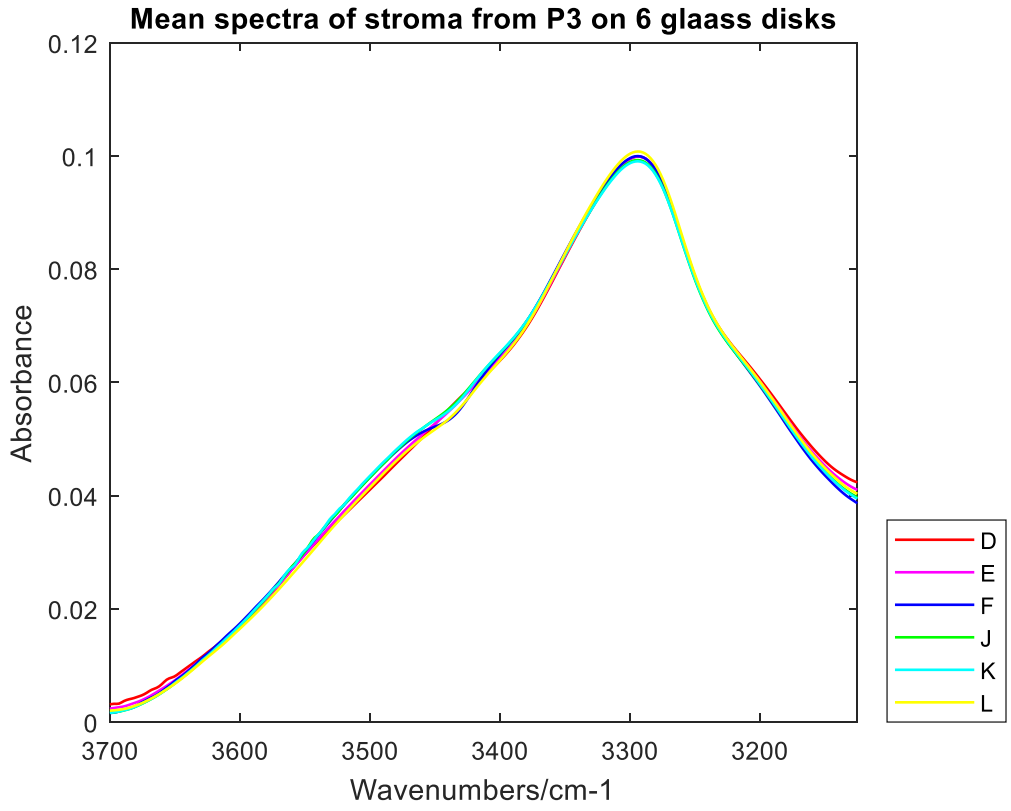
Mean spectra of stroma from P3 on 6 glaass disks
Absorbance
Wavenumbers/cm-1
0.12
0.1
0.08
0.06
0.04
0.02
0
3700
3600
3500
3400
3300
3200
D
E
F
J
K
L

(g)

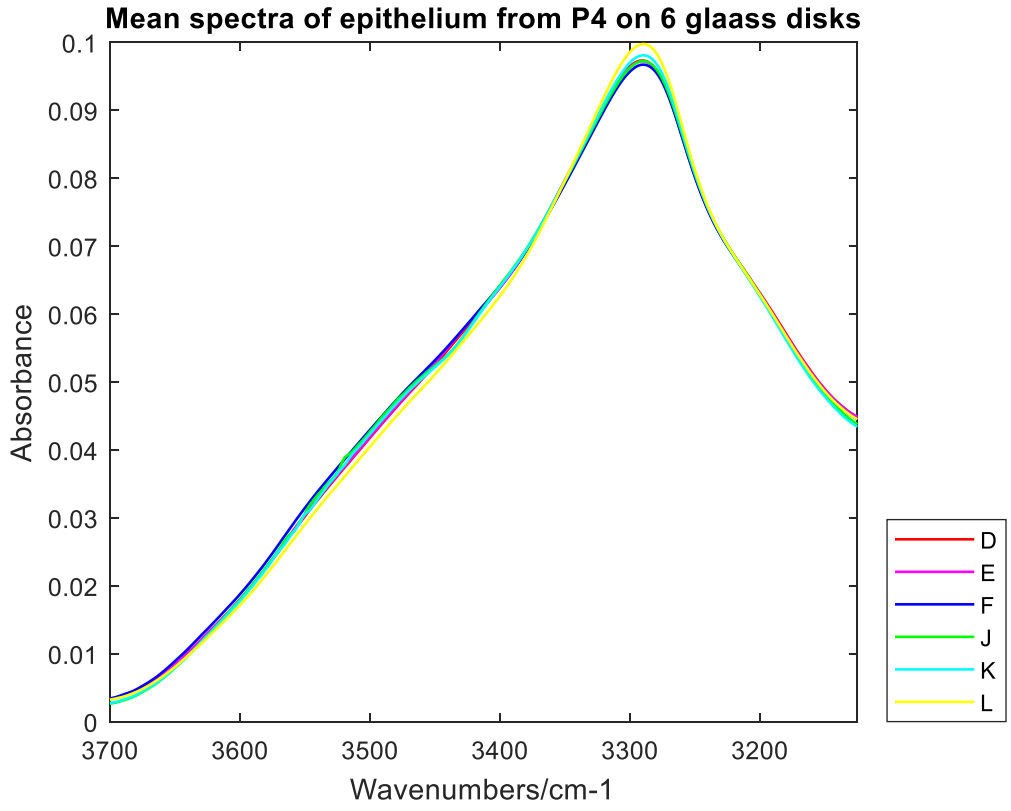
Mean spectra of epithelium from P4 on 6 glaass disks
Absorbance
Wavenumbers/cm-1
0.1
0.09
0.08
0.07
0.06
0.05
0.04
0.03
0.02
0.01
0
3700
3600
3500
3400
3300
3200
D
E
F
J
K
L

(h)

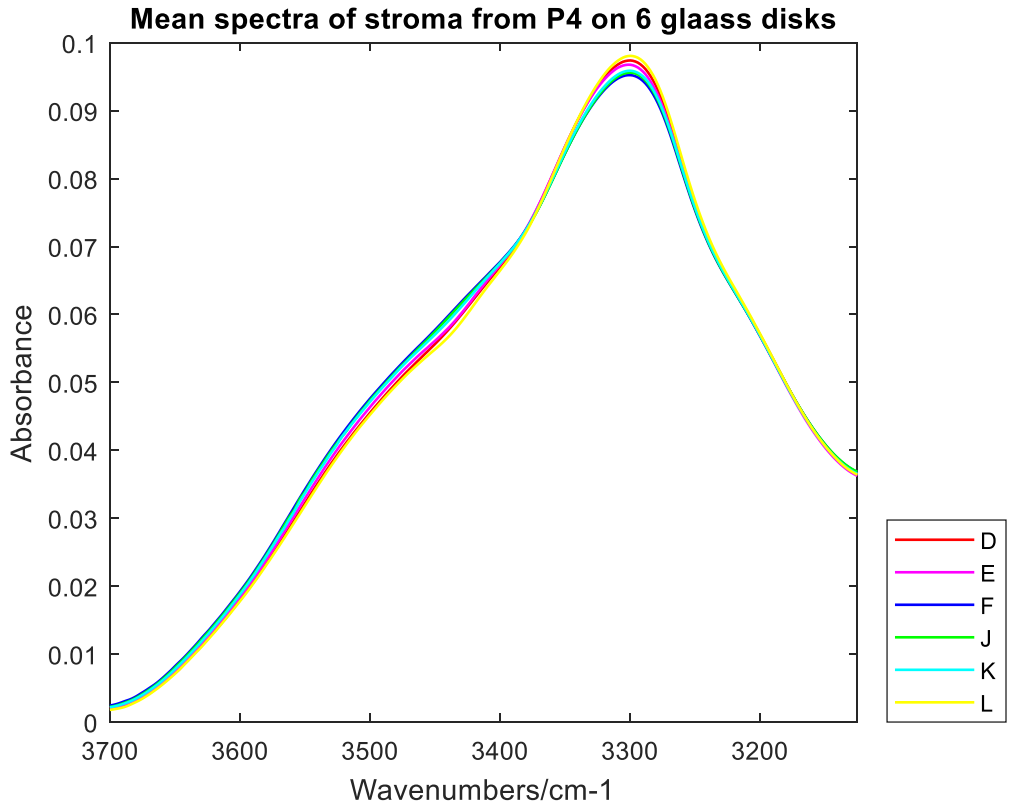

Figure7. 4 (a) (b) Mean spectra of epithelium & stroma on 6 glass slides in 3125 – 3700 cm^{-1} for P1(BPH). (c) (d) Mean spectra of epithelium & stroma on 6 glass slides in 3125 – 3700 cm^{-1} for P2(BPH). (e) (f) Mean spectra of epithelium & stroma on 6 glass slides in 3125 – 3700 cm^{-1} for P3(CaP). (g) (h) Mean spectra of epithelium & stroma on 6 glass slides in 3125 – 3700 cm^{-1} for P4(CaP).

7.2.3.2 The PCA of 6 glass slides

There is no noticeable difference among the mean spectra on 6 glass slides. Therefore, the difference of spectral data among different types of glass maybe could be indicated based on PCA. 200 spectra of stroma and epithelium on 6 glass slides were randomly selected. The PCA is based on these random spectra. Figure 7.5 shows the PCA results of 6 glass slides for 4 patients. Due to the similar PCA distribution between epithelium and stroma for every patient, there are only show the PCA figures of the stroma.

(a)

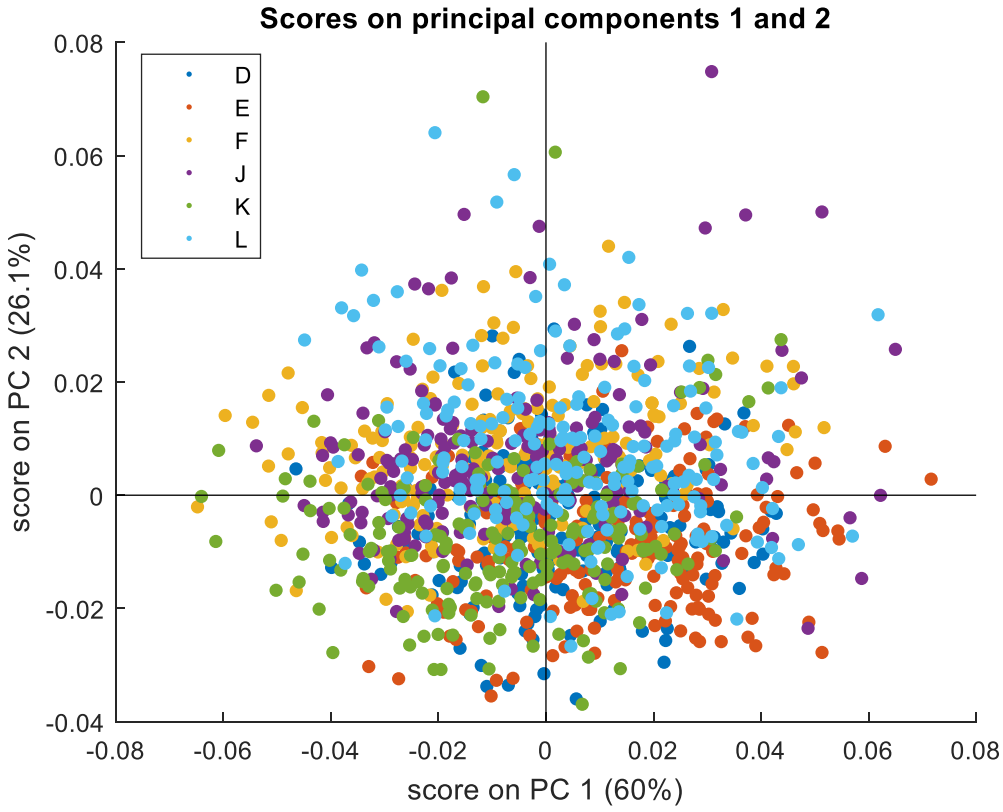
Scores on principal components 1 and 2
D
E
F
J
K
L
0.08
0.06
0.04
0.02
0
-0.02
-0.04
score on PC 2 (26.1%)
-0.08
-0.06
-0.04
-0.02
0
0.02
0.04
0.06
0.08
score on PC 1 (60%)

(b)

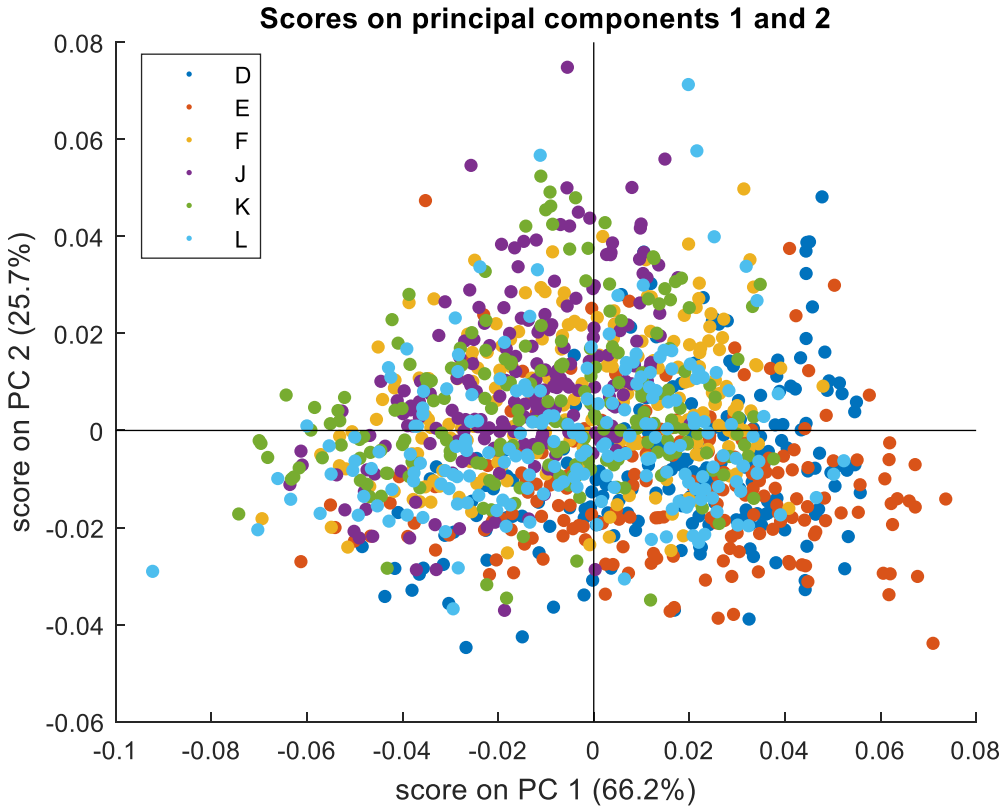
Scores on principal components 1 and 2
D
E
F
J
K
L
0.08
0.06
0.04
0.02
0
-0.02
-0.04
-0.06
score on PC 2 (25.7%)
-0.1
-0.08
-0.06
-0.04
-0.02
0
0.02
0.04
0.06
0.08
score on PC 1 (66.2%)

(c)

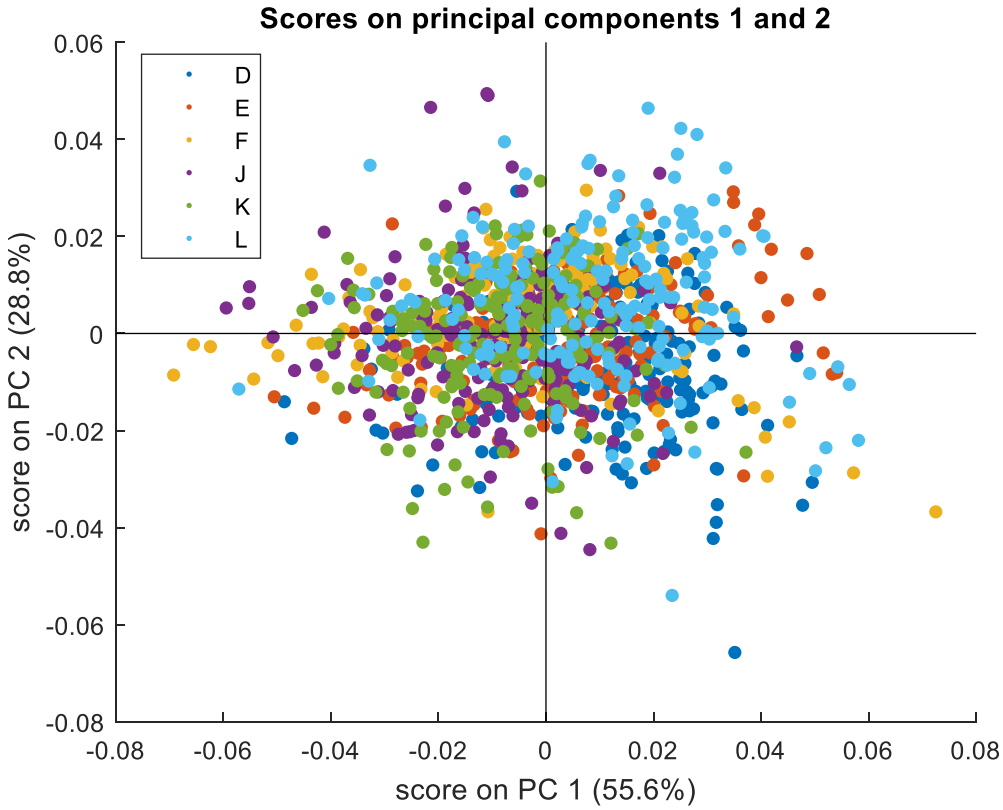

(d)

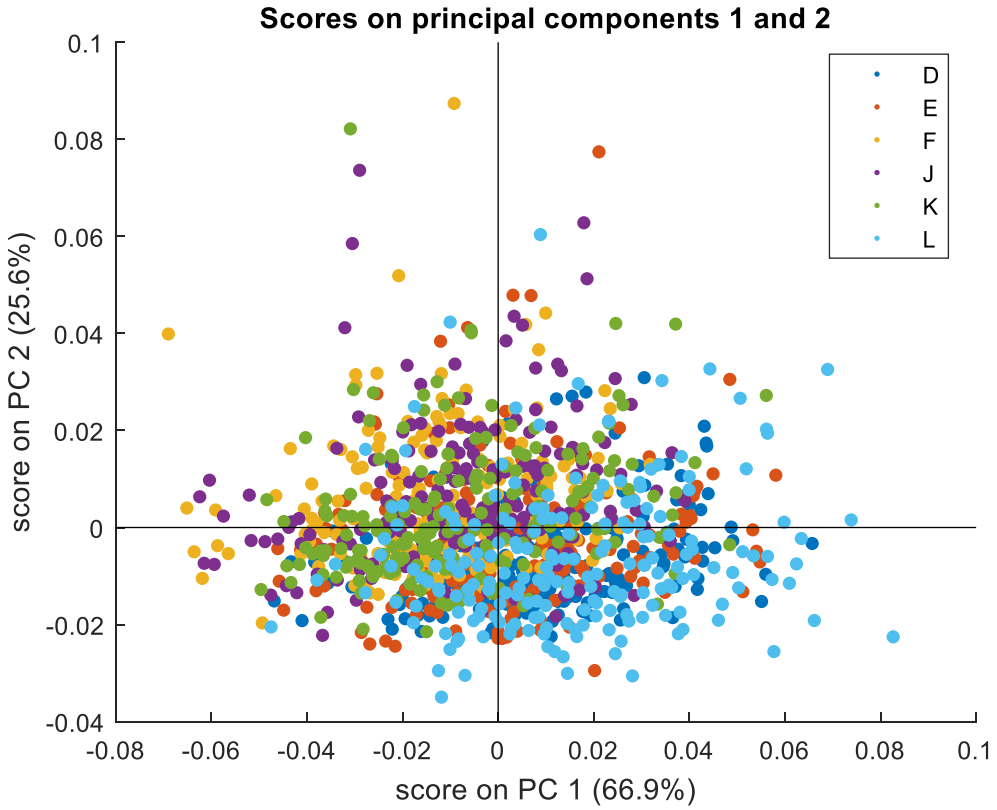

Figure7. 5 (a) The score plots of PC1 and PC2 of stroma on 6 glass slides for P1(BPH). (b) The score plots of PC1 and PC2 of stroma on 6 glass slides for P2(BPH). (c) The score plots of PC1 and PC2 of

stroma on 6 glass slides for P3(CaP). (d) The score plots of PC1 and PC2 of stroma on 6 glass slides for P4(CaP).

According to figure 7.5, it is accessible to see that there is no clear separation among the tissue sections on 6 glass slides. It indicates that the type of glass has little influence on the spectra of the same histological class.

7.2.3.3 The PCA of 4 patients

Figure 7.6 shows the PCA results of 4 patients on glass D. Due to the similar PCA distribution between 4 patients for every glass slide, only the PCA figures on glass D are shown. According to figure 7.6, there is no clear separation, but there is a separation trend, especially for the spectra of epithelium on glass D (figure 7.6(a)). The spectra of 4 patients are mainly distributed in the four different regions of the PCA scores plot, and it suggests that the spectral difference is caused by different patients.

(a)

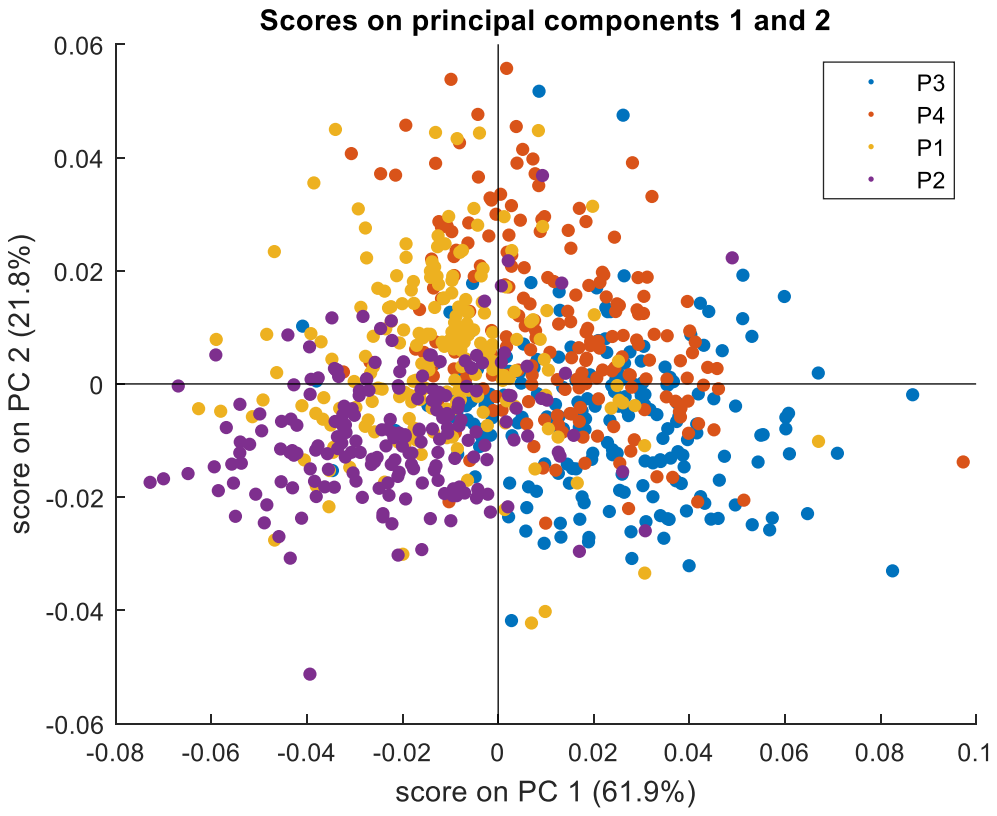

(b)

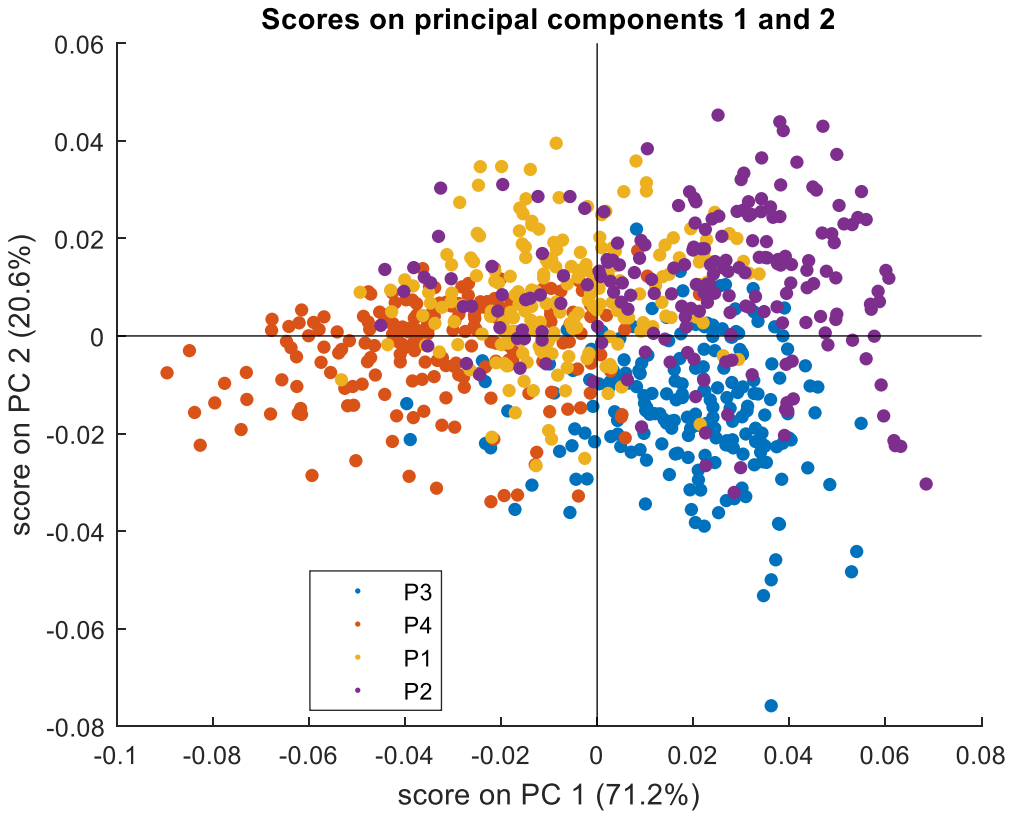

Figure7. 6 (a) The score plots of PC1 and PC2 of epithelium on glass D for 4 patients. (b) The score plots of PC1 and PC2 of stroma on 6 glass slides for 4 patients.

According to figure 7.6, the spectra of the epithelium of cancer and no-cancer could be almost separated by PC1. While for the spectra of stroma, cancer and non-cancer spectra are separated by PC2. The loading of PC1 of epithelium spectra and PC2 of stroma spectra from 4 patients on glass D is shown in figure 7.7 (a) and (b), respectively. According to figure 7.7, except that they go in the opposite direction, the spectral peaks of the two loadings are similar for epithelium and stroma spectra. The PC1 loading of epithelium spectra is taken as an example for the analysis.

(a)

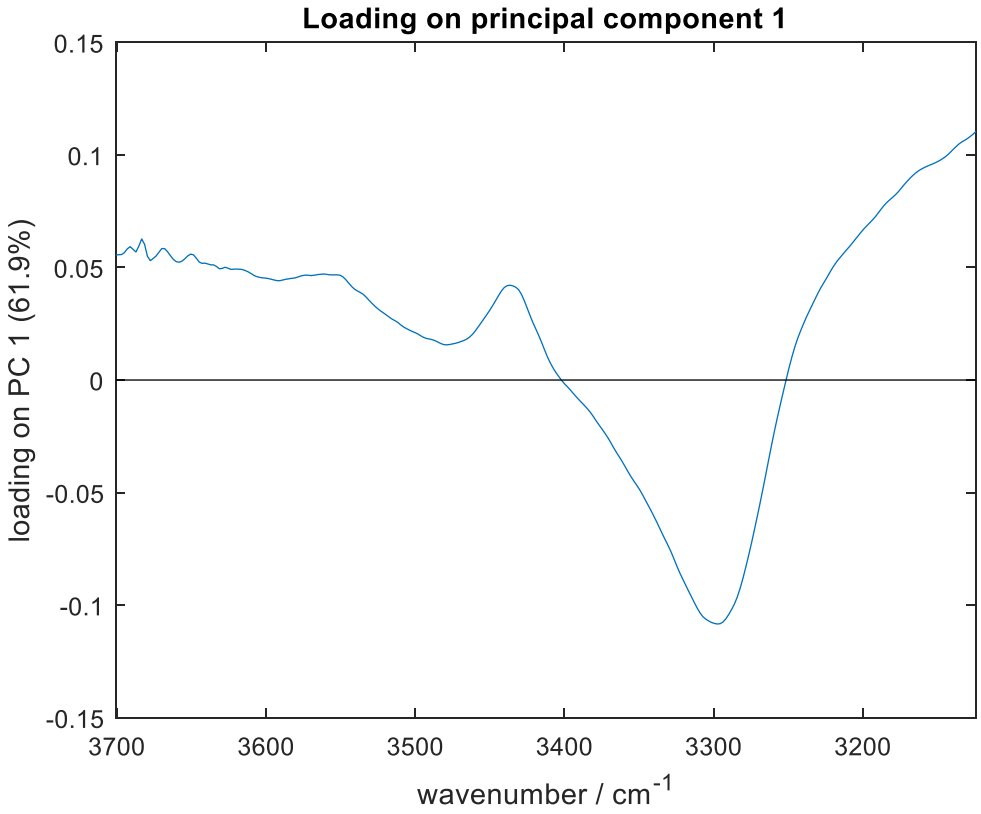

(b)

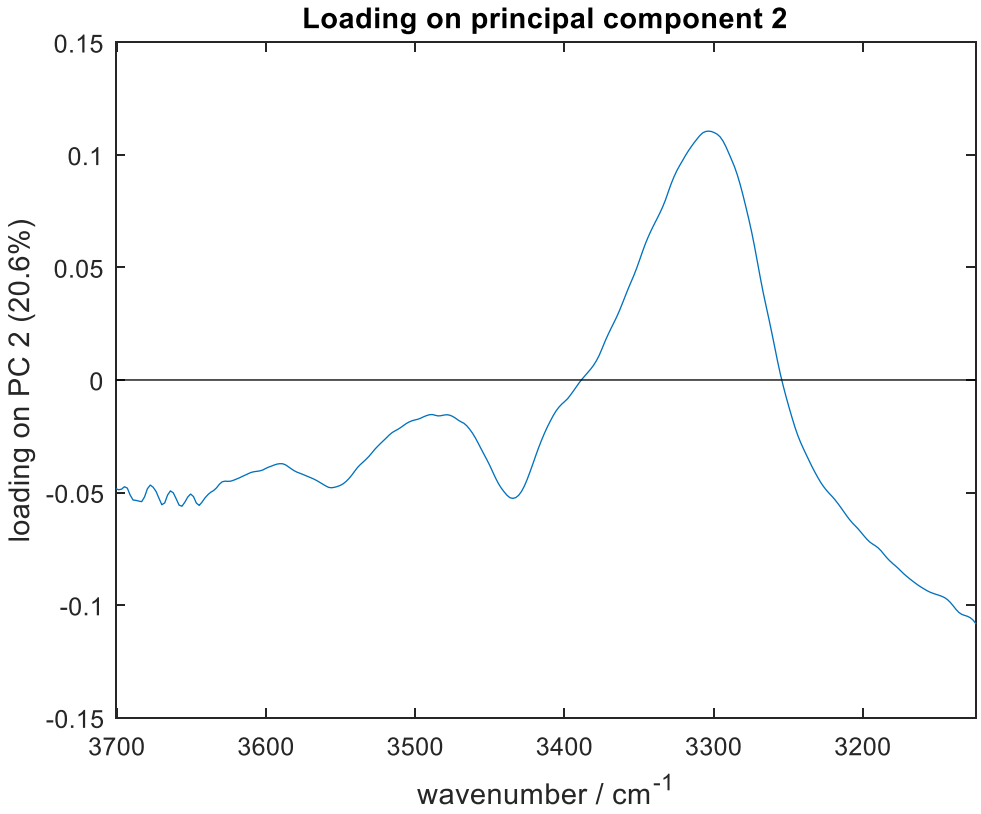

Figure7. 7 (a)The PC1 loading for PCA of epithelium spectra from 4 patients on glass D. (b) The PC2 loading for PCA of stroma spectra from 4 patients on glass D.

The loading of PC1 of epithelium spectra from 4 patients on glass D is shown in figure 7.7 (a). The PC1 is the significant component to represent the information of spectra. According to figure 7.7 (a), PC1 has two whole peaks in the range of 3125 – 3700 cm^{-1}. The prominent negative peak is located at 3298 cm^{-1}, which is related to amide A. The positive peak is located at 3437 cm^{-1}, which is associated with O-H asymmetric stretching. An overall consideration of negative and positive peaks in PC1, the loading of PC1 mainly results from the intensity of amide A. Therefore, the distribution of spectra on PC1 is nearly negatively correlated with the intensity of amide A. P1(BPH) & P2(BPH) are mainly distributed in the negative area, which means the intensity of amide A for non-cancer spectra is higher than cancer spectra.

7.2.3.4 The PCA of cancer & non-cancer patients

One of the objectives is achieving cancer detection. To find the difference between cancer and non-cancer spectra on the same glass slide, spectra of cancer and non-cancer are compared in 3125 – 3700 cm^{-1}. There are 2 BPH patients and 2 cancer patients. Therefore, it is meaningful to combine the spectra from 2 BPH patients and 2 cancer patients and become cancer and non-cancer groups. Because the results of the spectral comparison of cancer and non-cancer on the same glass are similar. Figure 7.8 shows the comparison of mean spectra on glass D, and figure 7.9 shows the PCA figures on glass D.

(a)

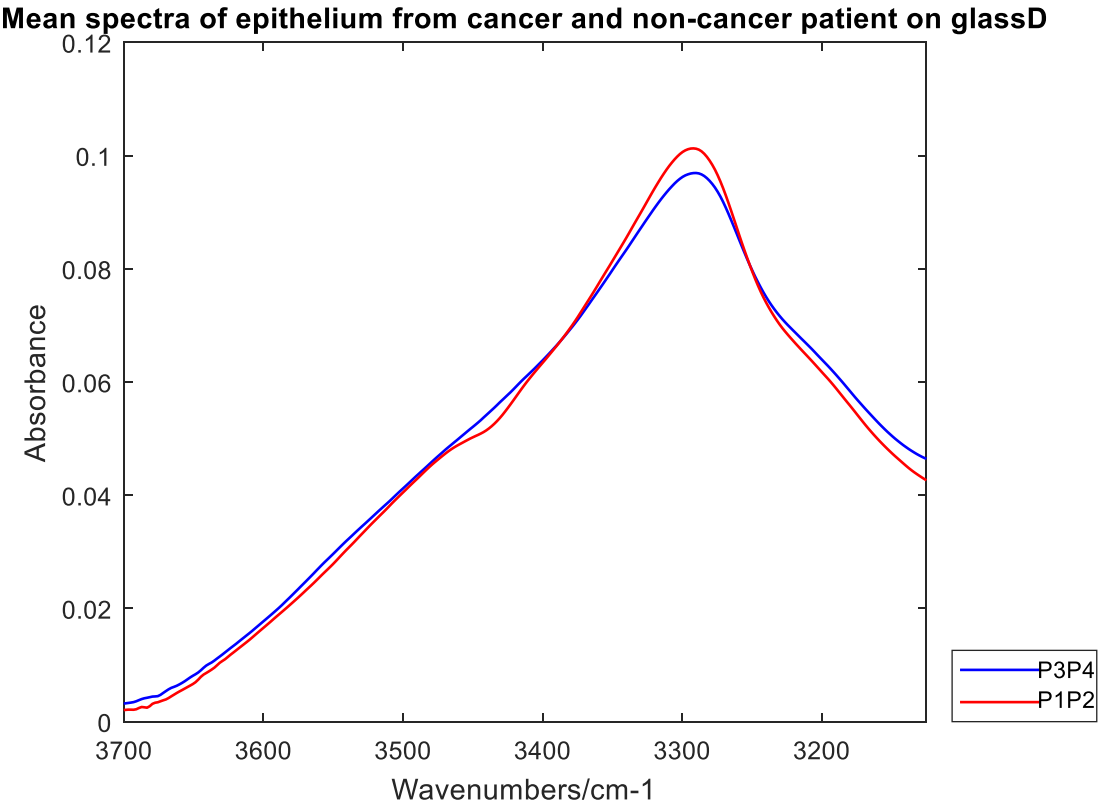

(b)

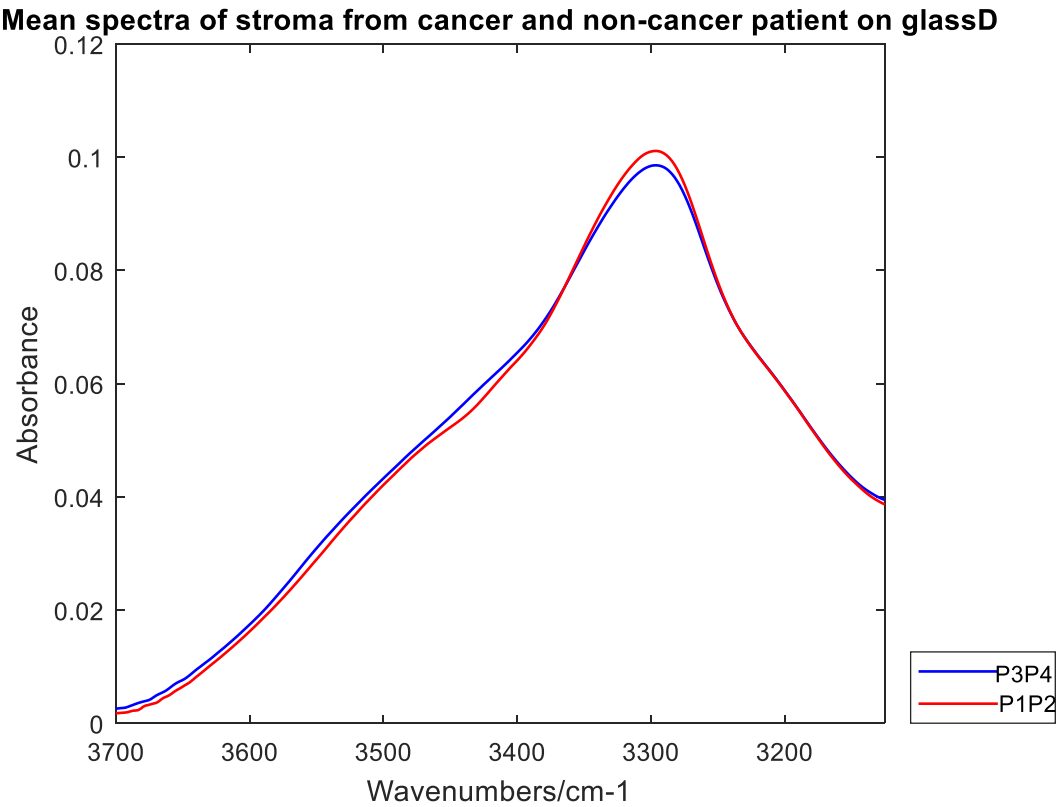

Figure7. 8 (a) the mean spectra of epithelium for cancer &non-cancer group on glass D. (b) the mean

spectra of stroma for cancer &non-cancer group on glass D

According to figure 7.8, not only for the mean spectra of the epithelium but also for the spectra of stroma, the intensity of amide A for the non-cancer group is higher than the cancer group. In addition, according to the comparison of the mean spectra of epithelium and stroma, the intensity of amide A of stroma spectra is a little higher than epithelium spectra.

According to figure 7.9, there is a nearly clear separation between cancer and non-cancer groups. The break is based on PC1. The loading of PC1 has two whole peaks. However, the most contribution is a negative peak located at 3298 cm^{-1} and it is related to amide A. Therefore, the spectra distribution is nearly negatively correlated with the intensity of amide A. Because the non-cancer group is located in a negative area on PC1, the intensity of amide A of epithelium spectra for the non-cancer group is higher than the cancer group.

(a)

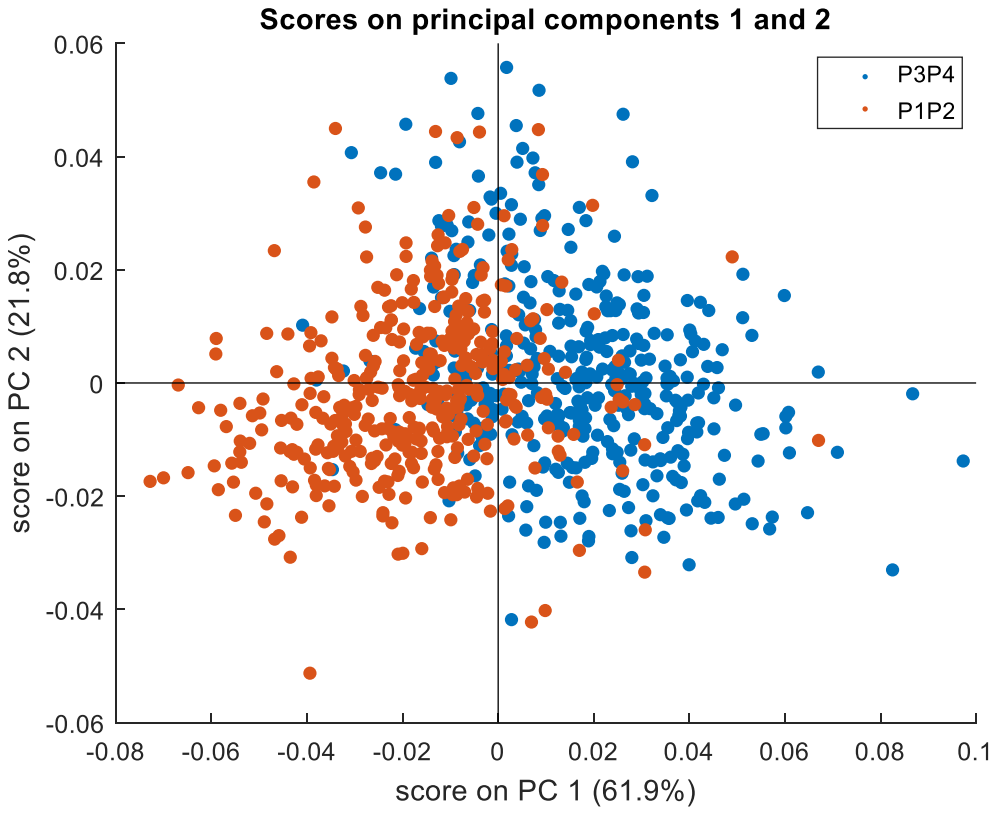

(b)

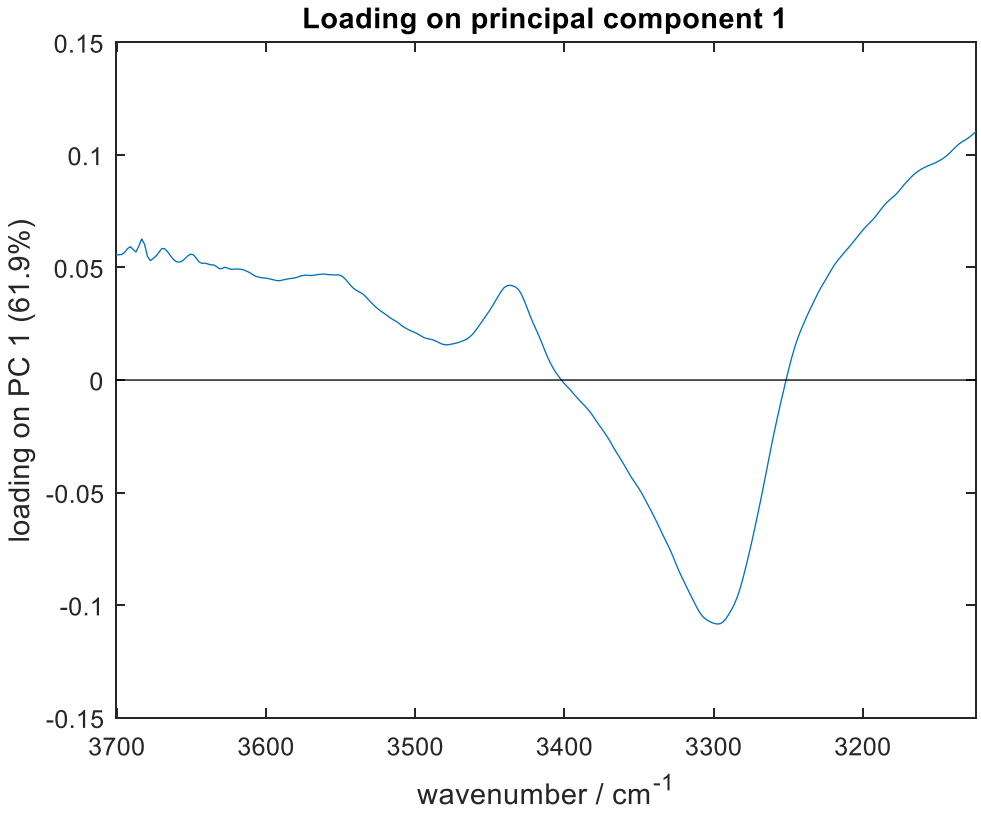

Figure7. 9 (a) The score plots of PC1 and PC2 of epithelium on glass D for cancer and non-cancer patients. (b) The PC1 loading for PCA of epithelium spectra on glass D for cancer and non-cancer patients.

7.2.3.5 Cancer detection by random forest on the same glass slide

The tissue slices from 4 patients (P1(BPH), P2(BPH), P3(CaP), P4(CaP)) are mounted on 6 different types of glass slides (glass D, E, F, J, K, L) in the experiment. For an easy description in the further report, " patient_glass " stand for a patient's tissue fixed on a type of glass slide. For example, "P1_D" represents the P1's tissue slice mounted on glass D. P1 _D and P2_D are BPH slides on glass D, P3_D and P4_D are cancer slides on glass D. For looking at the accuracy of cancer detection, there are 4 kinds of classification in total, which are P1_D & P3_D, P2_D & P3_D, P1_D & P4_D, P2_D & P4_D.

All spectra of a BPH tissue slice and a cancer tissue slide on the same glass slide are divided into two data sets. 80% of spectral data are used to train the classifier, and the

rest 20% of spectral data are used to test the classifier (table 7.9). The accuracy of cancer and non-cancer classification is applied to evaluate the classifier. In addition, epithelium and stroma are annotated and applied to train the model, respectively. And the accuracy of cancer detection by the spectra of epithelium and stroma is shown in table 7.10 and table 7.11, respectively.

Table7. 9 Classifier construction by Random forest (Take spectra of P1 & P3 on glass D as an example.)

	Training set	Test set
Model test	80% spectra of P1_D	20% spectra of P1_D
	80% spectra of P3_D	20% spectra of P3_D

Table7. 10 The accuracy of cancer detection by epithelium spectra on the same glass slide.

Model test (%)	P1(BPH) & P3(CaP)	P2(BPH) & P3(CaP)	P1(BPH) & P4(CaP)	P2(BPH) & P4(CaP)
Glass D	99.07	98.68	99.94	99.75
Glass E	98.39	99.90	99.46	99.90
Glass F	100	100	99.83	98.92
Glass J	99.03	99.20	99.71	99.86
Glass K	99.11	97.47	99.47	99.77
Glass L	95.49	92.76	97.18	97.35

Table7. 11 The accuracy of cancer detection by stroma spectra on the same glass slide.

Model test (%)	P1(BPH) & P3(CaP)	P2(BPH) & P3(CaP)	P1(BPH) & P4(CaP)	P2(BPH) & P4(CaP)
Glass D	99.24	98.89	98.59	99.87
Glass E	97.85	99.93	99.51	99.81
Glass F	99.96	100	96.52	99.30
Glass J	96.44	96.2	99.22	99.76
Glass K	98.41	97.36	99.03	99.37
Glass L	96.90	94.00	98.41	98.96

Table 7.10 and table 7.11 show there is very high accuracy for cancer detection on the same glass slide. Most of the accuracies are above 96%. It indicates the classifier has high precision to discriminate against cancer and non-cancer on the same glass slide for both by spectra of epithelium and stroma. Compared with the specific accuracies on the same glass slide, the cancer detection results by epithelium are slightly better than by stroma.

However, the detection only between two patients cannot ensure the classification is based on the biochemical difference rather than the patient's difference. Therefore, it is

meaningful to obtain cancer and non-cancer groups by combining the spectra of two CaP patients and two BPH patients, respectively. And table 7.12 shows the accuracy of cancer detection between the cancer group and the non-cancer group.

Table7. 12 The accuracy of cancer detection between cancer and non-cancer group on the same glass slide

Model test (%)	epithelium	stroma
Glass D	98.55	98.80
Glass E	99.16	98.63
Glass F	99.49	97.46
Glass J	99.12	97.19
Glass K	98.00	97.59
Glass L	93.10	95.79

According to table 7.12, the results indicate that both by spectra of epithelium and stroma cancer detection has a specific high accuracy on the same type of glass slide. The classification accuracy on the glass L is only above 93%, and the better results are training classifiers by the spectra of the epithelium. Except for glass L, the accuracy of cancer detection on the other glass slide is above 97%. To sum up, the accurate results indicate that SHP for cancer detection on the same type of glass slide is a possible way.

7.2.3.6 Cancer detection by random forest on the different glass slide

For clinical application, the main objective of the project is to look at the influence of glass type on cancer detection. Therefore, spectral data from one glass slide are used to train the classifier to distinguish between cancer and non-cancer patients. And the spectra from the other glass slide are used to test the classifier. If the classifier could achieve cancer detection on the different glass slides, it would indicate that the type of glass does not affect cancer detection. If not, the type of glass affects cancer detection.

Table 7.13 and Table 7.14 show the classification results of cancer and non-cancer groups on different types of glass slides by spectra of epithelium and stroma, respectively. The classification accuracy of cancer and non-cancer group is very

different on the various glass slide. Some classifiers have an excellent performance on cancer detection between some glass slides. The good results, in which the accuracy is more than 80%, are highlighted in yellow. But some classifiers have very bad classification between some glass slides.

According to the highlighting in Tables 7.13 and 7.14, it is easy to find that the cancer detection between glasses D & E or between glasses F & K & J could get a good classification result. It means that the differences in glasses D & E or in glasses F & K & J are smaller than the difference in cancer tissue. Therefore, the type of glass slide has a certain influence on cancer detection. But if the glass slides are similar, the effect on cancer detection could be lower. In addition, the comparison of the accuracy of cancer detection by epithelium and stroma spectra shows that the classifier trained by epithelium spectra could get better performance.

Table7. 13 The accuracy of cancer detection by epithelium spectra on a different glass slide

Accuracy (%)	Test on glass D	Test on glass E	Test on glass F	Test on glass J	Test on glass K	Test on glass L
Train on glass D		90.53	50.21	40.0	63.94	63.88
Train on glass E	84.87		40.17	37.54	48.0	66.3
Train on glass F	62.54	43.93		93.95	91.09	69.85
Train on glass J	66.48	68.63	97.16		91.23	67.76
Train on glass K	76.50	73.95	95.05	88.03		73.26
Train on glass L	85.53	83.72	86.23	82.19	84.08	

Table7. 14 The accuracy of cancer detection by stroma spectra on a different glass slide

Accuracy (%)	Test on glass D	Test on glass E	Test on glass F	Test on glass J	Test on glass K	Test on glass L
Train on glass D		92.16	59.47	58.10	69.86	48.42
Train on glass E	88.46		59.46	59.84	70.81	64.05
Train on glass F	70.53	60.49		85.08	88.95	65.77
Train on glass J	68.89	74.34	89.06		84.35	56.64
Train on glass K	79.83	76.54	89.43	81.88		72.45
Train on glass L	43.33	60.26	85.79	77.96	79.98	

7.2.4 Experiment 2 results

7.2.4.1 Mean spectra

Figure 7.10 show the mean spectra of epithelium and stroma on 6 glass slides for 4 patients in experiment 2. The background in experiment 2 is blank glass, and sample measurement includes coverslip, glue, tissue and glass, so the final spectra contain the information from coverslip, glue and tissue. There is only a pronounced peak at amide A (3298 cm^{-1}) for all of the mean spectra on six glass slides, which is amide A peak and caused by tissue. The broad band (3400-3600 cm^{-1}) is the most significant difference between experiments 1 and 2, and it is caused by the coverslip. In addition, the peak in 3400-3450 cm^{-1} is related to the O-H &N-H stretching. For experiment1, in this range, not only is the spectral intensity different but so is the spectral profile. This difference is caused by the glue and measurement method. While for experiment 2, there is a small positive peak in 3400-3450 cm^{-1} and is related to the glue. Although the glue has a significant effect on spectra, all of the mean spectra on 6 glass slides for 4 patients have the same shape and trend, and only the intensity of amide A is slightly different. Compared with the spectra of the same patients, the intensity of spectra from stroma is always higher than from epithelium.

(a)

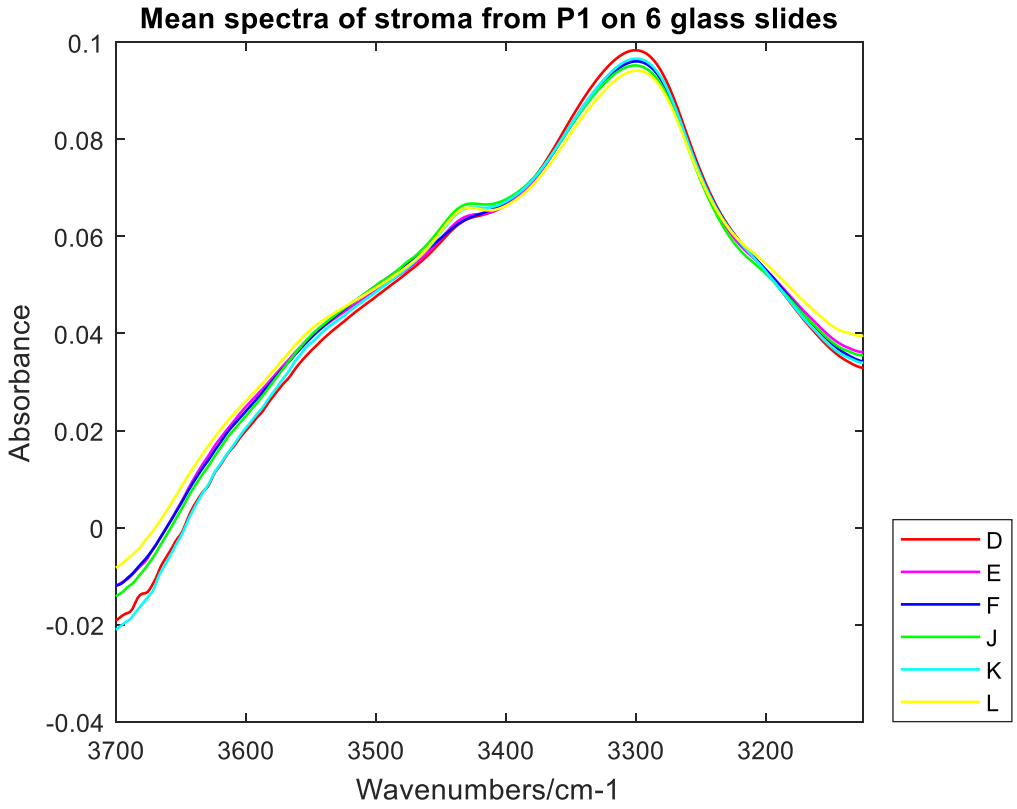
Mean spectra of stroma from P1 on 6 glass slides
Absorbance
0.1
0.08
0.06
0.04
0.02
0
-0.02
-0.04
3700
3600
3500
3400
3300
3200
Wavenumbers/cm-1
D
E
F
J
K
L

(b)

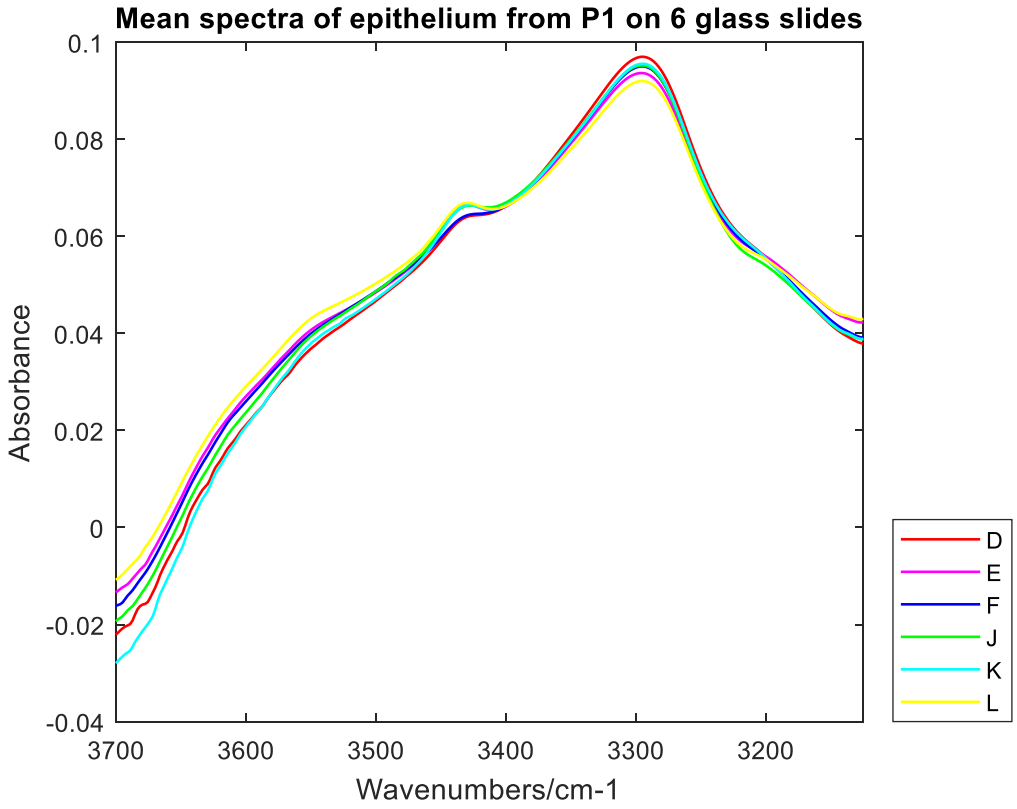
Mean spectra of epithelium from P1 on 6 glass slides
Absorbance
0.1
0.08
0.06
0.04
0.02
0
-0.02
-0.04
3700
3600
3500
3400
3300
3200
Wavenumbers/cm-1
D
E
F
J
K
L

(c)

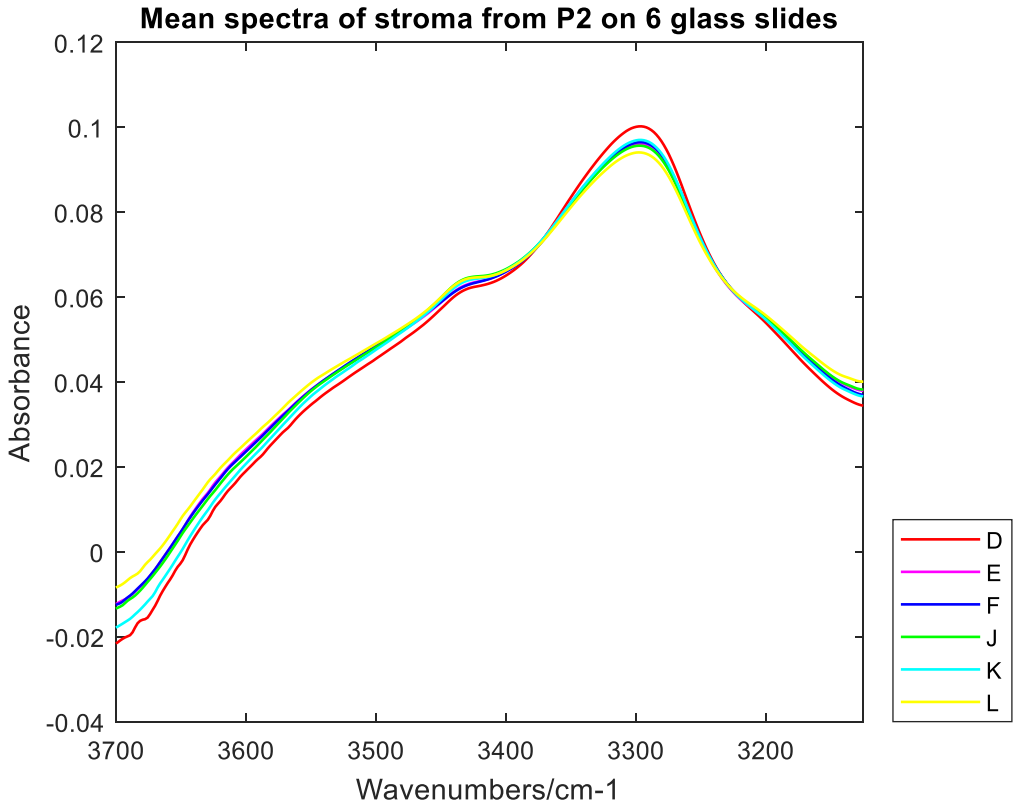
Mean spectra of stroma from P2 on 6 glass slides
Absorbance
0.12
0.1
0.08
0.06
0.04
0.02
0
-0.02
-0.04
3700
3600
3500
3400
3300
3200
Wavenumbers/cm-1
D
E
F
J
K
L

(d)

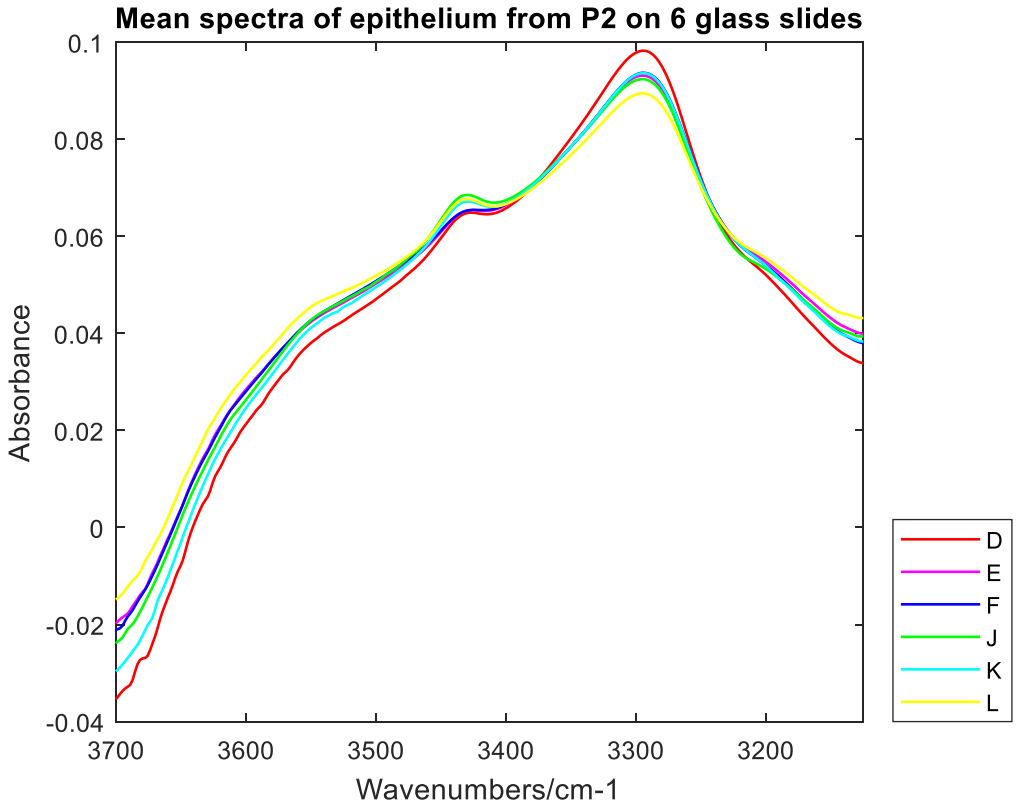
Mean spectra of epithelium from P2 on 6 glass slides
Absorbance
0.1
0.08
0.06
0.04
0.02
0
-0.02
-0.04
3700
3600
3500
3400
3300
3200
Wavenumbers/cm-1
D
E
F
J
K
L

(e)

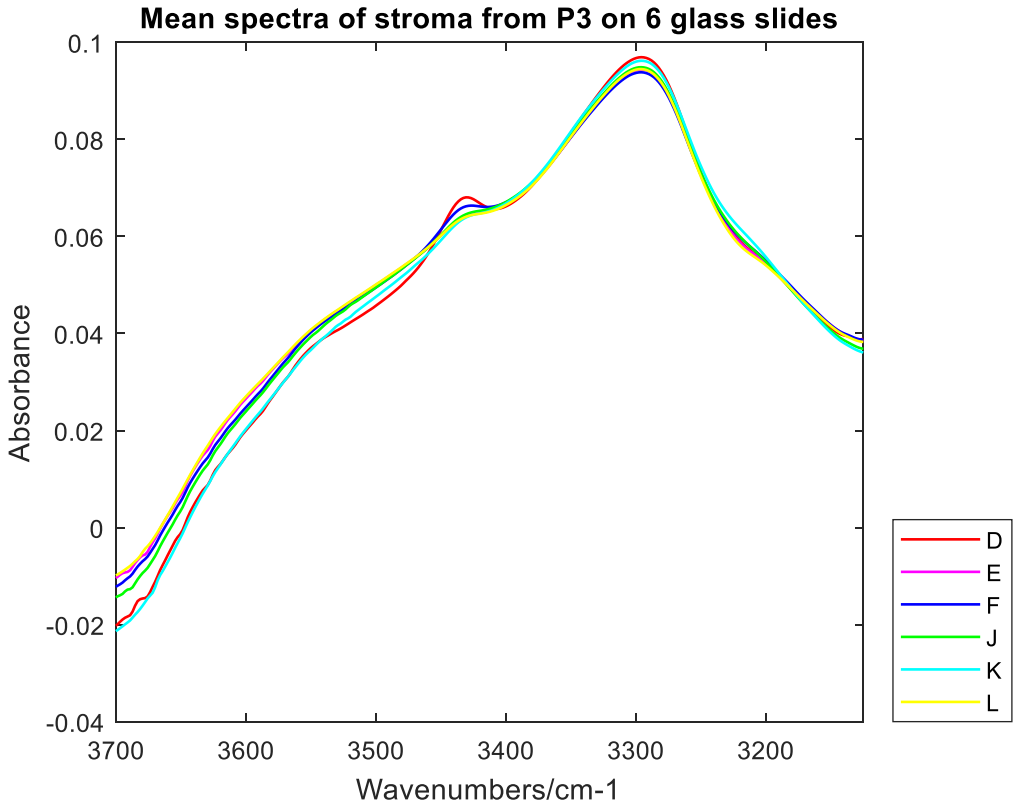
Mean spectra of stroma from P3 on 6 glass slides
Absorbance
0.1
0.08
0.06
0.04
0.02
0
-0.02
-0.04
3700
3600
3500
3400
3300
3200
Wavenumbers/cm-1
D
E
F
J
K
L

(f)

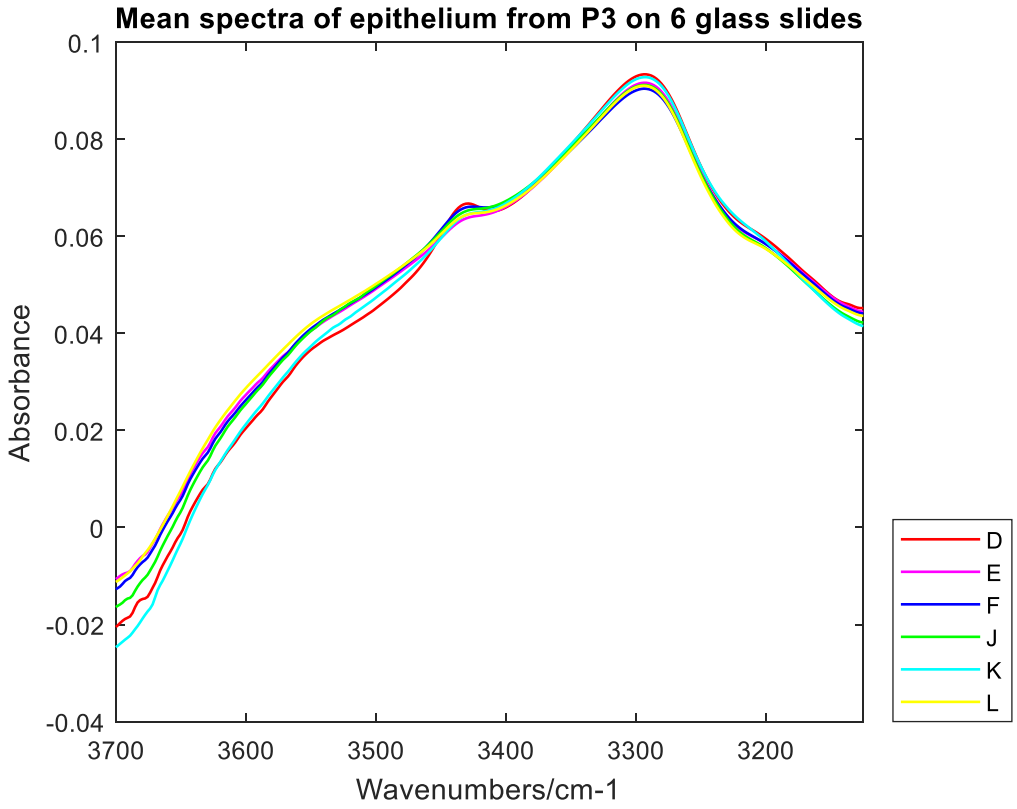
Mean spectra of epithelium from P3 on 6 glass slides
Absorbance
0.1
0.08
0.06
0.04
0.02
0
-0.02
-0.04
3700
3600
3500
3400
3300
3200
Wavenumbers/cm-1
D
E
F
J
K
L

(g)

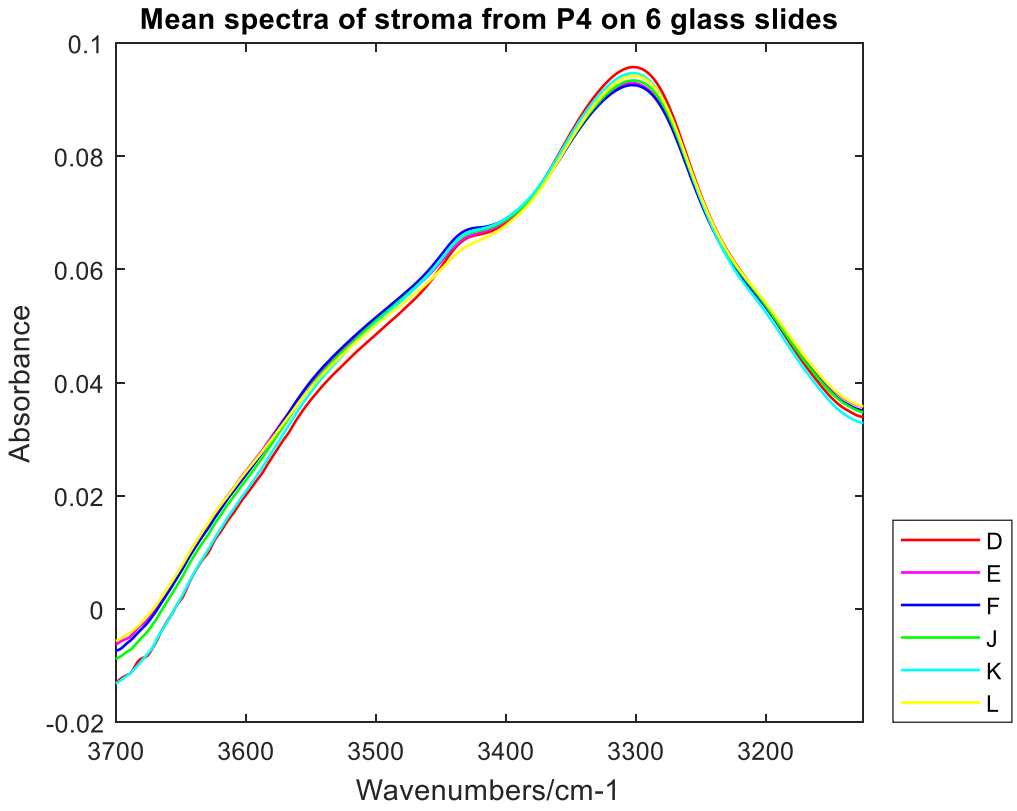
Mean spectra of stroma from P4 on 6 glass slides
Absorbance
0.1
0.08
0.06
0.04
0.02
0
-0.02
3700
3600
3500
3400
3300
3200
Wavenumbers/cm-1
D
E
F
J
K
L

(h)

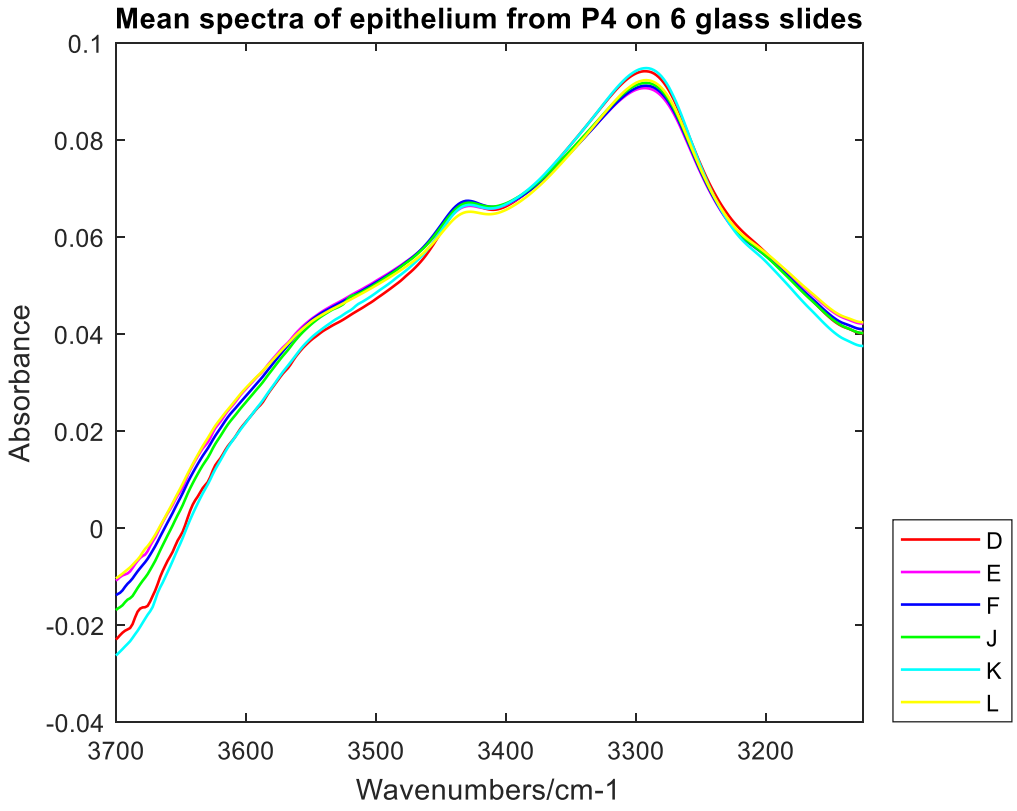
Mean spectra of epithelium from P4 on 6 glass slides
Absorbance
0.1
0.08
0.06
0.04
0.02
0
-0.02
-0.04
3700
3600
3500
3400
3300
3200
Wavenumbers/cm-1
D
E
F
J
K
L

Figure7. 10 (a) (b) Mean spectra of stroma & epithelium on 6 glass slides in 3125 – 3700 cm^{-1} or P1(BPH). (c) (d) Mean spectra of stroma & epithelium on 6 glass slides in 3125 – 3700 cm^{-1} for P2(BPH). (e) (f) Mean spectra of stroma & epithelium on 6 glass slides in 3125 – 3700 cm^{-1} for P3(CaP). (g) (h) Mean spectra of stroma & epithelium on 6 glass slides in 3125 – 3700 cm^{-1} for P4(CaP).

7.2.4.2 The PCA of 6 glass slides in experiment 2

Figure 7.11 is the PCA results of 6 glass slides for 4 patients. It can be seen that there is no clear separation among the tissue sections on 6 glass slides. It indicates that the type of glass has little influence on the spectra of the same histological class. Due to the similar PCA distribution between epithelium and stroma for every patient, there are only show the PCA figures of the stroma.

(a)

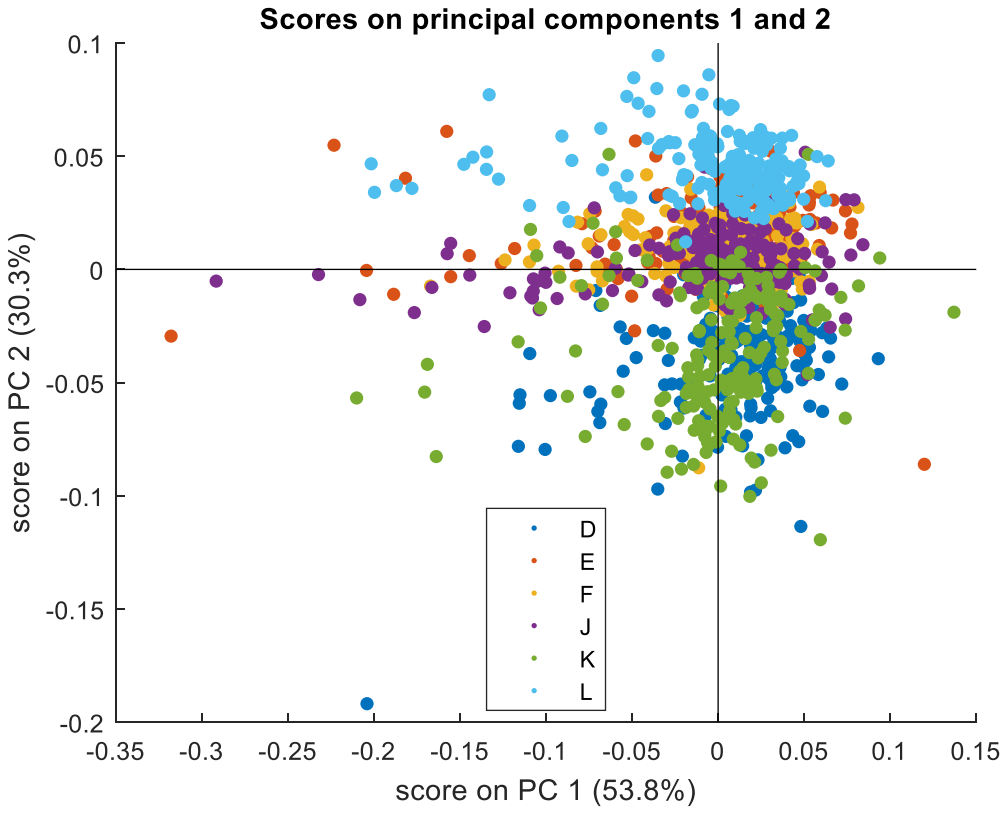

(b)

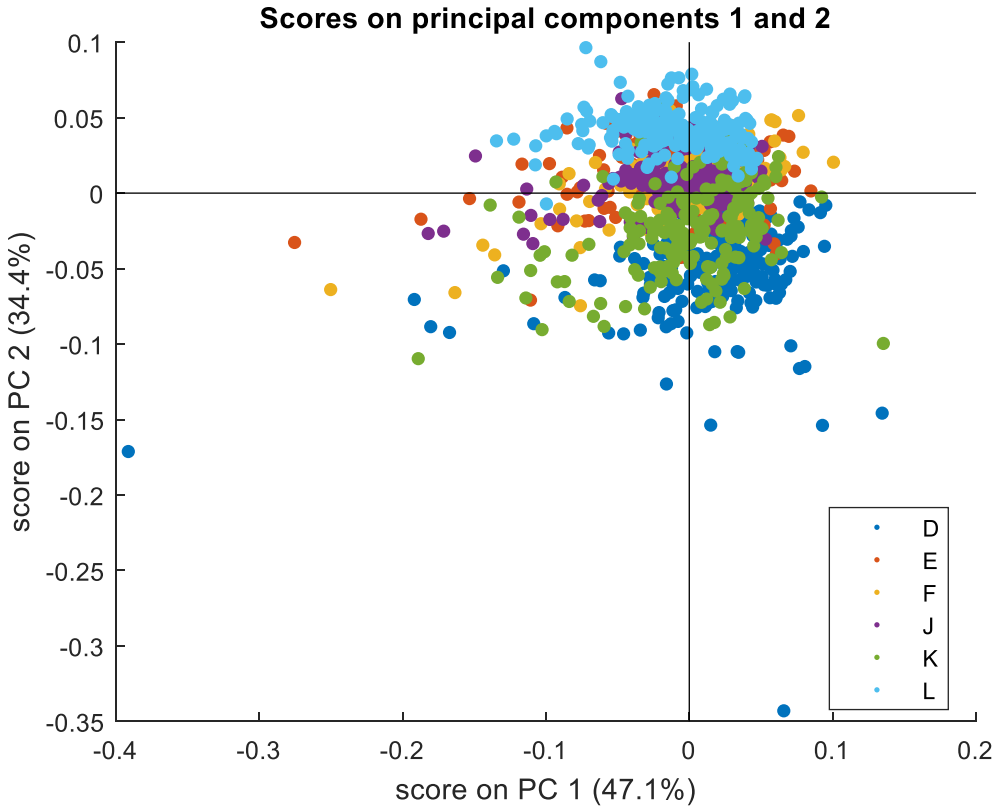
Scores on principal components 1 and 2
score on PC 2 (34.4%)
score on PC 1 (47.1%)
0.1
0.05
0
-0.05
-0.1
-0.15
-0.2
-0.25
-0.3
-0.35
-0.4
-0.3
-0.2
-0.1
0
0.1
0.2
D
E
F
J
K
L

(c)

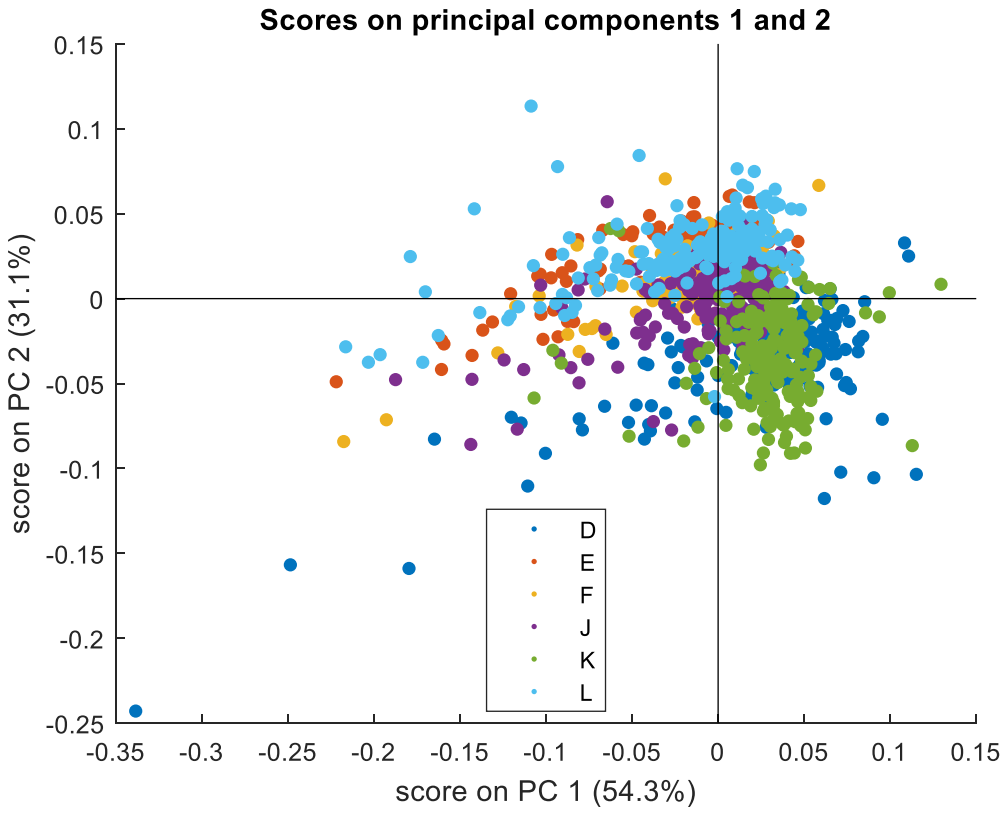
Scores on principal components 1 and 2
score on PC 2 (31.1%)
score on PC 1 (54.3%)
0.15
0.1
0.05
0
-0.05
-0.1
-0.15
-0.2
-0.25
-0.35
-0.3
-0.25
-0.2
-0.15
-0.1
-0.05
0
0.05
0.1
0.15
D
E
F
J
K
L

(d)

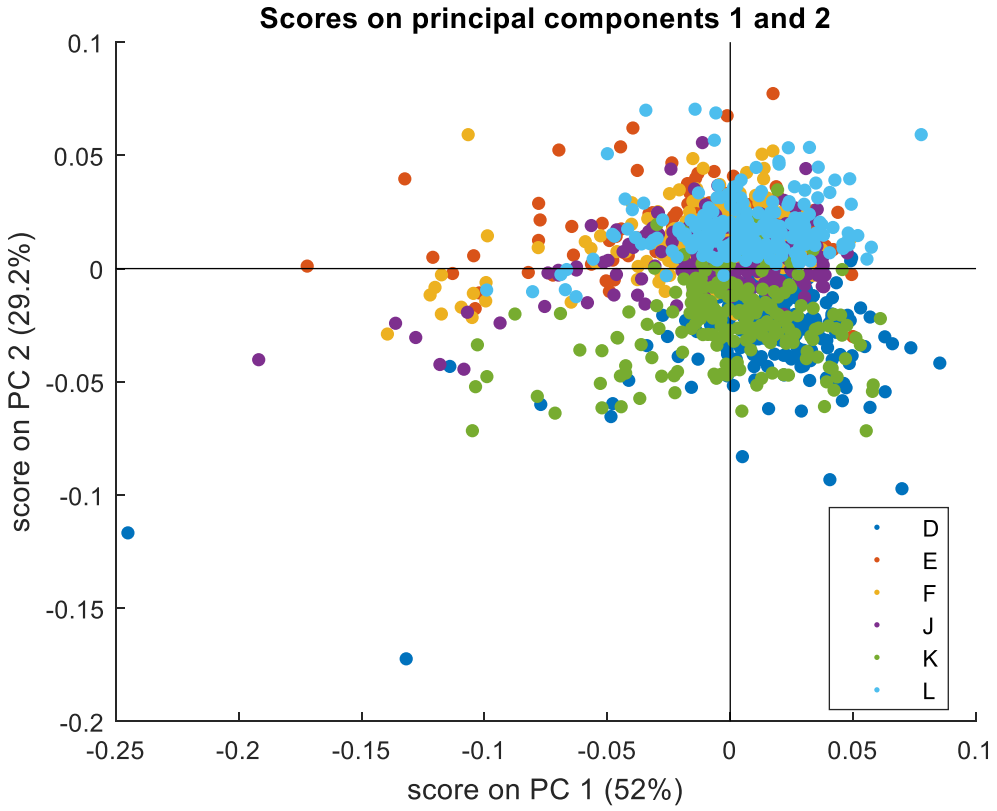

Figure7. 11 (a) The score plots of PC1 and PC2 of stroma on 6 glass slides for P1(BPH). (b) The score plots of PC1 and PC2 of stroma on 6 glass slides for P2(BPH). (c) The score plots of PC1 and PC2 of stroma on 6 glass slides for P3(CaP). (d) The score plots of PC1 and PC2 of stroma on 6 glass slides for P4(CaP).

7.2.4.3 The PCA of cancer & non-cancer patients

Figure 7.12 is the mean spectra of cancer and non-cancer group on glass D. Because of the similar figures on the other glass slide, the spectral comparison of two groups on glass D is an example.

(a)

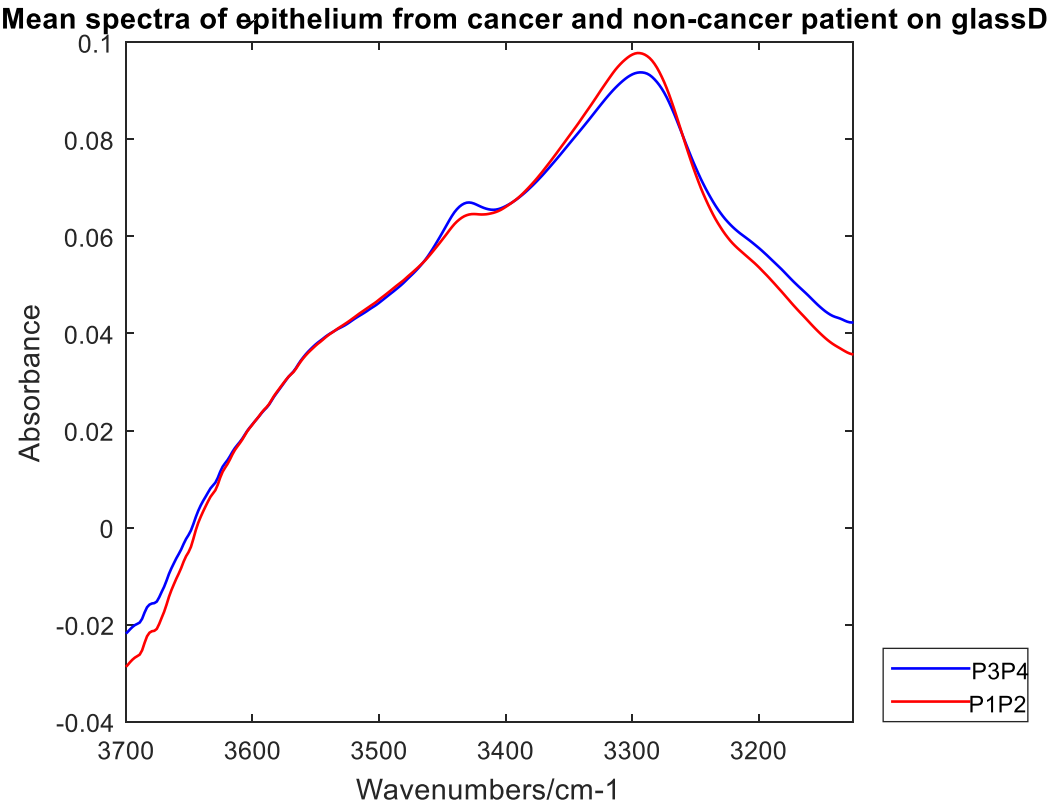
Mean spectra of epithelium from cancer and non-cancer patient on glassD
Absorbance
0.1
0.08
0.06
0.04
0.02
0
-0.02
-0.04
3700
3600
3500
3400
3300
3200
Wavenumbers/cm-1
P3P4
P1P2

(b)

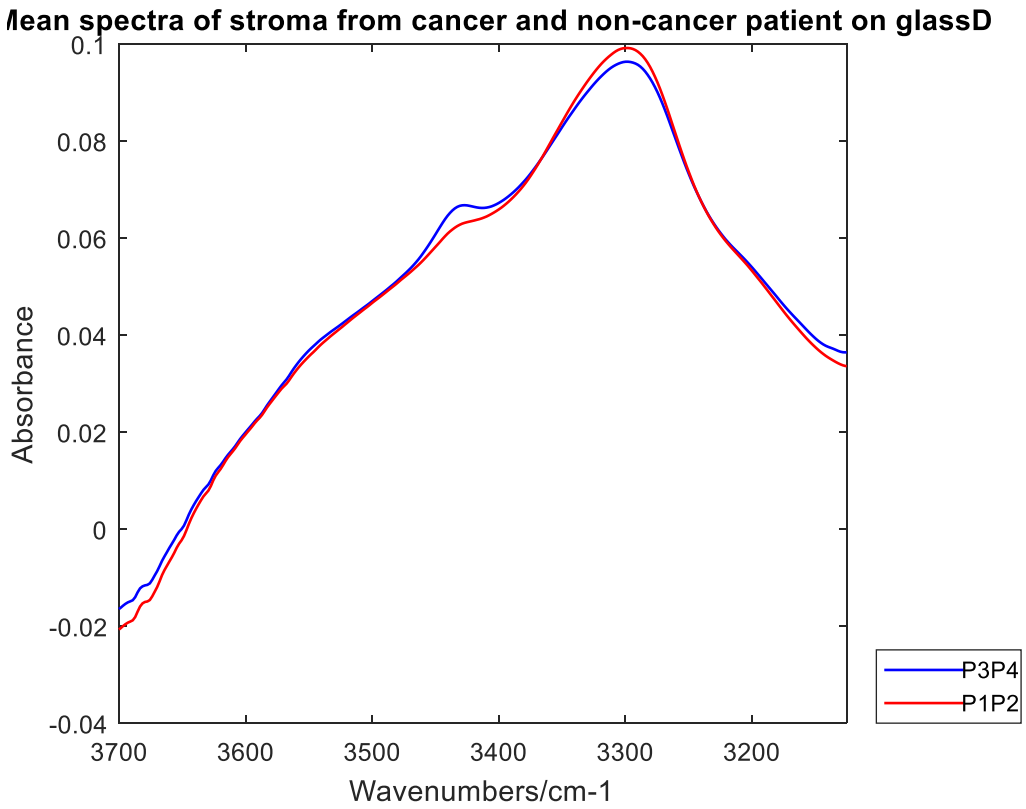
Mean spectra of stroma from cancer and non-cancer patient on glassD
Absorbance
0.1
0.08
0.06
0.04
0.02
0
-0.02
-0.04
3700
3600
3500
3400
3300
3200
Wavenumbers/cm-1
P3P4
P1P2

Figure7. 12 (a) the mean spectra of epithelium for cancer &non-cancer group on glass D. (b) the mean spectra of stroma for cancer &non-cancer group on glass D

According to figure 7.12, the intensity of amide A for the non-cancer group is higher than the cancer group for both spectra of epithelium and stroma. While for the peak in 3400-3450 cm^{-1}, the intensity for the cancer group is higher than the non-cancer group.

(a)

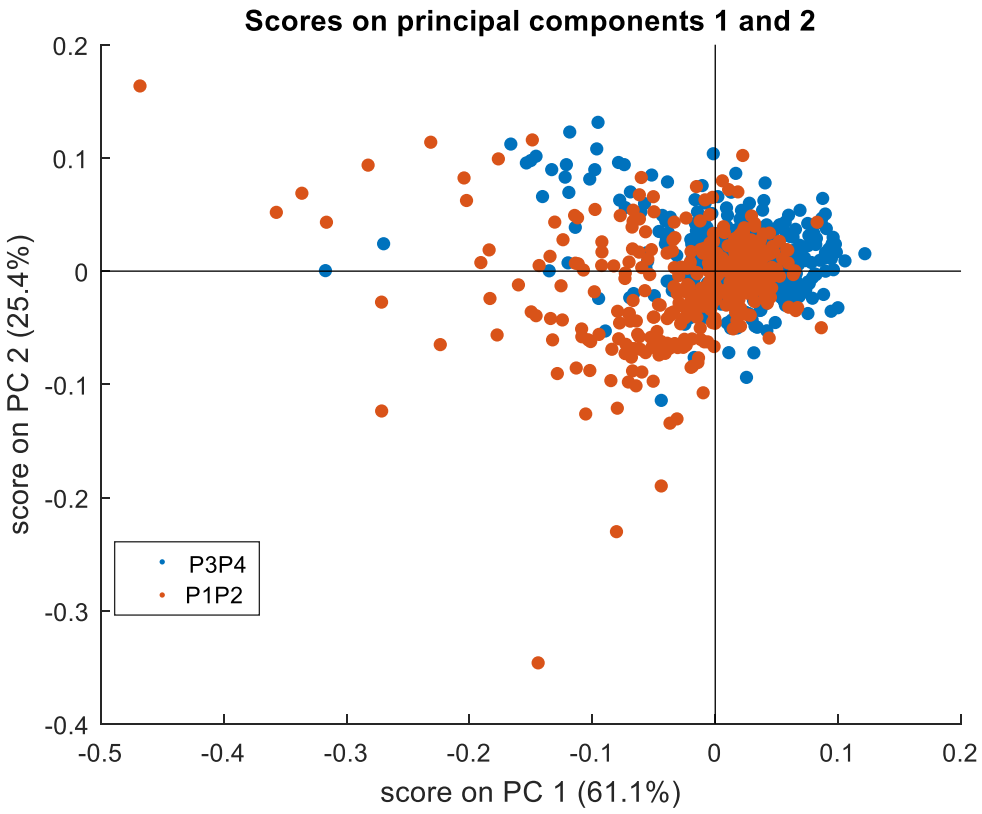

(b)

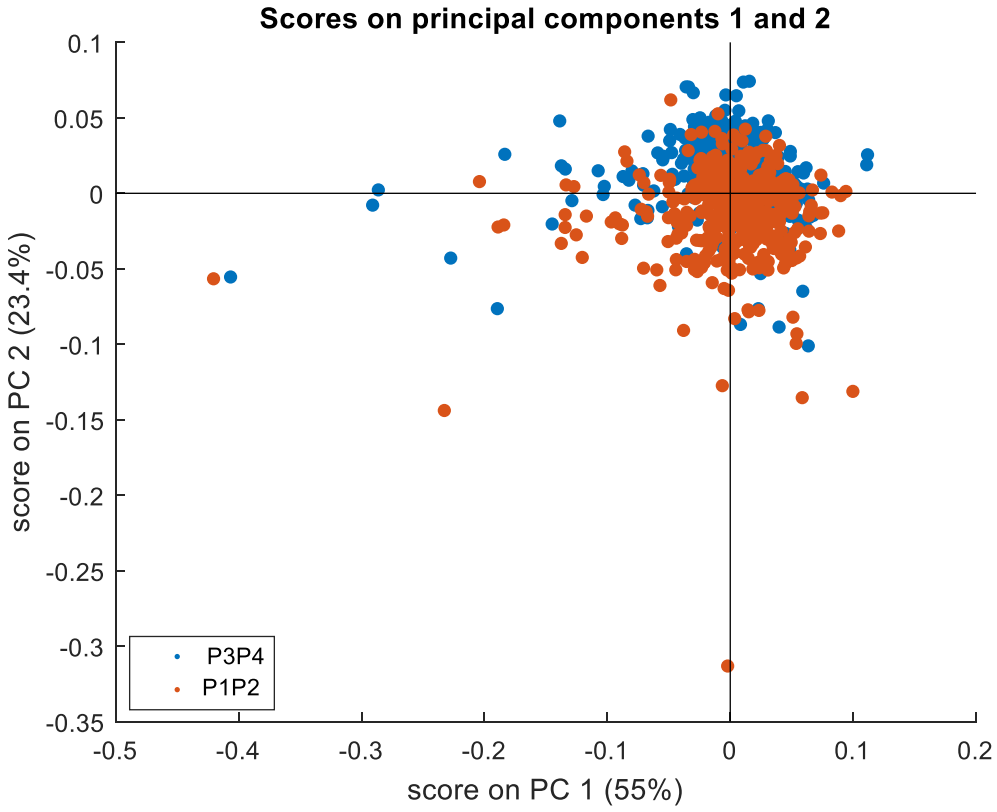

Figure7. 13 (a) The score plots of PC1 and PC2 of epithelium on glass D for cancer and non-cancer patients. (b) The score plots of PC1 and PC2 of stroma on glass D for cancer and non-cancer patients.

Figure 7.13 is the PCA plot of cancer and non-cancer spectra. There is no clear separation between the cancer and non-cancer groups for both spectra of epithelium and stroma on glass D.

7.2.4.5 Cancer detection by random forest on the same glass slide

PCA cannot separate cancer and non-cancer spectra on the same glass slide. It is essential to apply to the random forest. All of the spectra of cancer and non-cancer on the same glass slides are divided into two data sets. 80% of spectral data are used to train the classifier, and the rest 20% of spectral data are used to test the classifier. The accuracy of histological classification is applied to evaluate the classifier.

Table7. 15 Accuracy of cancer detection between cancer and non-cancer group on the same glass slide.

Model test (%)	epithelium	stroma
Glass D	98.80	98.61
Glass E	93.12	95.61
Glass F	99.13	99.36
Glass J	95.59	96.22
Glass K	92.29	92.41
Glass L	94.91	96.23

According to the accuracies in Table 7.15, all of the overall accuracies are above 0.920. It indicates the classifier has high accuracy in discriminating cancer and non-cancer groups on the same glass slides for both spectra of epithelium and stroma. However, the accuracy in experiment 2 is lower than in experiment 1. Therefore, more glue and coverslip maybe have a specific effect on cancer detection.

7.2.4.6 Cancer detection by random forest on the different glass slide

The main objective of the project is to look at the influence of glass type on cancer detection. Therefore, spectral data from one glass slide are used to train the classifier to distinguish between cancer and non-cancer patients. And the spectra from the other glass slide are used to test the classifier. If the classifier could achieve cancer detection on the different glass slides, it would indicate that the type of glass has no effect on cancer detection. If not, the type of glass affects cancer detection. The classification of cancer and non-cancer groups on different types of glass slides by spectra of epithelium and stroma are shown in table 7.16 and table 7.17, respectively. The accuracy, which is more than 80% is highlighted in yellow. The cancer detection results on different glass slides are changeable. Some classifiers have very bad classification between some glass slides. Compared with experiment 1, there are fewer good classification results in experiment 2.

Table7. 16 The accuracy of cancer detection by epithelium spectra on a different glass slide

Accuracy (%)	Test on glass D	Test on glass E	Test on glass F	Test on glass J	Test on glass K	Test on glass L
Train on glass D		65.43	94.10	43.20	60.04	36.87
Train on glass E	62.4		92.83	83.34	65.54	69.94
Train on glass F	76.73	77.09		70.95	62.27	35.53
Train on glass J	59.96	82.69	80.97		81.77	80.90
Train on glass K	61.63	64.61	75.69	87.26		64.77
Train on glass L	33.56	65.43	37.08	83.51	69.35	

Table7. 17 The accuracy of cancer detection by stroma spectra on a different glass slide

Accuracy (%)	Test on glass D	Test on glass E	Test on glass F	Test on glass J	Test on glass K	Test on glass L
Train on glass D		86.71	93.34	57.60	71.10	55.26
Train on glass E	66.77		92.14	81.95	59.61	65.29
Train on glass F	75.44	81.50		68.52	53.18	32.09
Train on glass J	66.54	89.31	77.03		83.73	72.37
Train on glass K	78.39	74.62	75.71	84.23		57.35
Train on glass L	35.78	62.69	50.79	64.10	64.49	

7.2.5 Cancer detection with glue removal

A previous study has shown that glue greatly affects all of the spectra in experiment 2. Therefore, glue removal is an essential process for experiment 2. Even for experiment 1, the background is a clear tissue-free area. Because the glue content on the background and sample scan is variable, the spectra information maybe plus or minus a small amount of glue. This is shown in the mean spectra of epithelium & stroma on the 6 glass slides (figure 7.4): some of the mean spectra have positive peaks and some of them have negative peaks in the range 3400-3450 cm^{-1}. Therefore, it is necessary to correct or remove glue from the spectra.

The glue removal in this project is based on the data processing by Matlab, and it is based on the principle of spectral subtraction. The specific process of glue removal has been discussed in chapter 5. The critical function of the glue removal code is the least-squares with known covariance (LSCOV). The corresponding coefficients can be calculated based on the LSCOV function and every small fit range. And the final coefficient is the mean coefficient of all fitness ranges.

The results of chapter 5 are that the reference spectra of glue removal is Matrigel, glue, and coverslip spectra, and the most suitable fit range for glue removal is range 1 (3278-3318 cm^{-1}, 3066-3106 cm^{-1}), range 3 (2950-2970 cm^{-1}, 2925-2945 cm^{-1}, 2867-2887cm^{-1}), and range 4 (3536-3576cm^{-1}, 2704-2744cm^{-1}). Figure 5.2 shows the reference spectra.

The glue effect on the spectra in this chapter is presented in 3400-3450 cm^{-1} for both two experimental results. For experiment 2, there is only a positive peak in this range. While for the spectra in experiment 1, there are both positive and negative peaks in this range. The comparison of spectral information under different situations is shown in table 7.18. According to table 7.18, the purpose of glue correction for a negative peak is to add some glue, while for a positive peak is to remove some glue. In addition, the broad band (3400-3600 cm^{-1}) for experiment 2 is also caused by coverslip.

Table7. 18 The spectral information in 3400-3450 cm^{-1} at different situations

Experiment	**3400 – 3450 cm^{-1}**	**Background Scan**	**Sample scan**	**Spectral information**
Experiment 1	Negative peak	More glue + coverslip + glass	Sample + coverslip + glass + less glue	Sample - some glue
	Positive peak	Less Glue + coverslip + glass	Sample + coverslip + glass + more glue	Sample + some glue
Experiment 2	Positive peak	Glass	Sample + coverslip + glass + more glue	Sample + glue +coverslip

Figure 7.14 shows the results of glue removal in experiment 1. Figure 7.14 (a) shows that the intensity of amide A is higher after glue removal because the effect of some glue is added. The intensity of amide A in figure 7.14 (b) is lower after glue removal because of glue removal. Figure 7.15 shows the results of glue removal in experiment 2. Therefore, the code of glue removal works in two experiments.

(a)

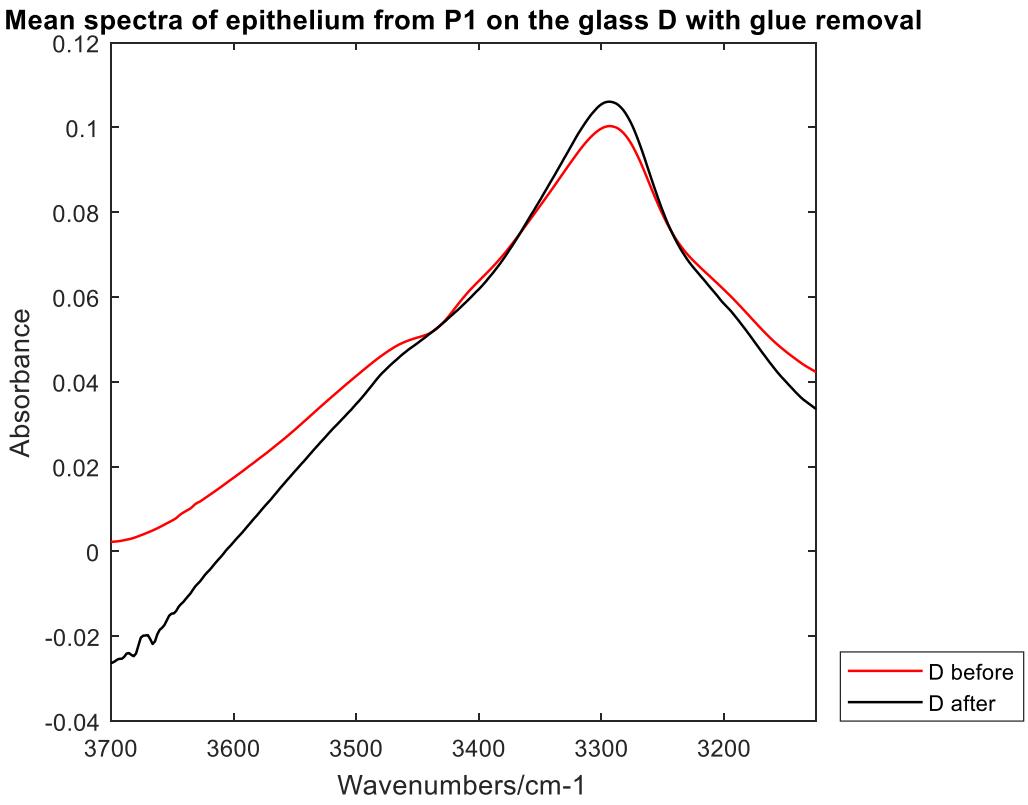

(b)

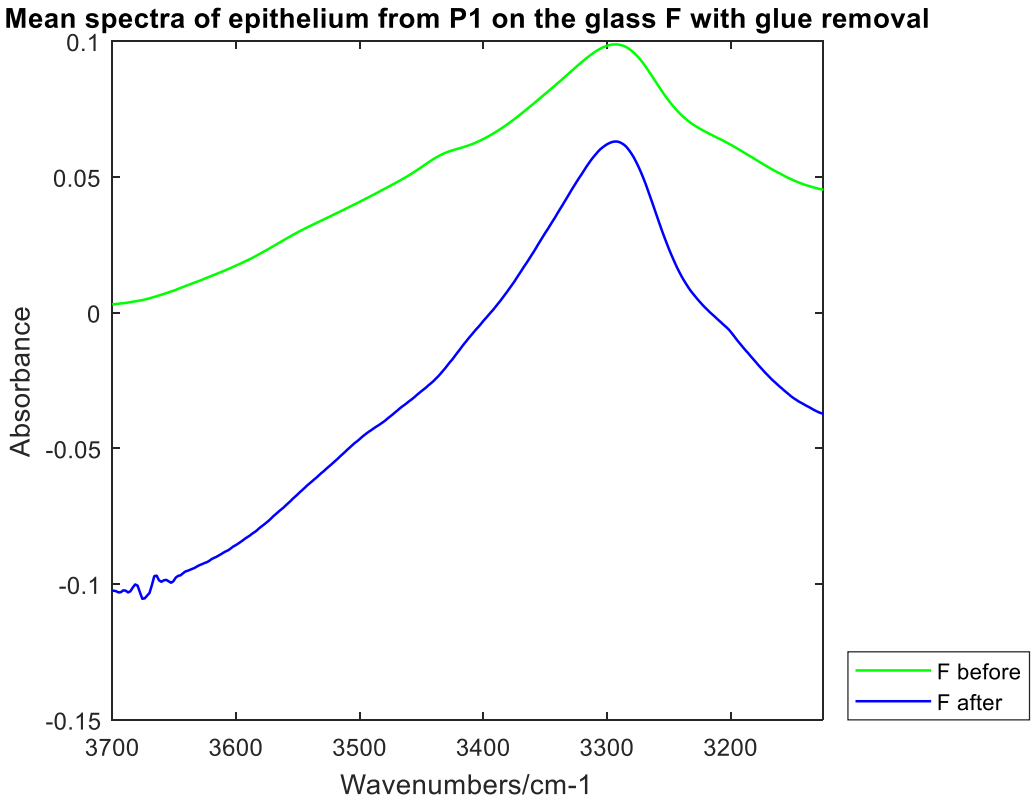

Figure7. 14 (a) Mean spectra of epithelium from P1 on the glass D with glue removal. (b) Mean spectra of epithelium from P1 on the glass F with glue removal.

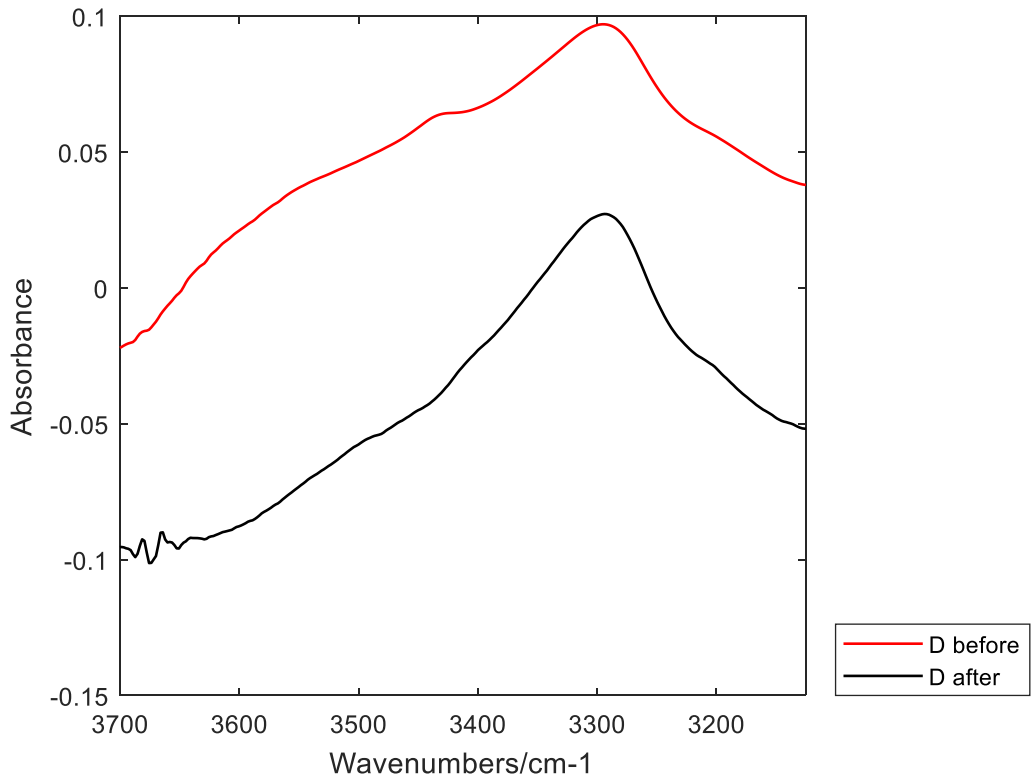

Figure7. 15 Mean spectra of epithelium from P1 on the glass D with glue removal.

7.2.5.1 Mean spectra with glue removal

Figure 7.16 shows all mean spectra of epithelium and stroma after removing glue on the 6 glass slides from 4 patients in experiment 1. Glue has an influence on the peak in 3400-3450 cm^{-1}. There is no pronounced peak in 3400-3450 cm^{-1} after glue removal. It indicates that the glue removal code has already worked on all spectra. Comparing the spectra on epithelium and stroma on 6 glass slides from the same patient, the intensity of amide A of stroma spectra is always slightly higher than the epithelium spectra.

(a)

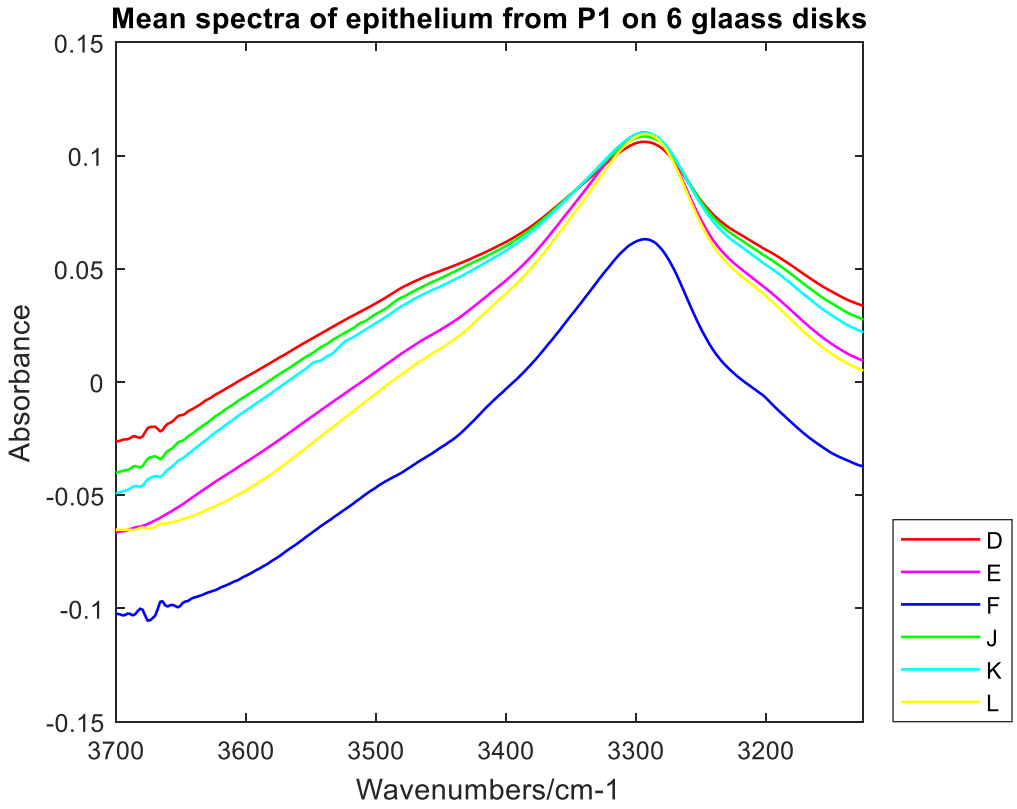
Mean spectra of epithelium from P1 on 6 glaass disks
Absorbance
0.15
0.1
0.05
0
-0.05
-0.1
-0.15
3700
3600
3500
3400
3300
3200
Wavenumbers/cm-1
D
E
F
J
K
L

(b)

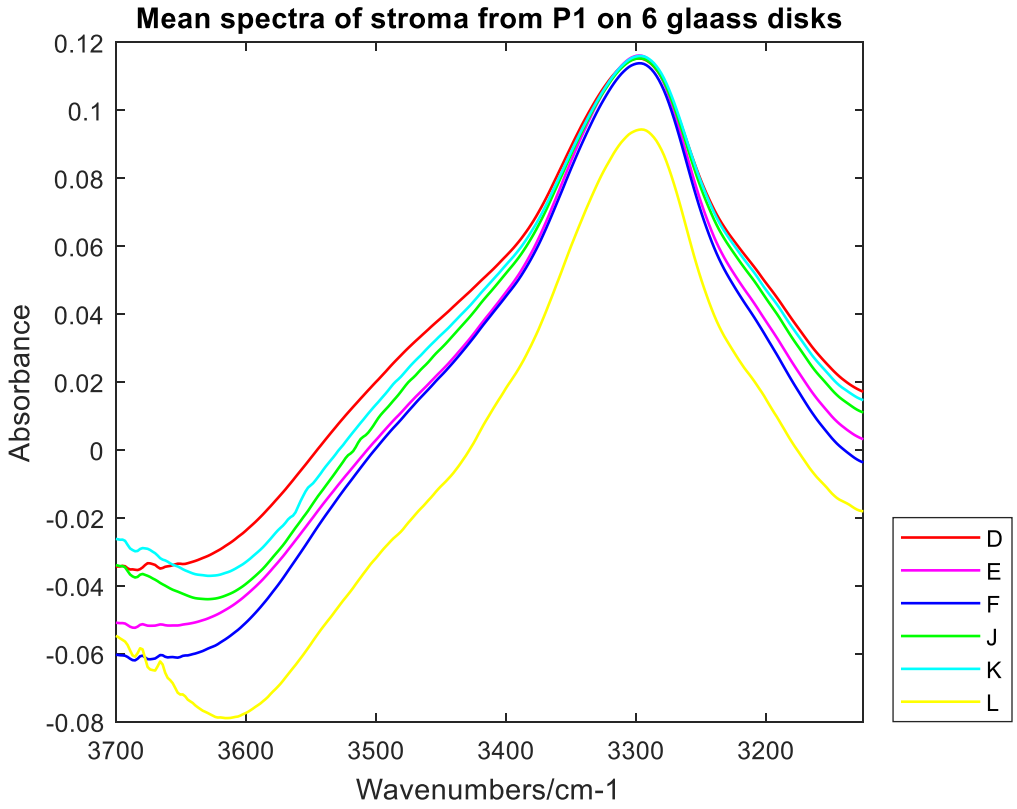
Mean spectra of stroma from P1 on 6 glaass disks
Absorbance
0.12
0.1
0.08
0.06
0.04
0.02
0
-0.02
-0.04
-0.06
-0.08
3700
3600
3500
3400
3300
3200
Wavenumbers/cm-1
D
E
F
J
K
L

(c)

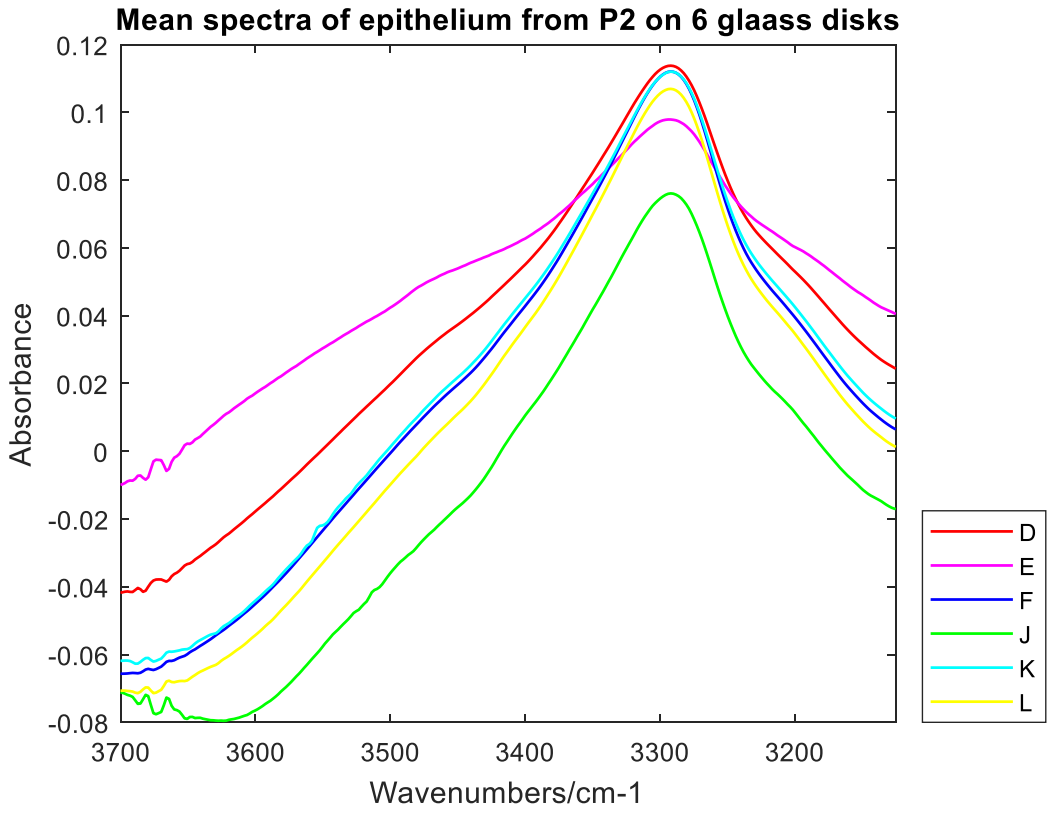
Mean spectra of epithelium from P2 on 6 glaass disks
Absorbance
0.12
0.1
0.08
0.06
0.04
0.02
0
-0.02
-0.04
-0.06
-0.08
3700
3600
3500
3400
3300
3200
Wavenumbers/cm-1
D
E
F
J
K
L

(d)

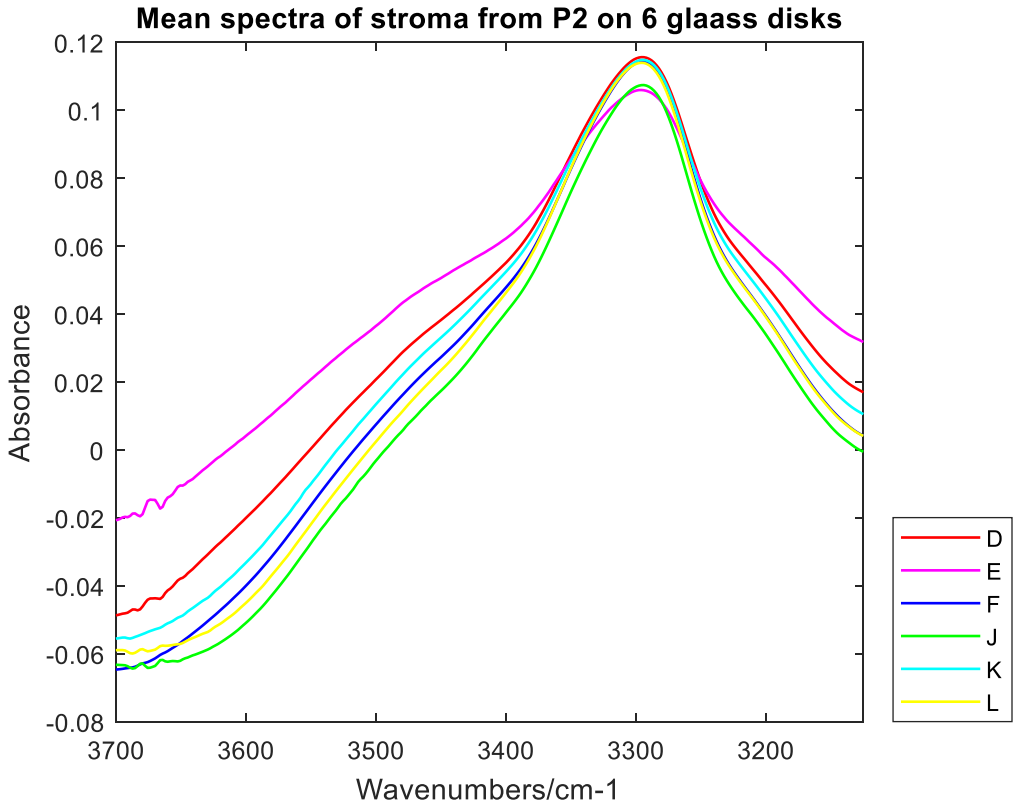
Mean spectra of stroma from P2 on 6 glaass disks
Absorbance
0.12
0.1
0.08
0.06
0.04
0.02
0
-0.02
-0.04
-0.06
-0.08
3700
3600
3500
3400
3300
3200
Wavenumbers/cm-1
D
E
F
J
K
L

(e)

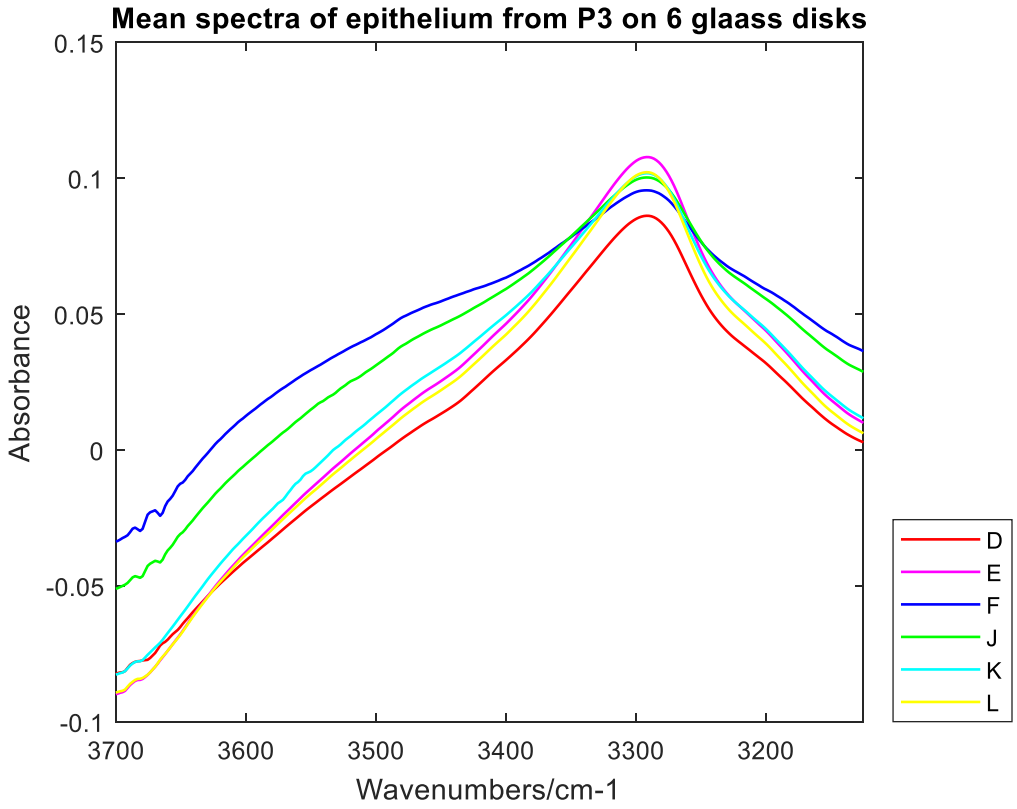
Mean spectra of epithelium from P3 on 6 glaass disks
Absorbance
0.15
0.1
0.05
0
-0.05
-0.1
3700
3600
3500
3400
3300
3200
Wavenumbers/cm-1
D
E
F
J
K
L

(f)

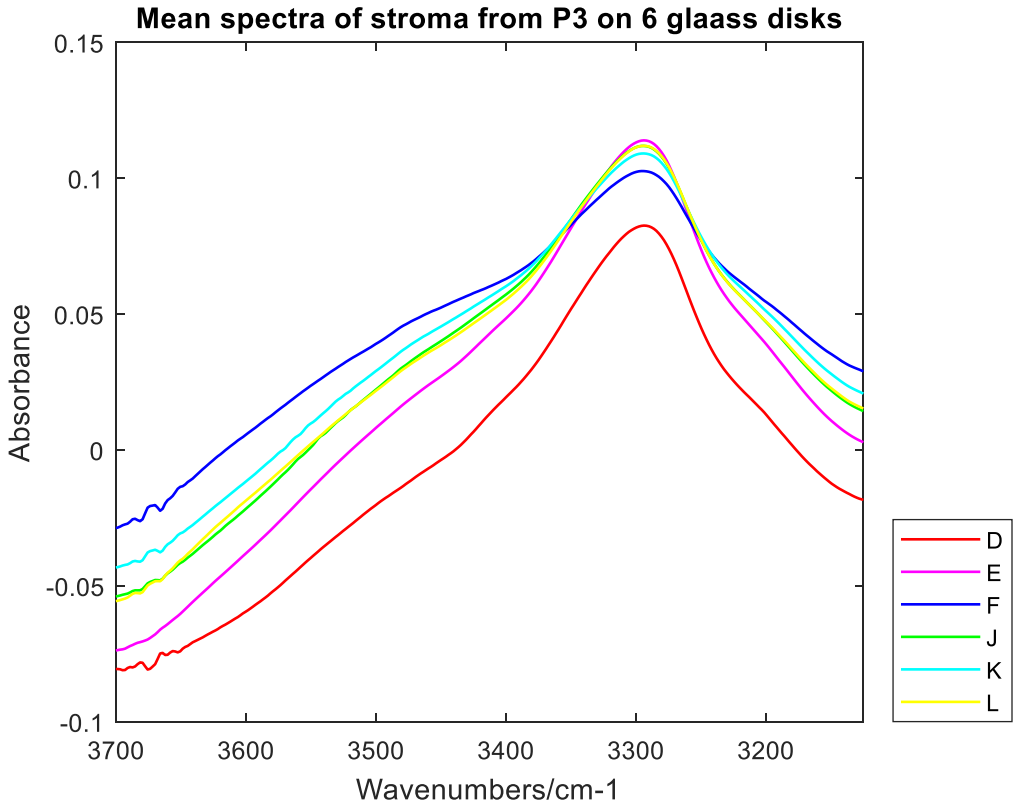
Mean spectra of stroma from P3 on 6 glaass disks
Absorbance
0.15
0.1
0.05
0
-0.05
-0.1
3700
3600
3500
3400
3300
3200
Wavenumbers/cm-1
D
E
F
J
K
L

(g)

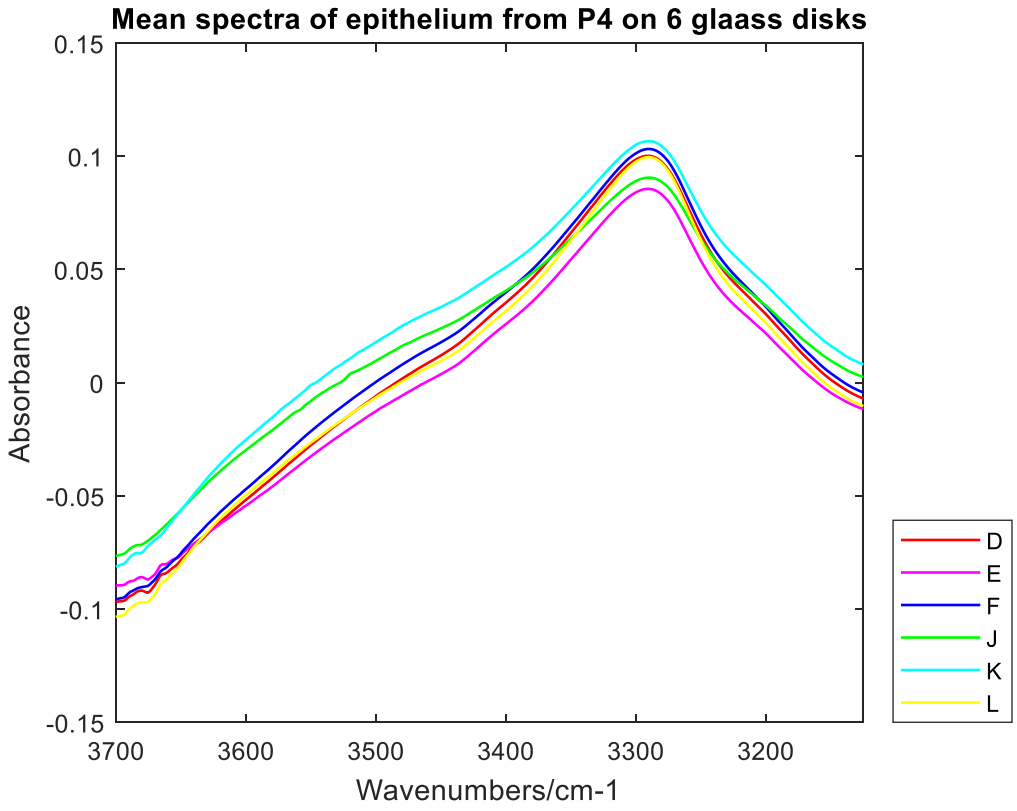
Mean spectra of epithelium from P4 on 6 glaass disks
Absorbance
0.15
0.1
0.05
0
-0.05
-0.1
-0.15
3700
3600
3500
3400
3300
3200
Wavenumbers/cm-1
D
E
F
J
K
L

(h)

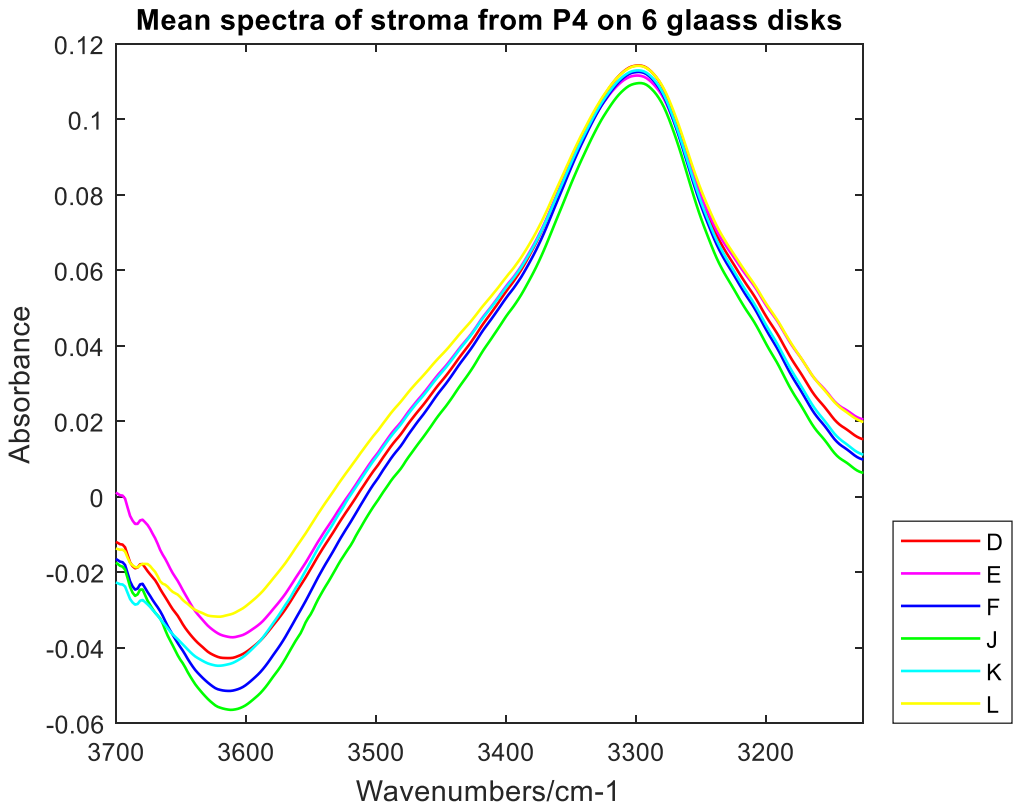
Mean spectra of stroma from P4 on 6 glaass disks
Absorbance
0.12
0.1
0.08
0.06
0.04
0.02
0
-0.02
-0.04
-0.06
3700
3600
3500
3400
3300
3200
Wavenumbers/cm-1
D
E
F
J
K
L

Figure7. 16 (a) (b) Mean spectra of epithelium & stroma on 6 glass slides for P1(BPH) after glue removal in experiment 1. (c) (d) Mean spectra of epithelium & stroma on 6 glass slides for P2(BPH) after glue removal in experiment 1. (e) (f) Mean spectra of epithelium & stroma on 6 glass slides for P3(CaP) after glue removal in experiment 1. (g) (h) Mean spectra of epithelium & stroma on 6 glass slides in for P4(CaP) after glue removal in experiment 1.

(a)

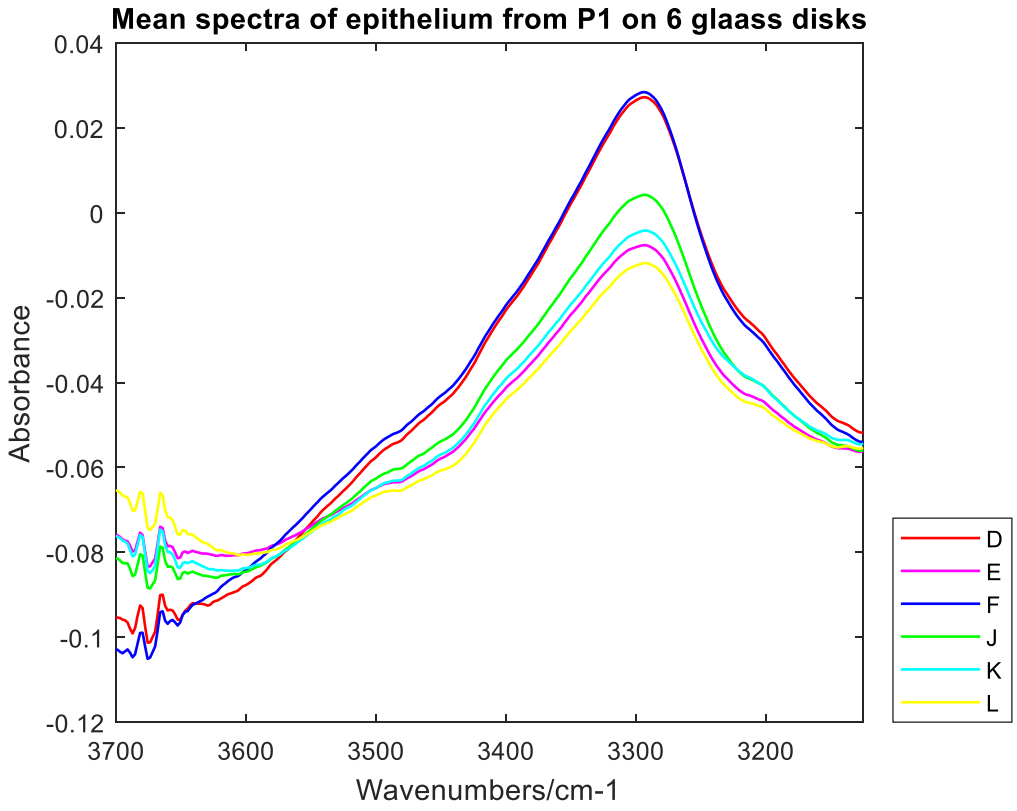

(b)

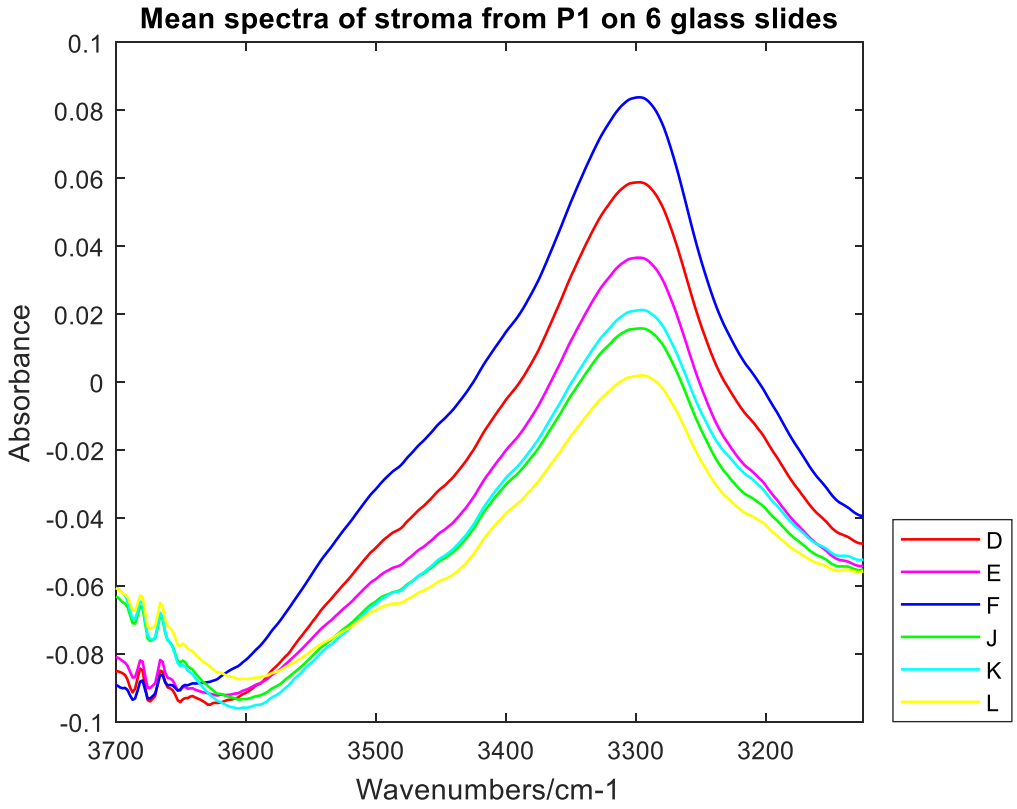
Mean spectra of stroma from P1 on 6 glass slides
Absorbance
0.1
0.08
0.06
0.04
0.02
0
-0.02
-0.04
-0.06
-0.08
-0.1
3700
3600
3500
3400
3300
3200
Wavenumbers/cm-1
D
E
F
J
K
L

(c)

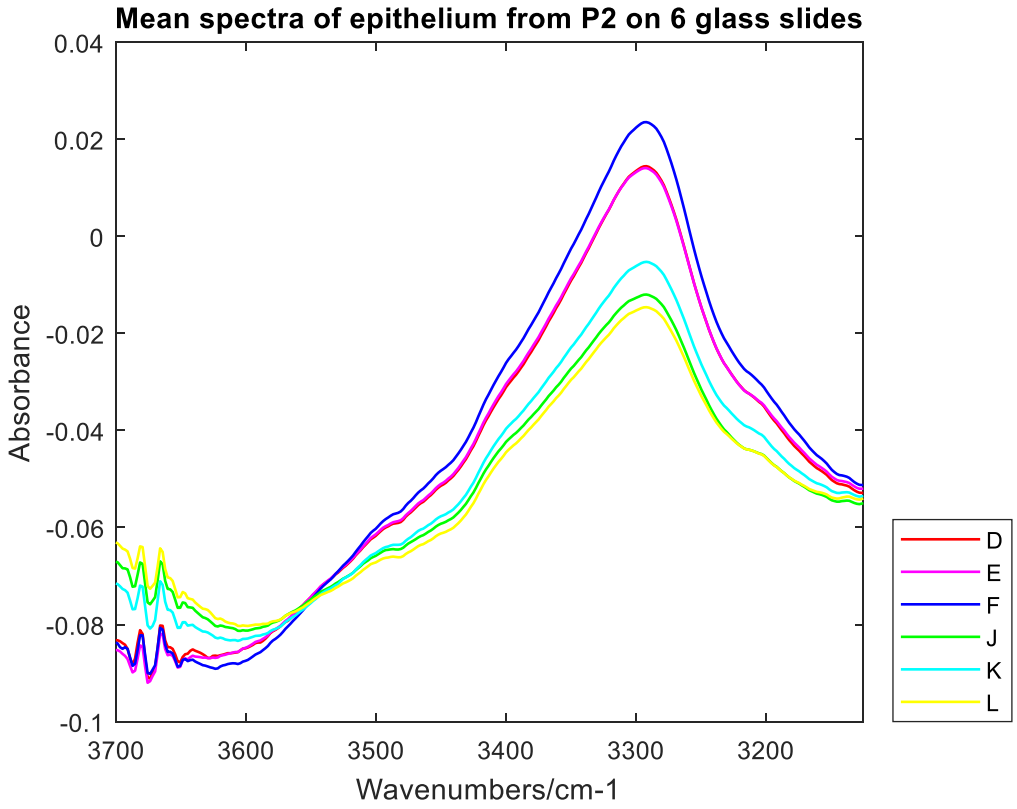
Mean spectra of epithelium from P2 on 6 glass slides
Absorbance
0.04
0.02
0
-0.02
-0.04
-0.06
-0.08
-0.1
3700
3600
3500
3400
3300
3200
Wavenumbers/cm-1
D
E
F
J
K
L

(d)

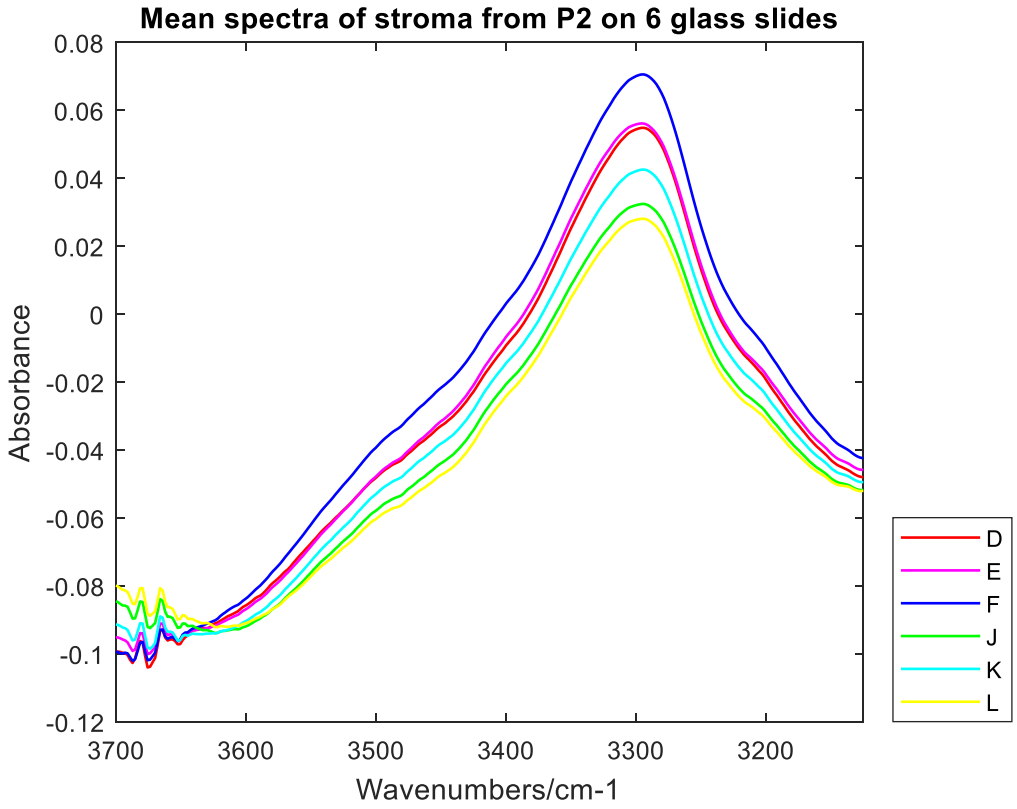
Mean spectra of stroma from P2 on 6 glass slides
Absorbance
0.08
0.06
0.04
0.02
0
-0.02
-0.04
-0.06
-0.08
-0.1
-0.12
3700
3600
3500
3400
3300
3200
Wavenumbers/cm-1
D
E
F
J
K
L

(e)

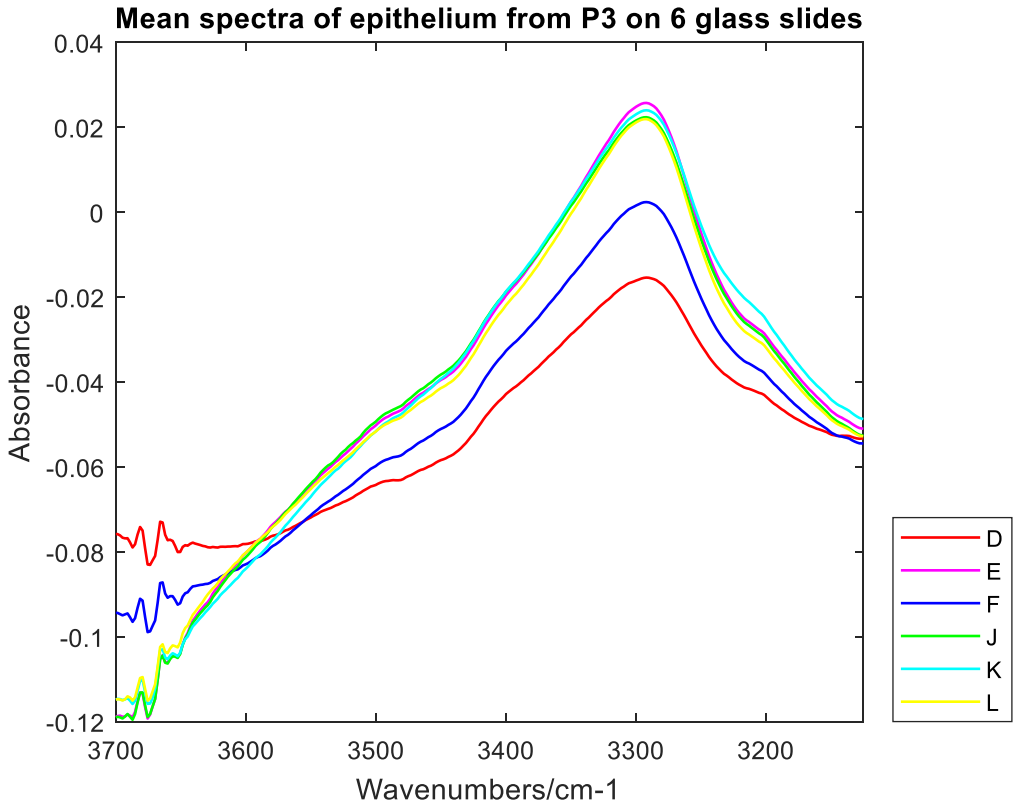
Mean spectra of epithelium from P3 on 6 glass slides
Absorbance
0.04
0.02
0
-0.02
-0.04
-0.06
-0.08
-0.1
-0.12
3700
3600
3500
3400
3300
3200
Wavenumbers/cm-1
D
E
F
J
K
L

(f)

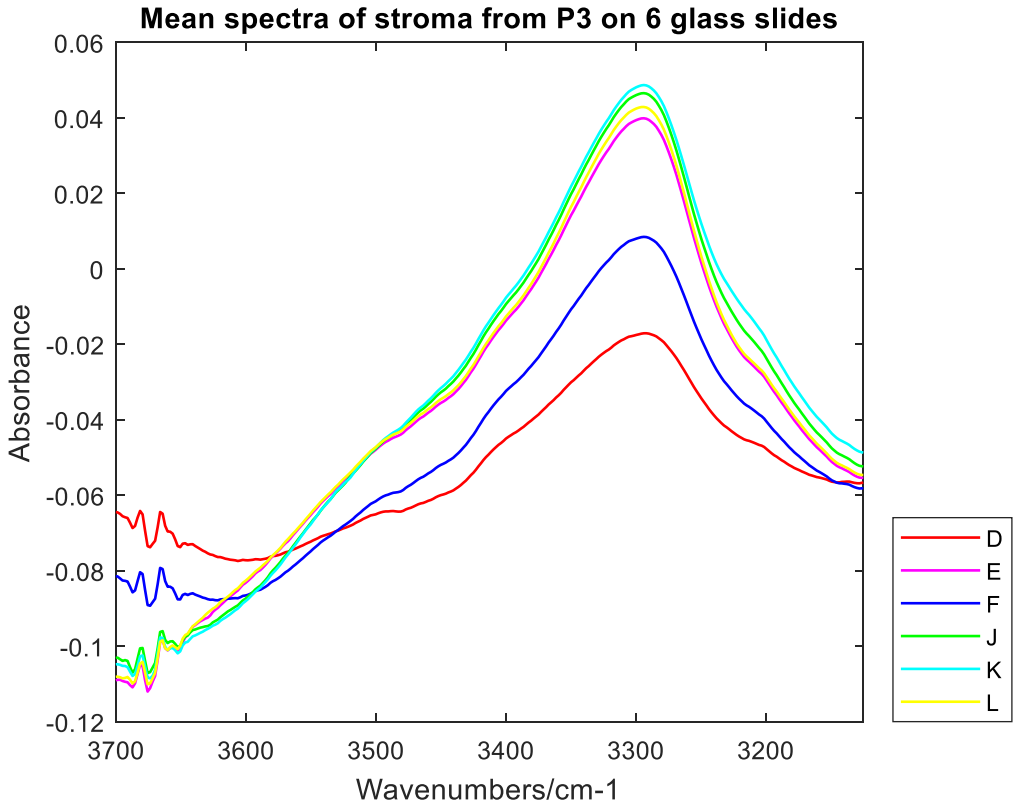
Mean spectra of stroma from P3 on 6 glass slides
Absorbance
0.06
0.04
0.02
0
-0.02
-0.04
-0.06
-0.08
-0.1
-0.12
3700
3600
3500
3400
3300
3200
Wavenumbers/cm-1
D
E
F
J
K
L

(g)

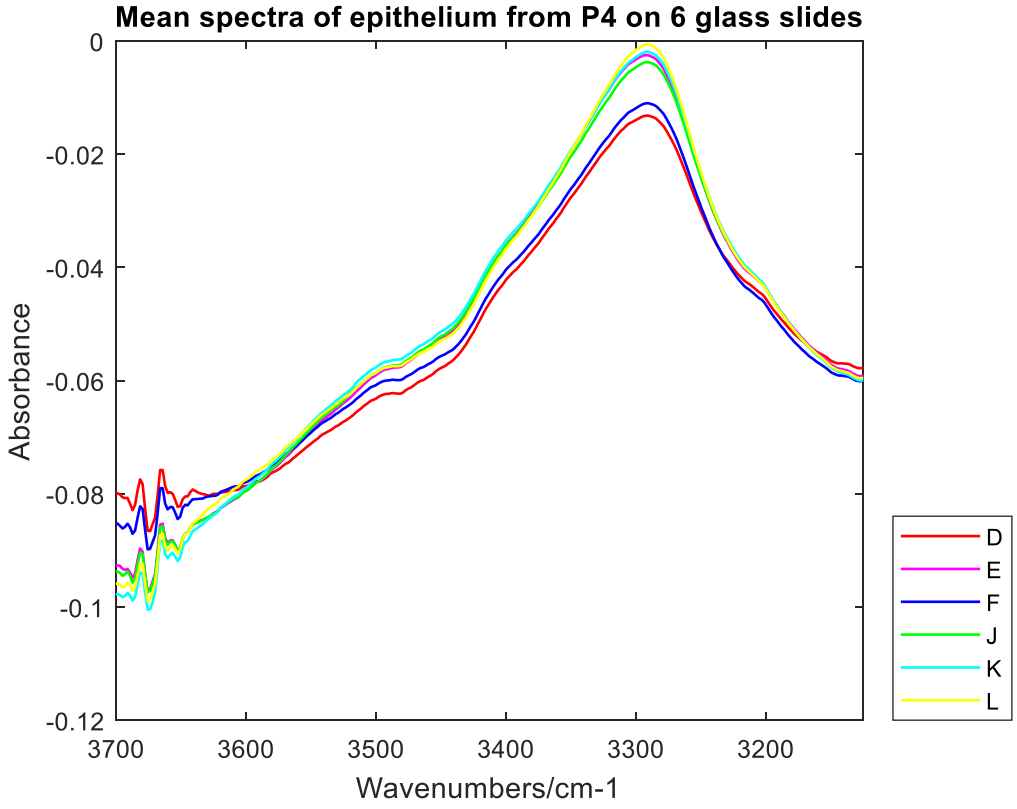
Mean spectra of epithelium from P4 on 6 glass slides
Absorbance
0
-0.02
-0.04
-0.06
-0.08
-0.1
-0.12
3700
3600
3500
3400
3300
3200
Wavenumbers/cm-1
D
E
F
J
K
L

(h)

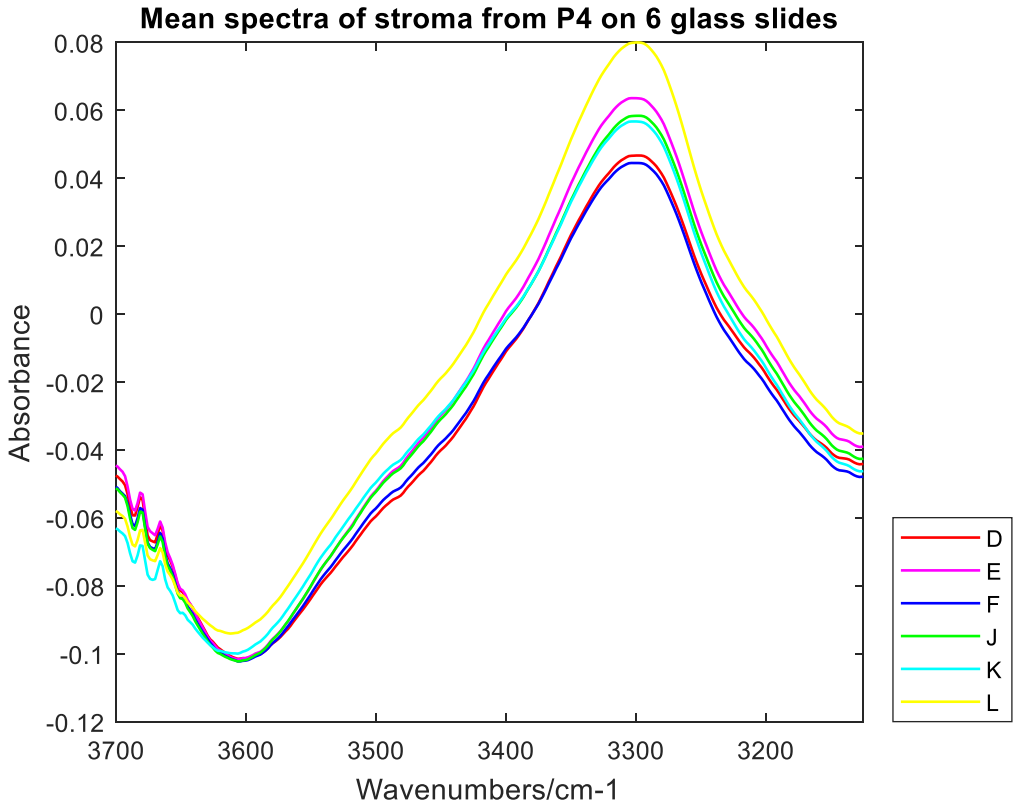

Figure7. 17 (a) (b) Mean spectra of epithelium & stroma on 6 glass slides for P1(BPH) after glue removal in experiment 2. (c) (d) Mean spectra of epithelium & stroma on 6 glass slides for P2(BPH) after glue removal in experiment 2. (e) (f) Mean spectra of epithelium & stroma on 6 glass slides for P3(CaP) after glue removal in experiment 2. (g) (h) Mean spectra of epithelium & stroma on 6 glass slides in for P4(CaP) after glue removal in experiment 2.

The mean spectra of epithelium and stroma from 4 patients with glue removal in experiment 2 are shown in figure 7.17. The apparent peak in 3400-3450 cm^{-1} have mainly been removed. However, the peaks in some of the epithelium spectra are not completely smoothed out and appear a little negative in some cases. Therefore there is a need to improve and optimise the parameters in further study. In addition, there is no broad peak in 3400-3600 cm^{-1} region indicating that the glue removal code has worked. Similar to the result in experiment 1, the intensity of amide A band of stroma is higher than that for epithelium.

7.2.5.2 The PCA of cancer & non-cancer patients with glue removal

Figure 7.18 and figure 7.19 show the comparison of mean spectra of cancer and non-cancer groups on glass D in experiments 1 and 2, respectively. For glue removal of both experiments, the intensity of the amide A band for the non-cancer group is always higher than cancer group and the peak intensity of stroma is higher than the epithelium.

(a)

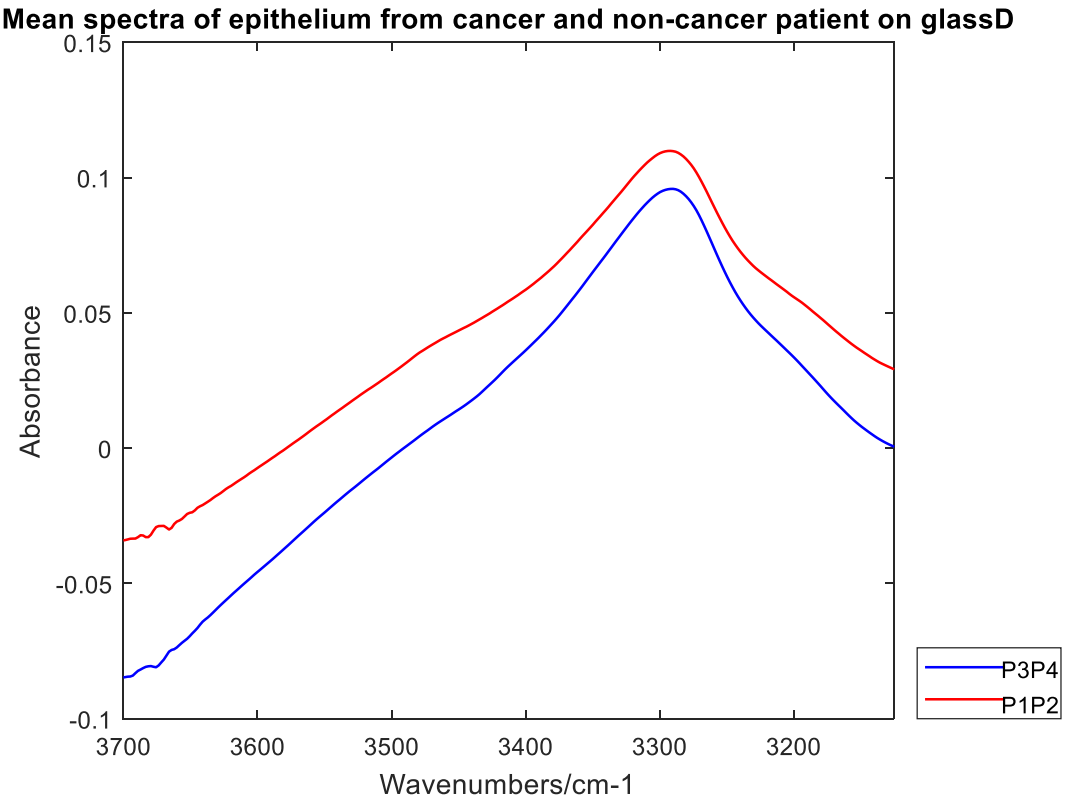

(b)

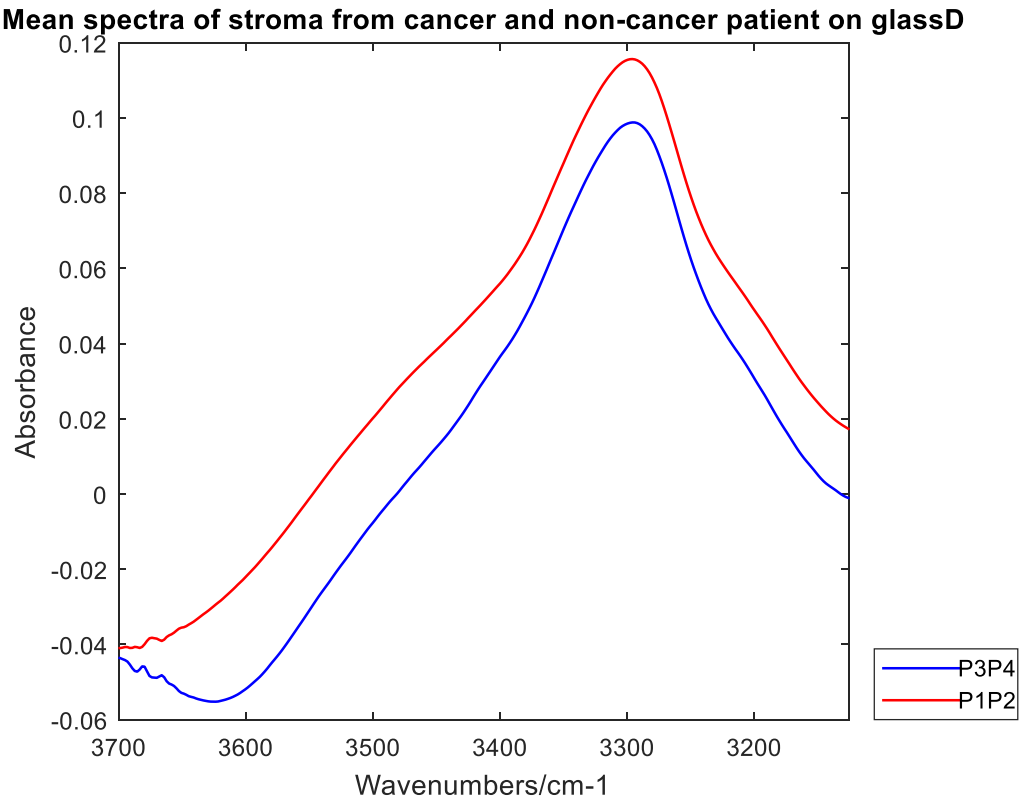

Figure7. 18 (a) the mean spectra of epithelium for cancer &non-cancer group on glass D with glue removal in experiment 1. (b) the mean spectra of stroma for cancer &non-cancer group on glass D with glue removal in experiment 1.

(a)

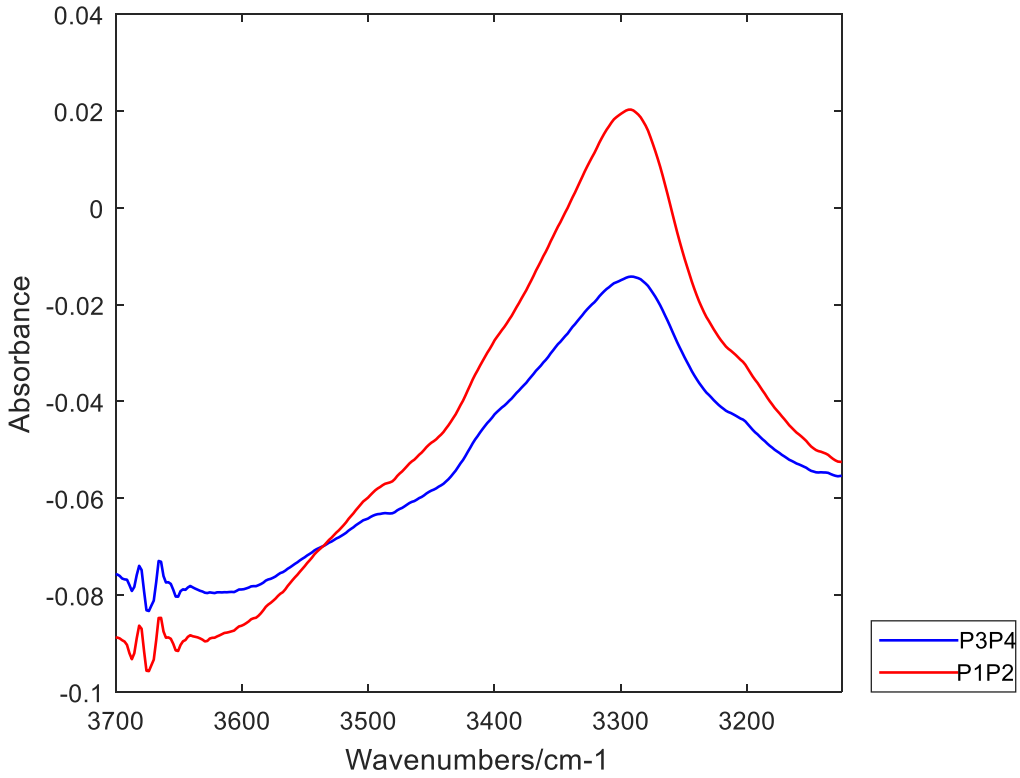

(b)

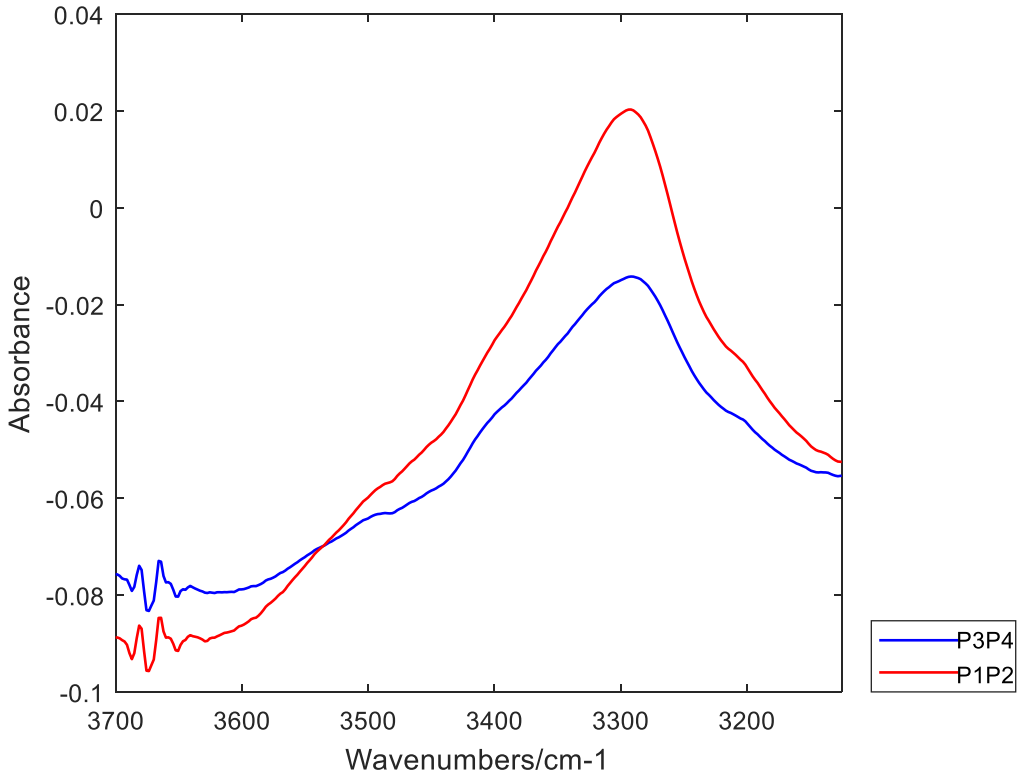

Figure7. 19 (a) the mean spectra of epithelium for cancer &non-cancer group on glass D with glue

removal in experiment 2. (b) the mean spectra of stroma for cancer &non-cancer group on glass D with glue removal in experiment 2.

Figures 7.20 and 7.21 show the PCA results of cancer and non-cancer group classification in experiments 1 and 2. Figure 7.20 indicates that the separation of cancer and non-cancer group is unclear. But the two groups still have a trend of separation and it depends on the PC1. The loading of PC1 has a positive feature which is located at around 3450 cm^{-1}. The positive peak is related to O-H stretching. Therefore, the distribution of spectra in PCA is correlated with the intensity at 3450 cm^{-1}. Because the cancer group is located in the negative area on PC1, the intensity of epithelium spectra at 3450 cm^{-1} for the cancer group is lower than the non-cancer group.

(a)

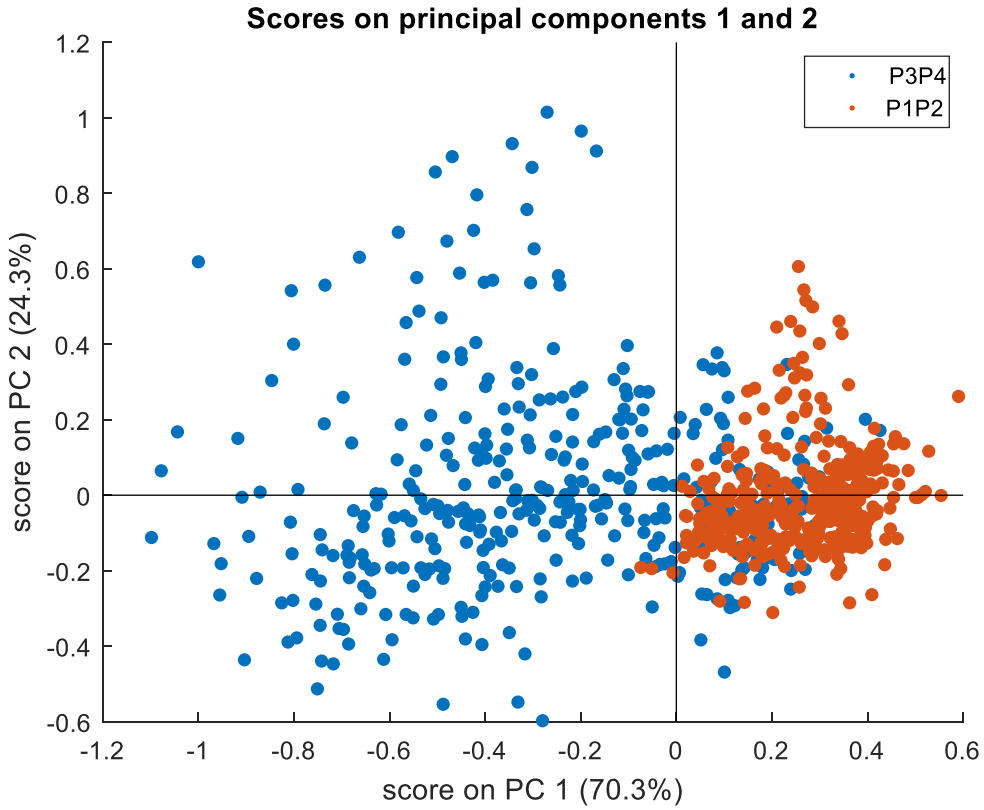
Scores on principal components 1 and 2
P3P4
P1P2
score on PC 2 (24.3%)
score on PC 1 (70.3%)
1.2
1
0.8
0.6
0.4
0.2
0
-0.2
-0.4
-0.6
-1.2
-1
-0.8
-0.6
-0.4
-0.2
0
0.2
0.4
0.6

(b)

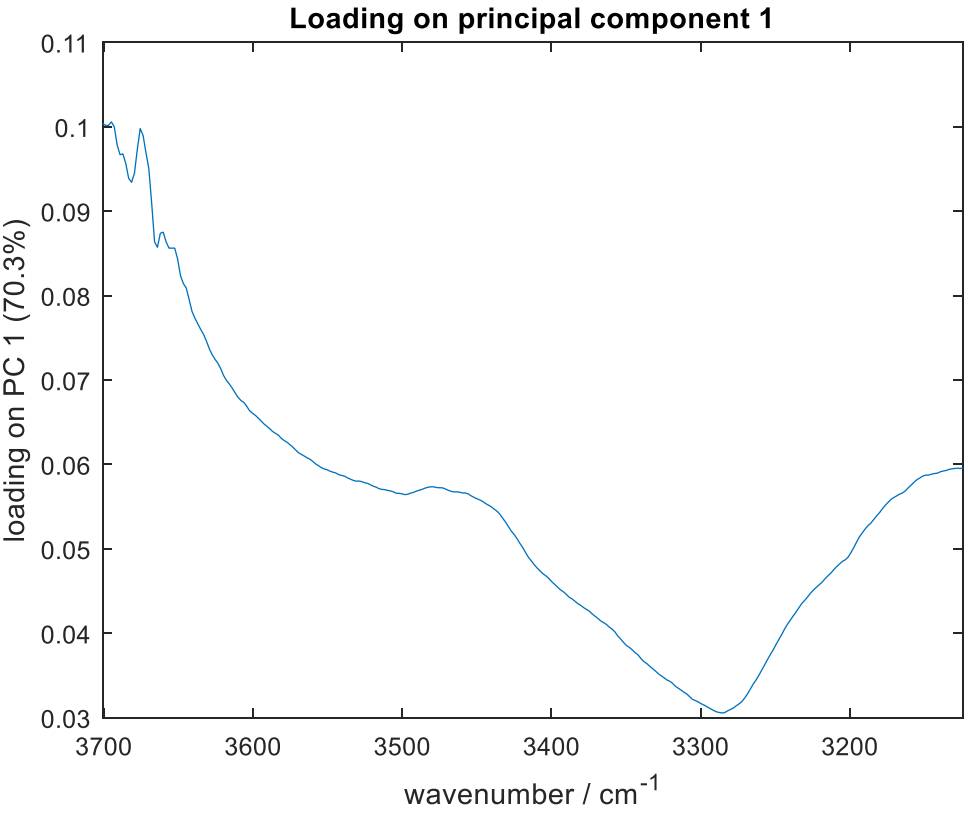
Loading on principal component 1
loading on PC 1 (70.3%)
wavenumber / cm-1
0.11
0.1
0.09
0.08
0.07
0.06
0.05
0.04
0.03
3700
3600
3500
3400
3300
3200

Figure7. 20 (a) The score plots of PC1 and PC2 of epithelium on glass D for cancer and non-cancer patients in experiment 1. (b) The PC1 loading for PCA of epithelium spectra on glass D for cancer and non-cancer patients in experiment 1.

According to figure 7.21, the separation of cancer and the non-cancer group with glue removal in experiment 2 is a little clearer, and it mainly depends on PC1 for separation. The loading of PC1 is shown in figures 7.21 (b). PC1 mostly has a positive peak, which is located at 3298 cm^{-1}. It means cancer and non-cancer group are separated based on amide A.

(a)

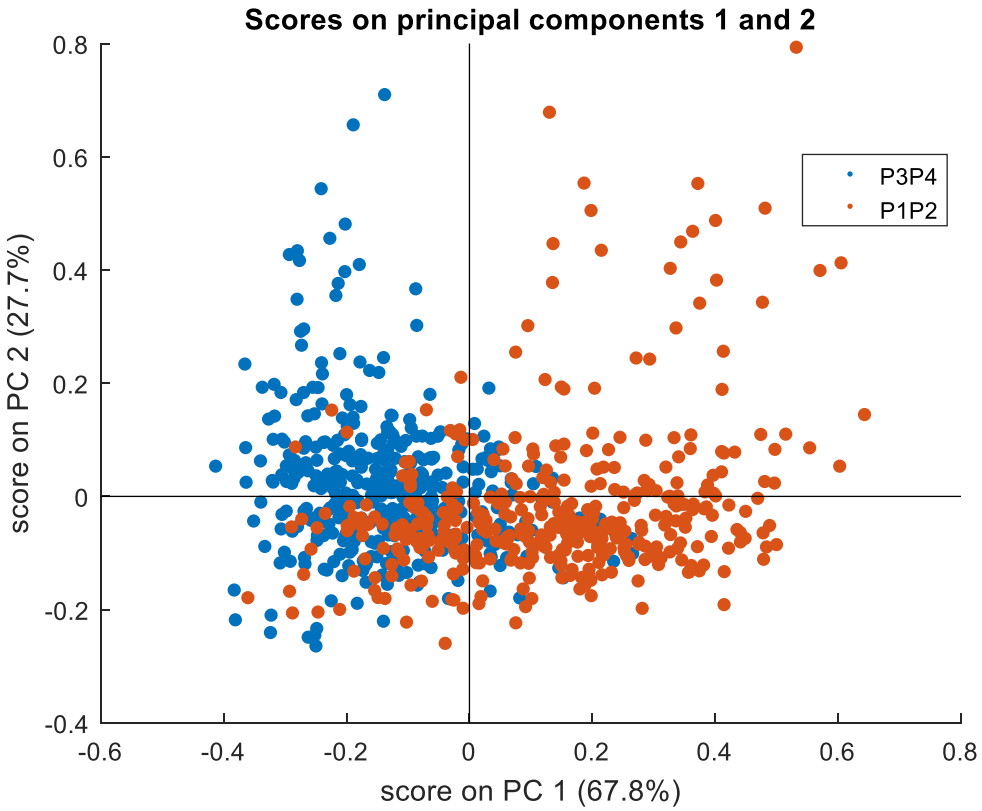

(b)

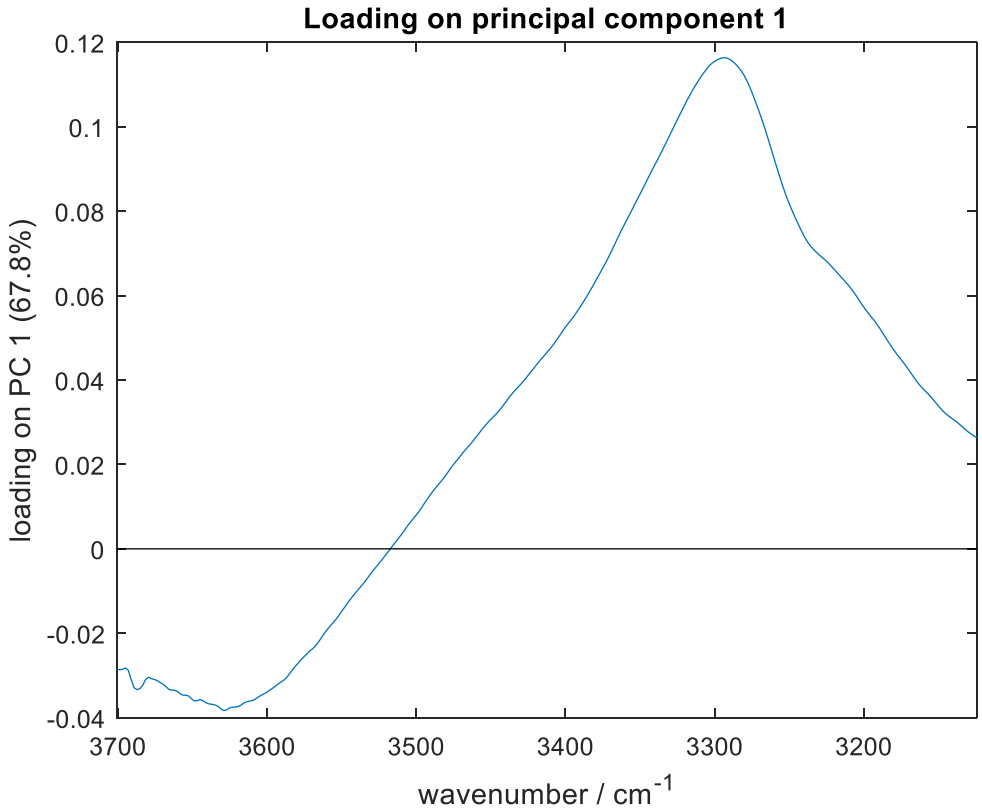

Figure7. 21 (a) The score plots of PC1 and PC2 of epithelium on glass D for cancer and non-cancer patients in experiment 2. (b) The PC1 loading for PCA of epithelium spectra on glass D for cancer and non-cancer patients in experiment 2.

7.2.5.3 Cancer detection by random forest on the same glass slide with glue removal

For both two experiments, the separation of spectra of cancer and non-cancer with glue removal on the same glass slide is not very clear based on PCA. It is necessary to achieve cancer detection by building a classifier.

The model test of cancer detection on the same glass slides is training a classifier using 80% of spectra of stroma or epithelium based on the random forest; the rest 20% of spectra are used to test whether the classifier could predict the spectrum belongs to. Tables 7.19 and 7.20 show the accuracy of the model test for cancer detection by the spectra of epithelium and stroma in experiments 1 and 2, respectively.

Table7. 19 The accuracy of cancer detection between cancer and non-cancer group on the same glass with glue removal in experiment 1.

Model test (%)	epithelium	stroma
Glass D	97.61	99.21
Glass E	98.78	99.23
Glass F	98.27	97.69
Glass J	97.74	97.37
Glass K	96.72	97.68
Glass L	92.51	97.96

For experiment 1 with glue removal, the accuracies of cancer detection between the cancer group and the non-cancer group are shown in table 7.19. According to table 7.19, cancer detection on the same glass slide has a specific high accuracy by both spectra of epithelium and stroma. Except for glass L, the accuracy of cancer detection on the other glass slide is all above 96.00%. In addition, the higher accuracy of the classification of cancer and non-cancer group is obtained by the spectra of the stroma.

Table 7.20 shows the accuracy of cancer detection on the same glass slide for spectra with glue removal in experiment 2. Compared with experiment 1 with glue removal, the accuracy of cancer detection on the same glass slide is lower in experiment 2 with glue removal and they are above 89.00%.

Table7. 20 The accuracy of cancer detection between cancer and non-cancer group on the same glass with glue removal in experiment 2.

Model test (%)	epithelium	stroma
Glass D	94.23	96.33
Glass E	89.99	90.73
Glass F	93.72	97.41
Glass J	94.60	92.28
Glass K	92.09	89.73
Glass L	93.76	93.26

7.2.5.4 Cancer detection by random forest on the different glass slide

To study the effect of glass type on cancer detection, the classifier is trained by spectral data from one glass slide and is tested by spectral data from the other glass slide. The results of the classification of cancer and non-cancer groups on different types of glass

slides by spectra of epithelium and stroma in experiments 1 and 2 are shown in table 7.21 and table 7.22, respectively. Table 7.21 and table 7.22 have highlighted the table cell in which the accuracy is above 80% in yellow. Most of the cancer detection accuracy between different glass slides is significantly lower. According to the number of highlighted cells, no matter for experiments 1 and 2,
the accuracy of the classification of cancer and non-cancer group on different glass slides by epithelium spectra could have a better result than by stroma spectra.

For experiment 1 with glue removal, most cancer detection accuracy between different glass slides is very low, but the accuracy is ok between a few glass slides. Table 7.21(a) shows that cancer detection on glass F&K and K&L could obtain good results using epithelium spectra. While by stroma spectra in table 7.21(b), cancer detection only on glass F&K could have high accuracy.

Table7. 21 (a) The accuracy of cancer detection by epithelium spectra on different glass slides with glue removal in experiment 1.

Accuracy (%)	Test on glass D	Test on glass E	Test on glass F	Test on glass J	Test on glass K	Test on glass L
Train on glass D		84.28	32.75	41.15	46.13	40.45
Train on glass E	71.62		38.49	47.38	59.25	63.33
Train on glass F	61.56	24.67		74.00	81.56	61.49
Train on glass J	71.55	49.68	85.19		68.53	56.03
Train on glass K	79.09	47.38	81.45	56.20		81.08
Train on glass L	49.35	25.75	83.01	73.84	80.57	

Table 7.21(b) The accuracy of cancer detection by stroma spectra on different glass slides with glue removal in experiment 1.

Accuracy (%)	Test on glass D	Test on glass E	Test on glass F	Test on glass J	Test on glass K	Test on glass L
Train on glass D		53.09	54.61	46.93	57.39	11.86
Train on glass E	47.48		58.18	63.97	40.80	46.09
Train on glass F	78.70	49.69		71.49	86.11	61.79
Train on glass J	57.69	37.02	66.86		47.69	31.67
Train on glass K	79.88	27.31	71.88	58.22		45.27
Train on glass L	20.39	44.70	60.61	47.32	65.97	

Table7. 22 (a) The accuracy of cancer detection by epithelium spectra on different glass slides with glue removal in experiment 2.

Accuracy (%)	Test on glass D	Test on glass E	Test on glass F	Test on glass J	Test on glass K	Test on glass L
Train on glass D		64.39	91.06	47.02	50.73	34.35
Train on glass E	66.79		82.94	88.44	83.08	84.55
Train on glass F	91.62	68.77		48.03	51.25	35.61
Train on glass J	52.92	82.84	60.04		91.02	88.69
Train on glass K	47.16	80.30	49.08	91.60		87.73
Train on glass L	33.50	70.05	42.05	86.20	84.30	

Table 7.22(b) The accuracy of cancer detection by stroma spectra on different glass slides with glue removal in experiment 2.

Accuracy (%)	Test on glass D	Test on glass E	Test on glass F	Test on glass J	Test on glass K	Test on glass L
Train on glass D		69.70	91.97	53.41	50.86	16.60
Train on glass E	73051		78.17	78.39	78.02	62.27
Train on glass F	86.3	67.75		49.81	54.26	21.08
Train on glass J	54.10	80.55	46.30		86.15	82.17
Train on glass K	60.29	81.26	53.61	89.50		74.03
Train on glass L	24.80	66.84	36.84	81.41	76.30	

While for experiment 2 with glue removal, the cancer detection results on different glass slides have better performance than experiment 1. The accuracy is ok only between more glass slides. Table 7.22 (a) shows that cancer detection on glass F&D,

glass E&J&K&L could obtain good results by epithelium spectra. While by stroma spectra in table 7.22 (b), cancer detection only on glass F&D, glass J&K could have high accuracy.

To sum up, the type of glass slide has a certain influence on cancer detection. However, maybe due to the similar composition or structure, there is little effect on cancer detection for some glass slides. In addition, the classifier of cancer detection on different glass slides trained by epithelium spectra could get better performance than when using stroma. It indicates the type of glass slide has less impact on cancer detection results for epithelium spectral data.

7.3 Error discussion

Similar to the error in chapter 6 (see section 6.3), the errors in chapter 7 are from measurement and data processes. It will take several days to measure all of the tissue samples, and the environmental changes during these days (temperature) would lead to an error. The different resolutions between the H&E brightfield and chemical images could lead to annotation and registration errors. Error for PCA and random forest results are caused by randomly selecting the spectra when reprocessing the spectral data every time. But the results change a little, only around ±3% and ±0.35% for PCA score and random forest accuracy, respectively.

7.4 Conclusion

The high accuracy of classification of cancer and non-cancer on CaF_2 indicates that SHP is a valuable method for cancer detection. The purpose of this report is to study whether the different types of glass could affect cancer detection. Two types of experimental methods are applied in this project. However, whichever method is used, the spectra could be affected by glue. Therefore, glue removal is a necessary process. Every

experimental result could be divided into two parts: spectra without glue removal and spectra with glue removal.

The biggest difference between the two experiments is the background scan. In experiment 1, the background is a clear and tissue-free area. According to chapters 5 and 6, the glue has less effect in experiment 1. While in experiment 2, the background is a blank glass slide, both glue and coverslip would have an influence on spectra. The glue removal has a considerable impact on the spectra in experiment 2.

Tissue sections from 4 patients are mounted on 6 kinds of glass slides, and P1(BPH), P2(BPH), P3(CaP) and P4(CaP) stand for the 4 patients. The cancer group is made of P3(CaP) and P4(CaP) spectra. The non-cancer group is made of P1(BPH) & P2(BPH) spectra.

For the spectra without glue removal in experiment 1, there is no separation for PCA results of 6 glass slides from the same patient. It means the type of glass slide has no effect on spectra. The classification of cancer and non-cancer group on the same glass slide by PCA has a good performance. It also has a high accuracy by random forest (accuracy above 97.00%), especially for the spectra of the epithelium. However, for the classification on the different glass slides, the accuracies are very different. The cancer detection on some of the glass slides could have good performance (accuracy above 80.00%), and the better results are also from the spectra of the epithelium. According to the detection result, the cancer detection between glasses D & E or between glasses F & K & J could get a good classification result. It means that the differences in glasses D & E or in glasses F & K & J are smaller than the difference in cancer tissue. Therefore, the type of glass slide impacts cancer detection, and the effect is lower for the spectra of epithelium than stroma.

While in experiment 2 without glue removal, PCA cannot separate all of the spectra on 6 glass slides from the same patient, and it cannot separate the spectra of cancer and

non-cancer groups on the same glass slide. It means the spectra difference between cancer and non-cancer group are less than spectra from experiment 1. Cancer detection only could achieve by random forest. Cancer detection accuracy on the same glass slide is above 92.00%, and it is slightly lower than experiment 1. For cancer detection on different glass slide, they have good results on glass J & E and glass J &K. it means the difference between glasses J & E, glasses J & K are smaller. In addition, for the cancer detection by epithelium spectra in experiment 2, the glasses J & L also have good performance.

There are certain separations between cancer and non-cancer groups by PCA for both two experiments after removing the glue. The accuracy of the classification of cancer and non-cancer group on the same glass slide is above 96.00% and 89.00% for experiment 1 and 2, respectively. And both of the accuracies are decreased after removing glue for two experiments. In addition, for both experimental spectra with glue removal, the better classification performance on the same glass slide is from the spectra of the stroma. But the spectra of stroma always have worse performance than epithelium on cancer detection on the different glass slides. It means the glass slide has more impact on cancer detection by stroma spectra after removing the glue.

Comparing the cancer detection on the same glass slide, spectra without glue removal always have better results than those with glue removal for both experiments. It means that the glue has a particular contribution to cancer detection. Compared with experiments 1 and 2, cancer detection on the same glass slide in experiment 1 always performs better than experiment 2. Although the spectra in experiment 2 have more effect on glue, they also have an effect on the coverslip. Therefore, experiment 1 is a better method than experiment 2.

For experiment 1, the better cancer detection results on the same glass slide are from epithelium spectra before removing the glue. The better results are from stroma spectra after removing the glue. Generally, the thickness of the glue on the normal epithelium

area is higher than the stroma area. The more glue in the epithelium has a certain contribution to cancer detection without glue removal. After removing glue, cancer detection only depends on the tissue. The thickness of the stroma is higher than the epithelium, so better classification results are from stroma spectra with glue removal. It also proves that glue has a specific effect on cancer detection.

Most of the cancer detection accuracy on the different glass slide is very low, and it indicates the type of glass slide has an effect on cancer detection. However, the accuracy among some of glass slides has good results, and the spectra of epithelium always have higher accuracy than stroma for both experiments with glue removal. It means that spectra of epithelium are less affected by the type of glass slide than stroma. As mentioned above, the normal epithelium area contains more glue, so the glue removal process has more significant changes on spectra of epithelium than stroma. This change could lead to the spectra with glue removal being more similar to the reference spectra (matrigel spectra). Therefore, the glue removal maybe would reduce the spectral difference among the glass slides. Thus, the type of glass slide has less impact on cancer detection by epithelium spectra with glue removal.

Compared with the results in chapter 6, the type of glass slide has a slight influence on tissue classification for spectra without glue removal, however, it has an impact on cancer detection. It indicates that the difference between epithelium and stroma is bigger than the difference in glass type and is bigger than the difference in spectra of cancer and non-cancer.

To sum up, cancer detection could be achieved by the spectra of epithelium and stroma on the same glass slide. SHP on glass slides is a potential method for cancer detection. But the type of glass slide has an impact on cancer detection. Therefore, the type of glass slide must be consistent during cancer detection.

7.5 Reference

[1] M. J. Baker *et al.*, ‘Using Fourier transform IR spectroscopy to analyze biological materials’, *Nat. Protoc.*, 2014.

[2] J. Doherty, Z. Zhang, K. Wehbe, G. Cinque, P. Gardner, and J. Denbigh, ‘Increased optical pathlength through aqueous media for the infrared microanalysis of live cells’.

[3] J. Tang, D. Kurfürstová, and P. Gardner, ‘Breast cancer detection using infrared spectral pathology from H&E stained tissue on glass slides’, *Clin. Spectrosc.*, vol. 3, p. 100008, Dec. 2021.

[4] M. J. Pilling, A. Henderson, J. H. Shanks, M. D. Brown, N. W. Clarke, and P. Gardner, ‘Infrared spectral histopathology using haematoxylin and eosin (H&E) stained glass slides: a major step forward towards clinical translation’, *Analyst*, vol. 142, no. 8, pp. 1258–1268, 2017.

[5] R. A. Shaw, H. H. Eysel, K. Z. Liu, and H. H. Mantsch, ‘Infrared Spectroscopic Analysis of Biomedical Specimens Using Glass Substrates’, *Anal. Biochem.*, vol. 259, no. 2, pp. 181–186, Jun. 1998.

[6] R. a Shaw, H. H. Eysel, K. Z. Liu, and H. H. Mantsch, ‘Infrared spectroscopic analysis of biomedical specimens using glass substrates.’, *Anal. Biochem.*, vol. 259, no. 2, pp. 181–6, 1998.

[7] M. J. Pilling, A. Henderson, J. H. Shanks, M. D. Brown, N. W. Clarke, and P. Gardner, ‘Infrared spectral histopathology using haematoxylin and eosin (H&E) stained glass slides: a major step forward towards clinical translation’, *Analyst*, vol. 142, no. 8, pp. 1258–1268, 2017.

[8] P. Bassan, J. Mellor, J. Shapiro, K. J. Williams, M. P. Lisanti, and P. Gardner, ‘Transmission FT-IR Chemical Imaging on Glass Substrates: Applications in Infrared Spectral Histopathology’, 2014.

Chapter 8

Conclusion and future work

8.1 Conclusion

Spectral histopathology (SHP) using H&E stained tissue on glass slides is a potential method to augment current pathology and help cancer diagnosis. There are many advantages if it were used as a pre-screening method for clinical application: 1) high speed of cancer detection, 2) no additional sample preparation process, 3) low cost, 4) no disruption to the pathologists' workflow. However, the most significant limitation of using glass slides is that the substrate is opaque in the rich fingerprint spectral region. The amide A envelope is the only band which could be used for SHP. In order to achieve the clinical translation of SHP, many fundamental studies need to be explored. The work presented in this thesis attempts to evaluate the influence of different types of glass substrates on the classification of tissue types and cancer detection using FTIR.

Glass is a non-crystalline amorphous solid consisting of a complex mixture of chemical components. Except for silicon dioxide, which is the main component, the types and proportions of other components are variable for different glass slides. There are many types of glass slides used in clinical histopathology. 12 different glass slides, which were produced by different manufacturers, were used in this project.

Chapter 4 compared the infrared spectra of 12 different types of blank glass slides. The infrared absorption of blank glass slide in 2000 – 3800 cm^{-1} is caused by hydroxyl and its related groups. Except for glass D, the rest of the glass slides cannot be separated by their infrared spectra. Furthermore, the rest of 11 glass slides could be divided into charged and non-charged glass slides. However, the PCA analysis still cannot completely separate the two groups of glass slides. Therefore, the types of glass slides generally have little effect on infrared spectra, and the spectral difference between the charged and non-charged glass slides is also very small. This is perhaps to be expected given that the charged surface layer is negligible in thickness compared with the bulk (~1 mm) glass slide.

For the tissue analysis, there are two experimental methods for comparison. The background of experiment 1 is a clear tissue-free area. While the background of experiment 2 is the blank glass. These two methods are compared for both tissue classification and cancer detection.

A glue removal method is developed and discussed in chapter 5. The existence of bands at 3400-3450 cm^{-1} and 3400-3600 cm^{-1} are related to the glue and the coverslip, respectively. The suitable removal method and fit range are compared to eliminate the interference of glue and coverslip. And the results indicate that the most appropriate glue removal method uses the spectra of glue, coverslip and Matrigel as references and the fit ranges 1: Matrigel peak (3278-3318cm^{-1}, 3066-3106cm^{-1}); fit range 3: glue peak & Matrigel peak (2950-2970cm^{-1}, 2925-2945cm^{-1}, 2867-2887cm^{-1}); fit range 4 coverslip & Matrigel peak (3536-3576 cm^{-1}, 2704-2744 cm^{-1}) for the fitting procedure.

Epithelium and stroma are essential components of the prostate tissue and have previously been used for IR based cancer detection[1]. Therefore, the classification of epithelium and stroma is used to evaluate the influence of glass type on tissue classification. A series of adjacent BPH tissue sections cut from the same tissue block are mounted on the 12 glass slides. For tissue classification on the same glass slide, the accuracy of discriminating epithelium and stroma is above 98.40% for two experiments. The results indicate that the tissue classification on the same glass slides based on the spectra can be easily achieved.

For tissue classification on the different glass slides without removing glue, except for glass A and glass I, most of the accuracies of distinguishing epithelium and stroma based on the spectra are above 90.57%. The results indicate that the glass slide type only slightly influences tissue classification, especially for experiment 1 without glue removal. However, after removing glue, the classification accuracy gets worse indicating that the glue removal introduces additional errors to the analysis.

Using either spectrum of epithelium or stroma could achieve cancer detection on the same glass slides, especially for experiment 1 without glue removal (above 97.19%). But accuracy is higher when using the spectra of epithelium. Spectra without glue removal always have higher cancer detection accuracy than glue removal for both experiments. It means that the glue contributes to cancer detection or introduces an additional random error that reduces the classification accuracy. Since glue has no biological relevance, it is likely that this relates to tissue density and porosity of the cancerous and non-cancerous tissue, which allows differing amounts of glue to penetrate, thus contributing a spectral difference. However, the accuracy of cancer detection always has poor performance on the different glass slides. Therefore, the type of glass slide has an impact on cancer detection.

In conclusion, the type of glass slide has a slight influence on spectra and tissue classification without glue removal, but it affects cancer detection. Glue has a contribution to tissue classification and cancer detection. In an ideal situation, the type of glass slide must be consistent in building a database to achieve cancer detection and the clinical translation of SHP. In addition, the spectra of epithelium in experiment 1 without glue removal are most suitable for cancer detection.

8.2 Future work

This project aims to study the effect of the type of glass slides on cancer detection, which is an important foundational work for SHP to obtain acceptance into clinical. The results indicate the type of glass slide affects cancer detection; thus, the type of glass slide should be kept consistent for spectral histopathology. However, further work is required to draw a more definitive conclusion because this project still has some shortcomings that need to be improved.

Firstly, in tissue classification and cancer detection work, only one adjacent tissue sample is mounted on every type of glass slide. It means there is only once sample preparation for every kind of slide. So, for tissue classification and cancer detection, the accuracy differences either be due to the glass itself or external factors during the sample preparation. For example, tissue classification in chapter 6 shows a big difference between the spectra on glass A and the other 11 glass slides, which caused the model trained by glass A cannot to be used to classify the epithelium and stroma on the other glass slides. It is unclear whether the spectral difference is caused by glass type or other factors during the sample preparation. Therefore, to eliminate the error from sample preparation, the same adjacent prostate tissue from the same BPH patient could be mounted on the 12 glass slide again as the second group. It means there are 24 adjacent tissue mounted on the 12 glass slides, and every type of glass slide has two adjacent prostate tissue. Similarly, the second group is also needed for cancer detection.

Secondly, only one patient was used for studying tissue classification, and only 4 patients were used for studying cancer detection. Therefore, it is necessary to prepare a series of adjacent tissue samples from more CaP and BPH patients for repeating the experiment and explore whether the experiment could get the same results about the influence of glass type on tissue classification and cancer detection.

Tissue microarray (TMA) is the most suitable sample for further research to improve

the above two shortcomings, even though fewer spectra could be selected than the whole prostate tissue. A schematic of the sample preparation is indicated in figure 8.1. Twelve adjacent prostate tissue are mounted on 6 different glass slides, and every type of glass slide have two adjacent tissue from the same patient. Figure 8.1 displays 12 prostate tissue cores from 6 BPH and 6 CaP patients. But the number of patients can also be appropriately increased when the experiment is really carried out.

Figure8. 1 The sample preparation design for future study.

Thus the spectra used for training the model on the same type of glass slide could be selected from two adjacent tissue samples, which could reduce the error caused by sample preparation. Suppose the models perform well on tissue classification or cancer detection on the different types of glass slides. In that case, it could prove the type of glass slide not affect tissue classification or cancer detection. If not, the kind of glass slide caused the spectral difference and bad performance on tissue classification or cancer detection. The above experimental design is to obtain more reliable and stable results about the effect of glass slides on tissue classification and cancer detection.

In addition, glue removal is one of the difficulties for data processing. Glue always has an impact on the spectra, no matter what experimental method is used. The project results indicated that the glue contributes to tissue classification and cancer detection. It is caused by the structural difference between epithelium and stroma. There is more holes for the normal epithelium. So the normal epithelium would contain more glue. In order to make sure the classification (epithelium & stroma, cancer & non-cancer) is based on the real tissue spectra, glue removal is necessary. Chapter 5 has already tried to remove the glue with algorithms in Matlab. The key problem in removing glue is finding the best fit range. Therefore, the future study for developing the glue removal method is optimizing the fit range based on constantly reprocessing the spectral data by the supercomputer.

High accuracy and affordability are the two critical aspects of clinical translation for SHP. Traditional substrate (CaF_2 or BaF_2) for infrared spectra at present is too expensive to be applied in the clinical field[2]. Therefore, using glass as a substrate is an important research field for the clinical application of SHP. Studies by Rutter el al. have proven that the thickness of the glass slide enable some data from the fingerprint region to be obtained.[3][4]. Coverslips (0.13-0.17 mm) could therefore be used to obtain the spectral data from the fingerprint range, but it still needs additional sample preparation above normal pathology procedure and the cover slips are considerably more fragile than the normal glass slides. The histopathology glass slide (around 1mm) is only transparent in the infrared region above 2000 cm^{-1}. The Amide A envelope is the only peak that could be used for SHP, which affects the accuracy of the classification. Kansiz used optical photothermal infrared (O-PTIR) spectroscopy combined with a quantum cascade laser (QCL) IR pump source to study cancer detection[5]. It was demonstrated that could obtain the IR spectra from lipid and fingerprint regions on cell lines but has yet to be fully demonstrated on biopsy tissue samples.

Compared with the above studies, using H&E stained tissue on the glass slides does not add additional sample preparation and cannot disturb the clinical histopathologist's

workflow. Cancer detection could be achieved only based on the amide A. This method in principle therefore the most straightforward method to push for the clinical translation for sample pre-screening and cancer detection.

Figure 8.2 describe the ideal workflow for the SHP used as a pre-screening process in the future. The traditional workflow for cancer detection is depicted by the blue arrow, and the pathologist has to examine all biopsy tissue and give detection results. SHP could be applied as a pre-screening process for clinical translation to reduce the pathologist's workload and detection time. As is shown in the yellow arrow in figure 8.2. just like a traffic light system, all H&E stained biopsy samples on the glass slide need to be detected by SHP. Only the samples, which are detected to be suspicious and cancerous, need to be given to the pathologist to make the final decision, while the normal samples could directly give the detection result.

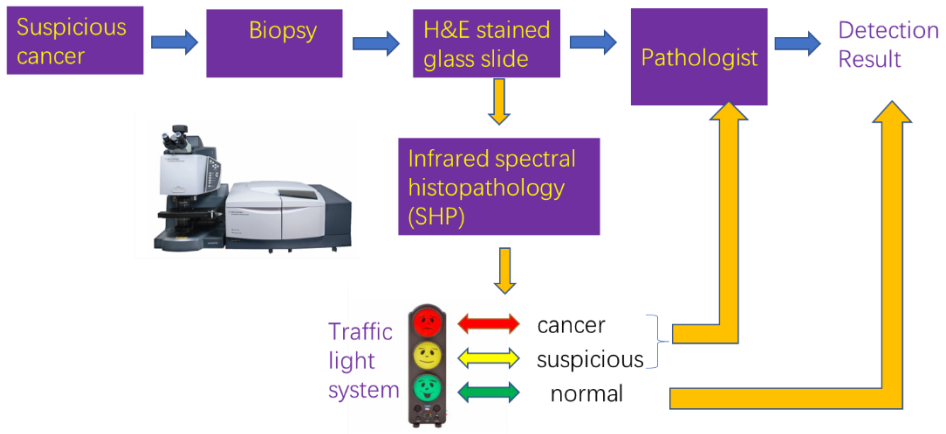

Figure8. 2 The workflow for clinical application of SHP in the future.

Many fundamental studies need to be considered to build a stable and reliable model for SHP. This project has explored the effect of glass type on cancer detection. Further study could discuss the impact of glue and coverslip on cancer detection. All of these studies could determine a very strict sample preparation protocol for the clinical application of SHP in the future.

8.3 Reference

[1] M. J. Pilling, A. Henderson, J. H. Shanks, M. D. Brown, N. W. Clarke, and P. Gardner, ‘Infrared spectral histopathology using haematoxylin and eosin (H&E) stained glass slides: a major step forward towards clinical translation’, *Analyst*, vol. 142, no. 8, pp. 1258–1268, 2017.

[2] M. J. Baker *et al.*, ‘Clinical applications of infrared and Raman spectroscopy: State of play and future challenges’, *Analyst*, vol. 143, no. 8, pp. 1735–1757, 2018.

[3] A. V. Rutter, J. Crees, H. Wright, D. G. Van Pittius, I. Yousef, and J. Sulé-Suso, ‘Fourier transform infrared spectra of cells on glass coverslips. A further step in spectral pathology’, *Analyst*, vol. 143, no. 23, pp. 5711–5717, 2018.

[4] A. V. Rutter *et al.*, ‘Identification of a Glass Substrate to Study Cells Using Fourier Transform Infrared Spectroscopy: Are We Closer to Spectral Pathology?’, *Appl. Spectrosc.*, vol. 74, no. 2, pp. 178–186, 2020.

[5] M. Kansiz, L. M. Dowling, I. Yousef, O. Guaitella, F. Borondics, and J. Sulé-Suso, ‘Optical Photothermal Infrared Microspectroscopy Discriminates for the First Time Different Types of Lung Cells on Histopathology Glass Slides’, *Anal. Chem.*, vol. 93, no. 32, pp. 11081–11088, 2021.